

PHOSPHIDO-BORANE COMPLEXES OF
GROUP I AND II METALS

by

James Martin Watson

A thesis submitted in partial fulfilment of the
requirements for the degree of

Doctor of Philosophy

Newcastle
University

September 2011

Abstract

The synthesis and characterisation of a range of novel phosphine-borane precursors is described: $\{(Me_3Si)_2CH\}PH(C_6H_4-2-CH_2OMe)(BH_3)$ (**39**), $\{(Me_3Si)_2CH\}PH(C_6H_4-2-SMe)(BH_3)$ (**40**), $\{(Me_3Si)_2CH\}PH(C_6H_4-2-OMe)(BH_3)$ (**41**) and $\{(Me_3Si)_2CH\}PH(C_6H_5)(BH_3)$ (**42**).

Treatment of **39** with *n*-BuLi, BnNa or BnK proceeds cleanly to give the corresponding alkali metal complexes, which are crystallised in the presence of THF, tmeda and pmdeta, respectively, to yield the adducts $[[\{(Me_3Si)_2CH\}P(BH_3)(C_6H_4-2-CH_2OMe)]ML]_2$ [ML = Li(THF), (**49**); ML = Na(tmeda), (**50**); ML = K(pmdeta), (**51**)].

Deprotonation of **40** with *n*-BuLi, BnNa or BnK, followed by crystallisation in the presence of THF, tmeda or pmdeta, respectively, yields the compounds $[\{(Me_3Si)_2CH\}P(BH_3)(C_6H_4-2-SMe)M(L)]_n$ [ML = Li(THF), $n = 2$ (**64**); ML = Na(tmeda), $n = \infty$ (**65**); ML = K(pmdeta), $n = 2$ (**66**)]. On heating a solution of **64** in the presence of free phosphine-borane **40**, concurrent formation of the corresponding phosphine $[\{(Me_3Si)_2CH\}PH(C_6H_4-2-SMe)]$ (**45**) and phosphido-bis(borane) $[\{(Me_3Si)_2CH\}P(C_6H_4-2-SMe)(BH_3)_2Li]$ (**72**) is observed *via* multinuclear NMR spectroscopy.

Treatment of **41** with *n*-BuLi, BnNa or BnK, yield the corresponding phosphido-boranes. Heating a solution of the lithium salt $[\{(Me_3Si)_2CH\}P(C_6H_4-2-OMe)(BH_3)Li(THF)]$ (**85**) in toluene, in the presence of one equivalent of tmeda yields the unexpected phosphine-substituted lithium alkoxide $[\{(Me_3Si)CH\}PH(C_6H_4-2-O)Li]_6$ (**89**) and the tertiary phosphine-borane $\{(Me_3Si)_2CH\}PMe(BH_3)(C_6H_4-2-OMe)$ (**90**), and a third unidentified phosphorus-containing compound. Repeating the experiment with the analogue $[\{(Me_3Si)_2CH\}P(C_6H_4-2-OMe)(BD_3)Li(THF)_n]$ (**104**), and monitoring the reaction using 2D and $^{31}P\{^1H\}$ NMR spectroscopy, indicates that the source of the P-H proton is the borane group. It was also found that heating a solution of **85** in toluene, in the presence of an excess of THF and one equivalent of tmeda results in another thermolytic reaction pathway, generating **90** and a phosphorus-containing compound, proposed to be the alkoxo-phosphido-borane $[\{(Me_3Si)_2CH\}P(BH_3)(C_6H_4-2-O)Li_2(tmeda)_2]$ (**91**). Reaction between CaI_2 and two

equivalents of $[\{(Me_3Si)_2CH\}P(C_6H_4-2-OMe)(BH_3)]K$ yields the cluster $[\{(Me_3Si)_2CH\}P(C_6H_4-2-O)(BH_3)Ca(THF)]_4$ (**108**) and **90**. **108** crystallises with an unusual Ca_4O_4 core, with two distinct calcium environments.

Reaction between **42** and *n*-BuLi, BnNa or BnK proceeds cleanly to give the corresponding alkali metal phosphido-boranes. The lithium salt crystallises in the presence of THF as a polymer $[\{(Me_3Si)_2CH\}P(C_6H_5)(BH_3)Li(THF)_2]_\infty$ (**115**), whilst the sodium salt crystallises in the presence of 12-crown-4 as the solvent-separated ion species $[\{(Me_3Si)_2CH\}P(C_6H_5)(BH_3)][Na(12-crown-4)_2]$ (**116**). The potassium salt crystallises in the presence of pmdeta as the adduct $[\{(Me_3Si)_2CH\}P(C_6H_5)(BH_3)K(pmdeta)]_2$ (**117**). The reaction between **42** and $PhCH_2K$ followed by addition of half an equivalent of either SrI_2 or BaI_2 , generates the corresponding alkaline-earth metal complexes $[\{(Me_3Si)_2CH\}P(C_6H_5)(BH_3)]_2Sr$ (**119**) and $[\{(Me_3Si)_2CH\}P(C_6H_5)(BH_3)]_2Ba$ (**120**).

A series of alkaline and alkaline earth metal phosphido-bis(borane) complexes have been prepared. The reaction between **42** and one equivalent of *n*-BuLi, $PhCH_2Na$ or $PhCH_2K$, followed by addition of $BH_3 \cdot SMe_2$, yields the corresponding phosphido-bis(borane) complexes. The lithium salt is crystallised in the presence of one equivalent of 12-crown-4 to yield the monomer $[\{(Me_3Si)_2CH\}P(C_6H_5)(BH_3)_2Li(12-crown-4)]$ (**123**), whilst the sodium and potassium salts are crystallised in the presence of THF to yield the adducts $[\{(Me_3Si)_2CH\}P(C_6H_5)(BH_3)_2Na(THF)_2]_2$ (**124**) and $[\{(Me_3Si)_2CH\}P(C_6H_5)(BH_3)_2K(THF)_2]_\infty$ (**125**). Deprotonation of **41** with $PhCH_2Na$ followed by reaction with $BH_3 \cdot SMe_2$ yields the corresponding salt, which is crystallised in the presence of 12-crown-4 as a solvent-separated ion pair $[\{(Me_3Si)_2CH\}P(C_6H_4-2-OMe)(BH_3)_2][Na(12-crown-4)_2]$ (**126**).

Treatment of two equivalents of **42** with one equivalent of either $MgBu_2$, $CaBn_2$ or $\{(Me_3Si)_2CH\}_2Sr$, followed by addition of $BH_3 \cdot SMe_2$ yield the corresponding salts, which are crystallised in the presence of THF as the adducts $[[\{(Me_3Si)_2CH\}P(BH_3)_2(C_6H_5)]_2Mg(THF)_4]$, (**128**), $[[\{(Me_3Si)_2CH\}P(BH_3)_2(C_6H_5)]_2Ca(THF)_4]$ (**129**) and $[[\{(Me_3Si)_2CH\}P(BH_3)_2(C_6H_5)]_2Sr(THF)_4]$ (**130**), respectively.

Acknowledgements

I would firstly like to thank my supervisor Dr Keith Izod for his unwavering support and guidance over the past four years, in both the production of this thesis and in the laboratory, and to whom I am extremely grateful. I would also like to thank past members of the group: Dr Corinne Wills, Dr John-Charles Stewart and Dr Ewan Clark, for all of their help and advice.

I would like to thank Dr Ross Harrington and Professor Bill Clegg for their help with X-crystallography, Professor William McFarlane for his expertise in NMR, and staff members past and present who have given their help during my PhD.

I would also like to thank my family and friends for their support, in particular my parents Martin and Elaine and step-mother Romy.

Finally, to Lynsey, who has given her support, encouragement and help throughout my PhD. I could not have done this without her, and so it is to my wife that I dedicate this thesis.

Publications from this work

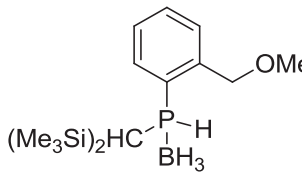
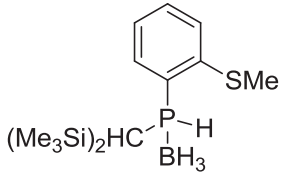
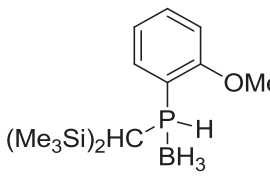
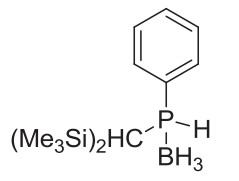
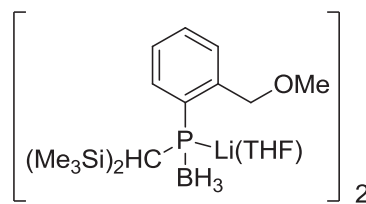
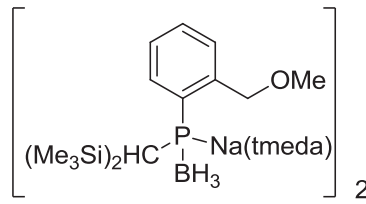
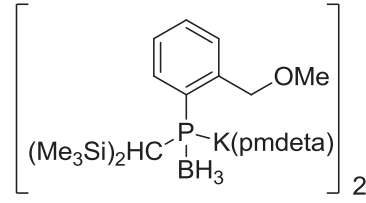
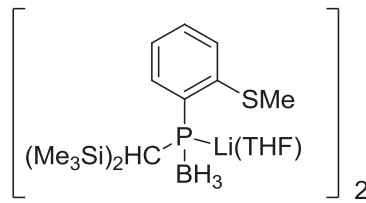
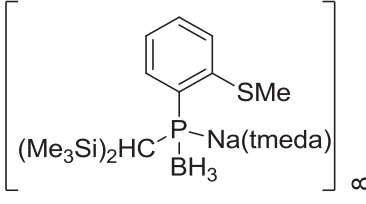
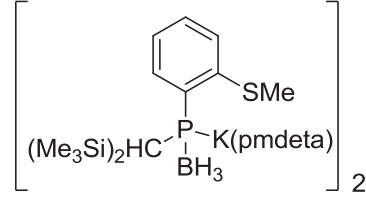
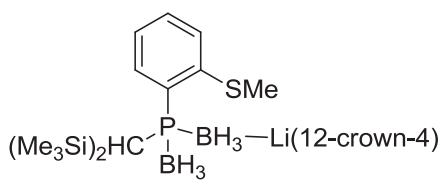
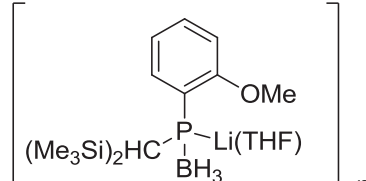
Chapter 4

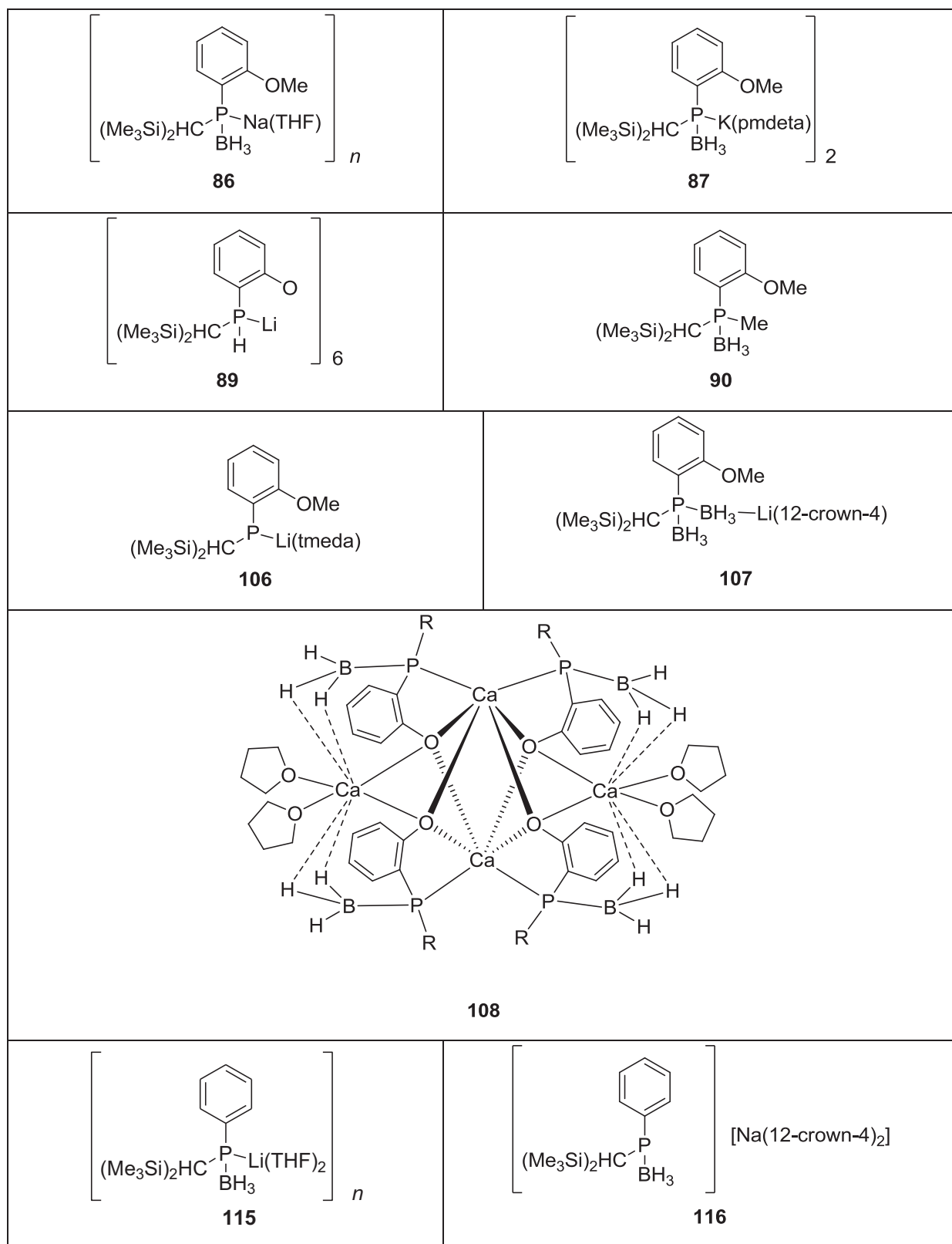
Synthesis, structures and stabilities of thioanisole-functionalised phosphido-borane complexes of the alkali metals. Keith Izod, James M. Watson, William Clegg and Ross W. Harrington. *Dalton Trans.* **2011**, 40, 11712.

List of Abbreviations

Bn	benzyl	q	quartet
d	doublet	s	singlet
dd	doublet of doublets	THF	tetrahydrofuran
dmp	dimesitylphenyl	tmeda	<i>N,N,N',N'</i> - tetramethylethylenediamine
dqd	doublet of quartet of doublets	t	triplet
<i>d</i>	deuterated		
{ ¹ H}	hydrogen decoupled		
Hz	hertz		
m	multiplet		
mes	mesityl		
mes*	2,4,6-tri- <i>t</i> -butylphenyl		
μ_n	<i>n</i> -bridging		
NMR	nuclear magnetic spectroscopy		
pmdeta	<i>N,N,N',N'',N'''</i> - pentamethyldiethylenetriamine		

Table of Important Compounds

 <p>39</p>	 <p>40</p>
 <p>41</p>	 <p>42</p>
 <p>49</p>	 <p>50</p>
 <p>51</p>	 <p>64</p>
 <p>65</p>	 <p>66</p>
 <p>72 (12-crown-4)</p>	 <p>85</p>



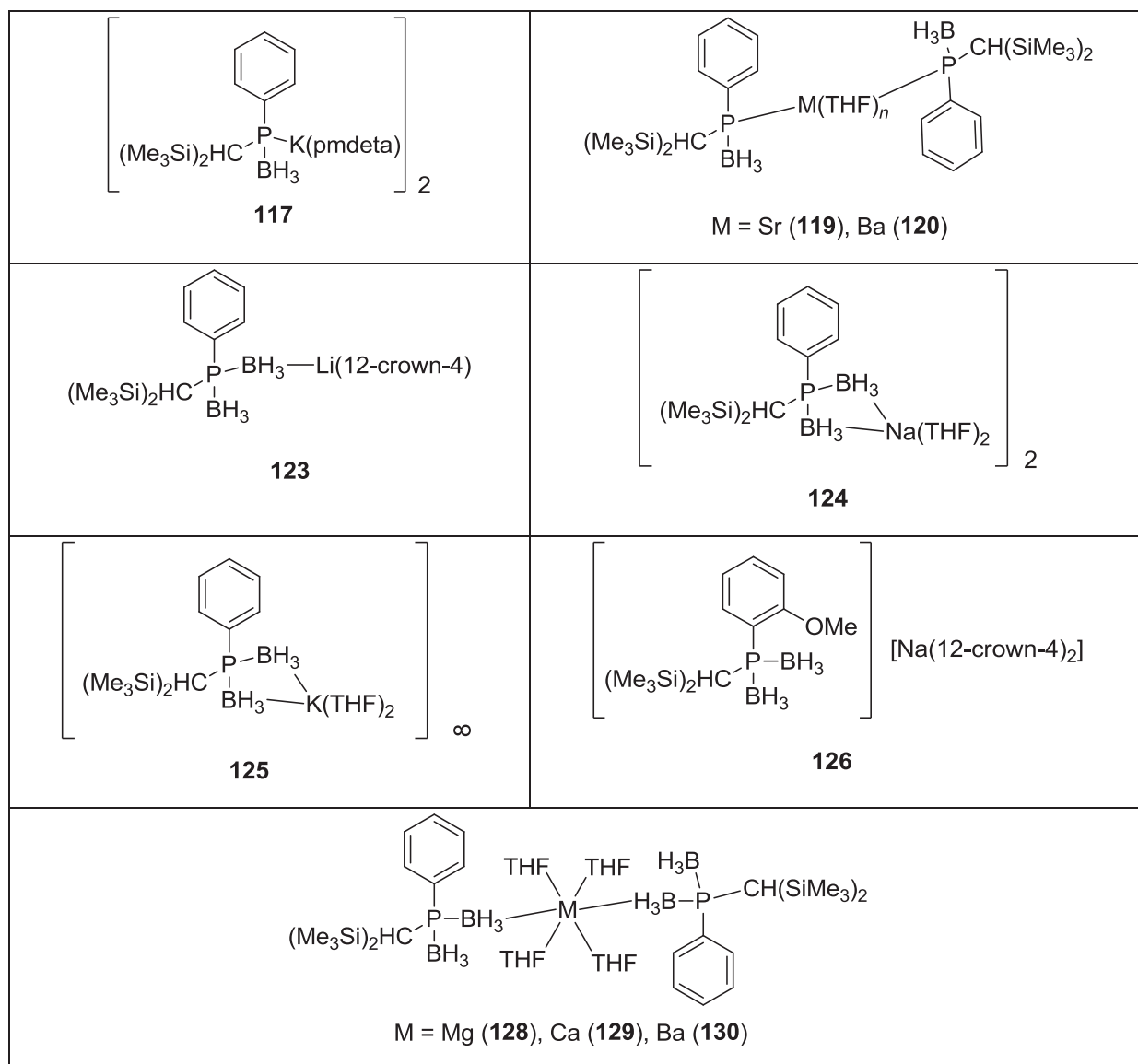


Table of Contents

Abstract	i
Acknowledgements	iii
Publications from this work	iv
List of abbreviations	v
Table of important compounds	vi
Table of contents	ix
Chapter 1. Introduction	1
1.1 Alkali metal organometallics	1
1.2 Phosphides	3
1.2.1 Alkali metal phosphides	4
1.2.1.1 Lithium organophosphides	4
1.2.1.2 Heavier alkali metal phosphides	10
1.2.1.3 Donor-functionalised phosphides	13
1.2.2 Alkaline earth metal phosphides	17
1.3 Phosphine-boranes	22
1.3.1 Introduction	22

1.3.2	Preparation	23
1.3.2.1	Preparation of phosphine-boranes from borohydrides	23
1.3.2.2	Preparation of phosphine-boranes from secondary chlorophosphines	24
1.3.3	Decomplexation of phosphine-boranes	25
1.3.4	Reactivity and functionalisation of phosphine-boranes	26
1.3.4.1	Hydrophosphination	28
1.3.4.2	Cross-coupling functionalisation	29
1.3.5	Summary	30
1.4	Phosphido-boranes	31
1.5	Summary	37
1.6	References	38
Chapter 2. Synthesis of Phosphine-Borane Precursors		45
2.1	Introduction	45
2.2	Synthesis of secondary phosphine-borane precursors	46
2.2.1	Synthesis of $\{(Me_3Si)_2CH\}PH(C_6H_4-2-CH_2OMe)(BH_3)$ (39)	46
2.2.2	Synthesis of $\{(Me_3Si)_2CH\}PH(C_6H_4-2-SMe)(BH_3)$ (40)	47
2.2.3	Synthesis of $\{(Me_3Si)_2CH\}PH(C_6H_4-2-OMe)(BH_3)$ (41)	48
2.2.4	Synthesis of $\{(Me_3Si)_2CH\}PH(C_6H_5)(BH_3)$ (42)	48
2.3	NMR spectroscopic characterisation of 39-42	49

2.4	Solid-state characterisation of phosphine-boranes	52
2.5	References	57
Chapter 3. Alkali metal complexes of a benzyl-methylether-functionalised phosphido-borane		60
3.1	Introduction	60
3.2	Synthesis of the alkali metal complexes [$\{(\text{Me}_3\text{Si})_2\text{CH}\}\text{P}(\text{C}_6\text{H}_4\text{-2-CH}_2\text{OMe})(\text{BH}_3)\text{M}(\text{L})$] [$\text{M}(\text{L}) = \text{Li}(\text{THF})$ (49), $\text{Na}(\text{tmeda})$ (50), $\text{K}(\text{pmdeta})$ (51)]	62
3.3	Solution-phase characterisation of compounds 49-51	63
3.4	Solid-state structures of compounds 49-51	64
3.4.1	Solid-state structure of 49	64
3.4.2	Solid-state structure of 50	67
3.4.3	Solid-state structure of 51	70
3.5	Conclusions	72
3.6	References	72
Chapter 4. Alkali metal complexes of a thioanisole-functionalised phosphido-borane		75
4.1	Introduction	75
4.2	Synthesis of the alkali metal complexes [$\{(\text{Me}_3\text{Si})_2\text{CH}\}\text{P}(\text{C}_6\text{H}_4\text{-2-SMe})(\text{BH}_3)\text{M}(\text{L})$] [$\text{M}(\text{L}) = \text{Li}(\text{THF})$ (64), $\text{Na}(\text{tmeda})$ (65), $\text{K}(\text{pmdeta})$ (66)]	76

4.3	Solution-phase characterisation of compounds 64-66	78
4.4	Solid-state structures of compounds 64-66	78
4.4.1	Solid-state structure of 64	78
4.4.2	Solid-state structure of 65	81
4.4.3	Solid-state structure of 66	83
4.5	Behaviour of 64 in solution	85
4.5.1	Photolytic reactivity of 64	85
4.5.2	Thermolytic reactivity of 64	86
4.5.3	Synthesis and solution-phase characterisation of 72·(12-crown-4)	88
4.6	Conclusions	89
4.7	References	90
 Chapter 5. Alkali metal and calcium complexes of anisole-functionalised phosphido-boranes		91
5.1	Introduction	91
5.2	Synthesis of alkali metal complexes [$\{(Me_3Si)_2CH\}P(C_6H_4-2-OMe)(BH_3)M(L)$] [$M(L) = Li(THF)$ (85), $Na(tmeda)$ (86), $K(pmdeta)$ (87)]	94
5.3	Solution-phase characterisation of 85-87	96
5.4	Solid-state structure of 87	96
5.5	Thermally-induced reactions of 85	99
5.6	Solution-phase characterisation of compound 89	104

5.7	Solid-state structure of compound 89	105
5.8	Synthesis and solution-phase characterisation of $\{(Me_3Si)_2CH\}PMe(BH_3)$ (C ₆ H ₄ -2-OMe) (90)	109
5.9	Investigation into the mechanism of formation of 89	109
5.9.1	Deuterated solvents	111
5.9.2	Synthesis of $\{(Me_3Si)_2CH\}PH(BH_3)(C_6H_4-2-OCD_3)$ (101) and $\{(Me_3Si)_2CH\}PH(BD_3)(C_6H_4-2-OMe)$ (102)	112
5.10	Identity of unknown compound A	115
5.11	Comparison between the stability of 85 and $[\{(Me_3Si)_2CH\}P(C_6H_4-2-$ OMe)Li(tmeda)] (106)	117
5.11.1	Synthesis and solution-phase characterisation of 106	118
5.11.2	Solid-state structure of 106	118
5.11.3	Reactivity of 106	119
5.12	Synthesis and solution-phase characterisation of $[\{(Me_3Si)_2CH\}P(C_6H_4-2-$ OMe)(BH ₃) ₂ Li(12-crown-4)] (107)	120
5.13	Synthesis of the alkaline earth metal complex $[\{(Me_3Si)_2CH\}P(C_6H_4-2-$ O)(BH ₃)Ca(THF) ₄] (108)	121
5.14	Solution-phase characterisation of 108	122
5.15	Solid-state structure of 108	126
5.16	Conclusions	128
5.17	References	129

Chapter 6. Alkali and alkaline earth metal complexes of a phenyl-functionalised phosphido-borane	134
6.1 Introduction	134
6.2 Synthesis of the alkali metal complexes [{(Me ₃ Si) ₂ CH}P(C ₆ H ₅)(BH ₃)M(L)] [M(L) = Li(THF) (115), Na(12-crown-4) ₂ (116), K(pmdeta) (117)]	135
6.3 Solution-phase characterisation of 115-117	137
6.4 Solid-state structures of 115, 116 and 117	141
6.4.1 Solid-state structure of 115	141
6.4.2 Solid-state structure of 116	145
6.4.3 Solid-state structure of 117	146
6.5 Synthesis of alkaline earth metal complexes [{(Me ₃ Si) ₂ CH}P(C ₆ H ₅)(BH ₃) ₂ M] [M = Sr(119), Ba(120)]	148
6.6 Solution-phase characterisation of 119 and 120	150
6.7 Conclusions	150
6.8 References	151
Chapter 7. Alkali and alkaline earth metal complexes of phosphido-bis(boranes)	153
7.1 Introduction	153
7.2 Synthesis and characterisation of the alkali metal complexes [{(Me ₃ Si) ₂ -CH}P(C ₆ H ₅)(BH ₃) ₂ M(L)] _n [M(L) = Li(12-crown-4), <i>n</i> = 1 (123), M(L) = Na(THF) ₂ , <i>n</i> = 2 (124), M(L) = K(THF) ₂ , <i>n</i> = ∞ (125)]	154

7.3	Synthesis and characterisation of the alkali metal complex [{(Me ₃ Si) ₂ CH}P(C ₆ H ₄ -2-OMe)(BH ₃) ₂][Na(12-crown-4) ₂] (126)	156
7.4	Solid-state structures of 123-126	157
7.4.1	Solid-state structure of 123	157
7.4.2	Solid-state structure of 124	159
7.4.3	Solid state structure of 125	160
7.4.4	Solid-state structure of 126	163
7.5	Synthesis and characterisation of the alkaline earth metal complexes [{(Me ₃ Si) ₂ CH}P(C ₆ H ₅)(BH ₃) ₂ M(THF) ₄] [M = Mg (128), Ca (129), Sr (130)]	164
7.6	Solid-state structures of compounds 128-130	166
7.7	Conclusions	174
7.8	References	174
Chapter 8. Conclusions		176
8.1	Effects of varying the peripheral donor on group I complexes of phosphido-boranes	176
8.2	Comparisons between group I complexes of the ligands [{(Me ₃ Si) ₂ CH}P(C ₆ H ₅)BH ₃] ⁻ and [{(Me ₃ Si) ₂ CH}P(C ₆ H ₅)(BH ₃) ₂] ⁻	184
8.3	Summary	185

Chapter 9. Experimental	186
9.1 General procedure	186
9.2 NMR spectroscopy and elemental analysis	186
9.3 Crystal structure determination	187
9.4 Preparative methods	187
9.5 References	207
Appendix 1:	208
Appendix 2: X-ray crystallographic data [enclosed CD]	211

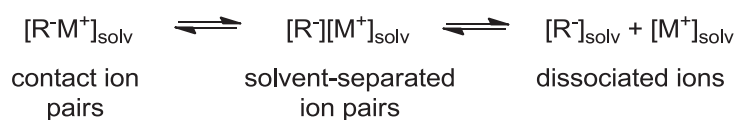
Chapter 1. Introduction

1.1 Alkali metal organometallics

The first examples of alkali metal organometallic reagents were organolithiums, reported by the pioneer Wilhelm Schlenk in 1914.^{1,2} Since then the numbers of alkali metal organometallics have vastly increased, as have their uses in chemical synthesis as either nucleophilic or basic reagents.^{3,4,5} However, our understanding of the chemistry that governs these compounds has not developed to the same extent. To gain an insight into the mechanistic behaviour of these reagents, it is crucial to know their molecular structures, i.e. the precise location of the atoms, and the level of solvation and aggregation.^{6,7} To this end, advances in X-ray crystallography over the past 30 years, alongside developments in *ab initio* calculations and analytical techniques such as NMR spectroscopy, have resulted in the full characterisation of a large number of organometallic complexes. Nevertheless, despite these advances, organometallic compounds of the heavier alkali metals (sodium, potassium, rubidium and caesium) have been less extensively investigated in comparison to lithium complexes due, at least in part, to the increased difficulty in handling these compounds.

In addition, much less attention has been paid to complexes of the alkali metals with organophosphorus ligands, although the factors that govern their structures and aggregation states are parallel to those observed in organometallics. This section will briefly discuss these factors, and highlight the trends that have been observed.

The behaviour of alkali metal organometallics in solution is very important in rationalising the reactivity of these compounds. Although it was previously assumed that the anionic ligand and cationic metal dissociate in solution, it is now accepted that the ligand is stabilised by the cation and contact ion pairs are often formed. The ion pairing can be divided into two categories: tight contact ion pairs with one solvent shell around the RM unit ($R = R_3C$, $M =$ alkali metal cation) and solvent separated ion pairs, in which the R^- and M^+ ions each become solvated and are shielded from each other (Scheme 1.1).⁵



Scheme 1.1. Solvated forms of an organometallic complex.

The structure and aggregation state of RM is most strongly dependent on the charge-to-size ratio of the metal cation M^+ . As the ionic radius of the alkali metals increases down the group, the charge to size ratio decreases, which affects electronic factors such as lattice energy and electronegativity, as shown in Table 1.1. The size of the cation has a significant effect on the coordination numbers; for example, complexes of lithium, the smallest alkali metal, typically favour a four-coordinated structure, whereas the larger potassium, rubidium and caesium cations can have coordination numbers of up to ten. Consequently complexes of the heavier alkali metals are more likely to undergo extensive aggregation, often leading to insoluble polymers that are difficult to crystallise or to characterise in solution.

	Ionic radius * ⁸ (Å)	Lattice energy (kJmol ⁻¹) $M^+(g) + Cl^-(g) \rightarrow MCl$	Pauling Electronegativity ⁹
Li	0.76	-834	0.98
Na	1.02	-769	0.93
K	1.38	-701	0.82
Rb	1.52	-680	0.82
Cs	1.67	-657	0.79

Table 1.1. Selected physical and electronic properties of the alkali metals (* for coord. no. 6).

The extent of aggregation also depends on the steric requirements of the organic ligand, with more bulky/branched substituents leading to lower aggregation states; e.g. ⁿBuLi is hexameric in cyclohexane and benzene, whereas the more branched ^tBuLi is tetrameric in the same solvents. Sterically demanding ligands such as mesityl (2,4,6-trimethylphenyl) and (Me₃Si)₂CH can counteract the aggregation effects associated with complexes of the larger alkali metals, by blocking the vacant coordination sites. Preventing formation of larger lattices increases the solubility of these complexes, thus allowing characterisation.

The presence of coordinating solvents such as THF and Et₂O, and other chelating donors such as pmdeta and tmeda usually results in lower aggregation states, as they can also occupy

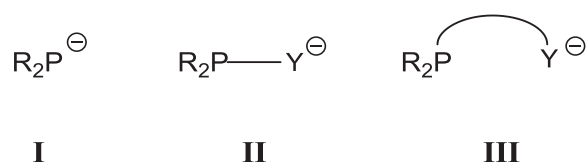
the vacant metal coordination sites [pmdeta = *N,N,N',N'',N'''*-pentamethyldiethylenetriamine; tmeda = *N,N,N',N''*-tetramethylethylenediamine].

In summary, the structures and reactivities of alkali metal organometallic reagents are a compromise between several factors including cation size, the steric requirements of the ligand and the presence of coligands. Aggregation is often observed in these complexes, with dimers trimers and ladder structures often observed. The degree of aggregation can be greatly reduced by occupying/blocking the vacant coordination sites of the alkali metal, which becomes more challenging with the larger alkali metals.

1.2 Phosphides

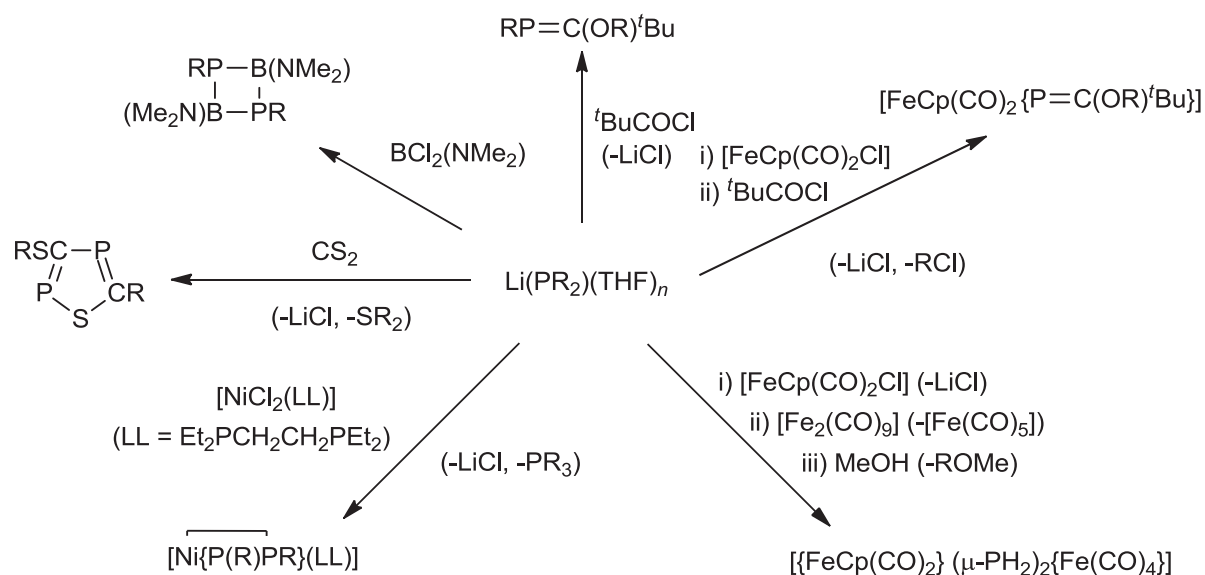
The interactions between alkali metal cations and P-donor ligands are expected to be weak and highly disfavoured due to Pearson's hard-soft acid-base principle.¹⁰ Indeed, theoretical calculations suggest that the bonding affinities in complexes between a soft phosphorus-based ligand and a hard alkali metal cation are much lower than those for the corresponding nitrogen-based complexes; the binding energies for the reaction $M^+ + PH_3 \rightarrow [M-PH_3]$ are calculated to be -26.7 and -17.4 kcal mol⁻¹ for Li⁺ and Na⁺, respectively, compared to those of Li⁺ NH₃ and Na⁺ NH₃, which are calculated to be -40.2 and -28.0 kcal mol⁻¹, respectively.^{11,12}

The low affinity of the alkali metal cation for phosphorus may be overcome by incorporating the P-donor site in an anionic ligand. Such ligands can be organised into three classes: ligands where the charge is localised on the phosphorus atom, i.e. phosphides (**I**), ligands where there is charge delocalisation towards phosphorus from an adjacent atom (**II**), or ligands where the negative charge is localised on an atom distant from the phosphorus (**III**).



The simplest complexes of the alkali metals with P-donor ligands are those of the type R_2P^- (**I**). The factors that affect the structures adopted by these complexes are parallel to those observed in organometallic compounds as discussed in 1.1.

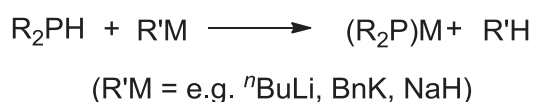
Due to the importance of alkali metal phosphide species as R_2P^- transfer reagents and nucleophiles in organic synthesis (examples of synthetic uses are shown in Scheme 1.2), interest in their solid-state structures has been growing considerably since the 1980s. However, the number of reports detailing the structures of alkali metal phosphides is still significantly less compared to their alkyl and amido counterparts.



Scheme 1.2. Some examples of $Li(PR_2)$ reactions.

1.2.1 Alkali metal phosphides

The synthesis of alkali metal organophosphides is usually achieved *via* the direct metalation of a primary or secondary phosphine with a strong base.

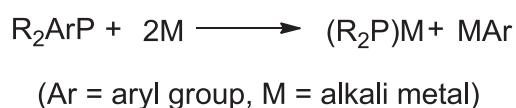


Whilst this is the most widely used method to synthesise these species, alternative routes to alkali metal phosphide complexes include:

i) Direct metalation of a phosphine with a heavier alkali metal.^{13,14}

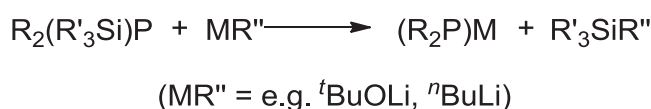


ii) P-C cleavage of an aryl-substituted tertiary phosphine with an alkali metal in a donor solvent e.g. THF, dioxane, or liquid ammonia.^{15,16,17}

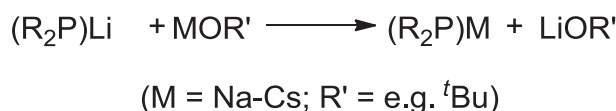


The side product MAr can be removed with a proton source e.g. ^tBuCl or NH₄Cl, however the P-C cleavage reactions are not straightforward, and the products depend on the substituents of the aryl group; the presence of electron donating groups (e.g. OMe, NMe₂, SMe etc.) tends to inhibit cleavage,¹⁵ although this depends also on the alkali metal.¹⁷

iii) P-Si cleavage of a tertiary phosphine with an alkali metal alkoxide, or alkali metal alkyl. This route has proved suitable for (Me₃Si)₂PM complexes, avoiding the need for complex synthesis of secondary phosphines.^{18,19,20}



iv) Metathesis between a lithium phosphide and a heavier alkali metal alkoxide.²¹



1.2.1.1 Lithium organophosphides

The first structurally characterised alkali metal phosphide was reported by R.A. Jones and co-workers in 1983.²² The deprotonation of ^tBu₂PH with ⁿBuLi in THF, followed by crystallisation from THF gave rise to the complex [Li₂(^tBu₂P)₂(THF)]₂ (**1**), which adopts a four-rung ladder structural motif, where two of the phosphide groups are triply bridging, and two are doubly bridging the lithium atoms (Figure 1.1). The Li-P distances in **1** range from 2.476(10) Å [Li(2)-P(2)] to 2.669(9) Å [Li(1)-P(1)].

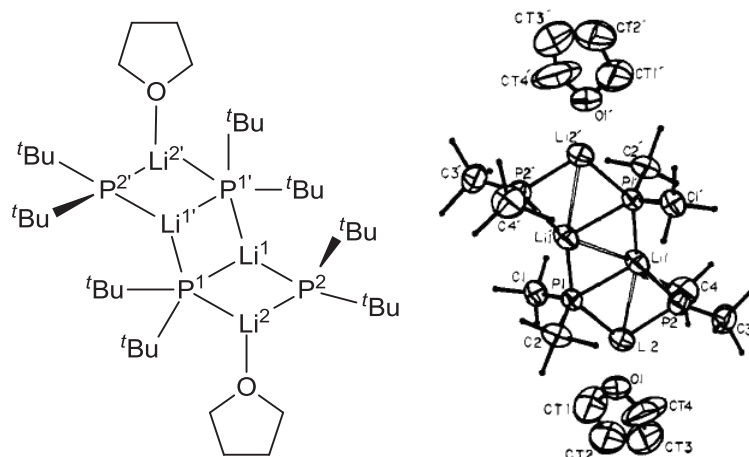


Figure 1.1. Structure of **1**.²²

A report by Steiglitz ten years later demonstrates that the ladder motif of this compound can be broken down by the addition of the bidentate ligand DME.²³ The modified complex $[\text{Li}(\text{tBu}_2\text{P})(\text{DME})]_2$ (**2**) consists of a dimer with a planar Li_2P_2 core (Figure 1.2) [$\text{Li}(1)\text{-P}(1\text{A}) = 2.600(6)$; $\text{Li}(1)\text{-P}(1) = 2.573(5)$ Å, $\text{P-Li-P} = 97.1(2)^\circ$].

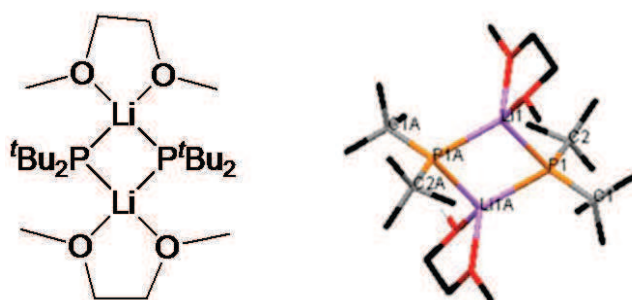


Figure 1.2. Structure of **2**.²³

Lithium diphenylphosphide was first characterised in 1984 as an adduct with 12-crown-4, and crystallises as a solvent separated ion pair.²⁴ Since then it has been characterised in a number of adducts with O- or N-donor ligands: $[\text{Li}(\text{PPh}_2)(\text{OEt}_2)]_\infty$ (**3**) and $[\text{Li}(\text{PPh}_2)(\text{THF})_2]_\infty$ (**4**) both crystallise as a chain of alternating Li^+ and PPh_2^- units, with greater solvation observed in **4** due to the smaller size of THF (Figure 1.3).²⁵

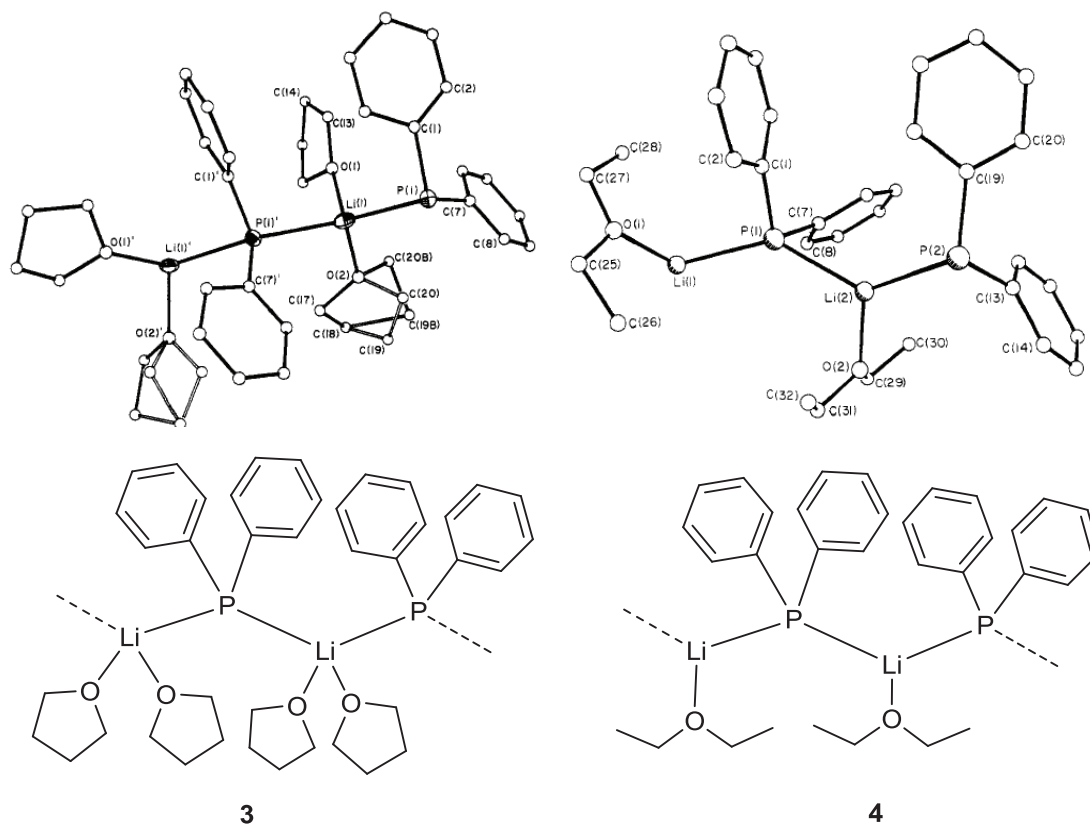


Figure 1.3. Structures of **3** and **4** [disorder in THFs for **3**].²⁵

The Li-P distances correlate well with the coordination number of Li; P-Li = 2.629-2.634 Å for **3** (4 coordinate Li) and 2.483-2.496 Å for **4** (3-coordinate Li). The tmeda adduct $[\text{Li}(\text{PPh}_2)(\text{tmeda})]_2$ adopts a dimeric structure with a planar Li_2P_2 core, whilst the pmdeta adduct $[\text{Li}(\text{PPh}_2)(\text{pmdeta})]$ crystallises as a monomer.

The simplest lithium phosphide LiPH_2 has been isolated as the polymeric adduct $[\text{Li}(\text{PH}_2)(\text{DME})]_\infty$ (**5**, Figure 1.4), which consists of an infinite zig-zag chain of alternating Li and P atoms, with an essentially linear Li-P-Li angle of $176.9(1)^\circ$ and a P-Li-P angle of $117.0(2)^\circ$.^{26,27} The linearity of the Li-P-Li angle is attributed to the low steric demands of the H atoms in the phosphide.

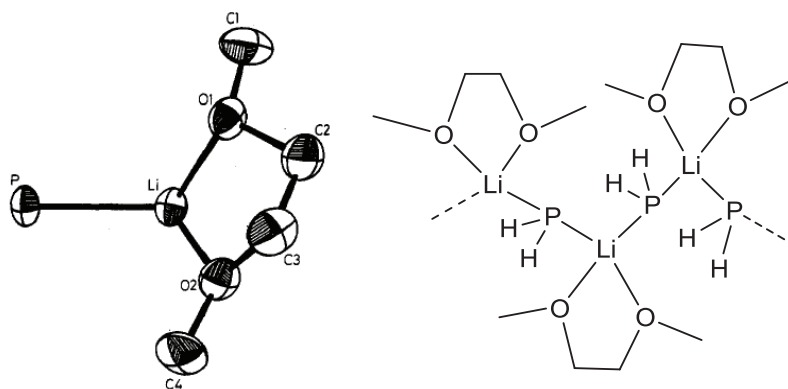


Figure 1.4. A short section of the polymeric structure of **5**.²⁶

Chelating or bridging alkali metal bis-phosphide complexes are useful synthons for the preparation of phosphorus macrocycles. For example, the compound $[1,2\text{-C}_6\text{H}_4(\text{PPh})_2\text{Li}(\text{tmeda})]_2$ (**6**, Figure 1.5) crystallises as a monomer, where each lithium ion is bound equivalently to the two phosphorus atoms. The coordination about each lithium ion is completed by a molecule of tmeda.²⁸

More recently, Power and co-workers were able to structurally characterise the novel phosphide $[\{\text{C}_6\text{H}_3\text{-}2,6(\text{C}_6\text{H}_2\text{-}2,4,6\text{-iPr}_3)\}\text{PhPLi}(\text{THF})_2]$ (**7**, Figure 1.6). The P–C(ipso) bond lengths in **7** were 1.836(2) and 1.830(3) Å for the terphenyl and phenyl linkages, respectively, with a Li–P contact of 2.478(4) Å, which suggests that this is a reasonably strong interaction. The large, bulky terphenyl groups are able to sterically protect the phosphorus, thus reducing the tendency to form P-bridging oligomers.²⁹

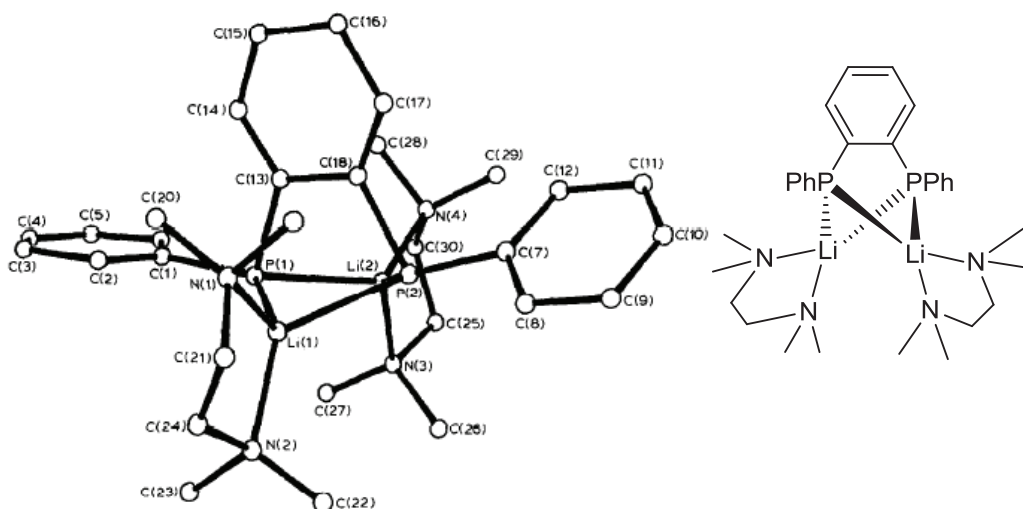


Figure 1.5. Structure of compound **6**.²⁸

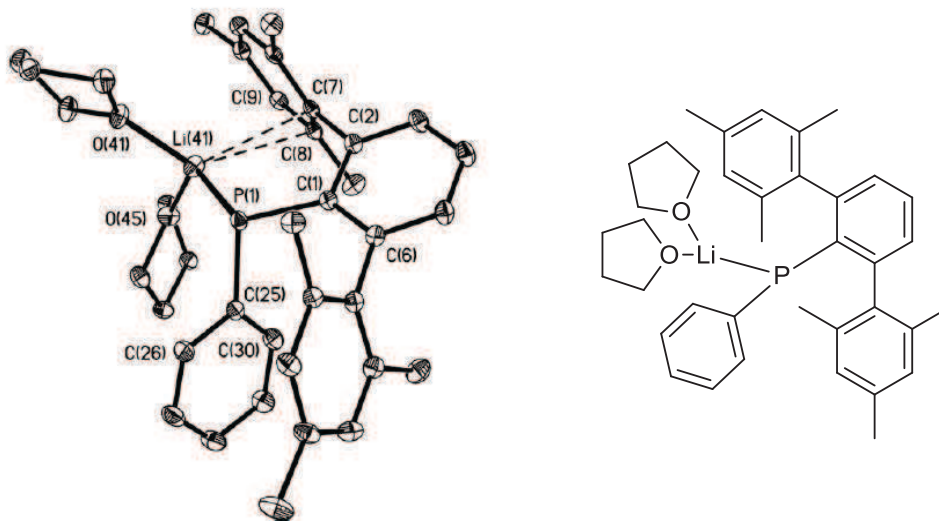


Figure 1.6. Structure of compound **7**.²⁹

A number of lithium phosphide complexes containing organosilicon substituents have also been synthesised and structurally characterised. Treatment of the secondary phosphine $(\text{Me}_3\text{Si})_2\text{PH}$ with ${}^n\text{BuLi}$ in cyclopentane yields the solvent-free, hexameric complex $[(\text{Me}_3\text{Si})_2\text{PLi}]_6$ (**8**, Figure 1.7).³⁰ The hexamer adopts a six-rung ladder motif in the solid state. This is in contrast to earlier reports of the solvated form of this compound when synthesised *via* the tertiary phosphine $\text{P}(\text{SiMe}_3)_3$, which forms a tetrameric ladder $[(\{\text{Me}_3\text{Si}\}_2\text{P})_2\text{Li}_2(\text{THF})]_2$ (Figure 1.8).²⁰ The formation of an extended ladder in **8** is inhibited by the steric demands of the SiMe_3 groups, which occlude the free coordination site on $\text{Li}(3)$.

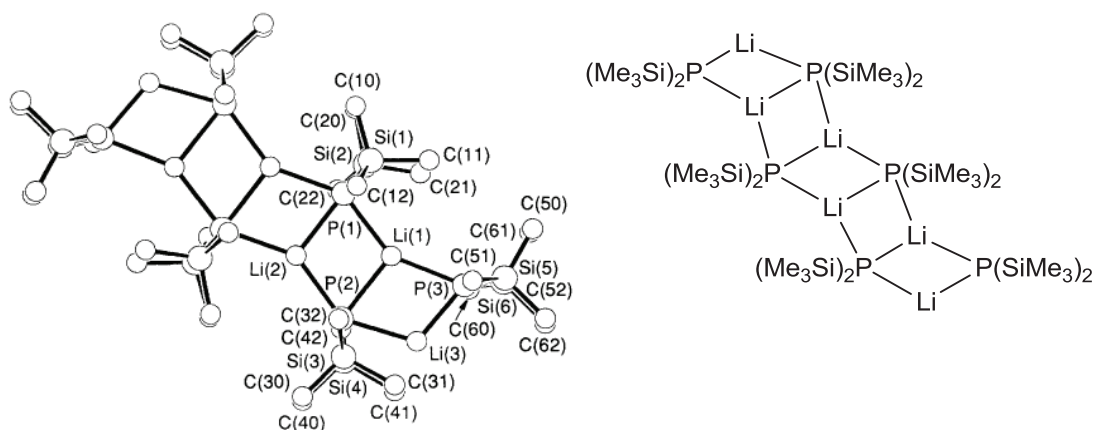


Figure 1.7. Structure of compound **8**.³⁰

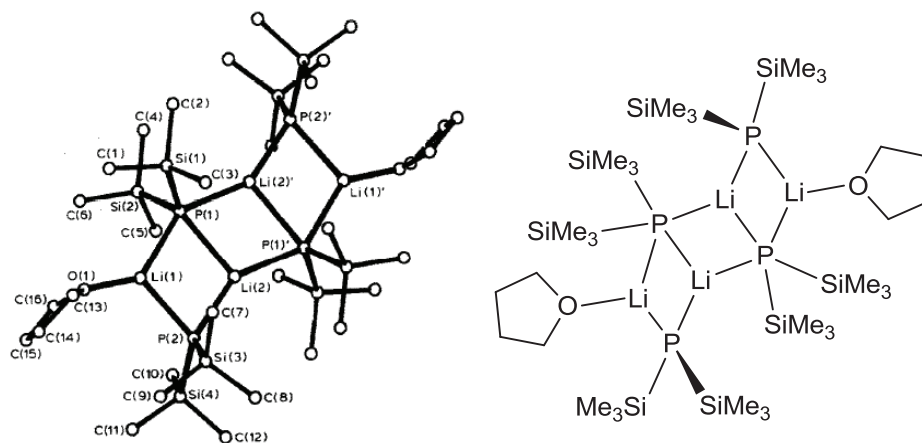


Figure 1.8. Structure of solvated **8**.²⁰

Examples of silicon-containing phosphides that adopt a dimeric or tetrameric structure are the compounds $[\{(\text{Ph}_3\text{Si})_2\text{P}\}\text{Li}]_2$ (**9**) and $[\{\text{P}(\text{Si}^i\text{Pr}_3)\}\{\text{P}(\text{Si}^i\text{Pr}_3)_2\}_3\text{Li}_4]$ (**10**, Figure 1.9).³¹ The large steric requirements of the SiPh_3 substituent in **9** prevent oligomerisation beyond a dimer and allow the isolation of a solvent-free complex. In addition to the P-Li contacts in the dimer, there are further contacts between the lithium and the phenyl rings: one phenyl ring from one $\text{P}(\text{SiPh}_3)_2$ ligand binds in a η^2 - fashion, whilst one ring from the other ligand binds in a η^1 - fashion to the metal. Compound **10** arises from deprotonation of $(^i\text{Pr}_3\text{Si})_2\text{PH}$ with $n\text{-BuLi}$. Formation of an additional $(^i\text{Pr}_3\text{Si})\text{PH}$ subunit is attributed to a Si-P cleavage that occurs on treatment with $n\text{-BuLi}$.

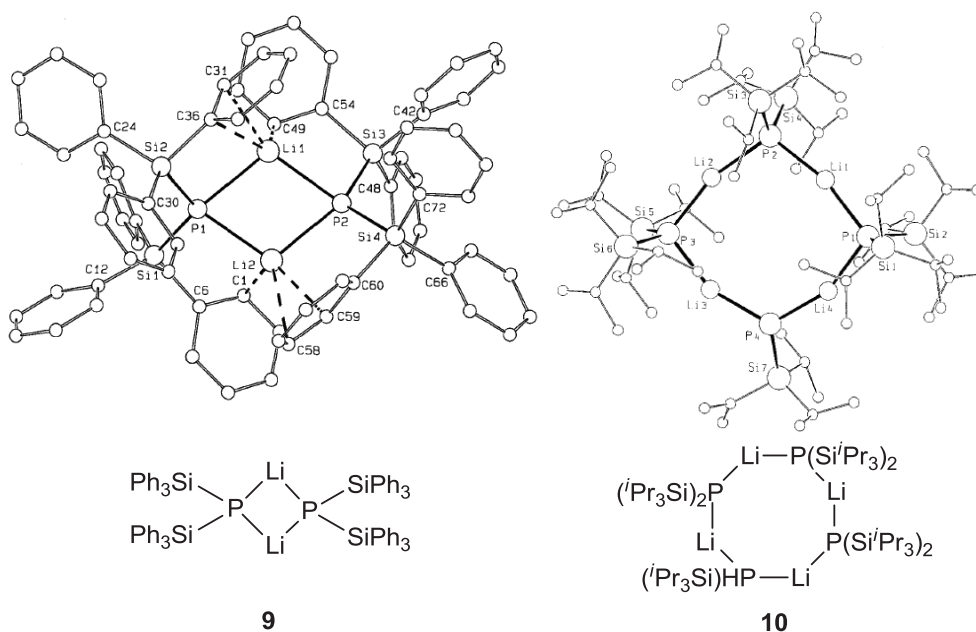


Figure 1.9. Structures of compounds **9** and **10**.³¹

1.2.1.2 Heavier alkali metal phosphides

Heavier alkali metal phosphides are important due to their enhanced reactivity over their lithium counterparts, and also with respect to the diversity of their solid state-structures. However, there are relatively few examples of heavier alkali metal phosphides, due to the larger size/charge ratios of the metals compared to lithium, leading to insoluble polymers that are difficult to crystallise and to characterise in solution. This can be counteracted by the use of sterically demanding substituents and/or the use of polydentate coligands (e.g. pmdeta, tmeda) to block or occupy vacant coordination sites.

The first heavier alkali metal phosphides to be structurally characterised were the sodium and potassium complexes $[(\text{mes})\{\text{F}^t\text{Bu}_2\text{Si}\}\text{P}]\text{M}(\text{THF})_2)_2$ [$\text{M} = \text{Na}$ (**11**), K (**12**); mes = mesityl].³² Compounds **11** and **12** adopt an 8-membered ring motif, where the metal cation is coordinated by a phosphorus atom from one ligand and a fluorine atom from the neighbouring ligand. The M-P and M-F bond distances are 2.890(1) and 2.383(2) Å, respectively, for **11**, and 3.230(1) and 2.643(1) Å, respectively, for **12**.

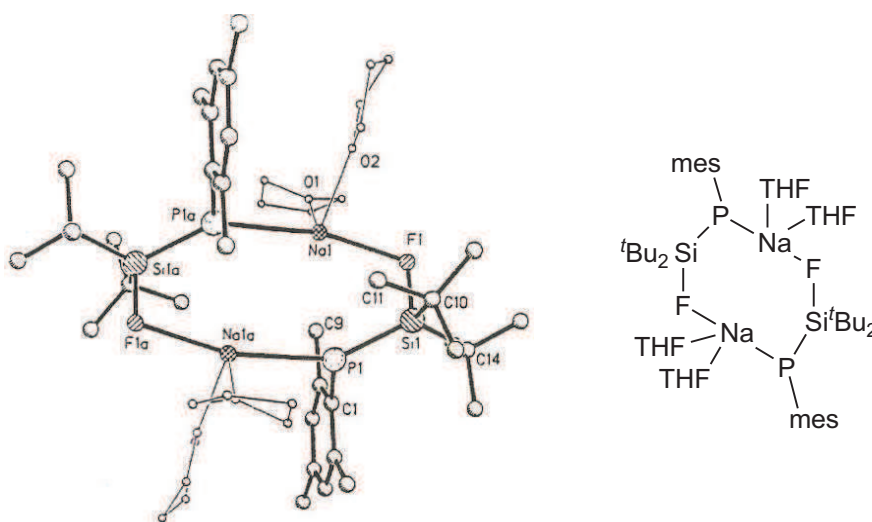


Figure 1.10. Structure of **11**.³²

The first simple sodium phosphide was reported by Raston and co-workers in 1995.³³ $[(\text{C}_6\text{H}_{11})\text{PHNa}(\text{pmdeta})_2]$ (**13**, Figure 1.11) crystallises as discrete centrosymmetric dimers with a planar central P_2Na_2 ring. The cyclohexyl substituents adopt a transoid position relative to the P_2Na_2 ring with both Na^+ cations achieving a five-coordinate geometry *via*

complexation with the tridentate pmdeta ligand, which prevents aggregation. Within the ring the P-Na distances [P-Na 2.883(8), P'-Na 2.936(7) Å] are comparable to those found in **11**.

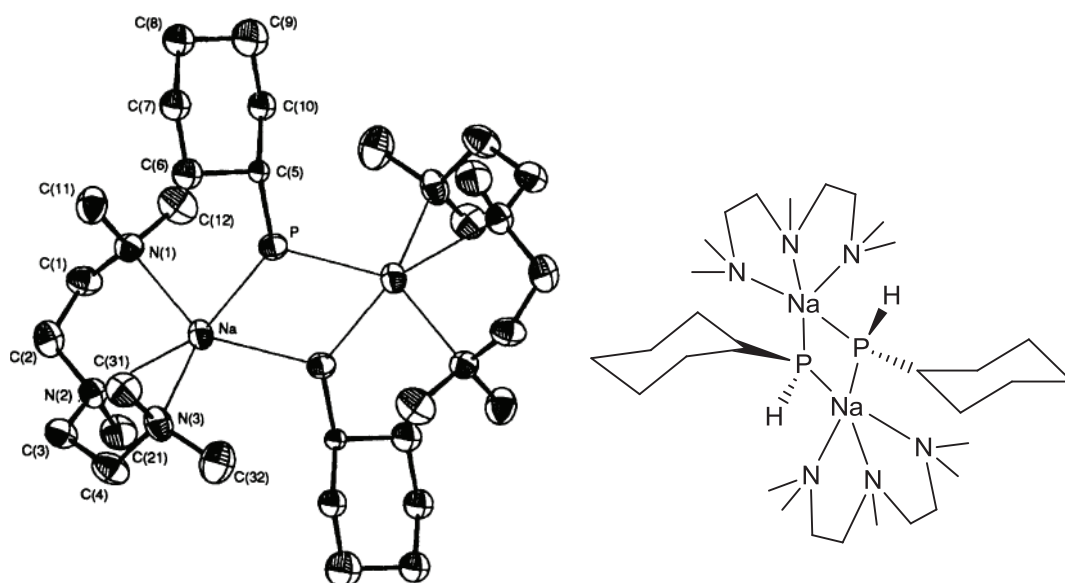


Figure 1.11. Structure of compound **13**.³³

There are several reports of caesium and rubidium phosphide complexes.³⁴⁻³⁶ Rabe and co-workers have isolated several complexes of these heavier alkali metals with mesityl- and supermesitylphosphides.^{34,35} Two such examples are $[\{(\text{mes}^*)\text{PH}\}\text{Cs}(\text{py})]_\infty$ (**14**, mes* = 2,4,6-tri-*t*-butylphenyl, Figure 1.12) and $[\{(\text{dmp})\text{PH}\}\text{Rb}]_4 \cdot (\text{toluene})$ (**15**, dmp = dimesitylphenyl, Figure 1.13). The caesium complex (**14**) crystallises as a ladder polymer in which the squares are alternately bridged and non-bridged by the pyridine ligands. The ladder also exhibits a twist of *ca.* 130° in one direction, followed by an equal twist in the opposite direction. There are several other base adducts of this compound that adopt similar ladder motifs.³⁴

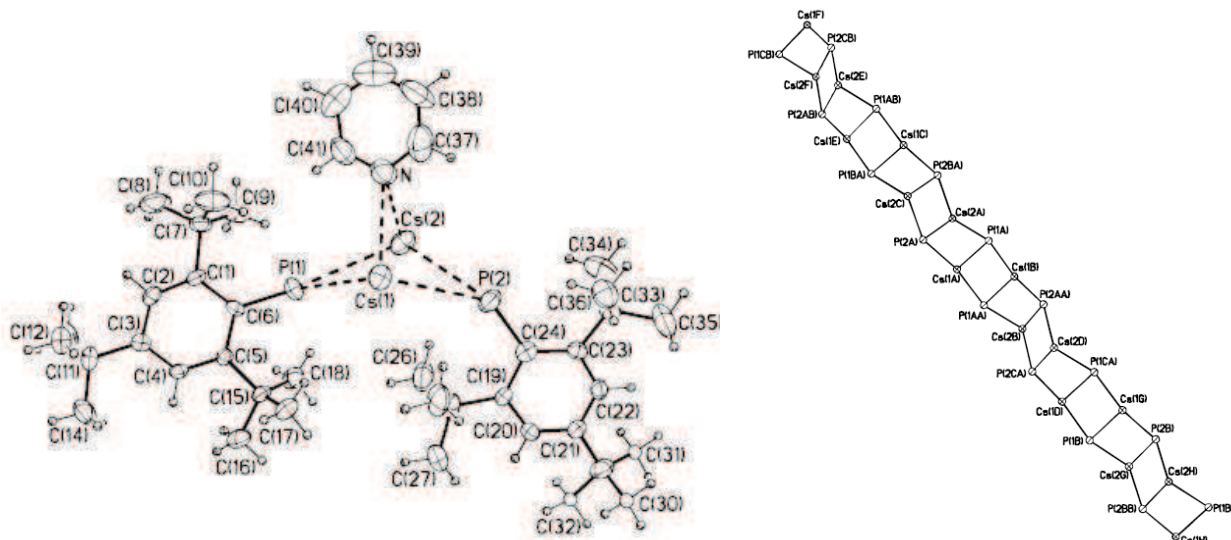


Figure 1.12. Structure of compound **14**.³⁴

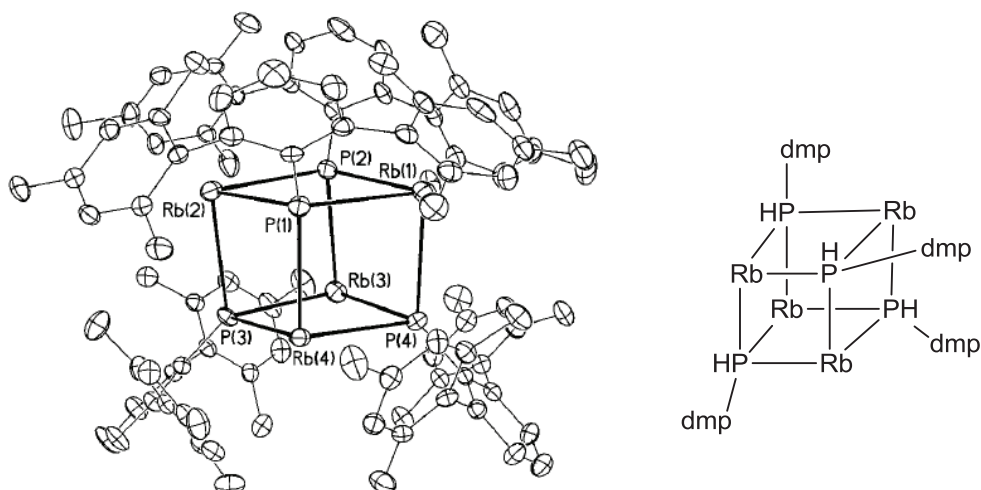


Figure 1.13. Structure of compound **15**.³⁵

Compound **15** crystallises as a tetramer with an unprecedented heterocubane structure, with each Rb atom coordinated by three phosphide ligands, with further coordination by multihapto interactions with two mesityl rings from two different dmp substituents. The NMR spectra of **15** suggest that this structure is retained in solution.³⁵

1.2.1.3 Donor-functionalised phosphides

Since the coordination of additional donor ligands to alkali metal complexes enhances reactivity by reducing the extent of aggregation, there have been several reports that have investigated the effects on aggregation of incorporating additional donor functionality into phosphide ligands.^{21,37-39} The first structurally characterised example was the compound $[\{(C_6H_4-2-OMe)_2P\}Na(diglyme)]_2$ (**16**, Figure 1.14).³⁷

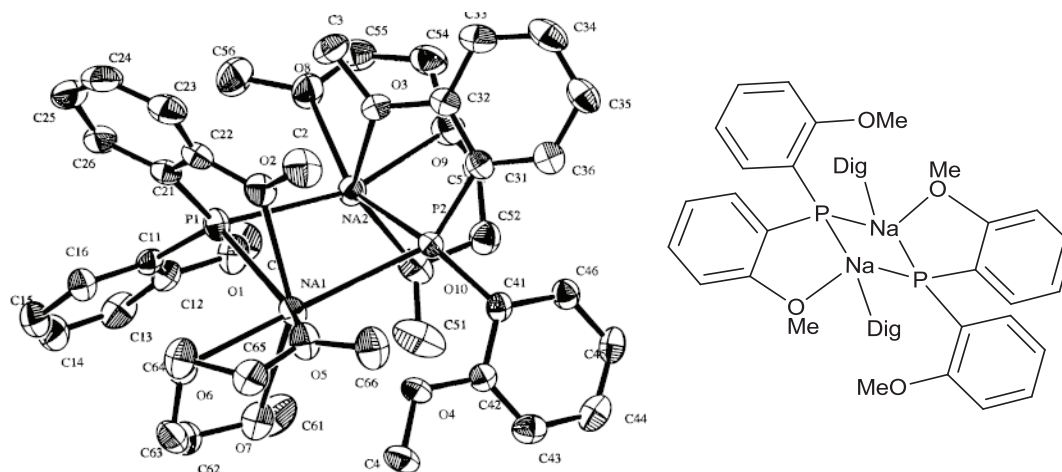


Figure 1.14. Structure of compound **16** [Dig = diglyme (MeO{C₂H₄}O{C₂H₄}OMe)].³⁷

Compound **16** was prepared by cleavage of (C₆H₄-2-OMe)₃P with Na in liquid ammonia/THF, and was crystallised as its diglyme adduct as discrete dimers. Each Na atom is coordinated to the P and one O atom of the phosphide ligand to give a 5-membered chelate ring; the second O atom of the phosphide ligand does not bind to the metal centre. Coordination to the sodium is completed by the P atom of the second phosphide, and three O atoms of a facially coordinated diglyme. Although **16** possess a P₂Na₂ core, this is not planar as in compounds **11** and **13**.^{31,32}

The related amino-functionalised phosphide complexes $[(\{Me_3Si\}_2CH)(C_6H_4-2-CH_2NMe_2)PM(L)]$ [M = Li, L = (THF)₂ (**17**), M = Na, L = tmeda (**18**), M = K, L = (pmdeta) (**19**)] have also been isolated and structurally characterised by Izod and co-workers.²¹ In each case, the phosphide ligand binds *via* its N and P atoms to the metal centres to give a puckered 6-membered chelate ring. However, in compounds **18** and **19**, there is a significant M⋯C contact to the *ipso* carbon directly attached to the P atom. The Na-P and K-P distances of 2.8396(9) and 3.2326(6) Å, respectively, are short compared to other Na-P and K-P distances.

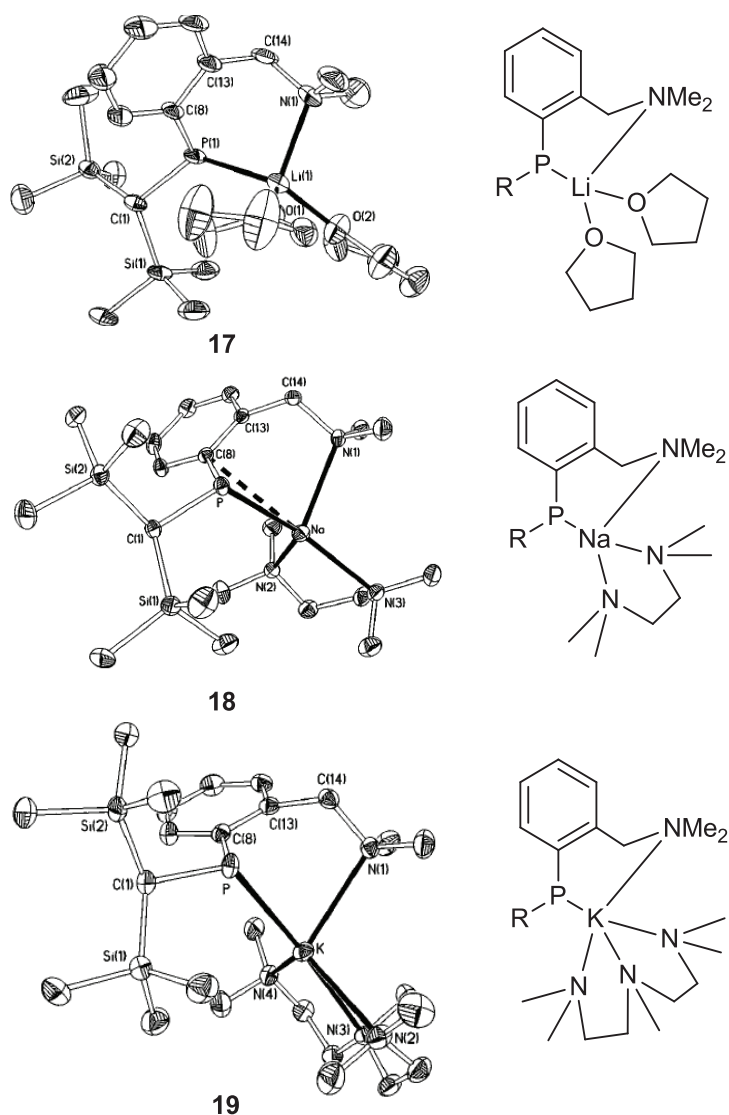
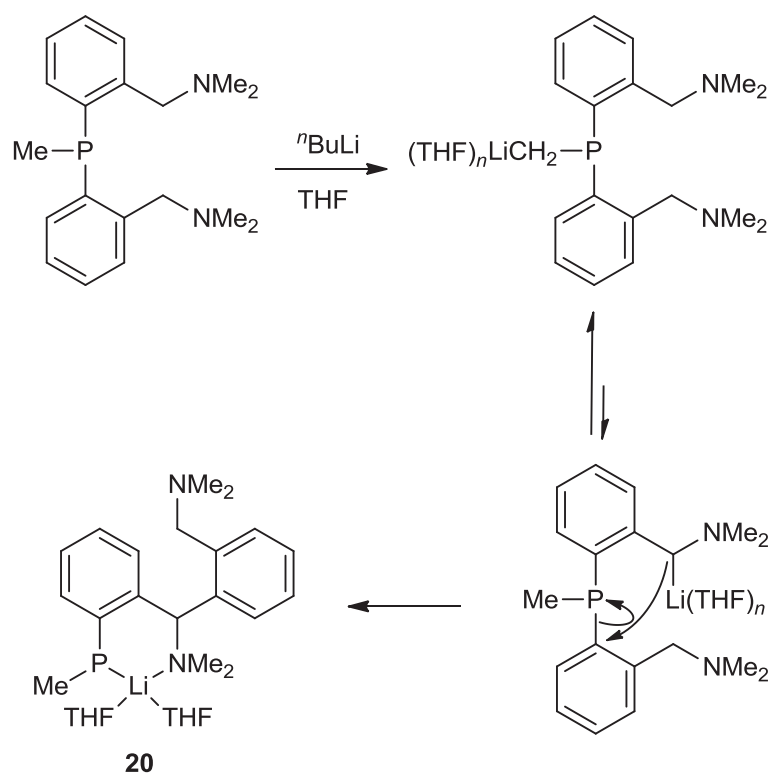


Figure 1.15. Structures of compounds **17**, **18** and **19**.²¹

The same group have also reported examples of amino-functionalised phosphides that have been prepared from the rearrangement of a tertiary phosphine: compounds $[\text{MeP}\{\text{C}_6\text{H}_4\text{-2-CH}(\text{C}_6\text{H}_4\text{-2-CH}_2\text{NMe}_2)\text{NMe}_2\}\text{Li}(\text{THF})_2]$ (**20**) and $[\textit{i}\text{PrP}\{\text{C}_6\text{H}_4\text{-2-CH}(\text{C}_6\text{H}_4\text{-2-CH}_2\text{NMe}_2)\text{NMe}_2\}\text{Li}(\text{THF})_2]$ (**21**).³⁹ Deprotonation of the tertiary phosphine $\text{MeP}(\text{C}_6\text{H}_4\text{-2-CH}_2\text{NMe}_2)_2$ with ${}^n\text{BuLi}$ in a solution of THF yields compound **20** exclusively. Similarly, treatment of a THF solution of the related tertiary phosphine $\textit{i}\text{PrP}(\text{C}_6\text{H}_4\text{-2-CH}_2\text{NMe}_2)_2$ with ${}^n\text{BuLi}$ yields only compound **21**. These compounds were formed *via* an unusual Smiles rearrangement, which is completely dependent on the presence of a strong donor solvent i.e. THF. The mechanism proposed for the formation of **20** (Scheme 1.3) proceeds *via* a phosphinomethanide intermediate, which is initially formed upon metalation.



Scheme 1.3. Formation of compound **20**.

In both cases the lithium ion is bound by the P and one of the N atoms of the ligands, generating a six-membered chelate ring with a bite angle of $97.39(15)^\circ$ and $95.4(2)^\circ$ for **20** and **21** respectively. These compare to a bite angle of $93.8(3)^\circ$ observed in compound **17**.²¹ The coordination sphere of each lithium ion is completed by two molecules of THF to give a distorted tetrahedral geometry.

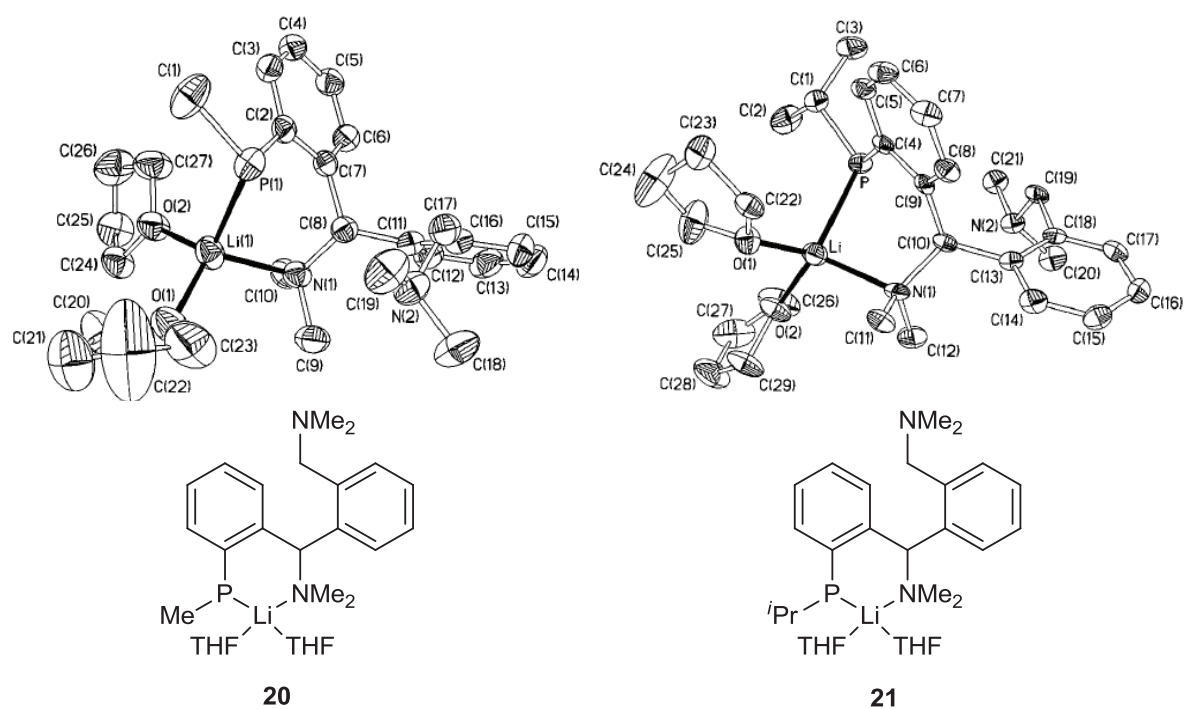


Figure 1.16. Structures of one independent molecule of **20** and **21**.³⁹

1.2.2 Alkaline earth metal phosphides

Complexes of the heavier alkaline earth metals (Ca^{2+} , Sr^{2+} , Ba^{2+}) have been shown to have catalytic activity in the hydrophosphination,⁴⁰ hydroamination^{41,42} and hydrosilylation⁴³ of alkenes and alkynes, and furthermore, have high reactivity that allows the synthesis of a wide range of derivatives.^{44,45} However, they have a tendency to form aggregates or solvates with neutral donor ligands due to their large ionic radii. Thus, the synthesis of phosphide complexes of group II metals requires sterically demanding substituents that can block the vacant coordination sites and prevent oligomerisation. Phosphide complexes with group II metals usually adopt one of four structural types (Figure 1.17) and are attracting much interest due to their high reactivity.⁴⁵⁻⁴⁷

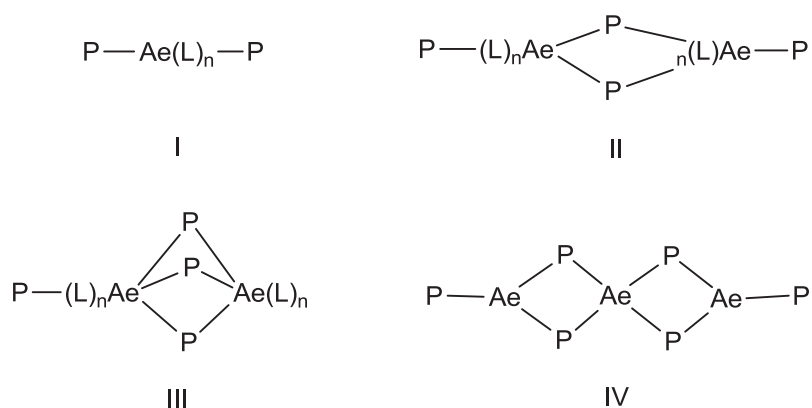


Figure 1.17. Typical structures adopted by group II complexes with phosphide ligands [P = PR₂, Ae = Alkaline Earth metal].

The first example of an alkaline earth metal phosphide to be characterised in the solid-state was reported in 1987 by Raston and co-workers, and has the formula [(PhPH)₂Mg(tmeda)] (**22**, Figure 1.18).⁴⁸

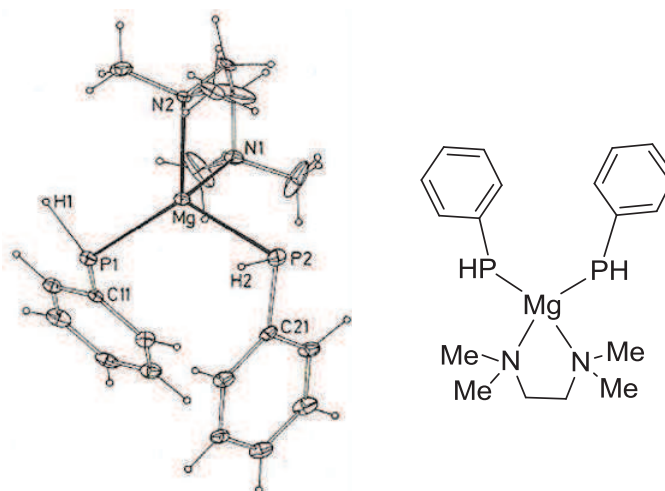


Figure 1.18. Structure of compound **22**.⁴⁸

The first structurally characterised diorganophosphide derivative of beryllium [(η⁵-C₅Me₅)Be(PBu^t₂)] (**23**, Figure 1.19), was reported in 1990.⁴⁹ Compound **23** crystallises as a monomer due to the steric bulk of the C₅Me₅ ligand which is bound to the beryllium in a η⁵-fashion. The Be-P bond length of 2.083(6) Å is much shorter than the Mg-P distance in **22** [2.592(5) Å], which is as expected.⁴⁸ The P-Be-ring centroid angle of 168.3(7)° suggests that there is some steric strain between the ^tBu groups on the phosphorus atom and the methyl substituents of the C₅Me₅ ligand. Notably, the Be-ring centroid distance [1.48(1) Å] is much shorter than that found in (C₅H₅)BeMe [1.907(5) Å].⁴⁹

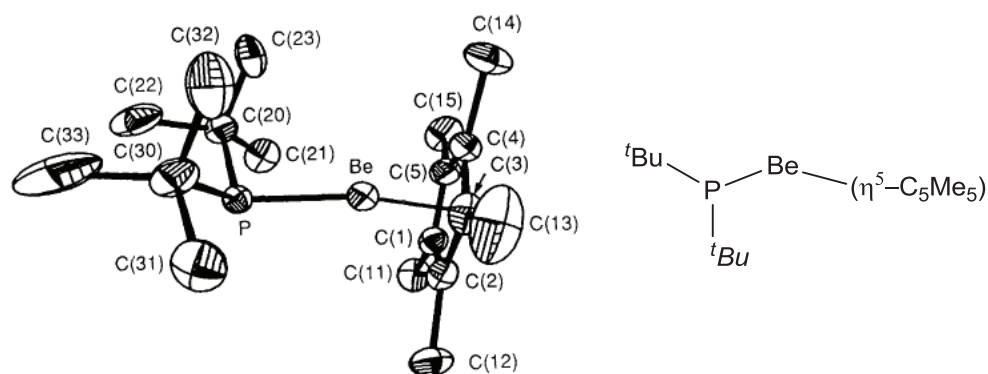


Figure 1.19. Structure of compound **23**.⁴⁹

The first strontium phosphide to be structurally characterised was the compound $[(\{\text{Me}_3\text{Si}\}_2\text{P})_2\text{Sr}(\text{THF})_4] \cdot \frac{1}{2}\text{THF}$ (**24**, Figure 1.20), reported by Westerhausen and co-workers.⁵⁰ The phosphide ligands adopt *trans* positions and are planar, and the normals of the Si_2P planes are nearly perpendicular to each other. Heating compound **24** in a vacuum yields $[\text{Sr}_2(\text{P}\{\text{SiMe}_3\}_2)_4(\text{THF})_3] \cdot \text{toluene}$ (**24a**), with three bridging and one terminal phosphide ligands.⁵⁰

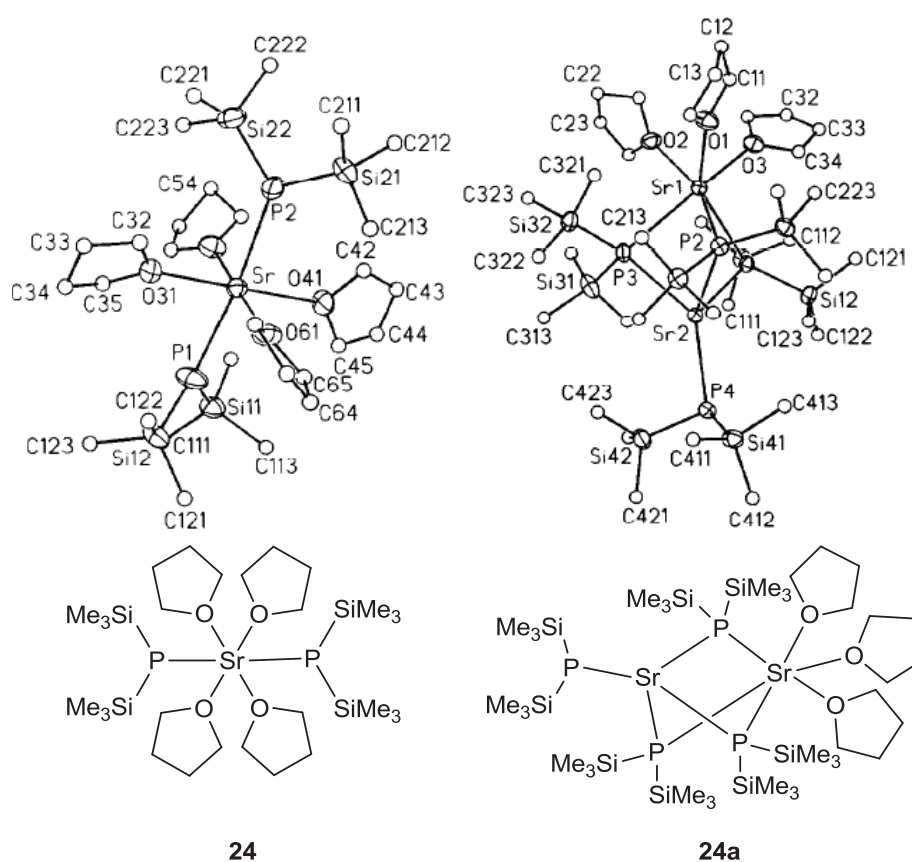
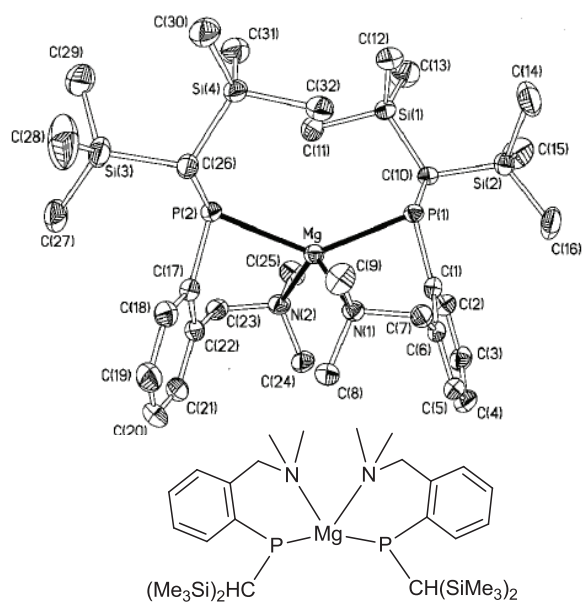


Figure 1.20. Structures of compounds **24** and **24a**.⁵⁰

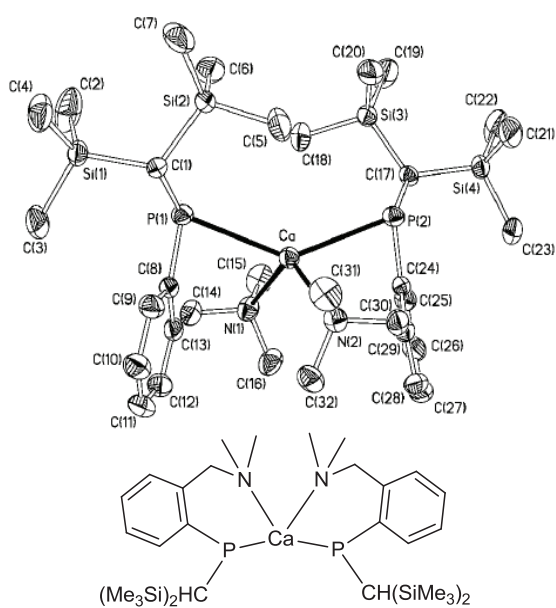
In 2002 Izod reported a series of alkaline earth metal complexes with the phosphide ligand $[\{(Me_3Si)_2CH\}P(C_6H_4-2-CH_2NMe_2)]^{-51}$. Compounds $[\{(Me_3Si)_2CH\}P(C_6H_4-2-CH_2NMe_2)]_2Mg$ (**25**) and $[\{(Me_3Si)_2CH\}P(C_6H_4-2-CH_2NMe_2)]_2Ca$ (**26**) are monomeric in the solid state with a four-coordinate metal centre, which adopts a distorted tetrahedral geometry. Two phosphide ligands are bound to each metal centre through their P and N atoms, forming two puckered 6-membered rings, with larger bite angles observed for **25** [$90.89(6)^\circ$] compared to **26** [$84.27(4)^\circ$] which is to be expected, due to the larger ionic radius of Ca^{2+} compared to Mg^{2+} (1.00 and 0.72 Å, respectively, for a 6-coordinate centre). The remaining angles about the metal centres are very similar for **25** and **26**, illustrating a high degree of flexibility of the phosphide ligands. The Mg-P distance of 2.556(1) Å is similar to Mg-P distances in other magnesium phosphides,^{47,48,52} which is unexpected due to the steric congestion about the Mg centre. In contrast, the Ca-P distances of 2.824(1) and 2.826(1) Å are the shortest of such distances to be reported.

The related compounds $[[\{(Me_3Si)_2CH\}P(C_6H_4-2-CH_2NMe_2)]_2Sr(THF)]$ (**27**) and $[[\{(Me_3Si)_2CH\}P(C_6H_4-2-CH_2NMe_2)]_2Ba(THF)]$ (**28**) crystallise as monomers. Compounds **27** and **28** are isostructural, with the metal centres adopting a five-coordinate, distorted square pyramidal geometry. The ligands bind to the metal centre through their N and P atoms to form the basal plane of the square pyramid, generating two puckered six-membered chelate rings. The coordination spheres of the metals in **27** and **28** are completed by a molecule of THF. A study of the dynamic behaviour of compounds **26**, **27** and **28** in solution showed that an equilibrium is established between their monomeric and dimeric forms, with the monomer favoured at low temperatures.

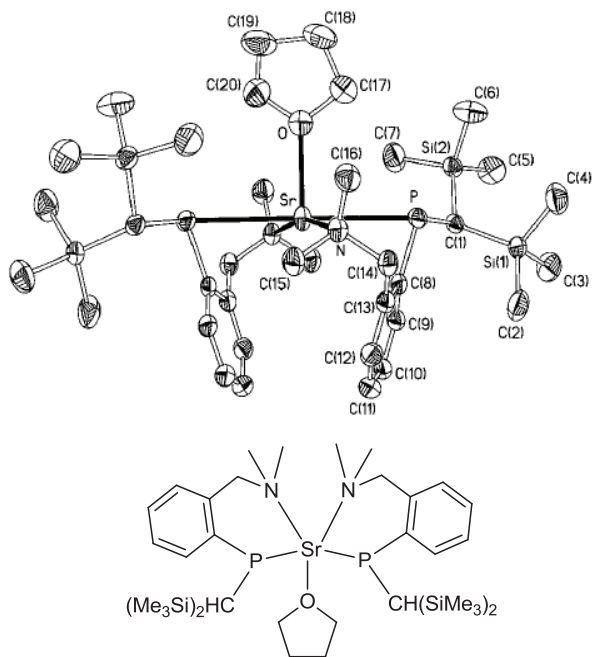
To summarise, complexes of phosphide anions with group I and II metals are a versatile class of compounds that exhibit much structural diversity. However, although there has been strong growth in the number of such complexes that have been isolated in the solid state in the past 30 years, there still remains a dearth of information, particularly with regards to the structures of heavier alkali and alkaline earth metal complexes.



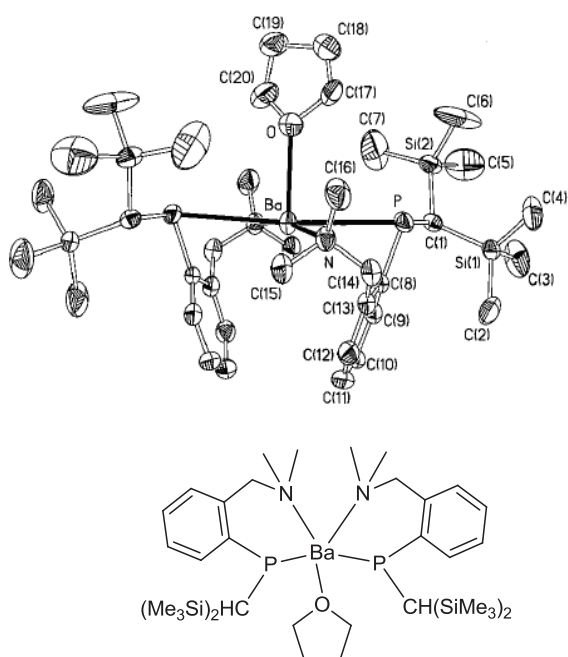
25



26



27



28

Figure 1.21. Structures of compounds 25 to 28.⁵¹

1.3 Phosphine-boranes

1.3.1 Introduction

Phosphine-boranes have several important features that make them interesting synthetic tools, and as such there has been an explosion of their use in organic synthesis over the past 30 years. These features include: a strong P-B bond, which is very stable and protects the phosphorus towards oxidation; reversible adduct formation; and activation of P-H or adjacent C-H bonds towards deprotonation. The air-stable, easy-to-handle properties of phosphine-boranes help overcome the usual problems associated with the handling and storage of air and moisture sensitive trivalent phosphines.

The first example of a phosphine-borane adduct, reported in 1890 by Besson, was the phosphine trichloroborane $\text{H}_3\text{P}\cdot\text{BCl}_3$.⁵³ 50 years later, Gamble and Gilmont continued with detailed investigations of phosphine-boranes, and reported the synthesis of the diborane diphosphine compound $\text{B}_2\text{H}_6\cdot 2\text{PH}_3$, at low temperatures, postulating the formula based on work by Stock on the amine analogue.^{54,55} However it was later found that the data collected was misinterpreted, and in fact the compound was monomeric in nature, and the true formula was the simple phosphine-borane adduct $\text{PH}_3\cdot\text{BH}_3$.⁵⁶

The methodology of the synthesis of alkyl-functionalised secondary phosphine-boranes of the general form $\text{R}_2\text{PH}\cdot\text{BH}_3$ (Figure 1.22) has since been greatly developed, and these species now constitute a unique class of compound with widespread application in synthesis.⁵⁵⁻⁵⁹

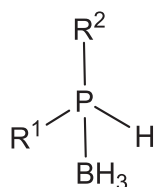


Figure 1.22. A secondary phosphine-borane.

1.3.2 Preparation

Formation of phosphine-borane adducts *via* direct reaction of diborane with a phosphine is now rarely used and instead is usually achieved through direct reaction of a phosphine (primary, secondary or tertiary) with $\text{BH}_3 \cdot \text{THF}$ or $\text{BH}_3 \cdot \text{SMe}_2$, where the weaker Lewis base is displaced by the more strongly donating phosphine, forming a dative covalent bond to the boron (Scheme 1.4).⁶²⁻⁶⁶



Scheme 1.4. Synthesis of a secondary phosphine-borane adduct.

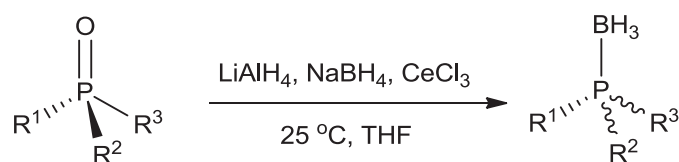
Similarly, phosphine/amine exchange reactions are also a well-established route to phosphine-borane adducts, where treatment of an amine-borane adduct with excess phosphine yields the phosphine-borane and free amine *via* an equilibrium process (Scheme 1.5).⁶⁷ The position of equilibrium in these processes is dependent on the donor abilities of the phosphine and amine and, as such, is defined by the electronic and steric effects of the substituents.



Scheme 1.5. Phosphine-borane and amine-borane equilibrium.

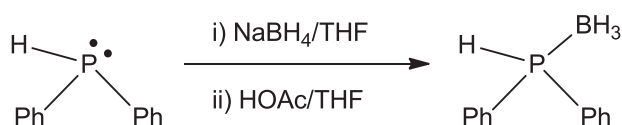
1.3.2.1 Preparation of phosphine-boranes from borohydrides

Alternatively, phosphine-boranes can be synthesised from phosphine oxides in a one pot reaction mixture of LiAlH_4 , NaBH_4 and CeCl_3 (Scheme 1.6).⁶⁸ The reaction does not proceed without CeCl_3 , which is postulated to have a dual role in the mechanism: it activates the phosphine oxide by coordination so that reduction with LiAlH_4 occurs readily,⁶⁹ and it activates NaBH_4 to facilitate the reaction with the intermediate phosphines to form the phosphine-boranes. This method can be used with secondary and tertiary phosphines, however the reduction step of the mechanism is followed by a rapid pseudorotation, leading to racemisation, so is unsuitable for preparing optically active phosphines.⁷⁰



Scheme 1.6. Synthesis of a phosphine-borane from a phosphide oxide.

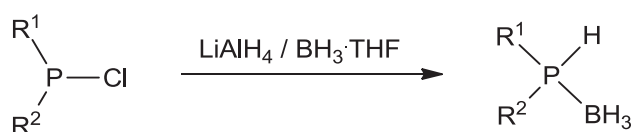
A more novel approach to accessing phosphine-borane adducts from NaBH_4 has been recently developed. A secondary phosphine can be reacted with NaBH_4 alongside a proton source, generating BH_3 *in situ* and generating the phosphine-borane in high yield (Scheme 1.7).⁷¹



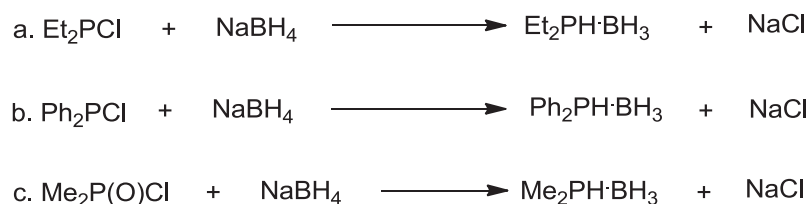
Scheme 1.7. Synthesis of a phosphine-borane *via* sodium borohydride and acetic acid.

1.3.2.2 Preparation of phosphine-boranes from secondary chlorophosphines

Secondary phosphine-boranes can also be prepared from secondary chlorophosphines in a one pot reaction, by treatment with LiAlH_4 and $\text{BH}_3\cdot\text{THF}$ (Scheme 1.8)⁷⁰ or with NaBH_4 (Scheme 1.9).^{72,73}



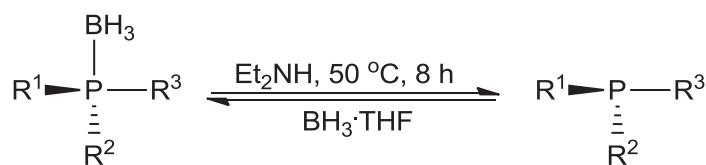
Scheme 1.8. Preparation of a secondary phosphine-borane from a chlorophosphine.



Scheme 1.9. Preparation of secondary phosphine-boranes from a chlorophosphine and NaBH_4 .

1.3.3 Decomplexation of phosphine-boranes

In section 1.3.1 it was mentioned that in the formation of phosphine-borane adducts, borane acts as a protecting group, thus allowing alternative chemistry to be performed; due to the relative ease in which phosphorus can be oxidised, the use of a protecting group means that selective oxidation can occur elsewhere in the molecule. Another important feature is that the formation of the adduct is reversible. Although a P-B bond is generally more stable than an N-B bond, the equilibrium that exists between phosphine/amine-borane adducts (as shown in Scheme 1.5) can be driven so that the borane group can migrate from phosphorus to nitrogen. This was first reported by Imamoto,^{68,70} who treated phosphine-boranes with a large excess of either diethylamine or morpholine to cleave the P-B bond in a variety of phosphine-boranes; this was found to occur with retention of chirality at phosphorus (Scheme 1.10). However, the use of secondary amines is not always suitable for deprotecting phosphine-boranes that contain other functional substituents. This problem was first solved by Le Corre *et al* who decomplexed phosphine-boranes containing carbonyl groups by treatment with dabco (1,4-diazabicyclo[2.2.2]octane) or tmeda.⁷⁴



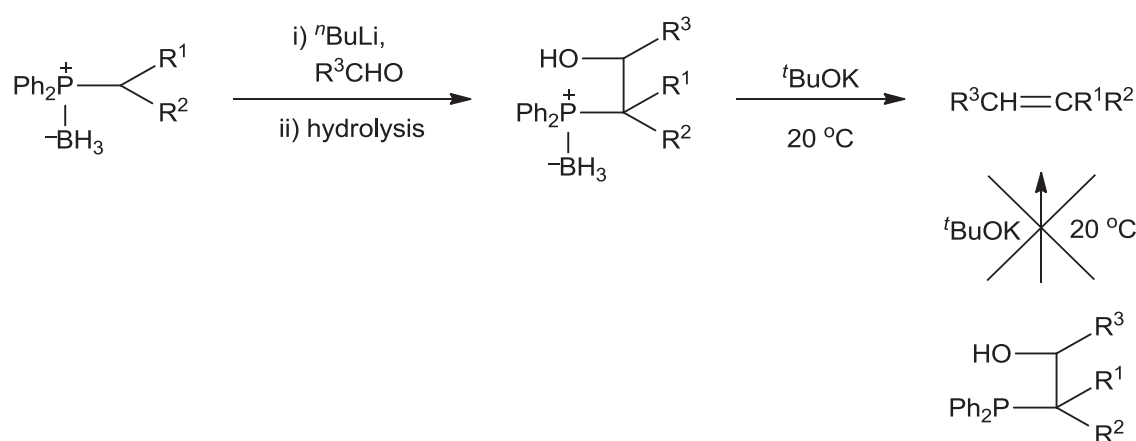
Scheme 1.10. Decomplexation of a phosphine borane with an amine

Decomplexation can also be achieved through the use of acids, such as methanesulfonic acid or trifluoromethanesulfonic acid,^{75,76} HBF_4 ,⁷⁷ or zeolites in combination with alcoholysis.⁷⁸ Mechanistically, the deprotection with acids is more complex.⁷⁹ For deprotection with HBF_4 , it has been shown that the fluoride of the reagent exchanges with the hydride on the borane moiety of the phosphine-borane, thus rendering it more easily attacked by water, leading to hydrolysis.

1.3.4 Reactivity and functionalisation of phosphine-boranes

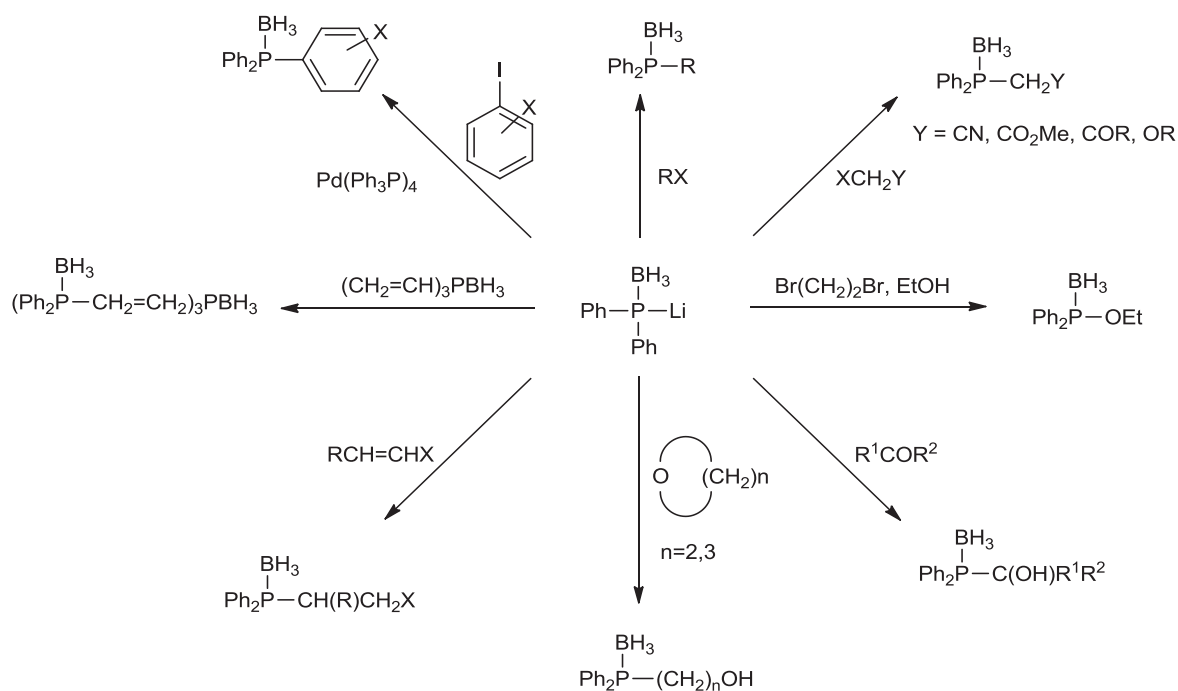
Phosphine-boranes are very versatile reagents, which is, in part, due to their increased reactivity over their phosphine precursors.^{68,80,81} The activation of phosphine-boranes towards deprotonation has been demonstrated by Le Corre and co-workers *via* the olefination of carbonyl compounds (Scheme 1.11); treatment of a hydroxy-functionalised phosphine-borane with ^tBuOK will proceed with elimination of an alkene, whereas the reaction is not observed with free phosphines.⁸²

Due to the wide scope of applications, this section will only focus on the uses of secondary phosphine-boranes in synthesis.



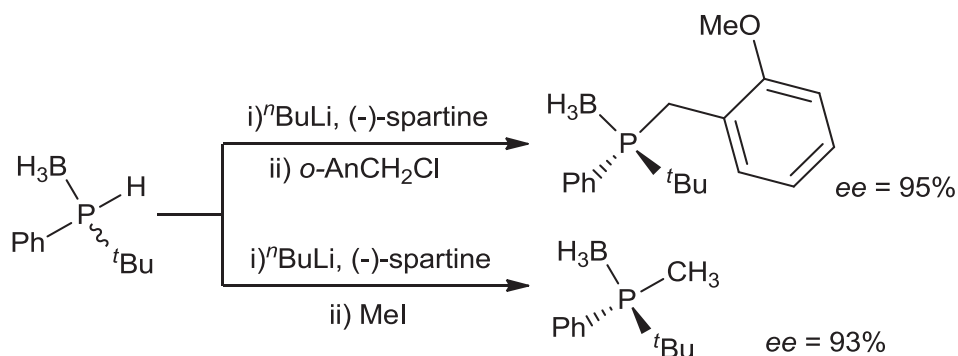
Scheme 1.11. Olefination reaction of phosphine-boranes and carbonyls.

The Imamoto group have investigated the reactions of secondary phosphine-boranes with a range of electrophiles in the presence of a base (e.g. $n\text{BuLi}$, NaH) to provide a variety of functionalised tertiary phosphine-boranes (Scheme 1.12).⁸³ In these reactions, the borane acts as both an activating and protecting group, and can be removed with an excess of amine (see also Scheme 1.10)



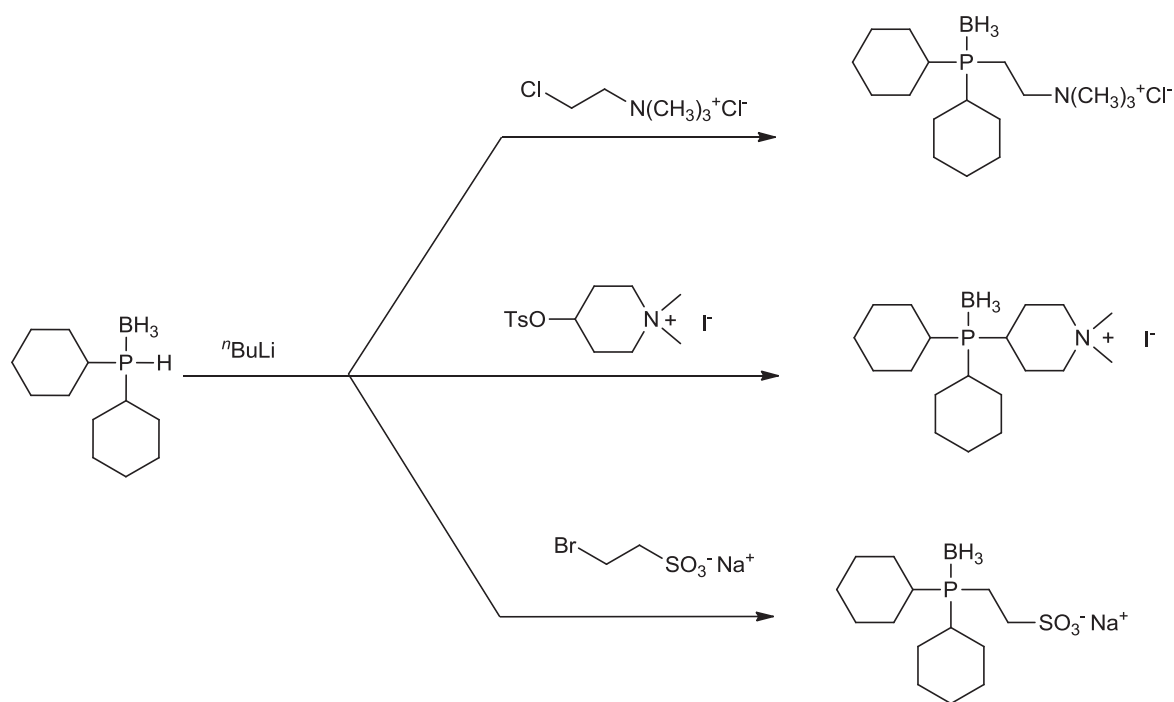
Scheme 1.12. Reaction of lithiated diphenylphosphine-borane with various electrophiles.

Livinghouse and Wolfe have synthesised a series of *P*-chiral phosphine-boranes prepared from a racemic secondary phosphine-borane precursor with excellent enantiocontrol *via* dynamic resolution/alkylation of the corresponding lithium derivative in the presence of (-)-sparteine (Scheme 1.13).⁸⁴ This may be followed by borane deprotection to yield chiral phosphines, which are well established as controller ligands for asymmetric processes.



Scheme 1.13. Synthesis of *P*-chiral phosphine-boranes.

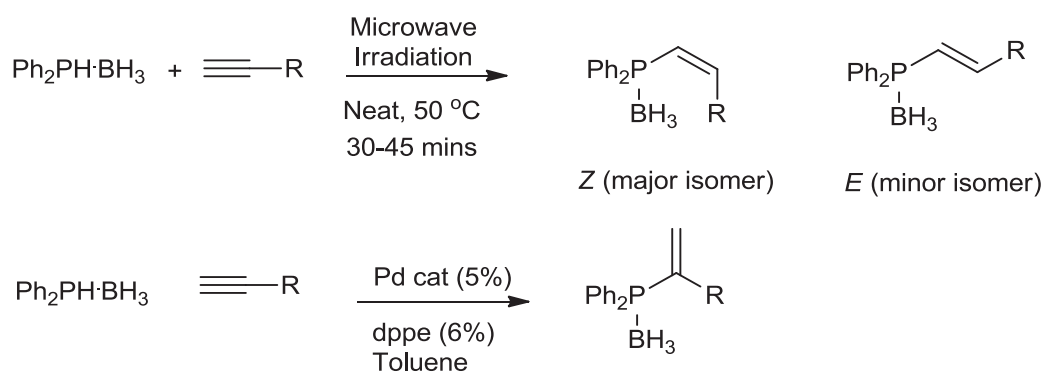
Grubbs and co-workers have synthesised a number of water-soluble aliphatic phosphines *via* secondary phosphine-borane intermediates. This approach was developed to generate phosphine-boranes that can bear ionic functionalities (Scheme 1.14).⁸⁵



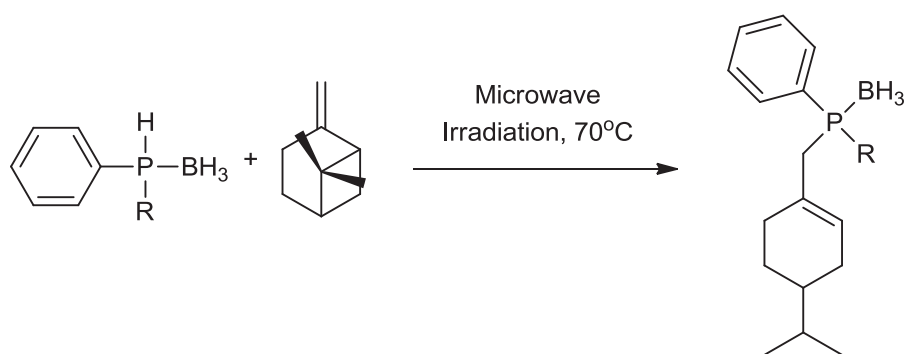
Scheme 1.14. Synthesis of water-soluble phosphine-boranes.

1.3.4.1 Hydrophosphination

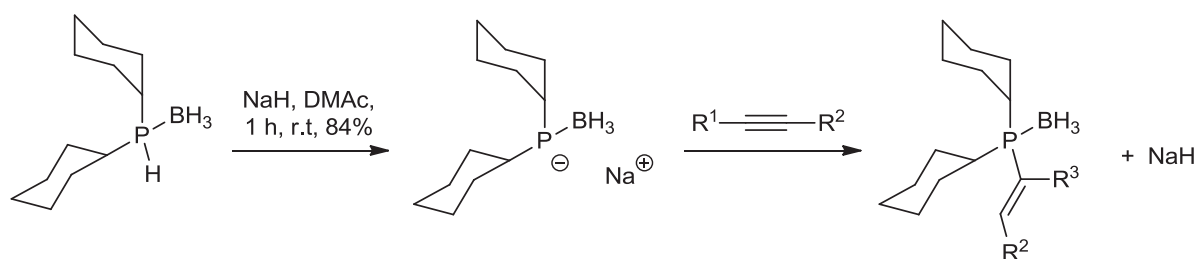
The utilisation of phosphine-boranes as a source of P-H bonds for hydrophosphination reactions has recently attracted much interest^{59,86-91} and was first described by Imamoto and co-workers.⁷⁰ Addition of a P-H bond across an unsymmetrical, unsaturated carbon – carbon bond can lead to two different isomers *via* Markovnikov (α -addition) or anti-Markovnikov (β -addition) addition, and is very challenging to control regioselectivity. However a number of hydrophosphination reactions of alkynes with phosphine-boranes have since been reported with improved yields and regio- and stereoselectivities. For example, it was observed that under thermal conditions, a mixture of alkyne and phosphine-borane yields only the anti-Markovnikov β -adduct, whilst in the presence of a Pd(0) catalyst, only the Markovnikov α -adduct is formed (Scheme 1.15).⁹² Subsequently, hydrophosphination reactions of secondary phosphine-boranes with unactivated alkenes have been reported: on heating diphenyl- or methylphenyl phosphine-boranes with a range of alkenes under microwave radiation, clean formation of the hydrophosphination product is observed (Scheme 1.16).⁹³ These types of reactions have also been shown to proceed catalytically using basic conditions with a number of alkynes and allenyl phosphine-oxides as shown in Scheme 1.17.⁹⁴



Scheme 1.15. Thermal and catalytic hydrophosphination of alkynes.



Scheme 1.16. Hydrophosphination of unactivated alkene.

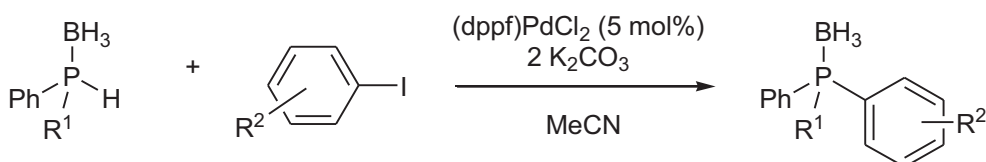


Scheme 1.17. Hydrophosphination of unactivated alkynes [DMAc = Dimethylacetamide].

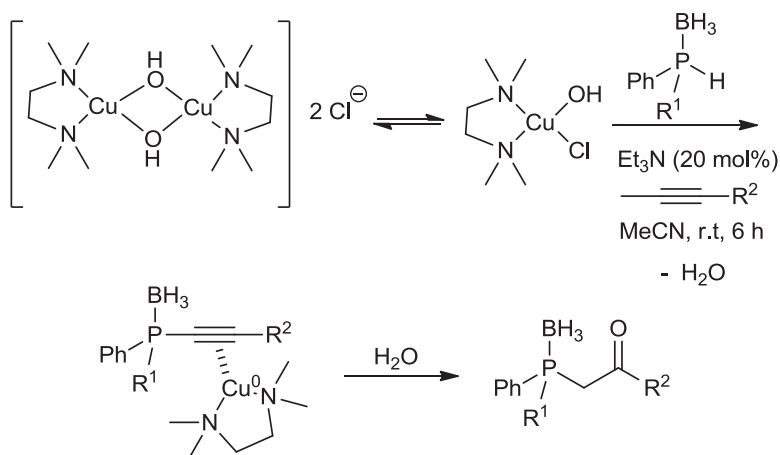
1.3.4.2 Cross-coupling functionalisation

Functionalisation of phosphine-boranes can also be achieved by metal-catalysed cross-coupling reactions. Pd-catalyzed coupling of aryl iodides with secondary phosphine-boranes yields tertiary phosphine-borane adducts (Scheme 1.18) in a process that is similar to the Buchwald-Hartwig cross-couplings known for amines and alcohols.^{95,96} Copper complexes have also been successfully utilised as a catalyst in P-C bond formation:

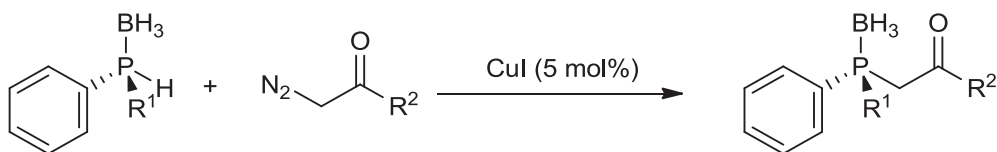
$[\text{Cu}^{\text{II}}(\text{OH})\cdot\text{tmeda}]_2\text{Cl}_2$ is able to cross-couple secondary phosphine-boranes with alkynes, which are believed to undergo subsequent hydrolysis of the triple bond to generate the corresponding ketone and regenerate the catalyst (Scheme 1.19).⁹⁷ Copper-amine adducts, generated *in situ* between CuI and a variety of diazo compounds, can also react with secondary phosphine-boranes. If chiral phosphine-boranes are used, these reactions can proceed with retention of chirality (Scheme 1.20).⁹⁸



Scheme 1.18. Pd-catalysed cross-coupling reaction [dppf = 1,1'-bis(diphenylphosphino)ferrocene].



Scheme 1.19. Cu-catalysed cross-coupling reaction and oxyfunctionalisation.



Scheme 1.20. Stereocontrolled Cu-catalysed cross-coupling reaction.

1.3.5 Summary

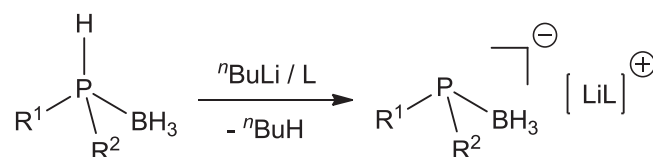
The examples given above demonstrate that phosphine-boranes are extremely useful synthetic intermediates. The stability of the P-B bond and the ability of borane to act as both

an activating and protecting group has been well exploited, particularly in the synthesis of *P*-chiral phosphines, with scope for the development of new, more efficacious phosphines. With increasing demand for ligands in asymmetric catalysis, there is no doubt that this area of chemistry will continue to grow.

1.4 Phosphido-boranes

Secondary phosphine-boranes are readily deprotonated to yield the corresponding phosphido-boranes. There are very few examples of phosphido-boranes that have been structurally characterised, as they are generally generated *in situ* in the preparation of (chiral) phosphines. However, phosphido-boranes are a unique class of compound which have the potential to form complexes with main group metals that contain unusual bonding modes between the ligand and metal centre. By studying their solid-state structures and the nature of the metal-ligand interactions, it can be possible to ‘fine tune’ their reactivity.

The first examples of phosphido-mono(borane) ligands coordinated to a main group metal were reported by Müller in 2003.⁹⁹ The deprotonation of either of the secondary phosphine-boranes Me₂PH(BH₃) or ^tBuPhPH(BH₃) with ⁿBuLi in the presence of tmeda or (-)-sparteine, respectively (Scheme 1.21), yields the compounds [Me₂P(BH₃)Li(tmeda)]_∞ (**29**) and [^tBuPhP(BH₃)Li{(-)-sparteine}] (**30**), respectively (Figure 1.23). Compound **29** crystallises as a polymer due to a series of Li-H-B interactions. The Li-P bond length of 2.620(4) Å is typical for lithium coordinated to an anionic phosphide, whilst it was found that the P-B bond lengthened to 1.945(3) Å compared to the phosphine-borane (1.898(1) Å). Compound **30** crystallises as a dimer, where metal-ligand contacts are formed exclusively due to Li-H-B interactions, which generates a central eight-membered ring. No P-Li contact is observed in the structure, which is possibly due to the steric bulk of the (-)-sparteine.



Scheme 1.21. Preparation of Compounds **29** (R¹ = R² = Me; L = tmeda) and **30** (R¹ = ^tBu, R² = Ph; L = (-)-sparteine).

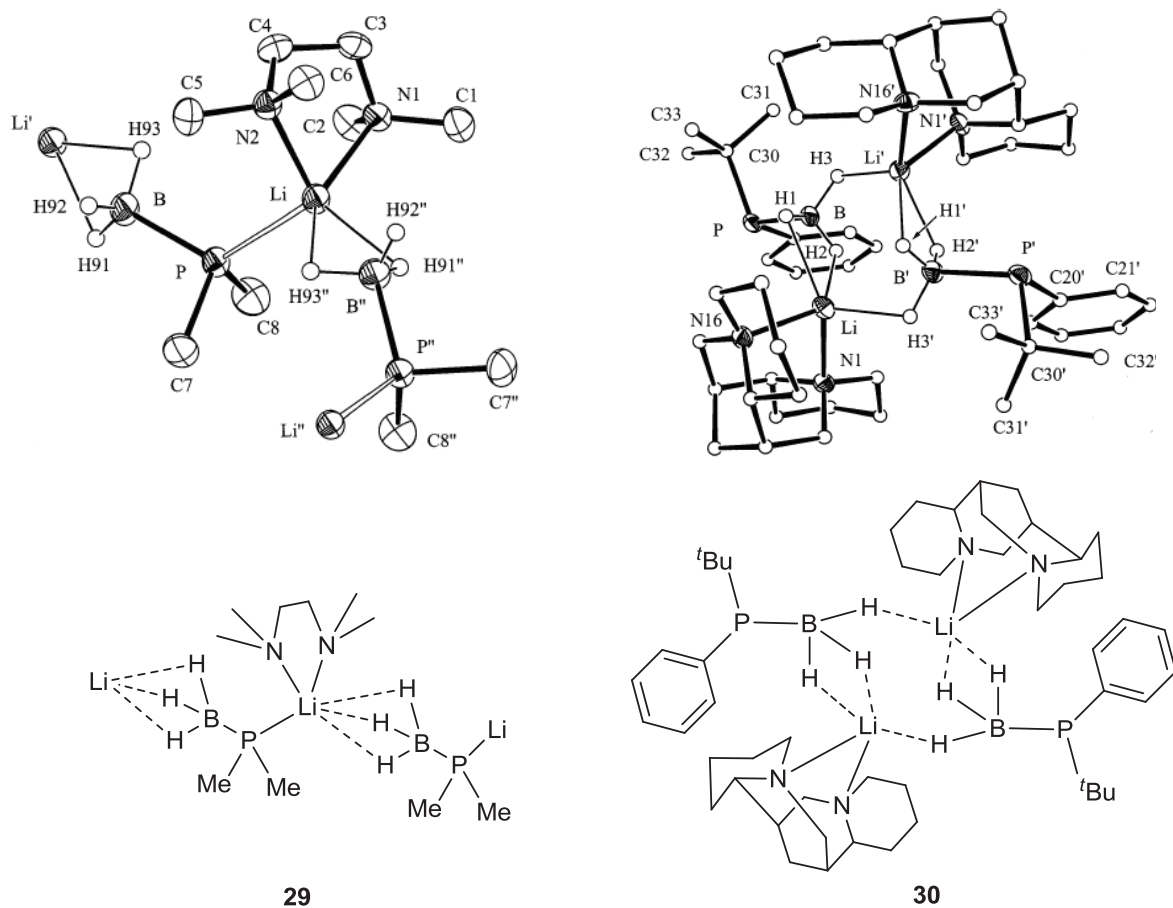


Figure 1.23. Structures of **29** and **30**.⁹⁹

Reaction of AlCl_3 with four equivalents of **29** yields the corresponding lithium aluminate $[\text{Al}\{\text{P}(\text{BH}_3)\text{Me}_2\}_4\text{Li}(\text{MeO}^t\text{Bu})]$ (**31**, Figure 1.24), which was the first homoleptic tetraphosphorus aluminate to be structurally characterised.⁹⁹

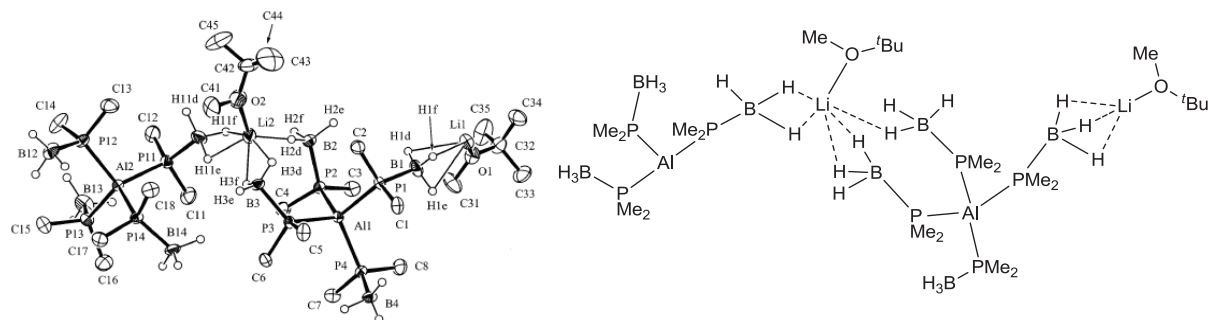


Figure 1.24. Structure of **31**.⁹⁹

Two examples of phosphido-boranes coordinated to the heavier alkali metal potassium have been reported by Wagner and co-workers.¹⁰⁰ The phosphine-boranes $\text{Ph}_2\text{P}(\text{BH}_3)$ and $t\text{Bu}_2\text{P}(\text{BH}_3)$ were deprotonated using KH at low temperatures, and crystallised in the presence of 18-crown-6 to yield compounds $[\text{Ph}_2\text{P}(\text{BH}_3)\text{K}(\text{18-crown-6})]$ (**32**) and $[t\text{Bu}_2\text{P}(\text{BH}_3)\text{K}(\text{18-crown-6})]$ (**33**), respectively (Figure 1.25). In compound **32**, a direct bond is formed between the P atom and the metal centre [K-P 3.320(2) Å] and there is an additional η^2 -coordination of the borane fragment [K...B 3.162 Å]. In compound **33**, there are two crystallographically independent molecules (only one is shown) but in both cases there is no direct P-K contact, most likely due to the fact that the larger *t*-butyl groups force the phosphorus away from the plane of the [K(18-crown-6)] adduct. In one of the molecules of **33**, coordination of the borane fragment to potassium is thought to be somewhere between a η^2 and η^3 interaction whereas the second ion-pair is linked *via* an η^3 -coordinated BH_3 .

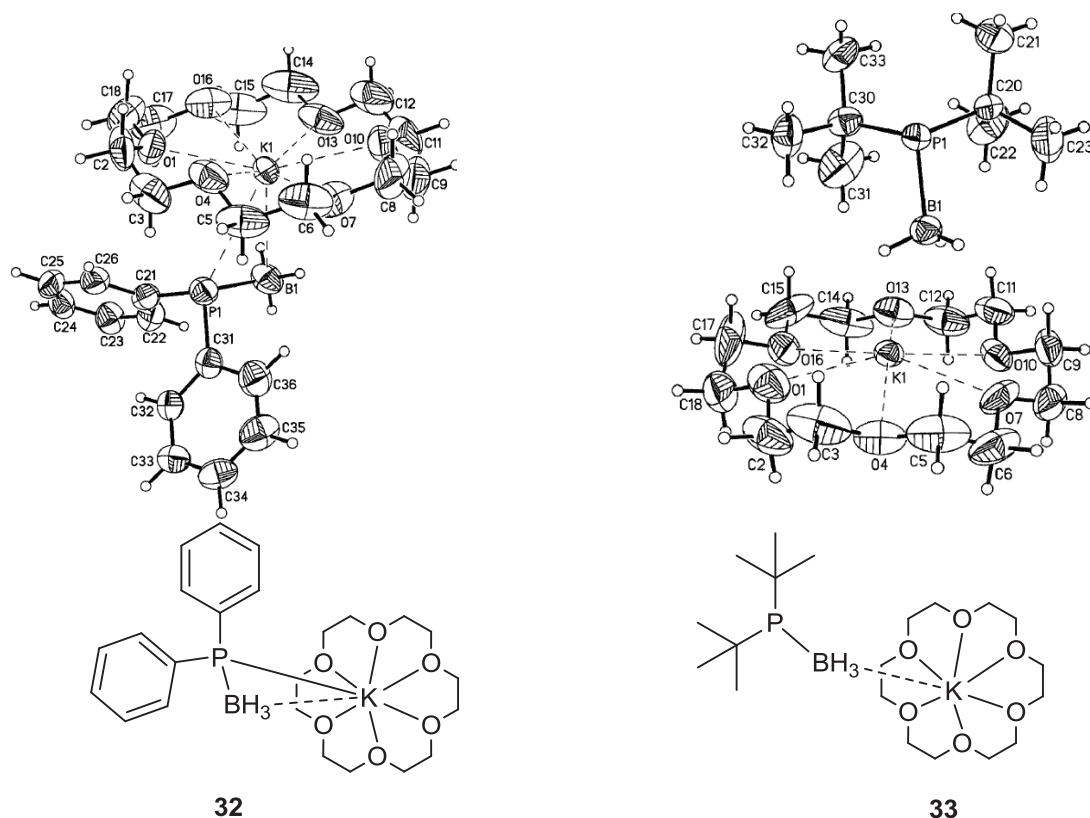


Figure 1.25. Structures of **32** and **33**.¹⁰⁰

The same group have also synthesised the bis(phosphido-borane) $[\{P(BH_3)(Ph)CH_2\}_2 K_2(THF)_4]_\infty$ (**34**), which crystallises as a polymer (*meso*-diastereoisomer shown in Figure 1.26). Both borane groups in the phosphido-borane ligand are coordinated to an adjacent potassium ion, and in turn, each potassium ion also bound to a borane group from a second ligand, forming a series of $BH_3 \dots K$ interactions, which forms the polymer. The coordination about each potassium is completed by two molecules of THF.¹⁰¹

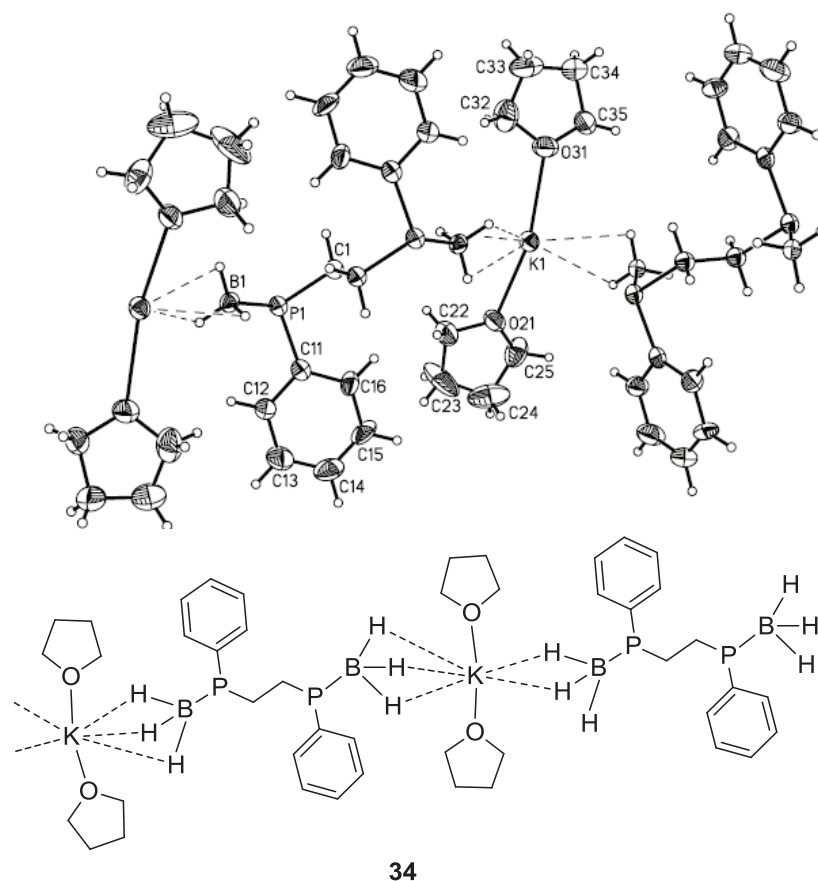
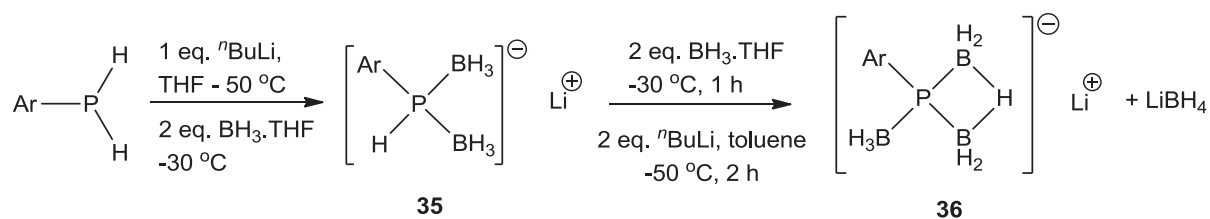


Figure 1.26. Structure of compound **34**.¹⁰¹

In 2001 Romanenko, Bertrand *et al* identified two phosphido-poly(boranes), which demonstrated that phosphide anions can be bound to two or three borane groups. The only previous examples of trivalent phosphorus bound to two or three boron atoms that had been characterised in the solid state were limited to polyhedral compounds, neutral diborylphosphines, and heterocyclic compounds.¹⁰²

The primary phosphine (mes*)PH₂ was deprotonated with an equimolar amount of ⁿBuLi in THF, and subsequent addition of two equivalents of BH₃·THF gave rise to the compound $[(mes^*)PH(BH_3)_2Li(THF)_3]$ (**35**). The phosphido-bis(borane) ligand is coordinated to lithium

through one of the borane fragments *via* an η^2 -interaction. The coordination sphere of lithium is completed by three molecules of THF. The borane bound to lithium is found to have a shorter P-B distance [P(1)-B(1) 1.955 Å] compared to the P-B distance in the ‘free’ BH₃ group [P(1)-B(2) 1.984 Å]. Further treatment of **35** with an excess of *n*BuLi and BH₃·THF at low temperature resulted in the formation of a new complex that crystallises as a dimer [(*mes**)P(BH₃)(μ -BH₂)₂H Li(THF)₂] (**36**, Scheme 1.22). Compound **36** is characterised by the presence of a four-membered heterocyclic ring with a hydride that bridges the two BH₂ groups.



Scheme 1.22. Synthesis of compounds **35** and **36** [Ar = 2,4,6-tri-*t*-butylphenyl].

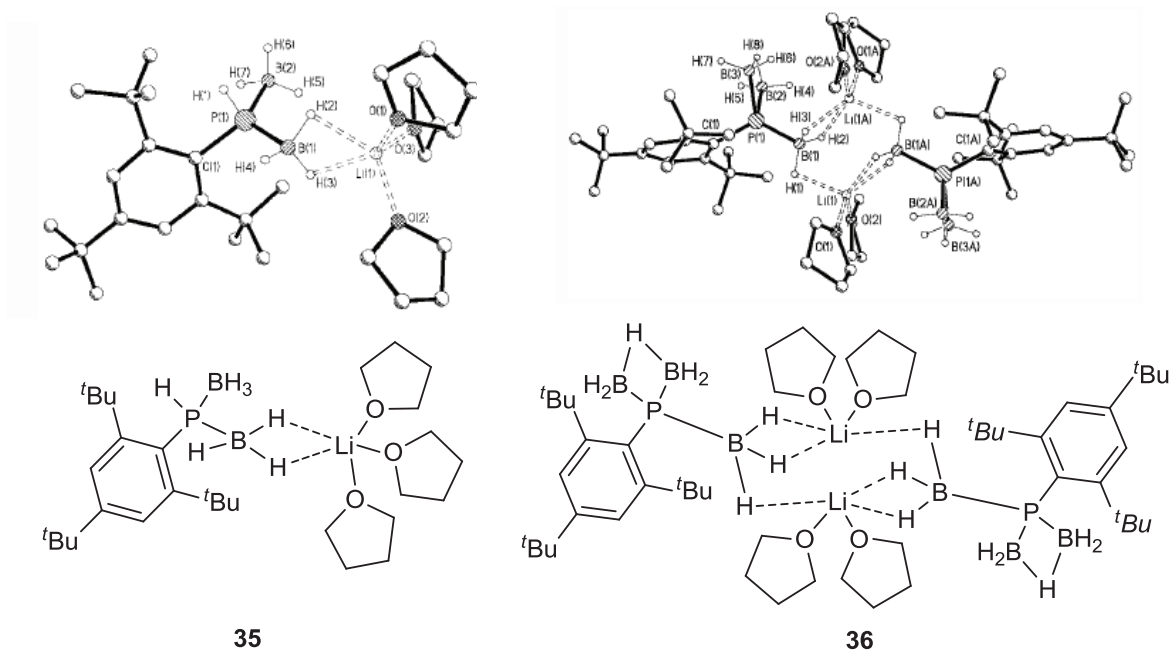


Figure 1.27. Structures of compounds **35** and **36**.¹⁰²

The only example of a phosphido-bis(borane) coordinated to a heavier alkali metal is $[\text{Ph}_2\text{P}(\text{BH}_3)_2\text{K}(18\text{-crown-6})]$ (**37**, Figure 1.28).¹⁰³ Compound **37** crystallises as a monomer with the ligand bound to the potassium ion through the hydrogen atoms of one of the borane groups in an η^3 fashion. Short contacts between one of the phenyl carbon atoms and the potassium ion [$\text{K}(1)\dots\text{C}(34) = 3.372(2) \text{ \AA}$] aid stabilisation of the molecular packing in the crystal lattice.

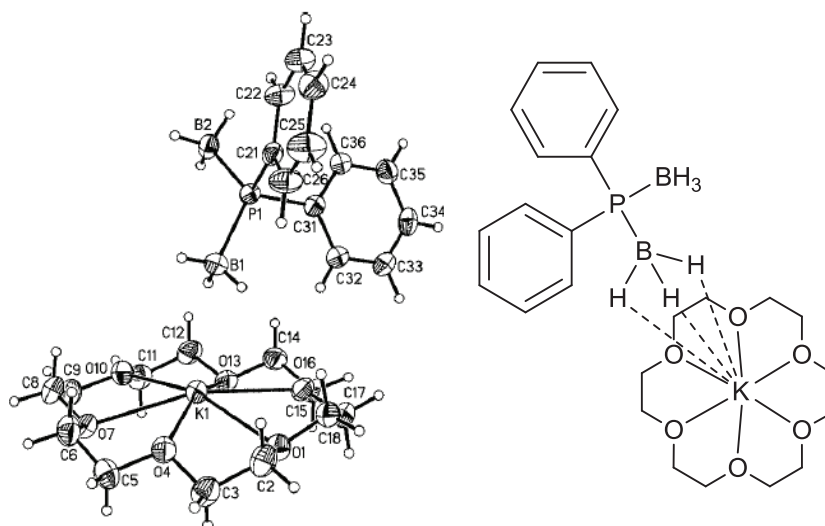


Figure 1.28. Compound **37**.¹⁰³

In 2009, Lancaster and co-workers synthesised a number of related phosphido-bis(borane) complexes, which possess (pentafluorophenyl)borane groups.¹⁰⁴ Of particular interest is the compound $[\text{Ph}_2\text{P}\{\text{B}(\text{C}_6\text{F}_5)_3\}(\text{BH}_3)\text{Li}(\text{Et}_2\text{O})_3]$ (**38**, Figure 1.29), which crystallises as a monomer, with the ligand bound to the lithium ion *via* an η^2 -type interaction from the BH_3 group. The $\text{Li}\dots\text{B}$ distance in **38** of $2.477(3) \text{ \AA}$ is similar to that of **35**, which is consistent with a $\eta^2\text{-BH}_3\text{-Li}$ interaction. As with **35**, the P-B distance for the Li-bound BH_3 group in **38** is considerably shorter than the P-B distance for the ‘free’ borane group.

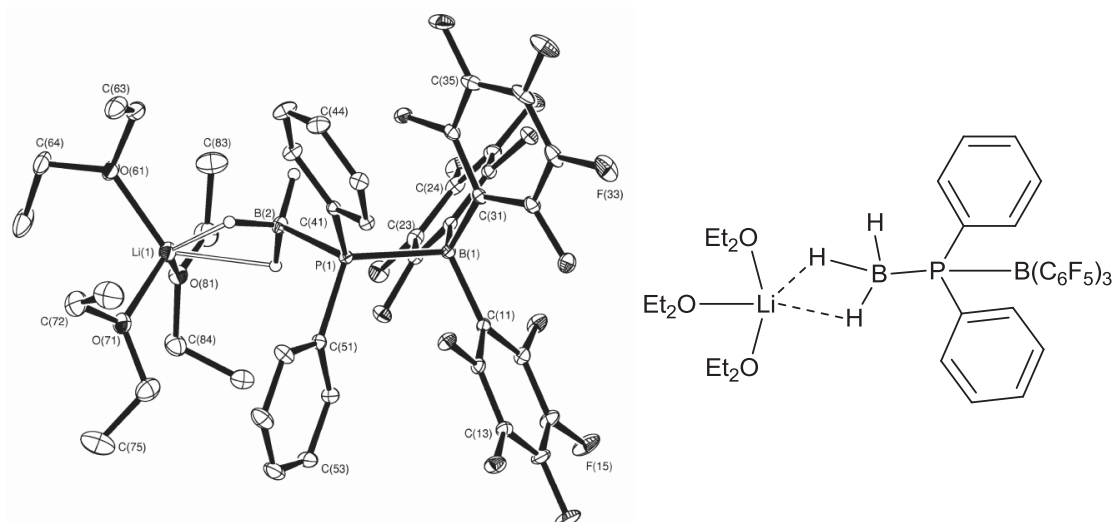


Figure 1.29. Compound 38.¹⁰⁴

Although there is only a small number of crystallographically-characterised phosphido-borane complexes with main group metals, there are several reports detailing the structures of phosphido-borane complexes with transition metals, these are discussed in chapter 3.

1.5 Summary

This chapter gives a brief overview of the factors that can affect the reactivity of alkali metal organometallic complexes, and reviews a diverse range of phosphide complexes with alkali and alkaline earth metals, exploring the factors which contribute to the unique structure and chemistry of each complex. The chapter also reviews the synthesis and applications of a wide-range of phosphine-boranes, with particular emphasis on the importance of the structures of the phosphido-borane intermediates, as this can help in our understanding of their reactivity. However, in general, there is a distinct lack of information on the structures of phosphido-boranes.

The work presented in this thesis will focus on the synthesis and solid-state structures of phosphido-boranes coordinated to alkali and alkaline earth metals, expanding upon the limited number examples found in the literature. There is a particular emphasis on the effect of introducing donor-functionality on the phosphorus, which will give a greater insight into the role played by a peripheral donor, and the factors that afford stability and that affect the

extent of aggregation in these species. Several new phosphido-bis(borane) complexes are also reported, including the first examples of alkaline earth metals coordinated to ligands of this type.

1.6 References

- (1) Schlenk, W.; Appendrodt, J.; Michael, A.; Thal, A. *Ber. Dtsch. Chem. Ges.* **1914**, 47, 473.
- (2) Schlenk, W.; Holtz, J. *Chem. Ber.* **1917**, 50, 262.
- (3) Weiss, E. *Angew. Chem. Int. Ed. Engl.* **1993**, 32, 1501.
- (4) Beswick, M. A.; Wright, D. S. in *Comprehensive Organometallic Chemistry II, Vol. 1* (Eds.: Abel, E; Stone, F. G. A; Wilkinson, G.), Pergamon, Oxford, **1995**, pp. 1.
- (5) Wardell, J. L. in *Comprehensive Organometallic Chemistry I, Vol. 1* (Eds.: Abel, E; Stone, F. G. A; Wilkinson, G.), Pergamon, Oxford, **1982**, pp 43.
- (6) Schleyer, P. v. R. *Pure Appl. Chem.* **1984**, 56, 151.
- (7) Schleyer, P. v. R. *Pure Appl. Chem.* **1983**, 55, 355.
- (8) Shannon, R. D. *Acta Cryst. Sect. A* **1976**, A32, 751.
- (9) *CRC Organic and Physical Chemistry* 6th Edⁿ, CRC Florida Press **2005**.
- (10) Pearson, R. G. *Chemical Hardness*; Wiley-VCH, Weinheim, **1997**.
- (11) Schleyer, P. v. R.; Clark, T.; Kos, A.; Spitznagel, G. W.; Rohde, C.; Arad, D.; Houk, K. N.; Rondan, N. G. *J. Am. Chem. Soc.* **1984**, 106, 6467.
- (12) Magnusson, E. *J. Phys. Chem.* **1994**, 98, 12558.
- (13) Smith, J. D. *Adv. Organomet. Chem.* **1998**, 43, 267.

- (14) Dreiss, M.; Pritzkov, H.; Skipinski, M.; Winkler, U. *Organometallics* **1997**, *16*, 5108.
- (15) Budzelaar, P. H. M.; van Doorn, J. A.; Meijboom, N. *Rec. Trav. Chim. Pays-Bas* **1991**, *110*, 420.
- (16) Van Doorn, J. A.; Frijns, J. H. G.; Meijboom, N. *Rec. Trav. Chim. Pays-Bas* **1991**, *110*, 1441.
- (17) Toth, I.; Hanson, B. E.; Davis, M. E. *Organometallics* **1990**, *9*, 675.
- (18) Uhlig, F.; Hummeltenber, R. J. *Organomet. Chem.* **1993**, *452*, C9.
- (19) English, U.; Hassler, K.; Ruhlandt-Senge, K.; Uhlig, F. *Inorg. Chem.* **1998**, *37*, 3532.
- (20) Hey, E.; Hitchcock, P. B.; Lappert, M. F.; Rai, A. K. *J. Organomet. Chem.* **1987**, *325*, 1.
- (21) Clegg, W.; Doherty, S.; Izod, K.; Kagerer, H.; O'Shaughnessy, P.; Sheffield, J.M. *J. Chem. Soc., Dalton Trans.* **1999**, 1825.
- (22) Jones, R. A.; Stuart, A. L.; Wright, T. C. *J. Am. Chem. Soc.* **1983**, *105*, 7459.
- (23) Steiglitz, G.; Neumüller, B.; Dehnicke, K. *Z. Naturforsch.* **1993**, *48b*, 156.
- (24) Hope, H.; Olmstead, M. M.; Power, P. P.; Xu, X. *J. Am. Chem. Soc.* **1984**, *106*, 819.
- (25) Bartlett, R. A.; Olmstead, M.; Power, P. P. *Inorg. Chem.* **1986**, *25*, 1243.
- (26) Jones, R. A.; Koschmieder, S. U.; Nunn, C. M. *Inorg. Chem.* **1987**, *26*, 3610.
- (27) Becker, G.; Hartmann, H. M.; Schwarz, W. *Z. Anorg. Allg. Chem.* **1989**, *577*, 9.
- (28) Anderson, D. M.; Hitchcock, P. B.; Lappert, M. F.; Leung, W.-P.; Zora, J. A. *J. Organomet. Chem.* **1987**, *333*, C13.

- (29) Rivard, E.; Sutton, A. D.; Fettinger, J. C.; Power, P. P. *Inorg. Chim. Acta* **2007**, *360*, 1278.
- (30) Hey-Hawkins, E.; Sattler, E. *J. Chem. Soc., Chem. Commun.* **1992**, 775.
- (31) Driess, M.; Pritzkow, H. *Z. Anorg. Allg. Chem.* **1996**, *622*, 1524.
- (32) Andrianarison, M.; Stalke, D.; Klingebiel, U. *Chem. Ber.* **1990**, *123*, 71.
- (33) Koutsantonis, G. A.; Andrews, P. C.; Raston, C. L. *J. Chem. Soc., Chem. Commun.* **1995**, 47.
- (34) Rabe, G. W.; Heise, H.; Yap, G. P. A.; Liable-Sands, L. M.; Guzei, I. A.; Rheingold, A. *Inorg. Chem.* **1998**, *37*, 4235.
- (35) Rabe, G. W.; Kheradmandan, S.; Liable-Sands, L. M.; Guzei, I. A.; Rheingold, A. *Angew. Chem. Int. Ed. Engl.* **1998**, *37*, 1404.
- (36) Rabe, G. W.; Riede, J.; Schier, A. *Acta Cryst. Sect. C* **1996**, *C52*, 1350.
- (37) Aspinall, H. C.; Tillotson, M. R. *Inorg. Chem.* **1996**, *35*, 5.
- (38) Toth, I.; Hanson, B. E.; Davis, M. E. *Organometallics* **1990**, *9*, 675.
- (39) Izod, K.; Clegg, W.; Liddle, S. T. *Organometallics* **2000**, *19*, 3640.
- (40) Crimmin, M. R.; Barrett, A. G. M.; Hill, M. S.; Hitchcock, P. B.; Procopiou, P. A. *Inorg. Chem.* **2007**, *26*, 2953.
- (41) Datta, S.; Roesky, P. W.; Blechert, S. *Organometallics* **2007**, *26*, 4392.
- (42) Crimmin, M. R.; Casely, I. J.; Hill, M. S. *J. Am. Chem. Soc.* **2005**, *127*, 2042.
- (43) Buch, F.; Brettar, J.; Harder, S. *Angew. Chem. Int. Ed. Engl.* **2006**, *45*, 2741.
- (44) Grigsby, W. J.; T., H.; Ellison, J. J.; Olmstead, M. M.; Power, P. P. *Inorg. Chem.* **1996**, *35*, 3254.

- (45) Westerhausen, M.; Digeser, M. H.; Nöth, H.; Seifert, T.; Pfitzner, A. *J. Am. Chem. Soc.* **1998**, *120*, 6722.
- (46) Westerhausen, M.; Digeser, M. H.; Wieneke, B.; Nöth, H.; Knizek, J. *Eur. J. Inorg. Chem.* **1998**, *1998*, 517.
- (47) Westerhausen, M.; Pfitzner, A. *J. Organomet. Chem.* **1995**, *487*, 187.
- (48) Hey, E.; Engelhardt, L. M.; Raston, C. L.; White, A. H. *Angew. Chem. Int. Ed. Engl.* **1987**, *26*, 81.
- (49) Atwood, J. L.; Bott, S. G.; Jones, R. A.; Koschmieder, S. U. *J. Chem. Soc., Chem. Commun.* **1990**, 692.
- (50) Westerhausen, M. *J. Organomet. Chem.* **1994**, *479*, 141.
- (51) Blair, S.; Izod, K.; Clegg, W. *Inorg. Chem.* **2002**, *41*, 3886
- (52) Gärtner, M.; Görls, H.; Westerhausen, M. *Inorg. Chem.* **2008**, *47*, 1397.
- (53) Besson, A. *Comptes Rendus* **1890**, *110*, 516.
- (54) Gamble, E. L.; Gilmont, P. *J. Am. Chem. Soc.* **1940**, *62*, 717.
- (55) Stock, A. *Ber* **1923**, *56B*, 789.
- (56) Rudolph, R. W.; Parry, R. W.; Farran, C. F. *Inorg. Chem.* **1966**, *5*, 723.
- (57) Paine, R. T.; Noth, H. *Chem. Rev.* **1995**, *95*, 343.
- (58) Carboni, B.; Monnier, L. *Tetrahedron* **1999**, *55*, 1197.
- (59) Brunel, J. M.; Faure, B.; Maffei, M. *Coord. Chem. Rev.* **1998**, *178-180*, 665.
- (60) Ohff, M.; Holz, J.; Quirnbach, M.; Borner, A. *Synthesis* **1998**, *1998*, 1391.
- (61) Gaumont, A.-C.; Carboni, B. *Science of Synthesis, Vol 6* **2004**, (Eds.: Kauffmann, D.; Matteson, D. S.), Thieme, Stuttgart, pp. 485.

- (62) Laneman, S. C. *Spec. Chem. Mag.* **2008**, 28.
- (63) Hurtado, M.; Ya'nez, M.; Herrero, R.; Guerrero, A.; Da'valos, J. Z.; Abboud, J.-L. M.; Khater, B.; Guillemin, J.-C. *Chem.-Eur. J.* **2009**, 15, 4622.
- (64) Chan, V. S.; Chiu, M.; Bergman, R. G.; Toste, F. D. *J. Am. Chem. Soc.* **2009**, 131, 6021.
- (65) Carreira, M.; Charernsuk, M.; Eberhard, M.; Fey, N.; van Ginkel, R.; Hamilton, A.; Mul, W. P.; Orpen, A. G.; Phetmung, H.; Pringle, P. G. *J. Am. Chem. Soc.* **2009**, 131, 3078.
- (66) Seitz, T.; Muth, A.; Huttner, G. *Chem. Ber.* **1994**, 127, 1837.
- (67) Yasue, T.; Kawano, Y.; Shimo, M. *Angew. Chem. Int. Ed. Engl.* **2003**, 42, 1727.
- (68) Imamoto, T.; Kusumoto, T.; Suzuki, N.; Sato, K. J. *J. Am. Chem. Soc.* **1985**, 107, 5301.
- (69) Imamoto, T.; Takeyama, T.; Kusumoto, T. *Chem. Lett.* **1985**, 1491.
- (70) Imamoto, T.; Osaiki, T.; Onoznuva, T.; Kusumoto, T.; Sato, K. J. *J. Am. Chem. Soc.* **1990**, 112, 5245.
- (71) McNulty, P.; Zhou, Y. *Tetrahedron Lett.* **2004**, 45, 407.
- (72) Burg, A. B.; Slota, P. J. *J. Am. Chem. Soc.* **1960**, 82.
- (73) Kuznetsov, N. T. *Zh. Fiz. Khim.* **1964**, 9, 1817.
- (74) Brisset, H.; Gourdel, Y.; Pellon, P.; Le Corre, M. *Tetrahedron Lett.* **1993**, 34, 4523.
- (75) Bradley, D.; Williams, G.; Lombard, H.; van Niekerk, M.; Coetlee, P. P.; Holzapfel, C. W. *Phosphorus, Sulfur.* **2002**, 177, 2799.
- (76) McKinsty, L.; Livinghouse, T. *Tetrahedron* **1995**, 51, 7655.
- (77) McKinsty, L.; Livinghouse, T. *Tetrahedron* **1994**, 35, 9319.

- (78) Van Overschelde, M.; Vervecken, E.; Modha, S. G.; Cogen, S.; van der Eycken, E.; van der Eycken, J. *Tetrahedron* **2009**, *65*, 6410.
- (79) McKinstry, L.; Overberg, J. J.; Soubre-Ghaoui, C.; Walsh, D. S.; Robins, K. A.; Toto, T. T.; Toto, J. L. *J. Org. Chem.* **2000**, *65*, 2261.
- (80) Cowley, A. H.; Damasco, M. C. *J. Am. Chem. Soc.* **1971**, 6815.
- (81) Bourumeau, K.; Gaumont, A.-C.; Denis, J.-M. *J. Organomet. Chem.* **1997**, *529*, 205.
- (82) Gourdel, Y.; Ghanimi, A.; Pellon, P.; Le Corre, M. *Tetrahedron Lett.* **1993**, *34*, 1011.
- (83) Imamoto, T. *Pure Appl. Chem.* **1993**, *65*, 655.
- (84) Wolfe, B.; Livinghouse, T. *Organometallics* **1981**, *120*, 5116.
- (85) Grubbs, R. H.; Mohr, B.; Lynn, D. M. *Organometallics* **1996**, *15*, 4317.
- (86) Gaumont, A.-C.; Gulea, M.; Levillain, J. *Chem. Rev.* **2009**, *178-180*. 665.
- (87) Mimeau, D.; Delacroix, O.; Join, B.; Gaumont, A.-C. *C. R. Chim.* **2004**, *7*. 845.
- (88) Delacroix, O.; Gaumont, A.-C. *Curr. Org. Chem.* **2005**, *9*. 1851.
- (89) Glueck, D. S. *Chem.-Eur. J.* **2008**, *14*. 7108.
- (90) Kolodiazhnyi, O. I. *Tetrahedron Asymmetry* **1998**, *9*, 1279.
- (91) Enders, D.; Saint-Dizier, A.; Lannou, M.-I.; Lenzen, A. *Eur. J. Org. Chem* **2006**, 29.
- (92) Mimeau, D.; Gaumont, A.-C. *J. Org. Chem.* **2003**, *68*, 7016.
- (93) Mimeau, D.; Delacroix, O.; Gaumont, A.-C. *Chem. Commun.* **2003**, 2928.
- (94) Busacca, C. A.; Farber, E.; DeYoung, J.; Campbell, S.; Gonnella, N. C.; Grinberg, N.; Haddad, N.; Lee, H.; Ma, S.; Reeves, D.; Shen, S.; Senanayake, C. H. *Org. Lett.* **2009**, *11*. 5594.

- (95) Gaumont, A.-C.; Hursthouse, M. B.; Coles, S. J.; Brown, J. M. *Chem. Commun.* **1999**, 63.
- (96) Schlumer, B.; Scholz, U. *Adv. Synth. Catal.* **2004**, 346, 1599.
- (97) Kumaraswamy, G.; Rao, G. V.; Murthy, A. N.; Sridhar, B. *Synlett* **2009**, 1180.
- (98) Kumaraswamy, G.; Rao, G. V.; Murthy, A. N.; Sridhar, B. *Synlett* **2006**, 1122.
- (99) Müller, G.; Brand, J. *Organometallics* **2003**, 22, 1463.
- (100) Dornhaus, F.; Bolte, M.; Lerner, H.-W.; Wagner, M. *Eur. J. Inorg. Chem.* **2006**, 5138.
- (101) Dornhaus, F.; Bolte, M.; Lerner, H.-W.; Wagner, J. *Organomet. Chem.* **2007**, 692, 2949.
- (102) Rudzevich, L. R.; Gornitzka, H.; Romanenko, V. D.; Bertrand, G. *Chem. Commun.* **2001**, 1634.
- (103) Dornhaus, F.; Bolte, M.; Lerner, H.-W.; Wagner, M. *Eur. J. Inorg. Chem.* **2006**, 1777.
- (104) Fuller, A.-M.; Mountford, A. J.; Scott, M. L.; Coles, S. J.; Horton, P. N.; Hughes, D. L.; Hursthouse, M. B.; Lancaster, S. J. *Inorg. Chem.* **2009**, 48, 11474.

Chapter 2. Synthesis of Phosphine-Borane Precursors

2.1 Introduction

Phosphine-boranes are highly valuable compounds due to their widespread applications in synthesis (see chapter 1.3). Deprotonation of secondary phosphine-boranes yields the corresponding anionic phosphido-boranes which are key intermediates in the synthesis of chiral phosphines. However, little is known about the structures of phosphido-boranes, as they are usually generated *in situ*, and as a result the factors that govern their structures and reactivities are not well understood.

In this project, several novel phosphine-boranes were prepared, with the general structure shown in Figure 2.1. The P-H group is activated towards deprotonation due to the presence of the BH₃ group directly bonded to phosphorus, thus phosphido-boranes are easily accessible upon treatment with a strong base. The bulky substituent (Me₃Si)₂CH confers several desirable properties, which include increased solubility, thermal stability, lipophilicity, and hindrance of high-order aggregation of the phosphido-borane complexes. Particular focus is paid to the introduction of peripheral donor functionality within the ligand, which can potentially provide additional stabilisation in the phosphido-borane complexes through intramolecular interactions between the peripheral donor atom and metal centre, resulting in the formation of a chelate ring. Changing the nature of the chelate ring *i.e.* varying the donor atom and ring size, can have a significant effect on the structures and consequently the reactivities of these phosphido-borane complexes. The borane group has also been shown to provide additional stabilisation through agostic-type B-H...M bonding modes with group I metals.¹⁻⁴

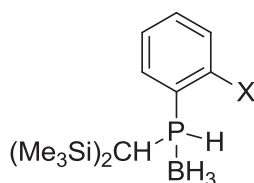


Figure 2.1. General structure of phosphine-borane precursor. X = CH₂OMe, SMe, OMe, H.

To probe the effects that peripheral donor groups have on the structures of phosphido-borane complexes, three donor-functionalised phosphine-borane precursors have been synthesised: $\{(Me_3Si)_2CH\}PH(C_6H_4-2-CH_2OMe)(BH_3)$ (**39**), $\{(Me_3Si)_2CH\}PH(C_6H_4-2-SMe)(BH_3)$ (**40**), and $\{(Me_3Si)_2CH\}PH(C_6H_4-2-OMe)(BH_3)$ (**41**). For comparison, the non-donor-functionalised $\{(Me_3Si)_2CH\}PH(C_6H_5)(BH_3)$ (**42**) was also synthesised.

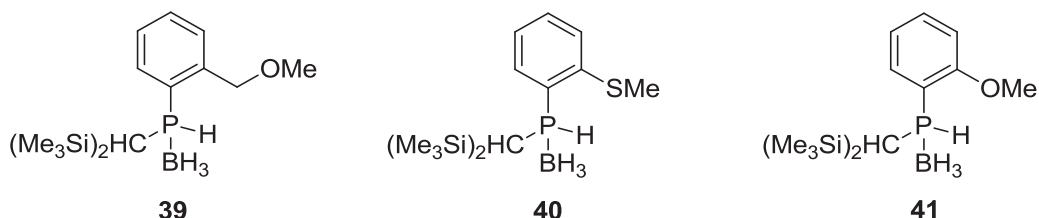
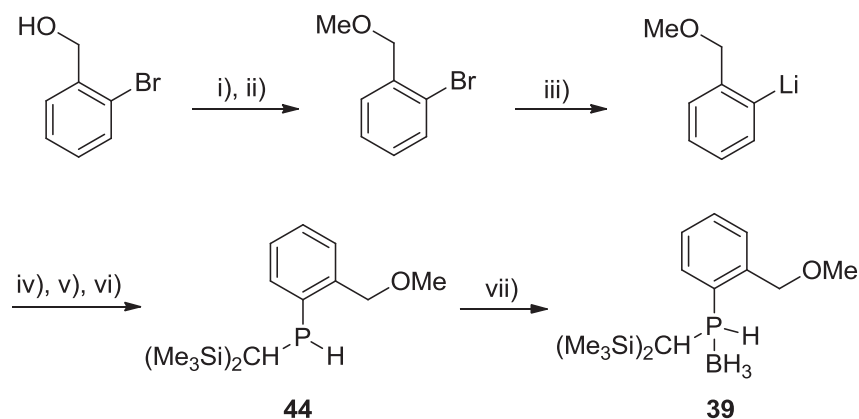


Figure 2.2. Donor-functionalised phosphine-boranes.

2.2 Synthesis of secondary phosphine-borane precursors

2.2.1 Synthesis of $\{(Me_3Si)_2CH\}PH(C_6H_4-2-CH_2OMe)(BH_3)$ (**39**)

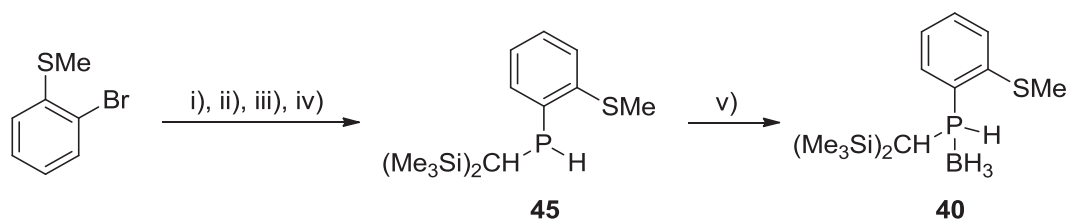
The preparation of **39** is shown in Scheme 2.1. Synthesis of 1-bromo-2-(methoxymethyl)benzene ($BrC_6H_4-2-CH_2OMe$) was achieved as previously reported.⁵ Treatment of $BrC_6H_4-2-CH_2OMe$ with nBuLi at low temperatures ($0\text{ }^\circ C$) yields $LiC_6H_4-2-CH_2OMe$ *via* a lithium-halogen exchange reaction; this compound was not isolated, but was generated and used *in situ*. The reaction between the lithium salt and a cold solution of $\{(Me_3Si)_2CH\}PCl_2$ (**43**)⁶ yields the monochlorophosphine $\{(Me_3Si)_2CH\}PCl(C_6H_4-2-CH_2OMe)$; the steric bulk of the $(Me_3Si)_2CH$ group and low reaction temperature allows for mono-substitution of **43**. The monochlorophosphine may be reduced *in situ* with $LiAlH_4$ to yield the secondary phosphine $\{(Me_3Si)_2CH\}PH(C_6H_4-2-CH_2OMe)$ (**44**). After an aqueous work-up, **44** may be isolated as a colourless oil. The phosphine-borane adduct was prepared by addition of $BH_3 \cdot SMe_2$ to a solution of **44** in Et_2O , and crystallised as colourless blocks from hot light petroleum in good yield (60%).



Scheme 2.1 Synthesis of **39**. Reagents and conditions: i) NaH, THF, 0°C, 1 h. ii) MeI, 0°C, 0.5 h. iii) ⁿBuLi, Et₂O, 0°C, 2 h. iv) {(Me₃Si)₂CH}PCl₂ (**43**), -78°C, 16 h. v) LiAlH₄, 35°C, 2 h. vi) Deoxygenated H₂O. vii) BH₃·SMe₂, THF, r.t., 1 h.

2.2.2 Synthesis of {(Me₃Si)₂CH}PH(C₆H₄-2-SMe)(BH₃) (**40**)

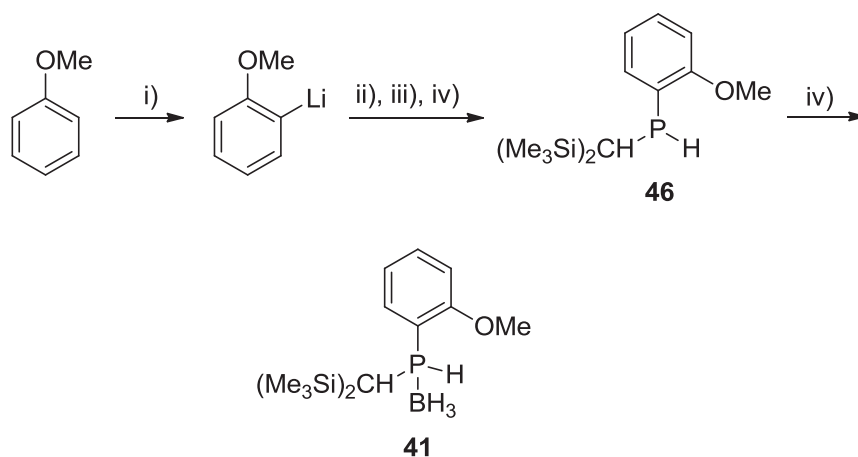
The preparation of **40** is shown in Scheme 2.2. The reaction between a cold solution of 2-bromothioanisole in Et₂O and ⁿBuLi yields (2-(methylthio)phenyl)lithium via a lithium-halogen exchange reaction. The *in situ*-generated lithium salt is added to a cold solution of **43**, to yield the chlorophosphine {(Me₃Si)₂CH}PCl(C₆H₄-2-SMe), which may be reduced *in situ* with LiAlH₄ to yield the secondary phosphine {(Me₃Si)₂CH}PH(C₆H₄-2-SMe) (**45**). After an aqueous work-up, **45** is isolated as a colourless oil. Addition of BH₃·SMe₂ to a solution of **45** in Et₂O yields the phosphine-borane {(Me₃Si)₂CH}PH(C₆H₄-2-SMe)(BH₃) (**40**), which may be crystallised from cold (-30 °C) *n*-hexane as colourless needles in excellent yield (83%).



Scheme 2.2. Synthesis of **40**. Reagents and conditions: i) ⁿBuLi, Et₂O, 0°C, 2 h. ii) {(Me₃Si)₂CH}PCl₂ (**43**), Et₂O, -78°C, 16 h. iii) LiAlH₄, 35°C, 2 h. iv) Deoxygenated H₂O. v) BH₃·SMe₂, THF, r.t., 1 h.

2.2.3 Synthesis of $\{(Me_3Si)_2CH\}PH(C_6H_4-2-OMe)(BH_3)$ (**41**)

The synthesis of **41** is shown in Scheme 2.3. The reaction between a cold solution of **43** in THF and one equivalent of (2-methoxyphenyl)lithium⁷ yields the corresponding monochlorophosphine $\{(Me_3Si)_2CH\}PCl(C_6H_4-2-OMe)$, which may be reduced *in situ* with $LiAlH_4$ to give the secondary phosphine $\{(Me_3Si)_2CH\}PH(C_6H_4-2-OMe)$ (**46**). After an aqueous work-up, **46** is isolated as a colourless oil. Treatment of a solution of **46** in Et_2O with $BH_3 \cdot SMe_2$ gives the phosphine-borane precursor $\{(Me_3Si)_2CH\}PH(C_6H_4-2-OMe)(BH_3)$ (**41**), which may be crystallised from light petroleum upon cooling ($-30\text{ }^\circ\text{C}$), in good yield (73%), as colourless blocks.

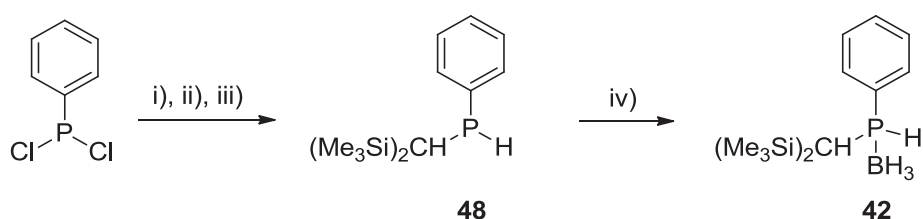


Scheme 2.3. Synthesis of **41**. Reagents and conditions: i) $nBuLi$, TMEDA, Et_2O , 16 h. ii) $\{(Me_3Si)_2CH\}PCl_2$ (**43**), THF, $-78\text{ }^\circ\text{C}$, 16 h. iii) $LiAlH_4$, $66\text{ }^\circ\text{C}$, 2 h. iv) Deoxygenated H_2O . v) $BH_3 \cdot SMe_2$, THF, r.t., 1 h.

2.2.4 Synthesis of $\{(Me_3Si)_2CH\}PH(C_6H_5)(BH_3)$ (**42**)

The non-donor-functionalised phosphine-borane **42** was synthesised as shown in Scheme 2.4. The reaction between $(Me_3Si)_2CHLi$ (**47**)⁶ and one equivalent of phenyldichlorophosphine in Et_2O at low temperature ($-78\text{ }^\circ\text{C}$) yields the monochlorophosphine $\{(Me_3Si)_2CH\}PCl(C_6H_5)$, which may be reduced with $LiAlH_4$ *in situ*, to generate the secondary phosphine $\{(Me_3Si)_2CH\}PH(C_6H_5)$ (**48**). After an aqueous work-up, **48** is isolated as a colourless oil. Reaction between a solution of **48** in Et_2O and one equivalent of $BH_3 \cdot SMe_2$ yields the

phosphine-borane adduct $\{(Me_3Si)_2CH\}PH(C_6H_5)(BH_3)$ (**42**), which may be crystallised from cold toluene ($-30\text{ }^\circ\text{C}$) as a colourless, air-stable solid in good yield (63%).



Scheme 2.4. Synthesis of **42**. Reagents and conditions: (i) $(Me_3Si)_2CHLi$ (**47**), Et_2O , -78°C , 16 h. ii) $LiAlH_4$, 35°C , 2 h. iii) Deoxygenated H_2O . iv) $H_3B \cdot SMe_2$, THF, r.t., 1 h.

2.3 NMR spectroscopic characterisation of 39-42

The 1H , $^{11}B\{^1H\}$, $^{13}C\{^1H\}$ and $^{31}P\{^1H\}$ NMR spectra of **39-42** are as expected. In the $^{31}P\{^1H\}$ NMR spectra each compound exhibits a broad quartet at -16.2 , -15.7 -22.3 and -8.6 ppm for **39-42**, respectively, due to coupling of the ^{31}P nucleus to the quadrupolar ^{11}B nucleus ($I = 3/2$, nat. ab. = 80.1%, $^1J_{PB} = 49.0$ Hz in each case); the magnitude of ^{31}P - ^{11}B coupling in secondary phosphine-boranes typically ranges between 38-58 Hz.⁸⁻¹² The $^{31}P\{^1H\}$ NMR spectrum of **41** is shown in Figure 2.3 for illustration. ^{31}P - ^{11}B coupling is confirmed in the corresponding $^{11}B\{^1H\}$ NMR spectra, which exhibit broad doublets at -39.8 , -40.1 , -40.6 and -40.6 ppm for **39-42**, respectively [$^1J_{PB} = 49.0$ Hz].

The quartets in the $^{31}P\{^1H\}$ spectra do not exhibit the expected signal ratio of 1:1:1:1, which may be a consequence of coupling to the ^{10}B isotope, which is also spin active but found in lower abundance than ^{11}B (^{10}B $I = 3$, nat. ab. = 19.9 %). The ^{10}B nucleus couples to ^{31}P to give a seven line multiplet, however the ^{31}P - ^{10}B coupling constant has a much lower value than for ^{31}P - ^{11}B ; the coupling of two nuclei is proportional to their magnetogyric ratios ($J_{ij} \propto \gamma_i \gamma_j$), which is approximately three times larger for ^{11}B than for ^{10}B ($\gamma = 8.58 \times 10^7$ and 2.87×10^7 rad $T^{-1}s^{-1}$, respectively).¹³ Therefore the observed signal in the $^{31}P\{^1H\}$ NMR spectra is a result of overlying ^{10}B and ^{11}B coupling, which is dominated by the more abundant ^{11}B isotope.

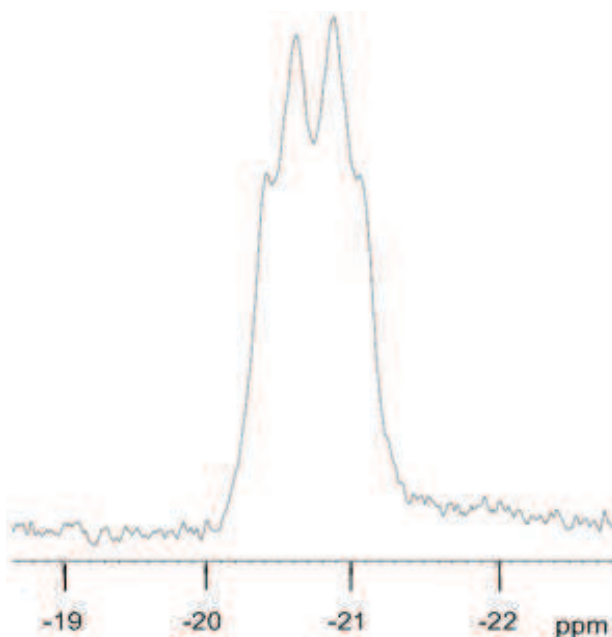


Figure 2.3. $^{31}\text{P}\{^1\text{H}\}$ NMR spectrum of **40** in CDCl_3 .

In the ^1H NMR spectra, the P-H signals are observed as a doublet of quartets of doublets in each compound, except for **42**, which has only been resolved as a doublet of quartets, lying at 5.97, 5.83, 6.04 and 5.72 ppm for **39-42** respectively (Figure 2.4). The splitting pattern is a result of the proton coupling to phosphorus, the borane protons and the adjacent C-H proton of the $\text{CH}(\text{SiMe}_3)$ group. The $^1J_{\text{PH}}$ coupling constants in **39-42** range from 359.0 to 385.0 Hz, and are consistent with values reported in related compounds;^{10,14-23} for example, for $\text{Ph}_2\text{P}(\text{BH}_3)$ $^1J_{\text{PH}} = 385$ Hz, whilst for $^t\text{BuPhP}(\text{BH}_3)$ $^1J_{\text{PH}} = 367$ Hz. The borane hydrogen atoms exhibit a broad quartet in the ^1H NMR spectra, and as a result cannot be easily identified or integrated. Therefore it is necessary to decouple the ^{11}B nucleus, which collapses the broad quartet into a sharp doublet of doublets, which are observed between 0.89 and 0.94, where $^2J_{\text{PH}} = 14.2, 14.7, 14.9, 15.3$ Hz, and $^3J_{\text{HH}} = 6.4, 7.1, 6.6$ and 6.6 Hz, for **39-42**, respectively. This effect can be seen in Figure 2.5, where the ^1H and $^1\text{H}\{^{11}\text{B}\}$ NMR spectra of compound **40** have been overlaid.

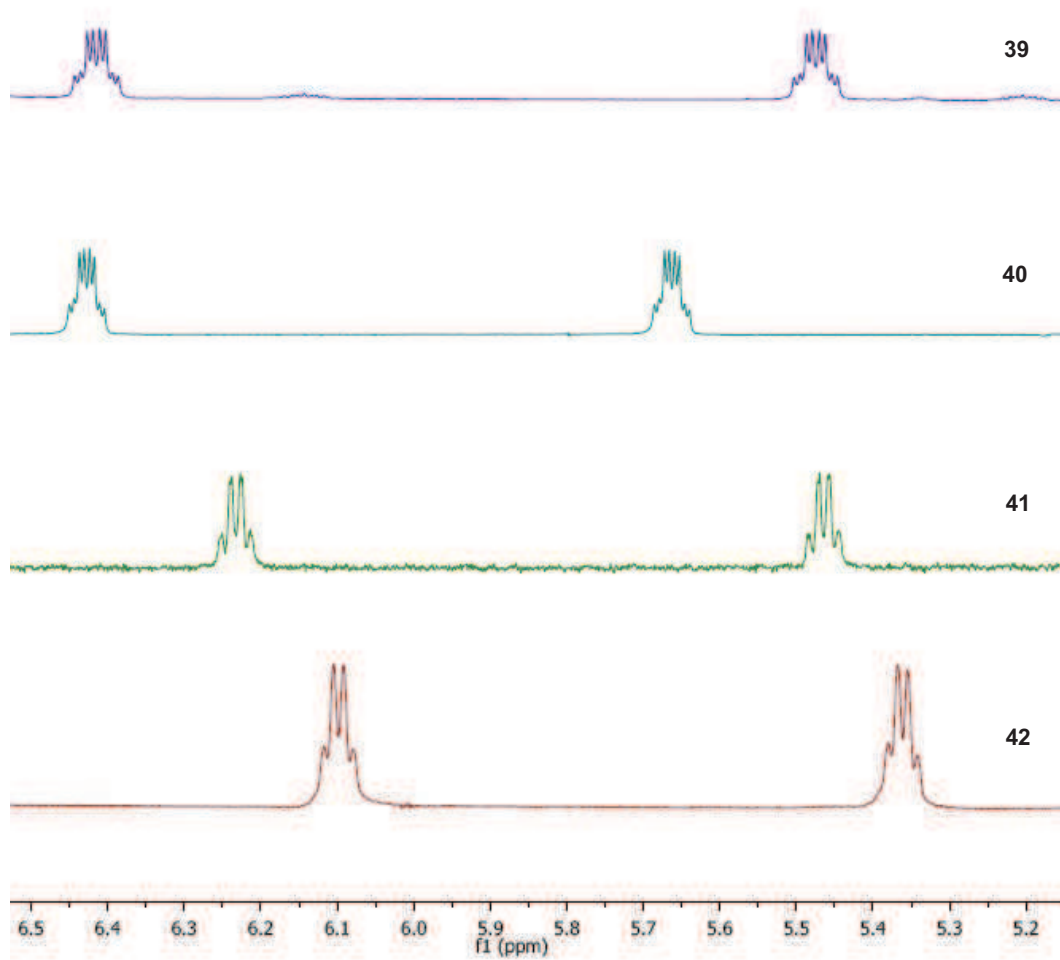


Figure 2.4. P-H region of the ¹H NMR spectra of compounds **39-42** in CDCl₃.

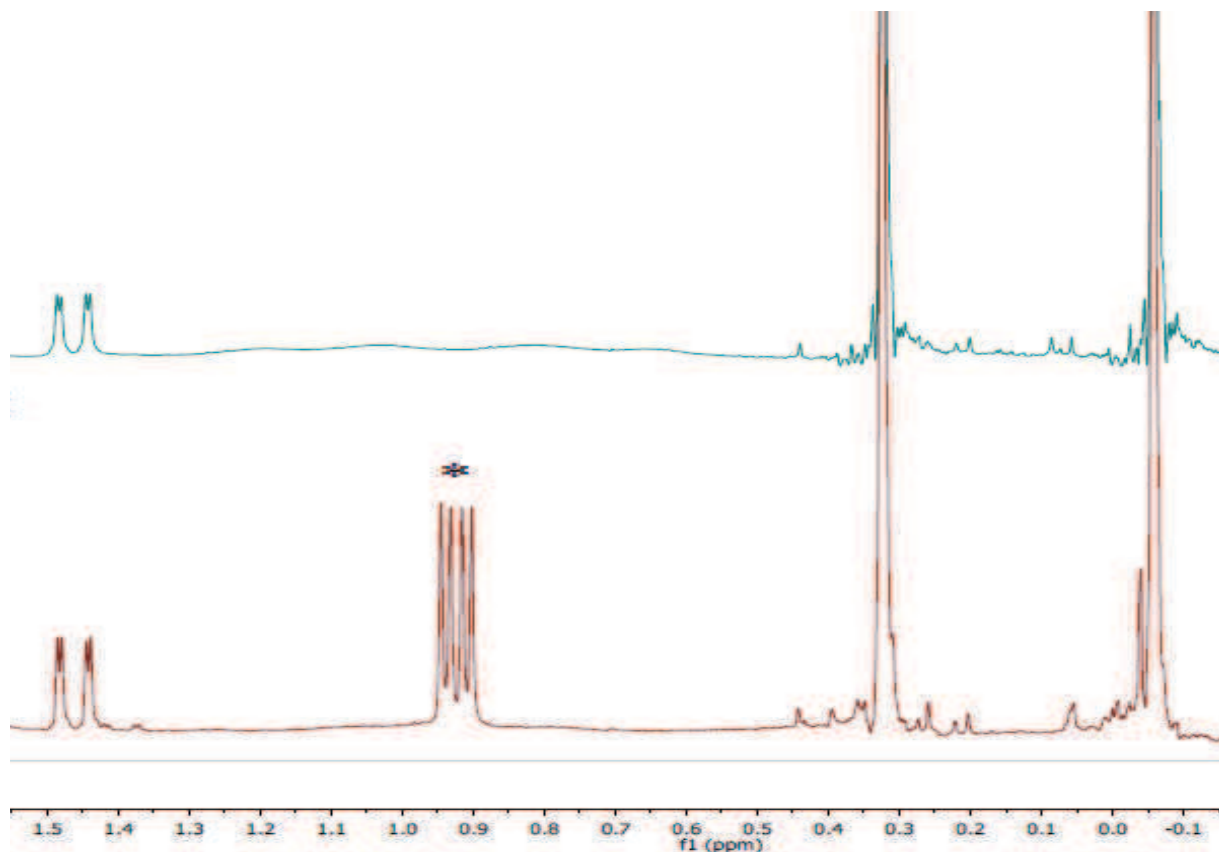


Figure 2.5. ^1H (above) and $^1\text{H}\{^{11}\text{B}\}$ (below) NMR spectra of compound **40** in CDCl_3 (* ^{11}B -decoupled borane hydrogens).

2.4 Solid-state structures of phosphine-boranes

X-ray diffraction studies of compounds **39**, **41** and **42** were carried out for comparison with the structures of the corresponding metalated phosphido-borane species (see chapters 3, 5, 6 and 7). The molecular structures of **39**, **41** and **42** are shown in Figures 2.6, 2.7 and 2.8 respectively, with selected bond lengths and angles shown in Tables 2.1, 2.2 and 2.3.

The P-B distances of 1.9232(18), 1.925(2) and 1.919(7) Å for **39**, **41** and **42** respectively, are very similar, and typical of P-B distances for secondary phosphine-boranes, which lie in the range of 1.91-1.95 Å.²⁴⁻³¹ The P-H distances in compounds **39**, **41** and **42** are identical to within experimental error [1.294(14), 1.32(2) and 1.35(4) Å respectively], and lie within the range of P-H distances that have previously been reported for related phosphine-boranes: 1.26-1.41 Å.²³⁻³⁰

The B-P-H angles for **39**, **41** and **42** fall in the typical range for phosphine-boranes [104-120.6°], however, the B-P-H angle is somewhat larger in **42** [118.1(15)°] than in **39** and **41** [110.8(7) and 110.6(9)°, respectively]. There are slight variations between the remaining bond angles about the phosphorus centre, but no significant differences; the sum of angles within the C₂PB framework for **39**, **41** and **42** are also identical to within experimental error [339.64, 339.68 and 340.07°, respectively].

In summary, the structures of **39**, **41** and **42** are unsurprising, with structural parameters, falling within typical values for secondary phosphine-boranes. However the non-donor functionalised **42** has a larger B-P-H bond angle in comparison to the donor-functionalised species.

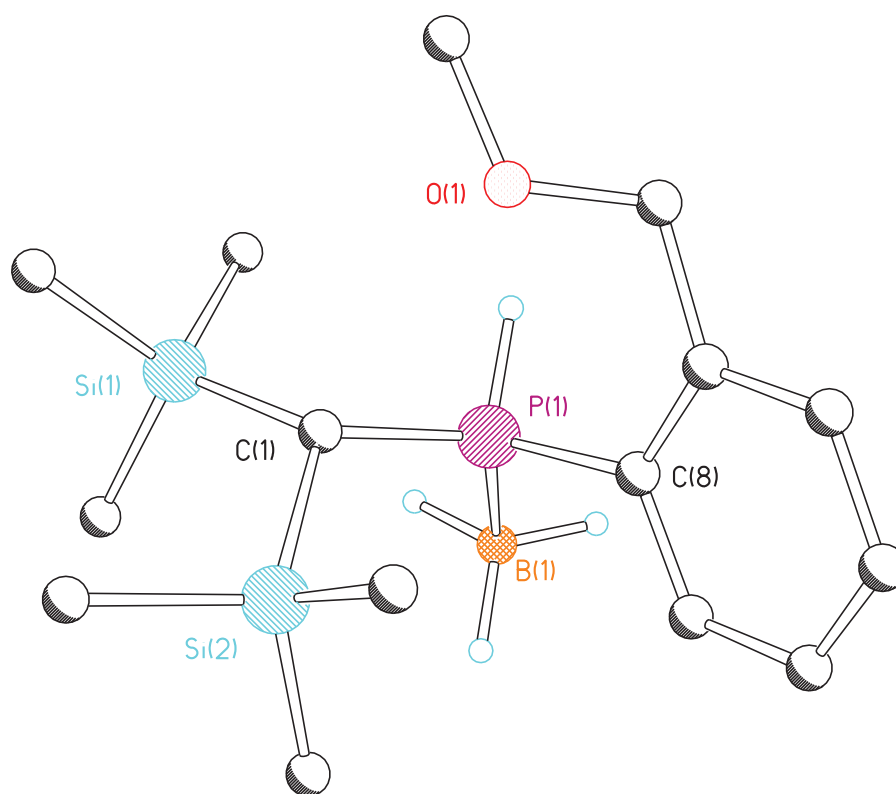


Figure 2.6. Structure of compound **39**. All C-bound H atoms omitted for clarity.

P(1)–B(1)	1.9232(18)	B(1)–P(1)–C(1)	118.23(7)
P(1)–C(8)	1.8135(14)	B(1)–P(1)–H(1)	110.8(7)
P(1)–C(1)	1.8101(13)	C(1)–P(1)–H(1)	103.4(6)
P(1)–H(1)	1.294(14)	B(1)–P(1)–C(8)	112.53(8)
B(1)–H(1C)	1.117(17)	C(1)–P(1)–C(8)	108.88(6)
B(1)–H(1A)	1.14(2)	C(8)–P(1)–H(1)	101.3(7)
B(1)–H(1B)	1.103(18)	P(1)–C(1)–Si(1)	113.09(7)
		P(1)–C(1)–Si(2)	115.60(7)
		Si(1)–C(1)–Si(2)	116.28(6)

Table 2.1. Selected bond lengths (Å) and angles (°) of compound **39**.

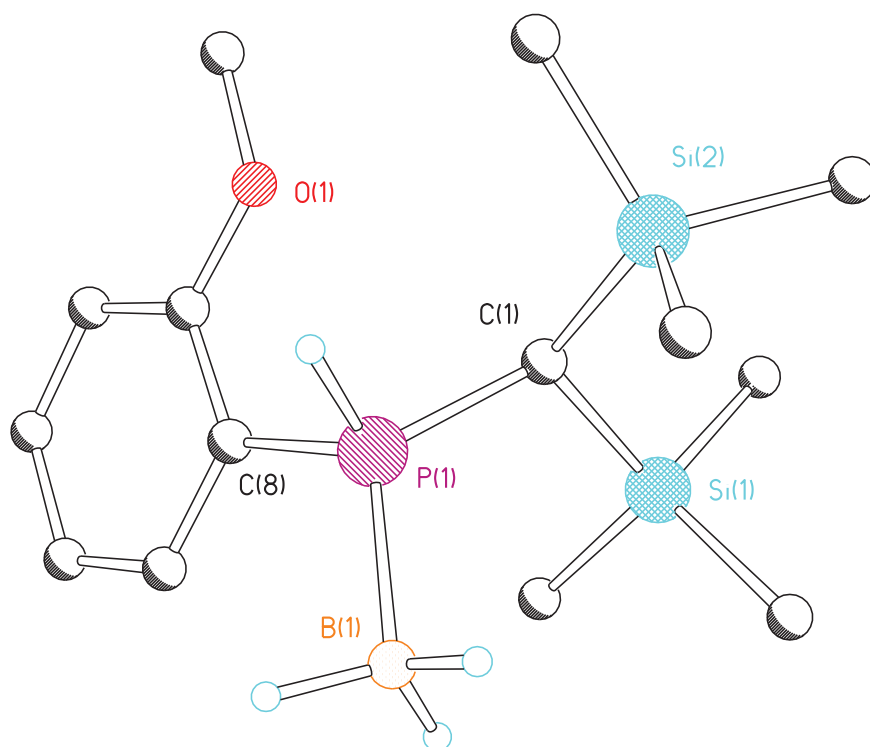


Figure 2.7. Structure of compound **41**. All C-bound H atoms omitted for clarity.

P(1)–B(1)	1.925(2)	B(1)–P(1)–C(1)	117.59(10)
P(1)–C(8)	1.8107(18)	B(1)–P(1)–H(1)	110.6(9)
P(1)–C(1)	1.8169(16)	C(1)–P(1)–H(1)	105.8(8)
P(1)–H(1)	1.32(2)	B(1)–P(1)–C(8)	112.72(9)
B(1)–H(1A)	1.05(2)	C(1)–P(1)–C(8)	109.37(8)
B(1)–H(1B)	1.11(2)	C(8)–P(1)–H(1)	98.9(9)
B(1)–H(1C)	1.10(2)	P(1)–C(1)–Si(1)	114.20(8)
		P(1)–C(1)–Si(2)	110.50(9)
		Si(1)–C(1)–Si(2)	117.95(9)

Table 2.2. Selected bond lengths (Å) and angles (°) of compound **41**.

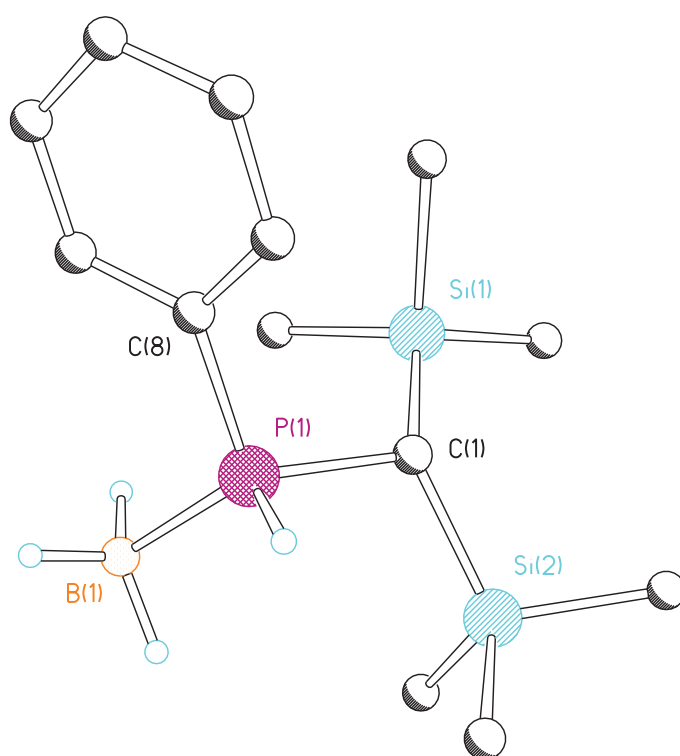


Figure 2.8. Structure of compound **42**. All C-bound H atoms omitted for clarity.

P(1)–B(1)	1.919(7)	B(1)–P(1)–C(1)	117.8(3)
P(1)–C(1)	1.814(4)	H(1)–P(1)–B(1)	118.1(15)
P(1)–C(8)	1.804(4)	H(1)–P(1)–C(1)	99.0(15)
P(1)–H(1)	1.35(4)	B(1)–P(1)–C(8)	113.9(3)
B(1)–H(1C)	1.17(6)	C(1)–P(1)–C(8)	108.37(17)
B(1)–H(1B)	1.02(6)	H(1)–P(1)–C(8)	96.9(15)
B(1)–H(1D)	1.05(5)	P(1)–C(1)–Si(1)	114.87(18)
		P(1)–C(1)–Si(2)	111.41(18)
		Si(1)–C(1)–Si(2)	117.39(18)

Table 2.3. Selected bond lengths (Å) and angles (°) of compound **42**.

2.5 References

- (1) Izod, K.; Wills, C.; Clegg, W.; Harrington, R. W. *Organometallics* **2005**, *25*, 38.
- (2) Izod, K.; Wills, C.; Clegg, W.; Harrington, R. W. *Dalton Trans.* **2007**, 3669.
- (3) Izod, K.; Wills, C.; Clegg, W.; Harrington, R. W. *Organometallics* **2007**, *26*, 2861.
- (4) Izod, K.; Bowman, L. J.; Wills, C.; Clegg, W.; Harrington, R. W. *Dalton Trans.* **2009**, 3340.
- (5) Bos, M. E.; Wulff, W. D.; Miller, R. A.; Chamberlin, S.; Brandvold, T. A. *J. Am. Chem. Soc.* **1991**, *113*, 9293.
- (6) Gynane, M. J. S.; Hudson, A.; Lappert, M. F.; Power, P. P.; Goldwhite, H. *J. Chem. Soc., Chem. Commun.* **1980**, 2428.
- (7) Slocum, D. W.; Book, G.; Jennings, C. A. *Tetrahedron Lett.* **1970**, *11*, 3443.
- (8) Bourumeau, K.; Gaumont, A.-C.; Denis, J.-M. *J. Organomet. Chem.* **1997**, *529*, 205.
- (9) Cowley, A. H.; Damasco, M. C. *J. Am. Chem. Soc.* **1971**, 6815.
- (10) Wolfe, B.; Livinghouse, T. *J. Org. Chem.* **2001**, *66*, 1514.
- (11) Carreira, M.; Charernsuk, M.; Eberhard, M.; Fey, N.; Ginkel, R. v.; Hamilton, A.; Mul, W. P.; Orpen, A. G.; Phetmung, H.; Pringle, P. G. *J. Am. Chem. Soc.* **2009**, *131*, 3078.
- (12) Petit, C.; Favre-Reguillon, A.; Mignani, G.; Lemaire, M. *Green Chem.* **2010**, *12*, 326.
- (13) Friebolin, H. *Basic One- and Two-Dimensional NMR spectroscopy*; 4th edn., Wiley VCH, Weinheim, 2005.
- (14) Rapp, B.; Drake, J. E. *Inorg. Chem.* **1973**, *12*, 2868.

- (15) Imamoto, T.; Osaiki, T.; Onoznuva, T.; Kusumoto, T.; Sato, K. *J. Am. Chem. Soc.* **1990**, *112*, 5245.
- (16) Grubbs, R. H.; Mohr, B.; Lynn, D. M. *Organometallics* **1996**, *15*, 4317.
- (17) Drake, J. E.; Simpson, J. *J. Chem. Soc., Chem. Commun.* **1967**, 249.
- (18) Van Overschelde, M.; Vervecken, E.; Modha, S. G.; Cogen, S.; Van der Eycken, E.; Van der Eycken, J. *Tetrahedron* **2009**, *65*, 6410.
- (19) McNulty, J.; Zhou, Y. *Tetrahedron Lett.* **2004**, *45*, 407.
- (20) Busacca, C. A.; Farber, E.; DeYoung, J.; Campbell, S.; Gonnella, N. C.; Grinberg, N.; Haddad, N.; Lee, H.; Ma, S.; Reeves, D.; Shen, S.; Senanayake, C. H. *Org. Lett.* **2009**, *11*, 5594.
- (21) Nagata, K.; Matsukawa, S.; Imamoto, T. *J. Org. Chem.* **2000**, *65*, 4185.
- (22) Bitterer, F.; Herd, O.; Kühnel, M.; Stelzer, O.; Weferling, N.; Sheldrick, W. S.; Hahn, J.; Nagel, S.; Rösch, N. *Inorg. Chem.* **1998**, *37*, 6408.
- (23) Panossian, A.; Fernández-Pérez, H.; Popa, D.; Vidal-Ferran, A. *Tetrahedron: Asymmetry* **2010**, *21*, 2281.
- (24) Anderson, B. J.; Guino-o, M. A.; Glueck, D. S.; Golen, J. A.; Di Pasquale, A. G.; Liable-Sands, L. M.; Rheingold, A. L. *Org. Lett.* **2008**, *10*, 4425.
- (25) Dorn, H.; Singh, R. A.; Massey, J. A.; Nelson, J. M.; Jaska, C. A.; Lough, A. J.; Manners, I. *J. Am. Chem. Soc.* **2000**, *122*, 6669.
- (26) Dorn, H.; Vejzovic, E.; Lough, A. J.; Manners, I. *Inorg. Chem.* **2001**, *40*, 4327.
- (27) Bader, A.; Pabel, M.; Willis, A. C.; Wild, S. B. *Inorg. Chem.* **1996**, *35*, 3874.
- (28) Day, M. W.; Mohr, B.; Grubbs, R. H. *Acta Cryst. Sect. C* **1996**, *C52*, 3106.

- (29) Pelczar, E. M.; Nytko, E. A.; Zhuravel, M. A.; Smith, J. M.; Glueck, D. S.; Sommer, R.; Incarvito, C. D.; Rheingold, A. L. *Polyhedron* **2002**, *21*, 2409.
- (30) Clark, T. J.; Rodezno, J. M.; Clendenning, S. B.; Aouba, S.; Brodersen, P. M.; Lough, A. J.; Ruda, H. E.; Manners, I. *Chem. Eur. J.* **2005**, *11*, 4526.
- (31) Dornhaus, F.; Bolte, M.; Lerner, H.-W.; Wagner, M. *J. Organomet. Chem.* **2007**, *692*, 2949.

Chapter 3. Alkali metal complexes of a benzyl-methylether-functionalised phosphido-borane

3.1 Introduction

Phosphido-borane complexes of the alkali metals are highly reactive intermediates, often used in the preparation of synthetically important chiral phosphines,^{1,2} but are usually generated *in situ* and as a result there are few examples of these compounds that have been characterised in the solid state (chapter 1.4). This is rather surprising given the considerable interest in complexes of organophosphides with main group metals (chapter 1.2), and in complexes of silyl anions of the type $(R_2SiMe)^-$, which are isoelectronic with phosphido-boranes.

There have, however, been a small number of reports detailing the solid-state structures of anionic phosphido-borane complexes with transition metals (Figure 3.1). These compounds can be prepared either *via* metathesis reactions between a transition metal halide and an alkali metal phosphido-borane complex (Scheme 3.1³) or *via* oxidative addition of a phosphine-borane adduct to a low oxidation state transition metal complex. Although these examples rarely demonstrate any B-H...M interactions,⁴ such as those observed in the group I complexes,^{3,5-9} the structures obtained provide an insight into the activity of transition metal-catalysed reactions with phosphine-boranes, such as dehydrogenation, dehydrocoupling or cross-coupling reactions.⁹⁻¹⁴

It has previously been shown that phosphides containing peripheral donor-functionality can provide additional stabilisation in complexes with group I and II metals through intramolecular interactions between the donor atom and the metal.¹⁵⁻¹⁷ However, to date there are no examples of donor-functionalised phosphido-borane complexes with main group metals that have been characterised in the solid-state. This chapter details the synthesis and characterisation of a series of phosphido-borane complexes prepared from compound **39** with alkali metals and considers the effects of cation size on structure.

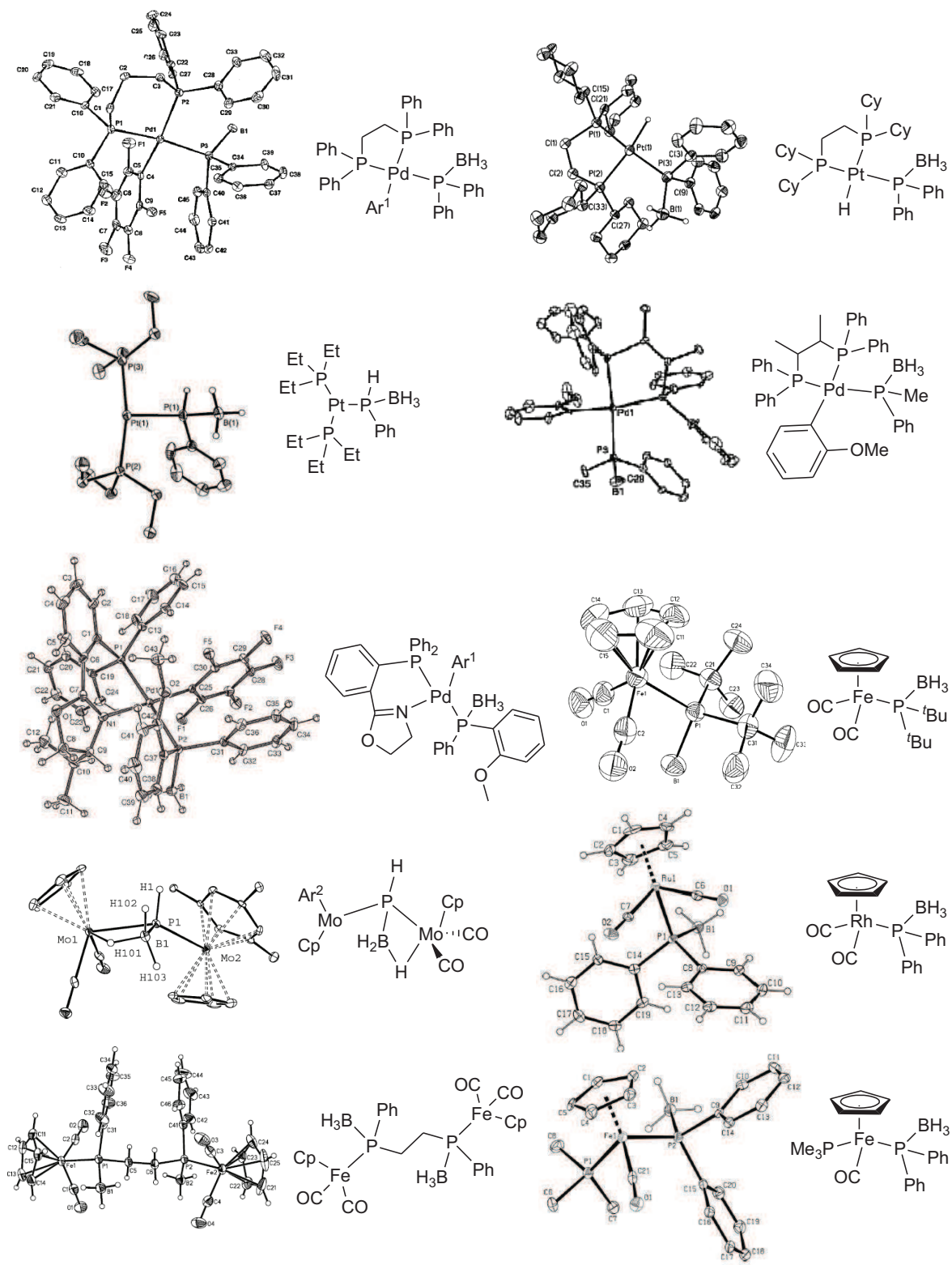
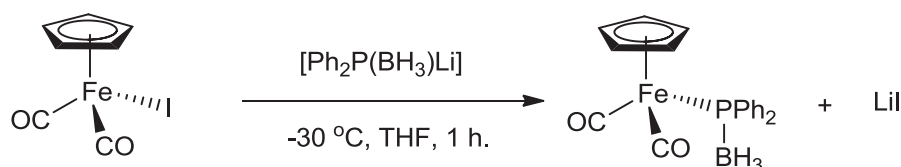


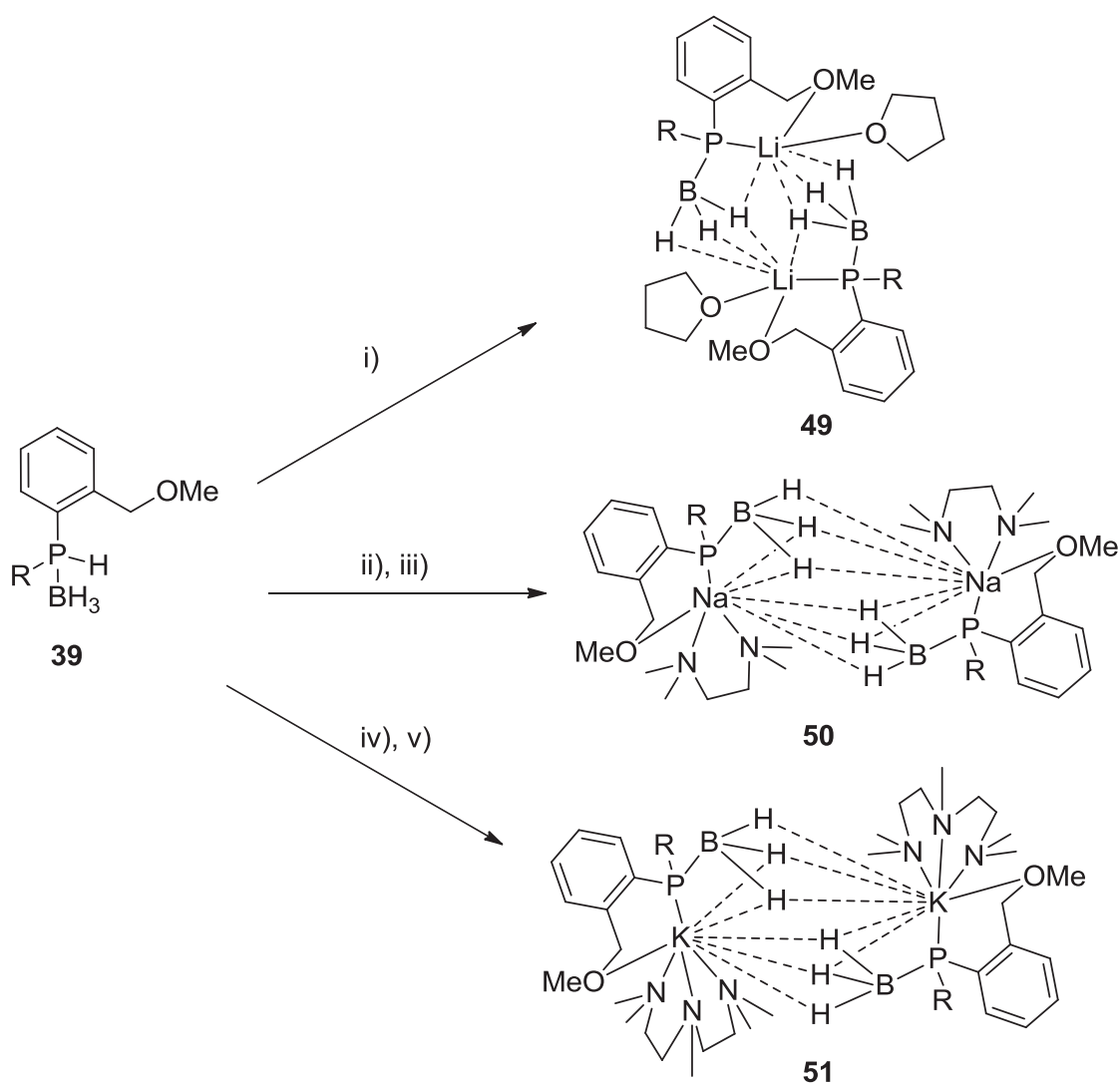
Figure 3.1. Phosphido-borane complexes with transition metals [Ar¹ = C₆F₅, Ar² = 1,3,5-tri-tert-butylphenyl].⁴⁻¹⁴



Scheme 3.1. Synthesis of a phosphido-borane complex with Fe *via* salt elimination.

3.2 Synthesis of the alkali metal complexes $[\{(\text{Me}_3\text{Si})_2\text{CH}\}\text{P}(\text{C}_6\text{H}_4\text{-2-CH}_2\text{OMe})(\text{BH}_3)\text{M}(\text{L})]_2$ [$\text{M}(\text{L}) = \text{Li}(\text{THF})$ (**49**), $\text{Na}(\text{tmeda})$ (**50**), $\text{K}(\text{pmdeta})$ (**51**)]

Treatment of **39** with one equivalent of $n\text{BuLi}$ in THF yields the corresponding phosphido-borane. Removal of the solvent gives a yellow solid, which may be crystallised from methylcyclohexane containing a few drops of THF as colourless needles of the adduct $[\{(\text{Me}_3\text{Si})_2\text{CH}\}\text{P}(\text{C}_6\text{H}_4\text{-2-CH}_2\text{OMe})(\text{BH}_3)\text{Li}(\text{THF})]_2$ (**49**). The reaction between **39** and one equivalent of either BnNa or BnK in THF yields the corresponding heavier alkali metal salts, which upon removal of the solvent yields a yellow and an orange solid, respectively. The sodium compound was crystallised from toluene in the presence of one equivalent of tmeda to yield colourless blocks of the adduct $[\{(\text{Me}_3\text{Si})_2\text{CH}\}\text{P}(\text{C}_6\text{H}_4\text{-2-CH}_2\text{OMe})(\text{BH}_3)\text{Na}(\text{tmeda})]_2$ (**50**), whereas the potassium compound was crystallised from toluene in the presence of pmdeta, also as colourless blocks, as the adduct $[\{(\text{Me}_3\text{Si})_2\text{CH}\}\text{P}(\text{C}_6\text{H}_4\text{-2-CH}_2\text{OMe})(\text{BH}_3)\text{K}(\text{pmdeta})]_2$ (**51**).



Scheme 3.2. Synthesis of compounds **49-51**. i) $n\text{BuLi}$, THF, 1 h, r.t. ii) BnNa , THF, 1h, r.t. iii) tmeda, toluene. iv) BnK , THF, 1h, r.t. vi) pmdeta, toluene [R = $(\text{Me}_3\text{Si})_2\text{CH}$].

3.3 Solution-phase characterisation of compounds **49-51**

Upon metalation, the $^{31}\text{P}\{^1\text{H}\}$ NMR signal shifts significantly from -16.2 ppm for **39** to -66.6, -65.3 and -64.2 ppm for **49**, **50** and **51**, respectively, consistent with single phosphido-borane ligand environments. The ^{31}P - ^{11}B coupling constants decrease with decreasing electronegativity of the cation, which occurs, approximately, in the order of 10 Hz increments [$^1J_{\text{PB}} = 49.0$ (**39**), 37.2 (**49**), 29.4 (**50**), and 19.6 Hz (**51**)], which is consistent with increasing ionic character of the P-M interaction.

The ^1H and $^{13}\text{C}\{^1\text{H}\}$ NMR spectra are as expected. In the ^1H NMR spectra the BH_3 protons exhibit a broad quartet at 0.6-0.8 ppm, which can be collapsed into a sharp doublet [$^2J_{\text{PH}} = 14.6$ (**49**), 5.5 (**50**), 5.0 Hz (**51**)] by decoupling the ^{11}B nucleus appearing at between 0.6 and 0.88 ppm for **49-50**. The diastereotopic Me_3Si groups appear as two sharp signals, whilst the CHP protons appear as unresolved singlets between 0.3 and 0.4 ppm. In the $^{13}\text{C}\{^1\text{H}\}$ NMR spectra, the SiMe_3 groups also appear as two separate signals, whereas the CH carbon adjacent to the phosphorus atom appears as a doublet at 8.01 and 8.26 ppm for **50** and **51** [$^1J_{\text{PC}} = 47.9$ (**50**), 49.8 Hz (**51**)], respectively, but does not appear in **49**.

3.4 Solid-state structures of compounds 49-51

3.4.1 Solid-state structure of 49

Compound **49** crystallises as discrete dimers; the molecular structure of **49** is shown in Figure 3.2 and details of selected bond lengths and angles are shown Table 3.1. Each lithium ion is bound to the P and O atoms of the phosphido-borane ligand, generating a six-membered chelate ring [P-Li-O bite angle $84.8(2)^\circ$]. The coordination sphere of each lithium ion is completed by a molecule of THF, an η^1 -interaction with one of the borane hydrogen atoms, and an η^3 - BH_3 interaction with the borane group from the adjacent phosphido-borane ligand in the dimer, such that each borane group acts as a μ_2 - η^1 : η^3 bridge between the lithium metal centres. The two halves of the dimer thus form a planar, pseudo-six-membered $[\text{PLi}(\text{BH}_3)]_2$ ring.

By comparison, the majority of structurally characterised group I complexes with isoelectronic silyl anions $(\text{R}_2\text{SiMe})^-$ crystallise as monomers,¹⁸⁻²² although the peripherally donor-functionalised compound $[\text{Ph}(\text{C}_5\text{H}_5\text{NCH}_2)\text{MeSiLi}(\text{THF})]_2$ (**52**) crystallises as a dimer with a Si_2Li_2 core.²³ However, unlike **49**, the two halves of the dimer in **52** are linked by the peripheral donor substituents of each ligand, which coordinate to the adjacent lithium ion in the dimer, thus forming intramolecular bridges (Figure 3.3).

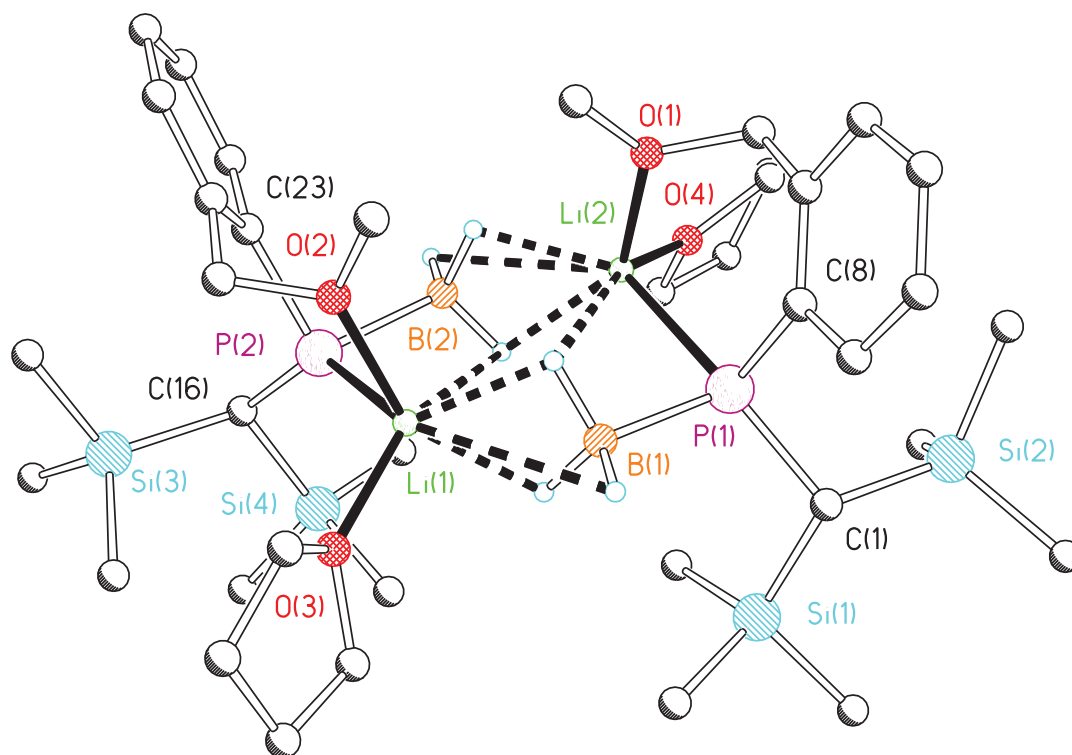


Figure 3.2. Structure of compound 49. All C-bound H atoms omitted for clarity.

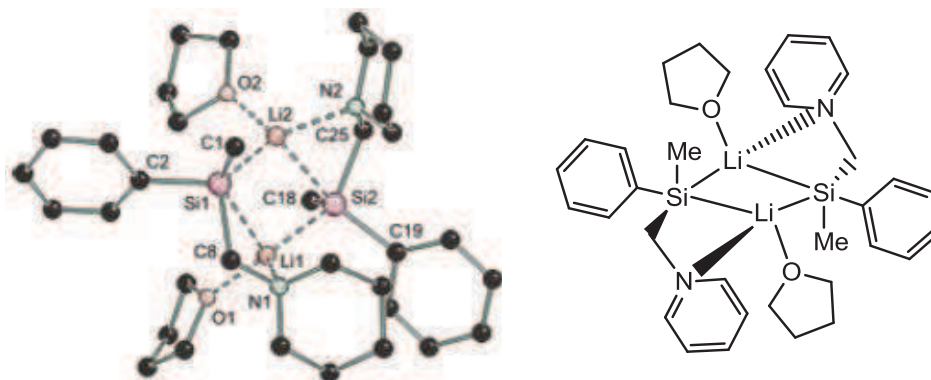


Figure 3.3. Structure of compound 52.²³

P(1)–Li(2)	2.611(6)	B(1)–P(1)–Li(2)	94.28(19)
P(2)–Li(1)	2.657(6)	B(2)–P(2)–Li(1)	98.86(19)
P(1)–B(1)	1.977(4)	B(1)–P(1)–C(8)	98.68(17)
P(2)–B(2)	1.983(4)	B(2)–P(2)–C(23)	98.25(17)
O(1)–Li(2)	1.988(6)	C(1)–P(1)–C(8)	102.05(15)
O(2)–Li(1)	1.982(7)	C(16)–P(2)–C(23)	103.08(16)
B(1)–Li(1)	2.370(8)	Li(2)–P(1)–C(8)	110.07(17)
B(2)–Li(2)	2.453(7)	Li(1)–P(2)–C(23)	107.08(18)
Li(1)–H(1A)	1.98(4)	P(2)–Li(1)–O(2)	89.5(2)
Li(1)–H(1B)	1.97(4)	P(1)–Li(2)–O(1)	84.8(2)
Li(2)–H(2C)	2.05(4)		

Table 3.1. Selected bond lengths (Å) and angles (°) for **49**.

The P–Li distance of 2.611(6) Å in **49** is only slightly shorter than the corresponding distance reported for [Me₂P(BH₃)Li(tmeda)] (**29**) [2.620(4) Å] but is typical of Li–P distances of 4-coordinate lithium phosphide complexes.^{24–27} The η³-BH₃...Li distances in **49** [1.98(4) Å] are comparable to similar η³-type borane-lithium interactions. For example, the Li–H distances in [Li(BH₄)(THF)₃] (**53**) are 2.02(4), 2.10(5) and 2.12(4) Å, and in the complex [Li(η³-BH₄)(NC₅H₄-4-Me)₃] (**54**) the Li–H distances are 2.10(2), 2.20(2) and 2.10(2) Å (Figure 3.4).^{28,29} The Li–H distances for the bridging borane hydrogen atoms in the dimer are 2.05(4) Å, which is consistent with other μ₂-η¹ bridges; for example, the η¹-BH₃-Li distances in [Li(BH₄)(MeNCH₂)₃] (**55**) is 2.08(1) Å,³⁰ while the corresponding distances in [LiBH₄(py-2-Me)₂] (**56**) are 2.134(6) and 2.184(7) Å.²⁹

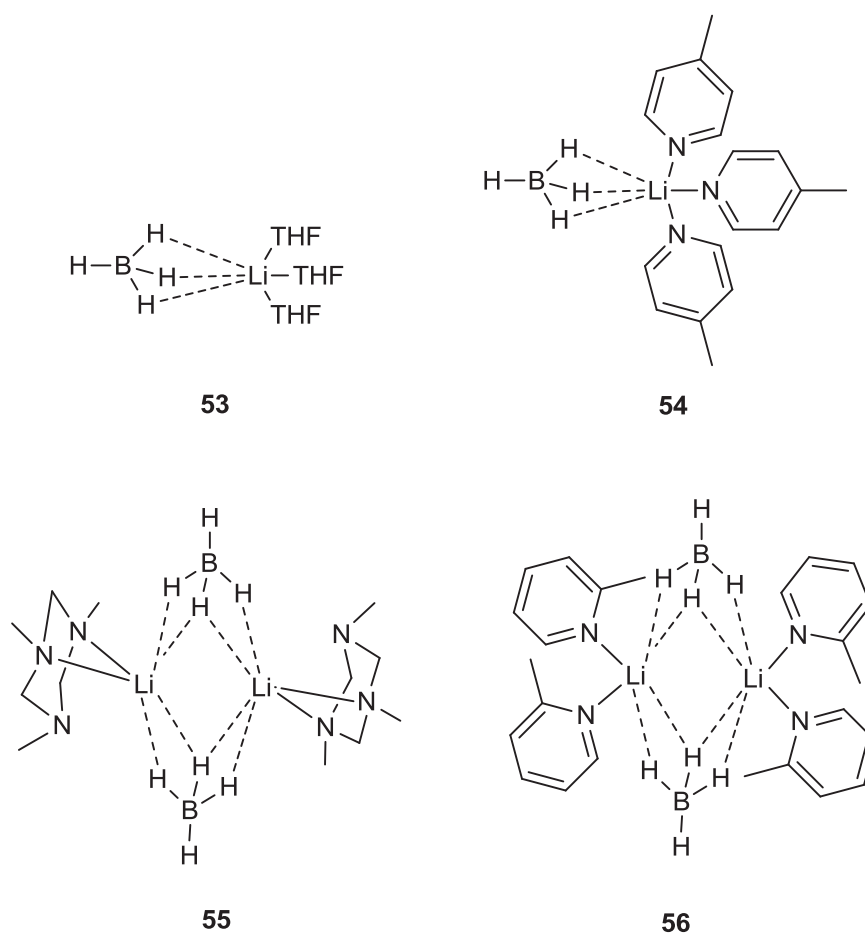


Figure 3.4. Structures of complexes **53-56**, which exhibit BH_n-Li interactions.

3.4.2 Solid-state structure of **50**

Compound **50** crystallises as discrete centrosymmetric dimers in which the phosphido-borane ligand adopts a tridentate coordination mode; the structure of **50** is shown in Figure 3.5 and selected bond length and angles are given in Table 3.2. Each phosphido-borane ligand binds the adjacent sodium ion through its P and O atoms to give a six-membered chelate ring [P(1)-Na(1)-O(1) bite angle 76.40(6)°], and in an η² fashion through two borane hydrogen atoms, which bridge the two sodium ions in the dimer. The third borane hydrogen of each group is η¹-bonded to the second sodium ion, such that each borane group acts as a μ₂-η²:η³ bridge between the cations, forming a rhombus-shaped pseudo-four-membered ring. The coordination of the sodium ions is completed by the N atoms of a chelating molecule of

tmeda. The η^2 and η^3 nature of the Na...B interactions in **50** is consistent with the bond distances observed [Na(1)-B(1) = 2.989(4), Na(1)-B(1A) = 2.844(3) Å].

The P-Na, O-Na and H-Na distances are longer than the corresponding bond lengths observed in compound **49** [P(1)-Na(1) 3.0528(13), P(1)-Li(1) 2.611(6) Å; O(1)-Na(1) 2.445(2), O(1)-Li(1) 1.988(6) Å; Na(1)-H(1B) 2.44(3), Li(1)-H(1B) 1.97(4) Å], whilst the P-Na-O bite angle of 76.4(6)° is significantly smaller than the P-Li-O angle in **49**, all of which are consistent with the greater ionic radius of sodium than lithium. The P-Na bond lengths in **50** lie just outside the range of previously reported P-Na distances (2.8-3.0 Å),^{16,31-33} however the Na-O distances in **50** of 2.445(2) Å are somewhat shorter than the related Na-O distances in [{(C₆H₄-2-OMe)₂P}Na(diglyme)]₂ (**16**) [2.531(3) and 2.563(3)].¹⁶

The Na-H distances in **50** [2.32-2.91 Å] are comparable with those in [Na(BH₄)(pmdeta)]₂ (**57**) [2.49(3)-2.58(3) Å], which also exhibits a μ_2 - η^2 : η^3 BH₃ binding mode. The Na...B distances in **57** [Na(1A)...B(1) 2.727(4), Na(1)...B(1) 2.867(4) Å] are similar to the corresponding η^2 -BH₃-Na and η^3 -BH₃-Na interactions observed in **50**.³⁰ Similarly, in [Na(η^3 -BH₄)(15-crown-5)(py)_{0.5}] (**58**), the Na-H bond lengths [2.28(2), 2.42(2), 2.74(2) Å] are comparable to those observed in **50**, but the Na...B distances [**58** 2.659(3) Å] are shorter in the former compound.²⁹

P(1)–Na(1)	3.0528(13)	P(1)–C(1)	1.882(3)
P(1)–B(1)	1.972(3)	P(1)–C(8)	1.855(3)
Na(1)–O(1)	2.445(2)	Na(1)–N(1)	2.639(7)
Na(1)–H(1AA)	2.91(4)	Na(1)–N(2)	2.542(3)
Na(1)–H(1BA)	2.32(4)		
Na(1)–H(1CA)	2.76(4)	P(1)–B(1)–Na(1)	72.70(11)
Na(1)–H(1B)	2.44(3)	C(1)–P(1)–C(8)	101.23(13)
Na(1)–H(1C)	2.91(4)	C(8)–P(1)–B(1)	96.90(14)
Na(1)–B(1)	2.989(4)	P(1)–Na(1)–O(1)	76.40(6)
Na(1)–B(1A)	2.844(3)	P(1)–Na(1)–B(1)	38.08(7)

Table 3.2. Selected bond lengths (Å) and angles (°) for **50**.

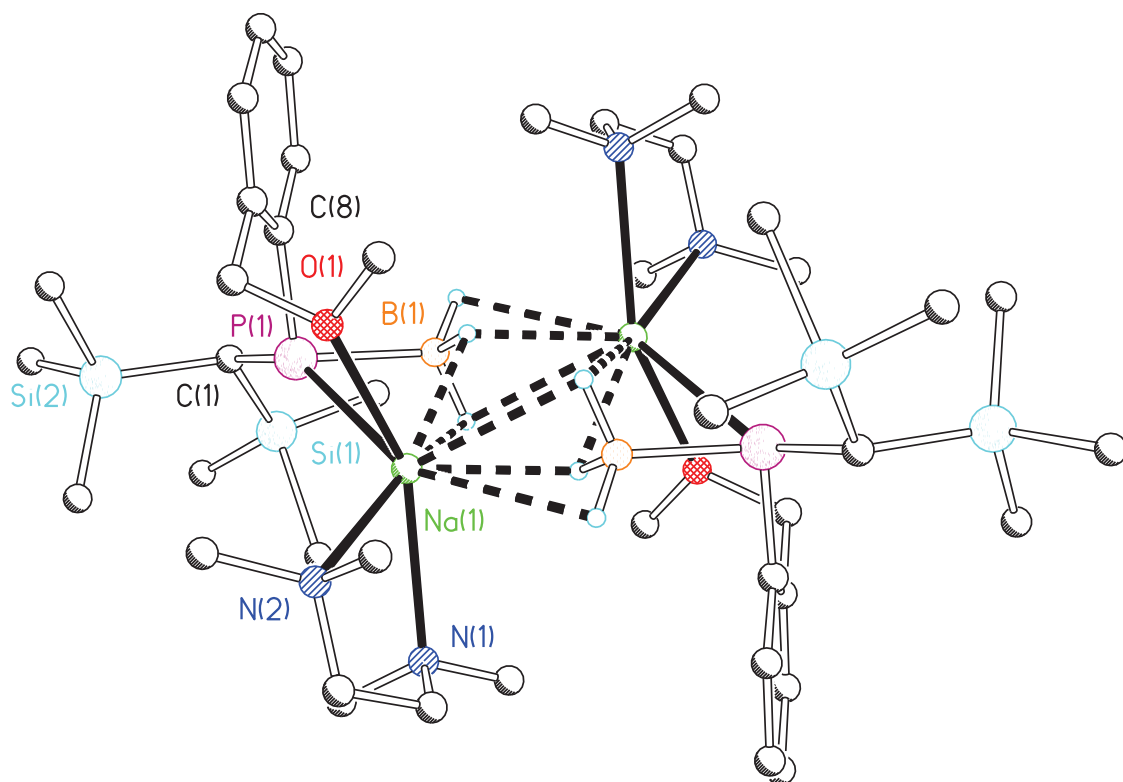


Figure 3.5. Structure of compound **50**. All C-bound H atoms omitted for clarity.

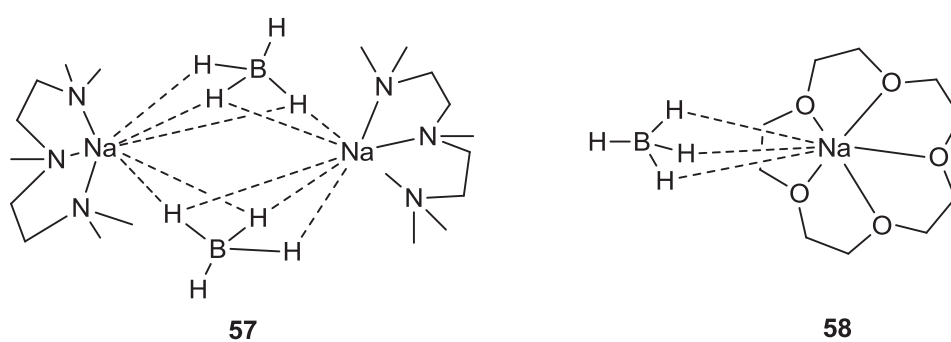


Figure 3.6. Structures of compounds **57** and **58**, which exhibit η^3 -Na-BH_n interactions.

3.4.3 Solid-state structure of **51**

Like **50**, compound **51** also crystallises as centrosymmetric dimers; the structure of **51** is shown in Figure 3.7, with selected bond lengths and angles shown in Table 3.3. Each potassium ion is bound by the P and O atoms of the adjacent phosphido-borane ligand, forming a six-membered chelate ring, and through the borane hydrogen atoms; the adjacent borane group binds in a η^2 -manner, and the second ligand binds in a η^3 -fashion, such that each borane group acts as a $\mu_2\text{-}\eta^2\text{:}\eta^3$ bridge between the two potassium ions. The coordination of each potassium ion is completed by the three nitrogen atoms and by a short Me...K contact with the central methyl group of a molecule of pmdeta, making the potassium ion pseudo-eight-coordinate.

The K-P bond length in **51** [3.7620(10) Å] is significantly longer than the corresponding distance in the related potassium salt **32** [3.320(2) Å], which also exhibits a P, BH_3 binding mode. The K(1)...B(1A) distance in **51** [3.322(3) Å] is also somewhat longer than the corresponding distance in **32** [3.162 Å], despite both having $\eta^2\text{-}BH_3$ coordination modes, whereas the K(1)...B(1) distance in **51** [3.103(3) Å] is slightly shorter than this, consistent with η^3 -coordination. The P-K-O bite angle of $60.74(3)^\circ$ in **51** is significantly smaller than the bite angles in **49** and **50**, which is consistent with the greater ionic radius of potassium than of sodium and lithium.

K(1)–P(1A)	3.7620(10)	K(1)–H(2)	2.970(19)
K(1)–N(1)	3.0339(19)	K(1)–H(3)	3.06(2)
K(1)–N(2)	2.9192(18)	K(1)–H(1A)	2.80(2)
K(1)–N(3)	2.9054(19)	K(1)–H(3A)	3.095(20)
K(1)–O(1A)	2.8239(16)		
K(1)–B(1)	3.103(3)	P(1A)–K(1)–O(1A)	60.74(3)
K(1)–B(1A)	3.322(3)	P(1A)–K(1)–B(1A)	31.82(4)
P(1)–B(1)	1.987(3)	B(1)–P(1)–C(1)	110.01(10)
P(1)–C(1)	1.894(2)	B(1)–P(1)–C(8)	99.18(10)
P(1)–C(8)	1.861(2)	C(1)–P(1)–C(8)	101.39(9)
K(1)–H(1)	2.816(18)	K(1A)–P(1)–B(1)	61.79(7)

Table 3.3. Selected bond lengths (Å) and angles ($^\circ$) of compound **51**.

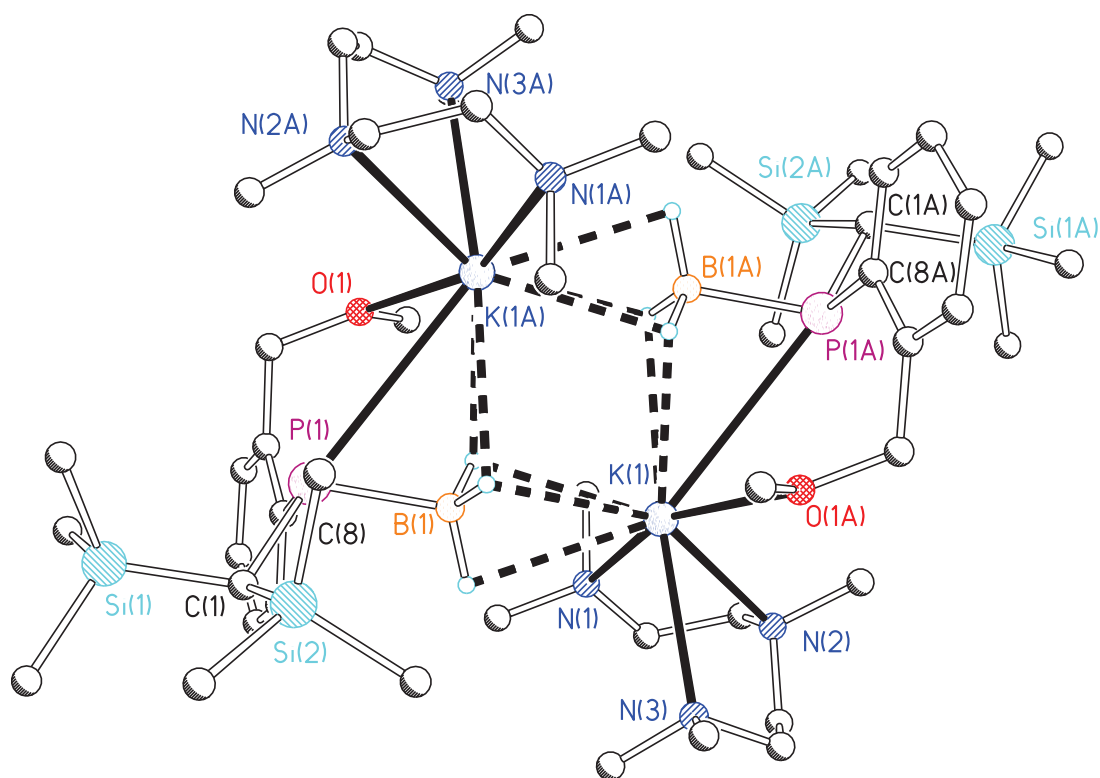


Figure 3.7. Structure of compound **51**. All C-bound H atoms eliminated for clarity.

The K-H distances in **51** are similar to other reported BH_n -K distances; for example the η^2 - BH_n distances in **51** [2.80(2) and 3.095(20) Å] are comparable to those in [K($H_2BC_5H_{10}$)(18-crown-6)] (**59**) [K(1)-H(1) 2.58(2), K(1)-H(2) 2.66(2) Å],²⁹ while the η^3 -type interactions [2.816(18), 2.970(19) and 3.06(2) Å] are similar to those in [K(BH_4)(18-crown-6)] (**60**, Figure 3.8) [K(1)-H(11) 2.85(6), K(1)-H(13) 2.61(8), K(1)-H(14) 2.77(7) Å].²⁹

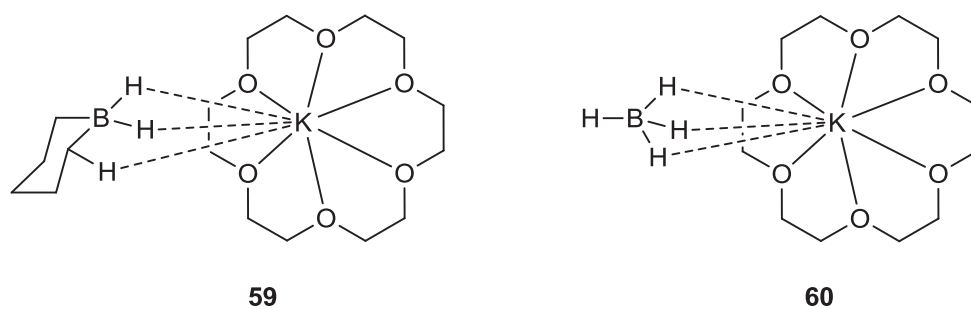


Figure 3.8. Structures of complexes which exhibit η^2 and η^3 K- BH_n interactions.

3.5 Conclusions

This chapter demonstrates that the alkali metal complexes of the phosphido-borane anion $[\{(Me_3Si)_2CH\}P(BH_3)(C_6H_4-2-CH_2OMe)]^-$ are readily accessible using straightforward synthetic procedures. Compounds **49-51** crystallise as dimers in the presence of THF, tmeda, or pmdeta, respectively, demonstrating ‘tridentate’ coordination of the phosphido-borane ligand, through P-M, B...M and O-M contacts with the metal centre. Compound **50** is the first example of a phosphido-borane complex with sodium.

The dimeric nature of the structures of these complexes is a result of agostic-type B-H-M interactions; within the lithium complex, the two halves of the dimer are bridged by the borane groups in a $\mu_2-\eta^1:\eta^3$ fashion, whereas the two halves of both the sodium and potassium complexes are bridged in a $\mu_2-\eta^2:\eta^3$ manner by the borane groups.

As expected, the P-M, O-M and BH-M distances increase with increasing radius of the cation, and likewise, the P-M-O and M-B-P bite angles decrease with increasing ionic radius of the alkali metal.

3.6 References

- (1) Imamoto, T.; Kusumoto, T.; Suzuki, N.; Sato, K. *J. Am. Chem. Soc.* **1985**, *107*, 5301.
- (2) Burk, M. J.; Pizzano, A.; Martín, J. A.; Liable-Sands, L. M.; Rheingold, A. L. *Organometallics* **2000**, *19*, 250.
- (3) Lee, K.; Clark, T. J.; Lough, A. J.; Manners, I. *Dalton Transactions* **2008**, 2732.
- (4) Amor, I.; García-Vivó, D.; García, M. E.; Ruiz, M. A.; Sáez, D.; Hamidov, H.; Jeffery, J. C. *Organometallics* **2007**, *26*, 466.
- (5) Müller, G.; Brand, J. *Organometallics* **2003**, *22*, 1463.
- (6) Dornhaus, F.; Bolte, M.; Lerner, H.-W.; Wagner, M. *Eur. J. Inorg. Chem.* **2006**, 5138.

- (7) Dornhaus, F.; Bolte, M.; Lerner, H.-W.; Wagner, M. *Eur. J. Inorg. Chem.* **2006**, 1777.
- (8) Rudzevich, L. R.; Gornitzka, H.; Romanenko, V. D.; Bertrand, G. *Chem. Commun.* **2001**, 1634.
- (9) Dornhaus, F.; Bolte, M.; Lerner, H.-W.; Wagner, M. *J. Organomet. Chem.* **2007**, 692, 2949.
- (10) Gaumont, A.-C.; Hursthouse, M. B.; Coles, S. J.; Brown, J. M. *Chem. Commun.* **1999**, 63.
- (11) Jaska, C. A.; Lough, A. J.; Manners, I. *Dalton Trans.* **2005**, 326.
- (12) Moncarz, J. R.; Brunker, T. J.; Glueck, D. S.; Sommer, R. D.; Rheingold, A. L. *J. Am. Chem. Soc.* **2003**, 125, 1180.
- (13) Jaska, C. A.; Lough, A. J.; Manners, I. *Inorg. Chem.* **2004**, 43, 1090.
- (14) Dorn, H.; Jaska, C. A.; Singh, R. A.; Lough, A. J.; Manners, I. *Chem. Commun.* **2000**, 1041.
- (15) Blair, S.; Izod, K.; Clegg, W.; Harrington, R. W. *Inorg. Chem.* **2004**, 43, 8526.
- (16) Aspinall, H. C.; Tillotson, M. R. *Inorg. Chem.* **1996**, 35, 5.
- (17) Clegg, W.; Doherty, S.; Izod, K.; Kagerer, H.; O'Shaughnessy, P.; M. Sheffield, J. *J. Chem. Soc., Dalton Trans.* **1999**, 1825.
- (18) Cai, X.; Gehrhus, B.; Hitchcock, P. B.; Lappert, M. F.; Slootweg, J. C. *J. Organomet. Chem.* **2002**, 643-644, 272.
- (19) Däschlein, C.; Strohmam, C. *Eur. J. Inorg. Chem.* **2009**, 2009, 43.
- (20) Strohmam, C.; Däschlein, C. *Chem. Commun.* **2008**, 2791.
- (21) Strohmam, C.; Däschlein, C.; Auer, D. *J. Am. Chem. Soc.* **2006**, 128, 704.

- (22) Wiberg, N.; Niedermayer, W.; Nöth, H.; Warchhold, M. *J. Organomet. Chem.* **2001**, 628, 46.
- (23) Strohmann, C.; Schildbach, D.; Auer, D. *J. Am. Chem. Soc.* **2005**, 127, 7968.
- (24) Jones, R. A.; Stuart, A. L.; Wright, T. C. *J. Am. Chem. Soc.* **1983**, 105, 7459.
- (25) Barlett, R. A.; Olmstead, M. M.; Power, P. P. *Inorg. Chem.* **1986**, 25, 1243.
- (26) Hey-Hawkins, E.; Kurz, S. *Phosphorus, Sulfur Silicon Relat. Elem.* **1994**, 90, 819.
- (27) Hey, E.; Weller, F. *Chem. Commun.* **1988**, 782.
- (28) Giese, H.-H.; Nöth, H.; Schwenk, H.; Thomas, S. *Eur. J. Inorg. Chem.* **1998**, 941.
- (29) Gálvez Ruiz, J. C.; Nöth, H.; Warchhold, M. *Eur. J. Inorg. Chem.* **2008**, 251.
- (30) Giese, H.-H.; Habereeder, T.; Nöth, H.; Ponikwar, W.; Thomas, S.; Warchhold, M. *Inorg. Chem.* **1999**, 38, 4188.
- (31) Andrianarison, M.; Stalke, D.; Klingebiel, U. *Chem. Ber.* **1990**, 123, 71.
- (32) Koutsantonis, G. A.; Andrews, P. C.; Raston, C. L. *J. Chem. Soc., Chem. Commun.* **1995**, 47.
- (33) Driess, M.; Pritzkow, H.; Skipinski, M.; Winkler, U. *Organometallics* **1997**, 16, 5108.

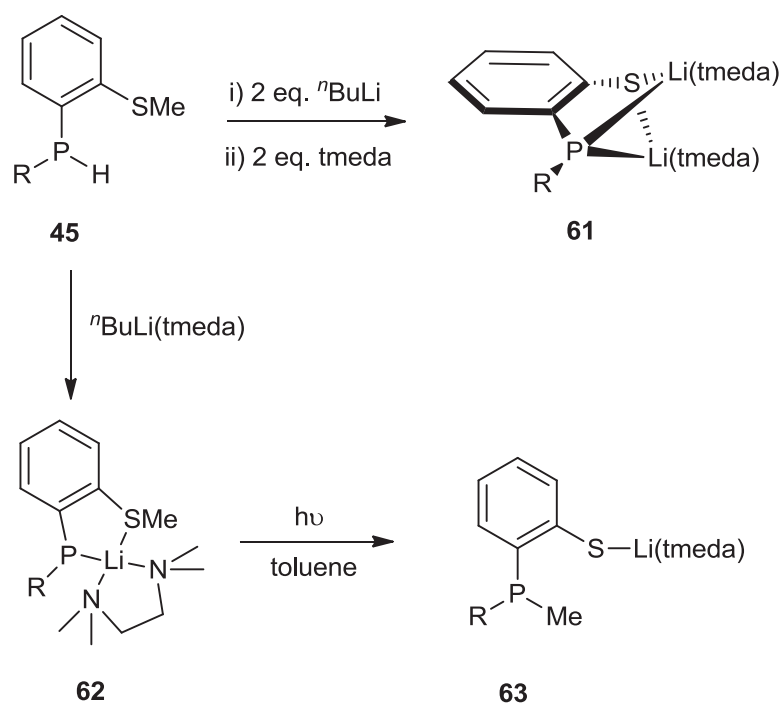
Chapter 4. Alkali metal complexes of a thioanisole-functionalised phosphido-borane

4.1 Introduction

In previous studies of thioanisole-substituted phosphines, it was found that compound **45** $\{(\text{Me}_3\text{Si})_2\text{CH}\}\text{PH}(\text{C}_6\text{H}_4\text{-2-SMe})$ exhibits unusual behaviour towards alkyllithium reagents.¹ The reaction between **45** and one equivalent of $^n\text{BuLi}$ in diethyl ether yields, after crystallisation in the presence of tmeda, half an equivalent of the dianion complex $[\{(\text{Me}_3\text{Si})_2\text{CH}\}\text{P}(\text{C}_6\text{H}_4\text{-2-S})\{\text{Li}(\text{tmeda})\}_2]$ (**61**) (Scheme 4.1), which results from simultaneous deprotonation and demethylation of the phosphine, leaving half an equivalent of **45** unchanged. Compound **61** may be accessed cleanly by reaction of **45** with two equivalents of $^n\text{BuLi}$ under the same conditions.

In comparison, reaction of **45** with one equivalent of $^n\text{BuLi}$ in the presence of tmeda yields the expected lithium phosphide $[\{(\text{Me}_3\text{Si})_2\text{CH}\}\text{P}(\text{C}_6\text{H}_4\text{-2-SMe})\text{Li}(\text{tmeda})]$ (**62**). However, compound **62** undergoes a rapid isomerisation in toluene upon exposure to ambient light, leading to the formation of the corresponding phosphine-thiolate $[\{(\text{Me}_3\text{Si})_2\text{CH}\}\text{PMe}(\text{C}_6\text{H}_4\text{-2-S})\text{Li}(\text{tmeda})]$ (**63**).

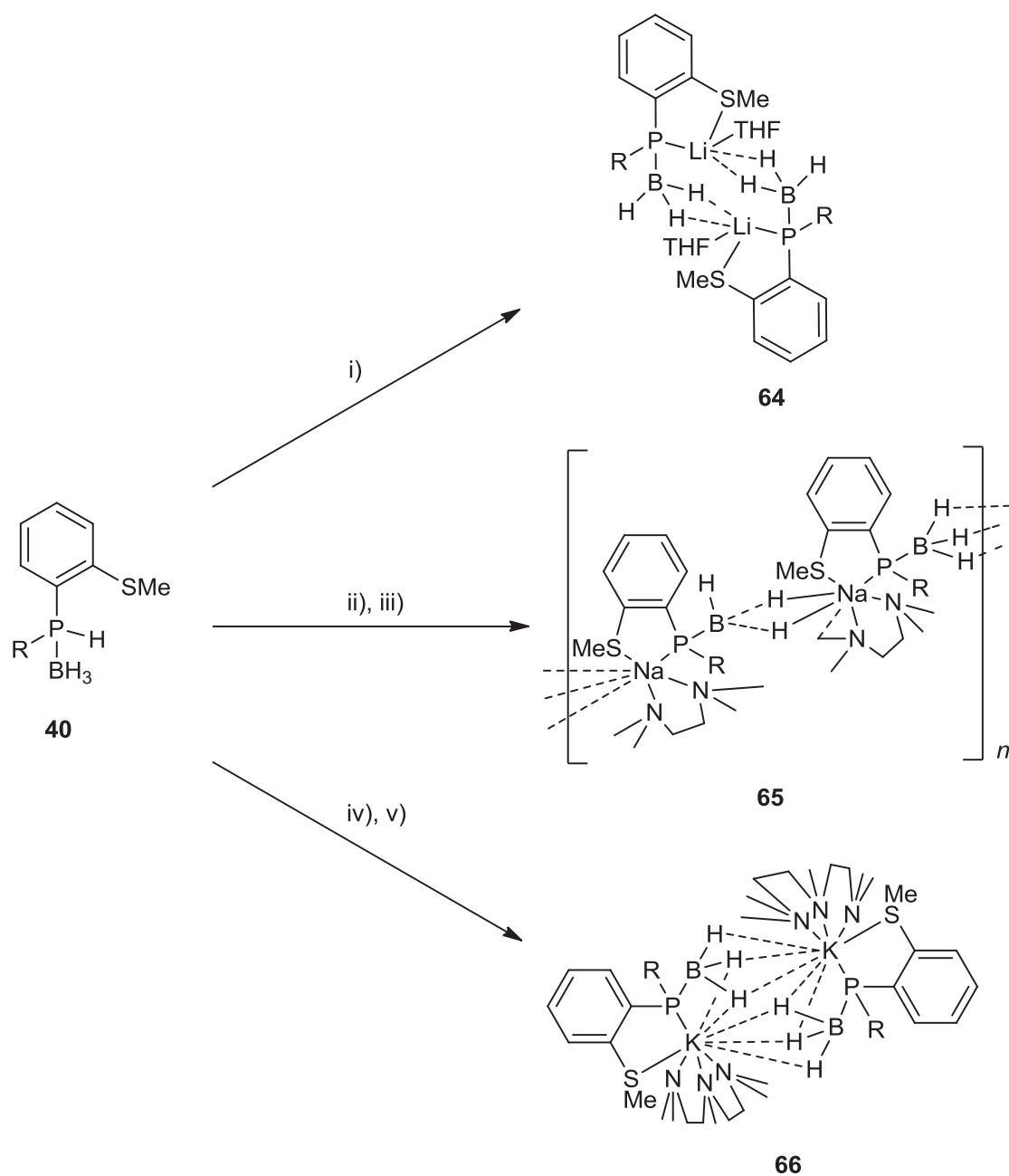
To obtain further insight into this unusual behaviour, this chapter considers the deprotonation of the related thioanisole-functionalised phosphine-borane **40**, exploring the effect that the borane adduct has on the ligand binding modes, and the photolytic/thermolytic stability of the corresponding phosphido-borane. For a comprehensive overview, a series of complexes with the group I metals (Li, Na and K) have been synthesised to also take into consideration the effect of cation size.



Scheme 4.1. Synthesis of compounds **61**, **62** and **63** [R = (Me₃Si)₂CH].

4.2 Synthesis of the alkali metal complexes [{(Me₃Si)₂CH}P(C₆H₄-2-SMe)(BH₃)M(L)]_n [M(L) = Li(THF), n = 2 (**64**), M(L) = Na(tmeda), n = ∞ (**65**), M(L) = K(pmdeta), n = 2 (**66**)]

The reaction between compound **40** and one equivalent of ⁿBuLi in THF proceeds cleanly to give the phosphido-borane complex [{(Me₃Si)₂CH}P(C₆H₄-2-SMe)(BH₃)Li(THF)]₂ (**64**), which was crystallised from cold toluene/THF as colourless blocks. Similarly, the reaction between **40** and one equivalent of either BnNa or BnK in THF yields the corresponding alkali metal salts, which were crystallised from cold toluene in the presence of either one equivalent of tmeda or pmdeta, respectively, as the adducts [{(Me₃Si)₂CH}P(C₆H₄-2-SMe)(BH₃)Na(tmeda)]_∞ (**65**), and [{(Me₃Si)₂CH}P(C₆H₄-2-SMe)(BH₃)K(pmdeta)]₂ (**66**). The syntheses of **64-66** are shown in Scheme 4.2.



Scheme 4.2. Synthesis of compounds 63-65. i) $t\text{BuLi}$, THF, 1 h, r.t. ii) BnNa , THF, 1h, r.t. iii) tmeda , toluene. iv) BnK , THF, 1h, r.t. vi) pmdeta , toluene [$\text{R} = (\text{Me}_3\text{Si})_2\text{CH}$].

4.3 Solution-phase characterisation of compounds 64-66

The room temperature $^1\text{H}\{^{11}\text{B}\}$, $^{13}\text{C}\{^1\text{H}\}$, $^{11}\text{B}\{^1\text{H}\}$, and $^{31}\text{P}\{^1\text{H}\}$ NMR spectra of complexes **64-66** indicate the presence of single phosphido-borane ligand environments. Upon metalation, the $^{31}\text{P}\{^1\text{H}\}$ NMR signals shift significantly upfield from -15.7 ppm for **40** to between -58.3 and -59.5 ppm for compounds **64-66**. The magnitude of the ^{31}P - ^{11}B coupling constant decreases steadily with decreasing electronegativity of the cation [$^1J_{\text{PB}} = 49.0$ (**40**), 39.2 (**64**), 29.4 (**65**) and 19.6 Hz (**66**)], which is consistent with increasing ionic character of the P-M interaction.

The ^1H NMR spectra of **64-66** are as expected, the diastereotopic SiMe_3 groups give rise to two sharp singlets between -0.05 and 0.11 ppm, and the BH_3 protons give rise to a broad quartet, which collapses into a sharp doublet on decoupling of the ^{11}B nucleus. The $^{13}\text{C}\{^1\text{H}\}$ NMR spectra are also as expected. The SiMe_3 carbons give rise to two signal, a doublet and a singlet between 1.5 and 2.9 ppm for **64** and **65** [$^3J_{\text{PC}} = 6.7$ Hz (**64** and **65**)], and a pair of doublets at 2.4 and 3.7 ppm [$^3J_{\text{PC}} = 6.71$ and 1.9 Hz, respectively] for **66**. The adjacent CH carbons appear as doublets between 6.9 and 8.0 ppm [$^1J_{\text{PC}} = 48.0$ (**64**) 43.2 (**65**) and 47.0 Hz (**66**)].

4.4 Solid-state structures of compounds 64-66

4.4.1 Solid-state structure of 64

Compound **64** crystallises as discrete centrosymmetric dimers; the molecular structure of **64** is shown in Figure 4.1 and selected bond lengths and angles are given in Table 4.1. Each lithium ion is coordinated by the P and S atoms of a phosphido-borane ligand to give a five-membered chelate ring [P-Li-S bite angle $77.28(7)^\circ$]. The coordination about each Li ion is completed by a molecule of THF, and by an η^2 - BH_3 contact with the borane group from the other phosphido-borane ligand in the dimer, resulting in pseudo-tetrahedral geometry at lithium. The two halves of the dimer, therefore, are linked *via* an essentially planar, pseudo-six-membered $[\text{PLi}(\text{BH}_3)]_2$ ring.

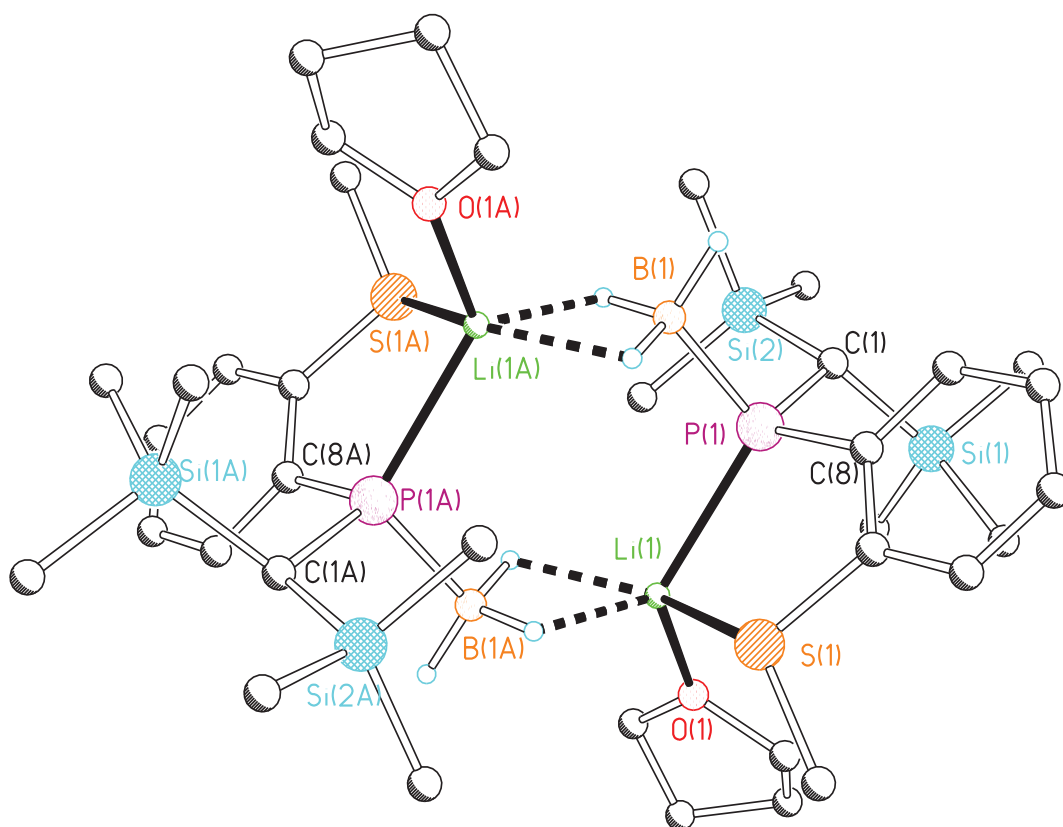


Figure 4.1. Structure of compound **64**. All C-bound H atoms omitted for clarity.

P(1)–Li(1)	2.527(3)	Li(1)–H(2A)	1.905(14)
S(1)–Li(1)	2.608(2)		
P(1)–B(1)	1.9618(18)	P(1)–Li(1)–S(1)	77.28(7)
P(1)–C(1)	1.8683(14)	B(1)–P(1)–Li(1)	109.30(8)
P(1)–C(8)	1.8459(13)	B(1)–P(1)–C(8)	100.40(7)
Li(1)···B(1A)	2.403(3)	B(1)–P(1)–C(1)	109.36(7)
Li(1)–O(1)	1.910(3)	Li(1)–P(1)–C(8)	109.31(7)
Li(1)–H(1A)	2.053(14)	Li(1)–P(1)–C(1)	123.28(7)

Table 4.1. Selected bond lengths (Å) and angles (°) of compound **64**.

The P-Li distance of 2.527(3) is slightly shorter than the corresponding distances in **29** and **49** [2.620(4) and 2.611(6) Å respectively], and also slightly longer than the P-Li distance in **62** [2.508(3) Å]. The S-Li distance in **64** of 2.608(2) Å is somewhat longer than the corresponding distance in **62** [2.543(3) Å] and is much longer than the related O-Li distance in **49** [1.988(6) Å], which is consistent with the larger atomic radius of sulphur compared to oxygen. The Li-H distances in **64** [2.053(14) and 1.905(14) Å] and the Li(1)...B(1A) distance [2.403(3) Å] are similar to those in **49** [Li-H: 1.97(4), 1.98(4) and 2.05(4) Å; Li...B: 2.453(7)], and are typical of complexes where there is an η^2 -BH₃-Li contact. For example, the Li-H distances and Li...B distance in Li[(η^2 -BH₄)(py)₃] (**67**) are 2.06 and 1.90 Å, and 2.401(7) Å, respectively (Figure 4.2); the corresponding distances in the complex Li[(η^2 -BH₄)(HN^{*i*}Pr₂)] (**68**) are 2.03(1) and 1.93(1) Å, and 2.358(3) Å, respectively, whilst the compound Li[(η^2 -BH₄)(THF)₂(py-2-NH₂)] (**69**) has a Li...B distance of 2.41(1) Å.^{2,3}

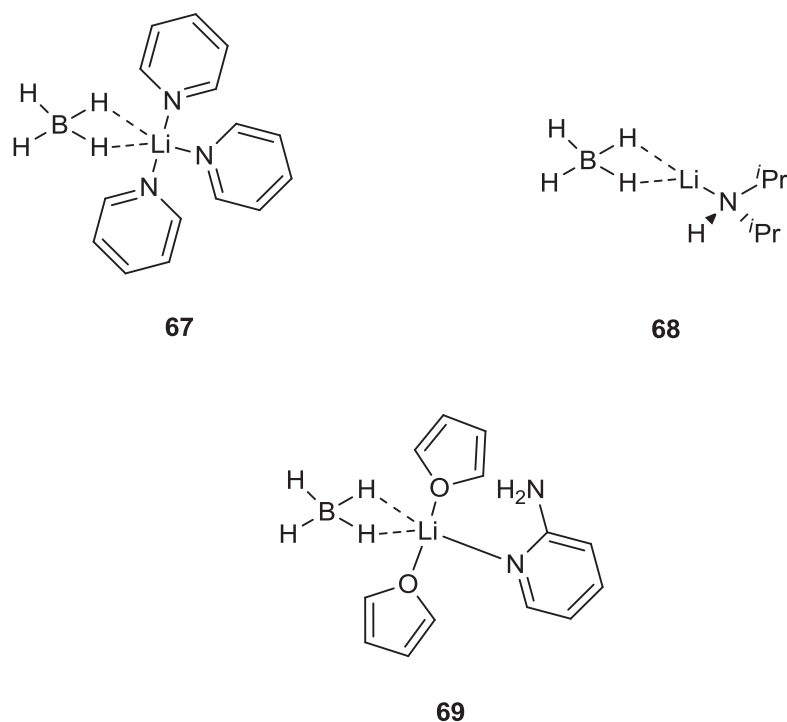


Figure 4.2. Structures of complexes which exhibit η^2 -BH₄-Li interactions.

4.4.2 Solid-state structure of **65**

Compound **65** crystallises as a linear polymer with two crystallographically independent molecular units per asymmetric unit. The structure of **65** is shown in Figure 4.3, and selected bond lengths and angles are shown in Table 4.2. The sodium ions are coordinated by the P and S atoms of a phosphido-borane ligand to generate a five-membered chelate ring [P-Na-S bite angles 62.93(4) and 63.43(4)°], and by two N atoms of a chelating molecule of tmeda. The coordination of Na(1) is completed by an η^2 -BH₃ interaction from the adjacent phosphido-borane unit in the polymer chain and a short contact to one of the methylene carbon atoms of the tmeda co-ligand [Na(1)...C(17) 3.126(4) Å], whereas the coordination of Na(2) is completed by η^3 -coordination of a BH₃ group from the adjacent polymer unit.

P(1)–Na(1)	2.9661(17)	Na(2)–H(1CA)	2.51(4)
P(2)–Na(2)	2.9474(16)	Na(2)–B(1B)	2.646(4)
S(1)–Na(1)	3.0441(19)		
S(2)–Na(2)	3.0735(18)	P(1)–Na(1)–S(1)	62.93(4)
P(1)–B(1)	1.951(4)	P(1)–Na(1)–B(2)	140.40(12)
C(17)–Na(2)	3.126(4)	P(2)–Na(2)–S(2)	63.43(4)
Na(2)–N(3)	2.523(3)	P(2)–Na(2)–B(1B)	137.57(12)
Na(2)–N(4)	2.533(3)	B(1)–P(1)–Na(1)	119.87(17)
Na(1)–H(2B)	2.64(3)	B(2)–P(2)–Na(2)	118.70(15)
Na(1)–H(2C)	2.35(3)	B(1)–P(1)–C(1)	110.23(18)
B(2)–Na(1)	2.694(4)	B(1)–P(1)–C(8)	105.98(19)
Na(2)–H(1AA)	2.54(3)	C(1)–P(1)–C(8)	105.55(16)
Na(2)–H(1BA)	2.63(3)		

Table 4.2. Selected bond lengths (Å) and angles (°) of compound **65**.

The P-Na distances of 2.9661(17) and 2.9474(16) Å are typical of P-Na distances in related sodium phosphide complexes, which range from 2.8-3.0 Å,⁴ and are similar to the corresponding distance in compound **50** [3.0528(13) Å]. The S-Na distances in **65** of 3.0441(19) and 3.0735(18) Å are longer than the related distance in **64**, which is consistent with the larger ionic radius of sodium. The Na(1)...B(2) distance of 2.646(4) Å is somewhat

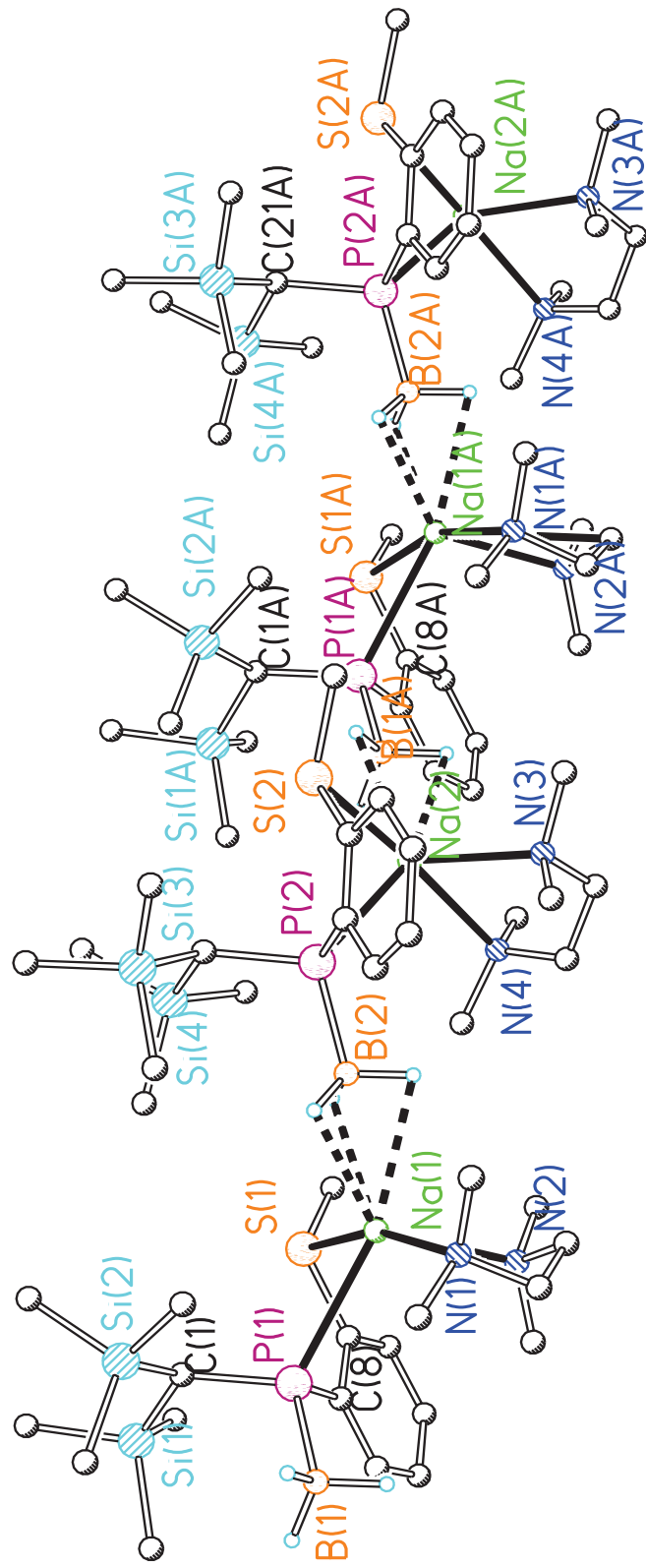


Figure 4.3. Structure of compound 65. All C-bound H atoms omitted for clarity.

shorter than typical $\eta^2\text{-BH}_n\text{-Na}$ distances, for example, the Na...B distances in $\text{Na}_2(\eta^2\text{-BH}_4)_2(\text{triglyme})$ (**70**) and $\text{NaBH}_4(\text{py})_3$ (**71**) are 2.830(2) and 2.927(3) Å, respectively (Figure 4.4),⁶ whilst the Na(2)...B(1B) distance of 2.694(4) Å is similar to other $\eta^3\text{-BH}_n\text{...Na}$ distances; for example, the $\eta^3\text{-BH}_4\text{...Na}$ distances in $[\text{Na}(\eta^3\text{-BH}_4)(15\text{-crown-5})(\text{py})_{0.5}]$ (**58**) are 2.7298 Å.⁵

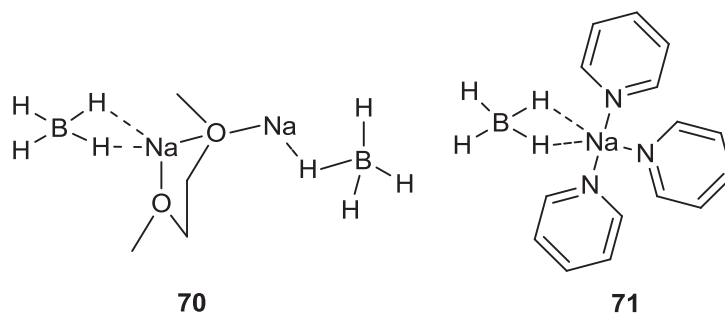


Figure 4.4. Structures of a section of compound **70** and compound **71**.

4.4.3 Solid-state structure of **66**

The structure of **66** is shown in Figure 4.5, with selected bond lengths and angles given in Table 4.3. Compound **66** crystallises as discrete centrosymmetric dimers in which the phosphido-borane ligands adopt a tridentate coordination mode, each binding to an adjacent potassium ion through its P and S atoms, and in an η^2 manner, through the BH_3 group. The borane groups are also coordinated to the second potassium ion in the dimer through an η^3 type interaction, such that each borane acts as a $\mu_2\text{-}\eta^2\text{:}\eta^3$ bridge between the two potassium ions, forming a rhombus-shaped pseudo-four-membered $\text{K}_2(\text{BH}_3)_2$ ring. The coordination about each potassium ion is completed by the three N atoms of a molecule of pmdeta, and by a short K...C contact from the central methyl group of the pmdeta ligand.

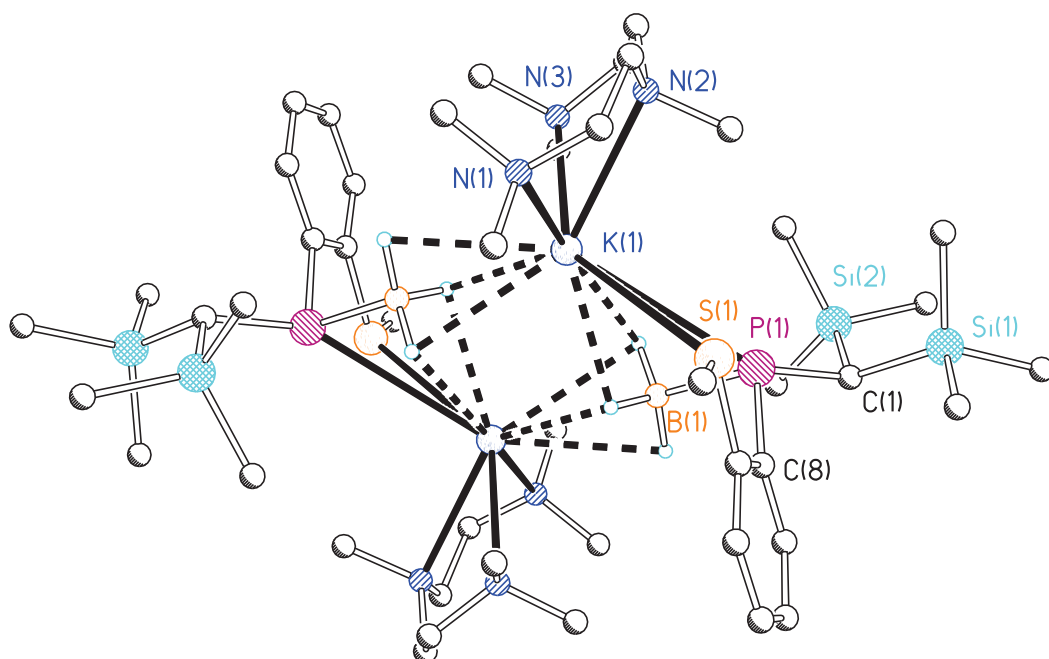


Figure 4.5. Structure of **66**. All C-bound H atoms omitted for clarity.

K(1)–P(1)	3.6617(6)	K(1)–H(1CA)	2.74(2)
K(1)–S(1)	3.7568(7)	K(1)–C(19)	3.266(2)
K(1)–B(1)	3.243(2)	P(1)–C(1)	1.8852(17)
K(1)–B(1A)	3.047(2)	P(1)–C(8)	1.8473(18)
K(1)–H(1A)	3.01(2)		
K(1)–H(1C)	2.77(2)	P(1)–K(1)–S(1)	49.666(12)
P(1)–B(1)	1.975(2)	P(1)–K(1)–B(1)	32.52(4)
K(1)–N(1)	2.9039(17)	B(1)–K(1)–B(1A)	94.71(5)
K(1)–N(2)	2.8912(16)	B(1)–P(1)–C(1)	112.54(9)
K(1)–N(3)	2.9099(17)	B(1)–P(1)–C(8)	97.38(9)
K(1)–H(1AA)	3.01(2)	C(1)–P(1)–C(8)	102.41(8)
K(1)–H(1BA)	2.97(2)	K(1)–P(1)–B(1)	62.01(7)

Table 4.3. Selected bond lengths (Å) and angles (°) of compound **66**.

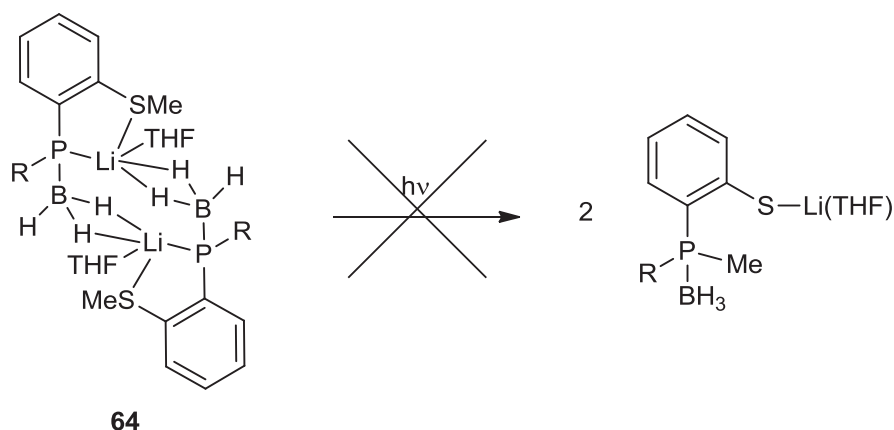
The K-P distance in **66** of 3.6617(6) Å is significantly longer than the corresponding distance in [Ph₂P(BH₃)K(18-crown-6)] (**32**) [3.320(2) Å],⁶ which supports the argument that K-P interactions in ‘tridentate’ phosphido-boranes, where there is additional coordination to potassium from a peripheral donor-atom, such as in compounds **51** and **66**, are considerably weaker than in ‘bidentate’ phosphido-boranes, such as **32**. The K-S distance in **66** of 3.7568(7) Å is much longer than the corresponding Li-S and Na-S distances in compounds **64** and **65** [2.608(2) and 3.0441(19) Å, respectively] which is consistent with the larger ionic radius of potassium. Similarly, the P-K-S bite angle [49.666(12)°] is considerably smaller than the corresponding P-M-S angles in **64** and **65** [77.28(7) and 62.93(4)°, respectively], which again is consistent with the larger ionic radius of potassium.

The K(1)...B(1) and K(1)...B(1A) distances in **66** of 3.243(2) and 3.047(2) Å, respectively, are consistent with the relative η²- and η³-BH₃ coordination modes, but are slightly shorter than the related distances in compound **51** [3.322(3) and 3.103(3) Å, respectively]. The K-H distances of **66** [2.74(2)-3.047(2) Å], however, are similar to those observed in compound **51** [2.816(18)-3.095(20)].

4.5 Behaviour of **64** in solution

4.5.1 Photolytic reactivity of **64**

In an effort to ascertain if these species undergo S-Me cleavage under photolytic conditions, NMR samples of compounds **64-66** in THF were exposed to both ambient light and a 10 W fluorescent light, whilst being monitored *via* ³¹P NMR spectroscopy. However, after long periods of exposure to light, compounds **64-66** showed no evidence of rearrangement, which was confirmed by ¹H{¹¹B} NMR spectroscopy. This suggests that these phosphido-borane species are photolytically stable (Scheme 4.3) compared to their phosphide counter-parts, which rapidly rearrange to give the corresponding tertiary phosphine-functionalised thiolate.

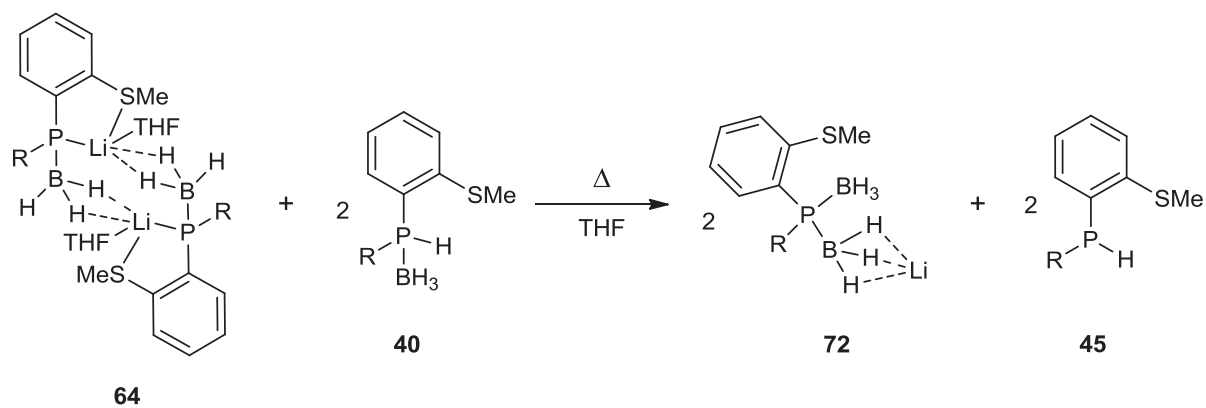


Scheme 4.3. Proposed photolytic rearrangement of **64** [R = (Me₃Si)₂CH].

4.5.2 Thermolytic reactivity of **64**

Although **64** is stable towards photolysis, it was found that the compound can undergo a thermally-induced rearrangement in the presence of phosphine-borane **40**. Heating a solution of a 1:1 mixture of **64** and **40** in THF to 50 °C for 16 h results in conversion of the phosphido-borane and **40** into a mixture of the corresponding lithium phosphido-bis(borane) [$\{(Me_3Si)_2CH\}P(C_6H_4-2-SMe)(BH_3)_2Li$] (**72**), which is observed in the $^{31}P\{^1H\}$ NMR spectrum as a broad multiplet at -4.6 ppm, and the secondary phosphine **45** in a 1:1 ratio (Scheme 4.4). It is thought that the rearrangement results from the abstraction of borane from **40** by the anionic phosphido-borane, which has greater basic character.

Unfortunately **72** could not be isolated from these thermolysis reactions, however the $^{31}P\{^1H\}$, ^{31}P , 1H and $^{11}B\{^1H\}$ NMR spectra of samples taken from the reaction solution are consistent with a mixture of **72** and **45** (^{31}P NMR spectra shown in Figure 4.6).



Scheme 4.4. Conversion of **64** in the presence of **40** into **72** and **45** upon thermolysis [R = (Me₃Si)₂CH].

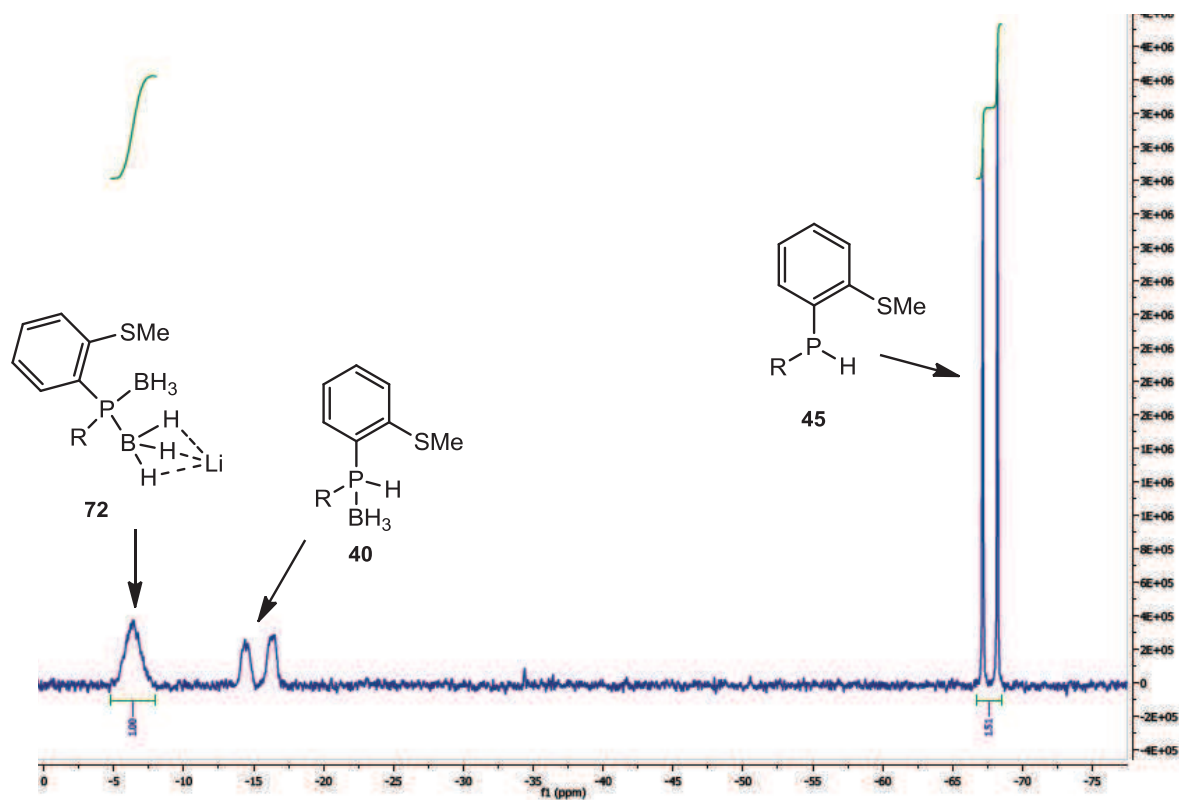
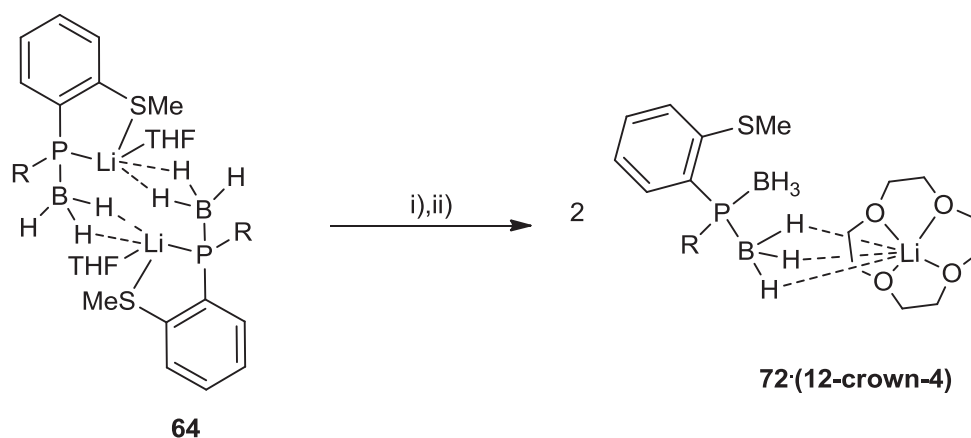


Figure 4.6. Undecoupled ³¹P NMR spectrum of **72** and **45**, from the thermolysis of **64** in the presence of **40** in THF, after 16 h at 50°C [R = (Me₃Si)₂CH].

4.5.3 Synthesis and solution-phase characterisation of **72**·(12-crown-4)

To confirm the identity of **72**, this compound was prepared using a direct route. The reaction between a solution of **64** and two equivalents of $\text{BH}_3\cdot\text{SMe}_2$ yields the corresponding phosphido-bis(borane) [$\{(\text{Me}_3\text{Si})_2\text{CH}\}\text{P}(\text{C}_6\text{H}_4\text{-2-SMe})(\text{BH}_3)_2\text{Li}$] (**72**) upon removal of the solvent. The product was isolated as the adduct [$\{(\text{Me}_3\text{Si})_2\text{CH}\}\text{P}(\text{C}_6\text{H}_4\text{-2-SMe})(\text{BH}_3)_2\text{Li}$ (12-crown-4)] (**72**·(12-crown-4)) as a colourless solid (Scheme 4.5).

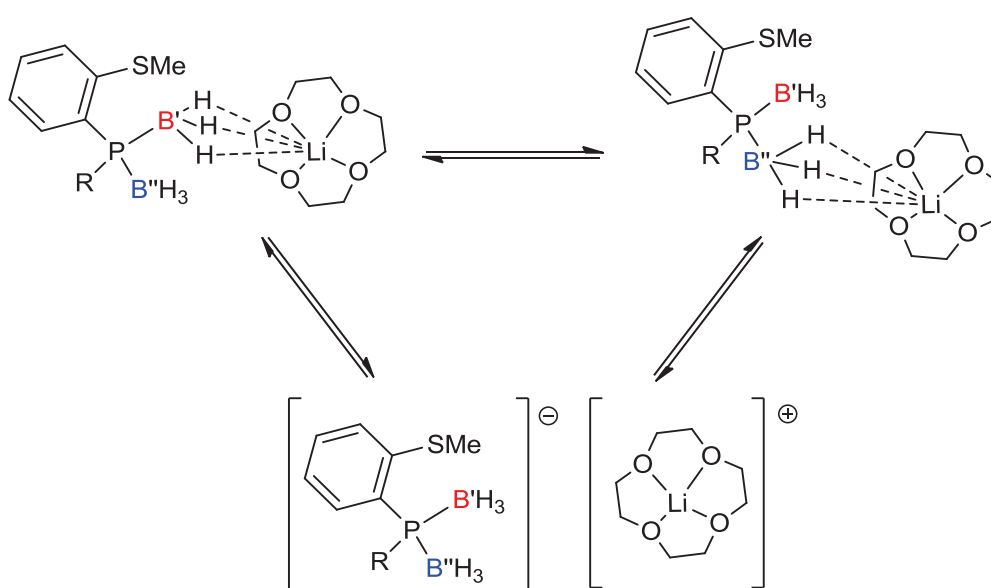


Scheme 4.5. Synthesis of **72**·(12-crown-4). i) 2 eq. $\text{BH}_3\cdot\text{SMe}_2$, THF, 1h, r.t. ii) 2 eq. 12-crown-4, toluene [R = $(\text{Me}_3\text{Si})_2\text{CH}$].

Upon addition of the second equivalent of borane, the $^{31}\text{P}\{^1\text{H}\}$ NMR signal at -59.5 ppm for **64** is replaced by a new, very broad signal at -4.6 ppm, which is indistinguishable from that of the sample of **72** prepared from the thermolysis of **64**. This chemical shift is typical of phosphido-bis(borane) complexes, which have previously demonstrated a relatively downfield shift in comparison to phosphido-boranes. For example, the $^{31}\text{P}\{^1\text{H}\}$ NMR spectrum of the potassium complex [$\text{Ph}_2\text{P}(\text{BH}_3)\text{K}(18\text{-crown-6})$] (**32**) gives rise to a signal at -28.8 ppm,⁶ whereas the related complex [$\text{Ph}_2\text{P}(\text{BH}_3)_2\text{K}(18\text{-crown-6})$] (**37**) has a ^{31}P chemical shift of -11.1 ppm.⁷ Although the signal observed in the $^{31}\text{P}\{^1\text{H}\}$ NMR spectrum of **72** is a very broad multiplet, the P-B coupling can be resolved in the $^{11}\text{B}\{^1\text{H}\}$ NMR spectrum where $^1J_{\text{PB}}$ is measured as 68.6 Hz, which is significantly larger than the P-B coupling constant in **64** [$^1J_{\text{PB}} = 39.2$ Hz].

The ^1H NMR spectrum of **72**·(12-crown-4) in THF is as expected; the six BH_3 protons appear as a broad signal at 0.8 ppm, which, upon decoupling of the ^{11}B nucleus, resolve as a

sharp doublet [$^2J_{\text{PH}} = 10.5 \text{ Hz}$]. That all six borane protons appear to be identical would suggest that in solution there is either rapid exchange between the borane groups coordinating with the lithium ion (Scheme 4.6), or that the compound exists as a separated ion pair in THF. In the $^{13}\text{C}\{^1\text{H}\}$ NMR spectrum the SiMe_3 carbons appear as a singlet at 3.1 ppm, whilst the adjacent CH carbon appears as a doublet at 7.0 ppm; the magnitude of the P-C coupling in $72 \cdot (12\text{-crown-4})$ [$^1J_{\text{PC}} = 3.8 \text{ Hz}$] is smaller compared to the mono(borane) compounds **64-66** [$^1J_{\text{PC}} = 48.0 \text{ Hz}$].



Scheme 4.6. Exchange between borane coordination to lithium in $72 \cdot (12\text{-crown-4})$ in THF [$\text{R} = (\text{Me}_3\text{Si})_2\text{CH}$].

4.6 Conclusions

The lithium, sodium and potassium complexes of the phosphido-borane anion $[\{(\text{Me}_3\text{Si})_2\text{CH}\}\text{P}(\text{C}_6\text{H}_4\text{-2-SMe})]^-$ have been successfully prepared *via* relatively straightforward synthetic procedures. In the solid state, the structures vary significantly with increasing radii of the alkali metal and can adopt unique structural motifs: the structure of complex **64** is a dimer linked through $\eta^2\text{-BH}_3$ type interactions; compound **65** crystallises as a linear polymer, where each unit is joined by a series of alternating $\eta^3\text{-BH}_3$ and $\eta^2\text{-BH}_3$ interactions; and compound **66** is a dimer, where the BH_3 groups bridge the two potassium

ions in a $\mu_2\text{-}\eta^2\text{:}\eta^3$ fashion. As with the previously reported phosphido-boranes, the $\text{BH}_3\text{-M}$ interactions in these complexes are an essential feature of their structures.

Unlike the related phosphide, **64** showed no photolytic reactivity upon exposure to ambient or fluorescent light. This would suggest that the formation of a P-B bond sufficiently perturbs the electronics of this system, so that methyl migration is disfavoured.

An investigation of the thermolytic reactivity of **64** in solution led to the observation that a borane migration can occur in the presence of **40**, which results in the formation of the corresponding phosphido-bis(borane) complex **72** and the secondary phosphine **45**. This behaviour has not previously been reported.

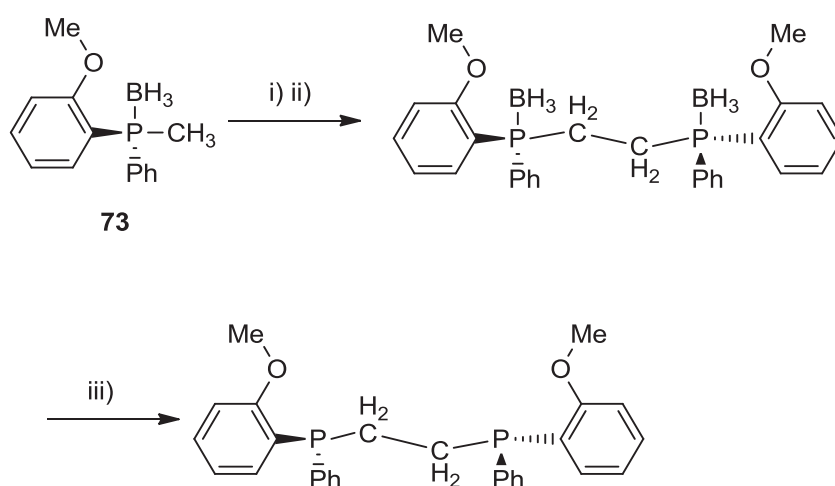
4.7 References

- (1) Blair, S.; Izod, K.; Harrington, R. W.; Clegg, W. *Organometallics* **2003**, *22*, 302.
- (2) Giese, H.-H.; Habereeder, T.; Nöth, H.; Ponikwar, W.; Thomas, S.; Warchhold, M. *Inorg. Chem.* **1999**, *38*, 4188.
- (3) Giese, H.-H.; Habereeder, T.; Knizek, J.; Nöth, H.; Warchhold, M. *Eur. J. Inorg. Chem.* **2001**, 1195.
- (4) Izod, K. *Adv. Inorg. Chem.* **2000**, *50*, 33.
- (5) Gálvez Ruiz, J. C.; Nöth, H.; Warchhold, M. *Eur. J. Inorg. Chem.* **2008**, 251.
- (6) Dornhaus, F.; Bolte, M.; Lerner, H.-W.; Wagner, M. *Eur. J. Inorg. Chem.* **2006**, 5138.
- (7) Dornhaus, F.; Bolte, M.; Lerner, H.-W.; Wagner, M. *Eur. J. Inorg. Chem.* **2006**, 1777.

Chapter 5. Alkali metal and calcium complexes of anisole-functionalised phosphido-boranes

5.1 Introduction

The first example of an anisole-functionalised phosphine-borane was the chiral compound $\text{PhP}(\text{BH}_3)(\text{CH}_3)(\text{C}_6\text{H}_4\text{-2-OMe})$ (**73**) reported by Imamoto and co-workers in 1985. This compound allowed a rapid route to the synthesis of the optically pure 1,2-ethanediylbis[(*o*-methoxyphenyl)phenylphosphine] (DIPAMP), which is an extremely useful ligand in catalytic asymmetric hydrogenation reactions (Scheme 5.1).¹



Scheme 5.1. Synthesis of DIPAMP. i) $^t\text{BuLi}$, THF, -78°C , 2 h. ii) CuCl_2 , 2 h. iii) Et_2NH , 50°C , 10 h.

To date, the only example of a structurally characterised anisole-functionalised phosphido-borane is the palladium complex $[(2\text{-}(2\text{-}(\text{Ph}_2\text{P})\text{C}_6\text{H}_4)\text{-4-}^i\text{Pr-4,5-C}_3\text{NO})\text{Pd}(\text{C}_6\text{F}_5)(\text{PhP}(\text{BH}_3)(\text{C}_6\text{H}_4\text{-2-OMe}))]$ (**74**, Figure 5.1).² There are, however, several examples of anisole-functionalised phosphides coordinated to group I, II and lanthanide metals.³⁻⁹ These systems have demonstrated that complex stabilisation can be afforded through an intramolecular chelate effect between the oxygen atom and metal centre.

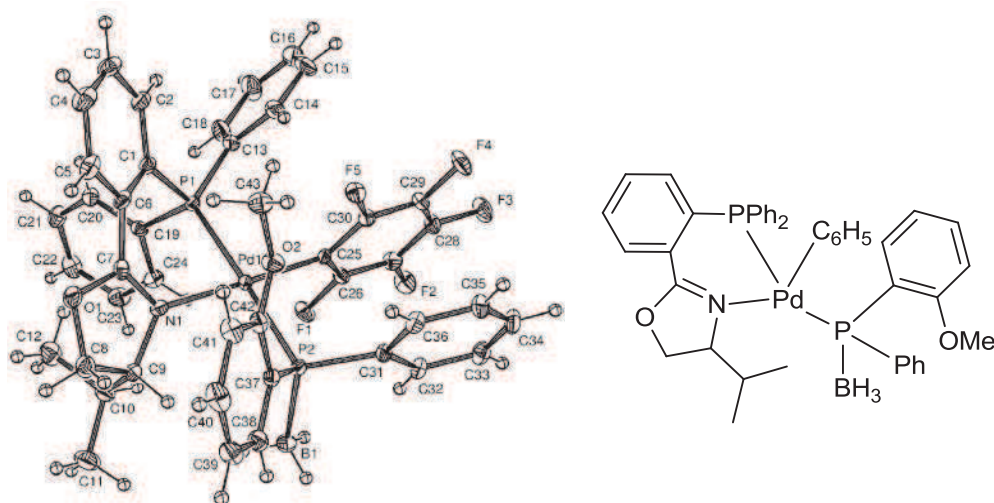


Figure 5.1. Structure of compound **74**.²

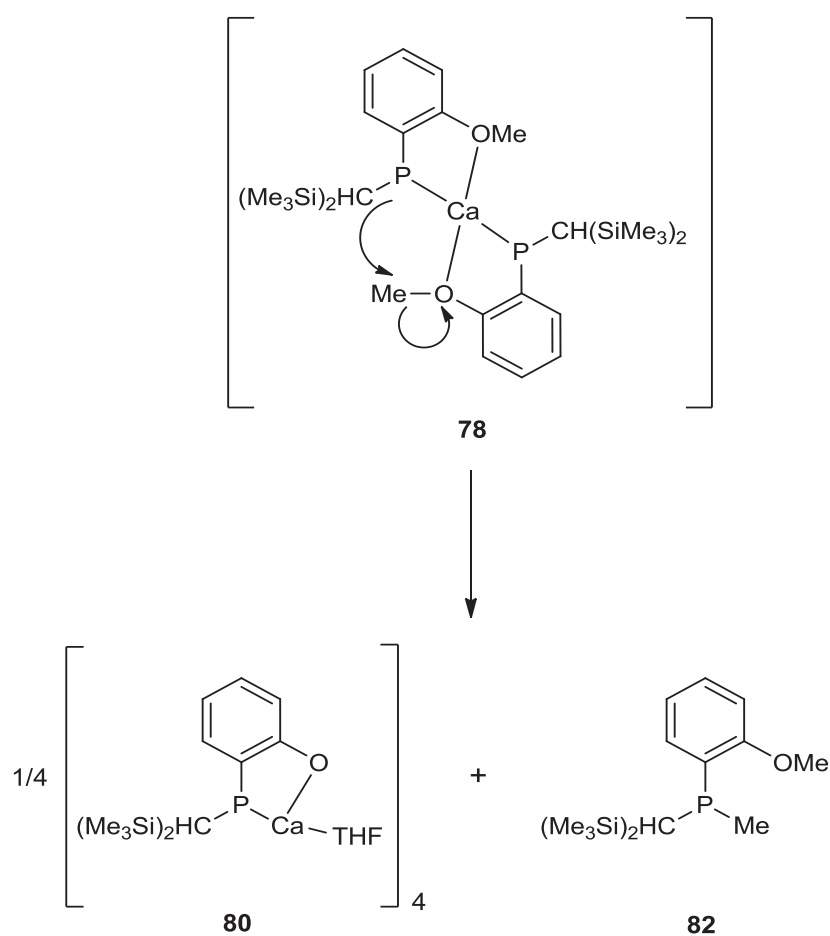
The chemistry of group II and lanthanide metal complexes with the phosphide ligand $[\{(Me_3Si)_2CH\}P(C_6H_4-2-OMe)]^-$ has been well established.⁶⁻¹⁰ The compounds $([\{(Me_3Si)_2CH\}P(C_6H_4-2-OMe)]_2Sr(THF)_2)$ (**75**), $([\{(Me_3Si)_2CH\}P(C_6H_4-2-OMe)]_2Ba(THF)_3)$ (**76**) and $([\{(Me_3Si)_2CH\}P(C_6H_4-2-OMe)]_2Sm(DME)(THF))$ (**77**) crystallise as discrete molecular species in which the phosphide ligands bind the metal centers *via* their P and O donors to give five-membered chelate rings.^{6,10} The strontium atom in **75** adopts a distorted *trans*-octahedral geometry, whilst both the Ba and Sm metal centers in **76** and **77** adopt a distorted pentagonal bipyramidal geometry. Compounds **75-77** are stable in the solid state and in THF solution at room temperature.

In contrast, the related complexes $([\{(Me_3Si)_2CH\}P(C_6H_4-2-OMe)]_2Ca(THF)_2)$ (**78**) and $([\{(Me_3Si)_2CH\}P(C_6H_4-2-OMe)]_2Yb(THF)_2)$ (**79**) undergo rapid decomposition to yield $([\{(Me_3Si)_2CH\}P(C_6H_4-2-O)Ca(THF)]_4)$ (**80**) and $([\{(Me_3Si)_2CH\}P(C_6H_4-2-O)Yb(THF)]_4)$ (**81**), respectively, and the side product $(\{(Me_3Si)_2CH\}PMe(C_6H_4-2-OMe))$ (**82**).^{7,9} Compounds **80** and **81** are isostructural in the solid state, and both crystallise as tetrameric clusters, adopting Ca_4O_4 and Yb_4O_4 cuboidal cores, respectively. They are thought to arise from rapid migration of a methyl group from the oxygen atom of one phosphide ligand to the phosphorus atom of the second ligand in the complex (Scheme 5.2).

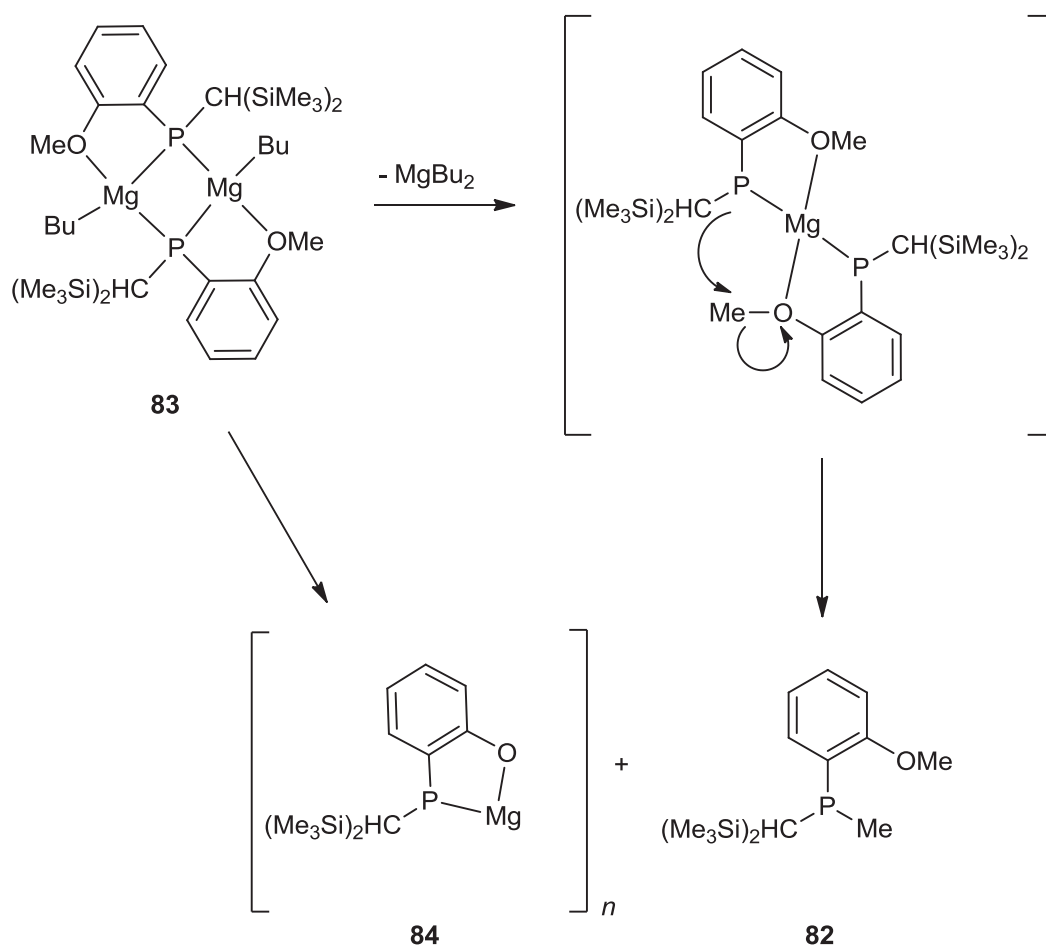
Similarly, the compound $([\{(Me_3Si)_2CH\}P(C_6H_4-2-OMe)Mg(C_4H_9)]_2)$ (**83**) is observed by NMR spectroscopy to undergo rapid decomposition, to yield **82** and a new magnesium phosphide compound.⁸ Although this new compound could not be isolated for full

characterisation, it is proposed to be the magnesium alkoxophosphide $[\{(Me_3Si)_2CH\}P(C_6H_4-2-O)Mg(THF)_n]_m$ (**84**), which could arise directly from the Grignard-like compound **83**. Alternatively, **83** may be subject to a Schlenk-type equilibrium in solution, generating the homoleptic phosphide $[\{(Me_3Si)_2CH\}(C_6H_4-2-OMe)P\}_2Mg]$ and one equivalent of Bu_2Mg , followed by methyl migration in a similar fashion to that observed in the formation of **80** and **81**.

The different reactivities of **75-79** and **83** suggest that the ligand cleavage reactions are dependent upon the Lewis acidity of the metal centre.



Scheme 5.2. Formation of **80** and **82** through facile C-O cleavage of compound **78**.



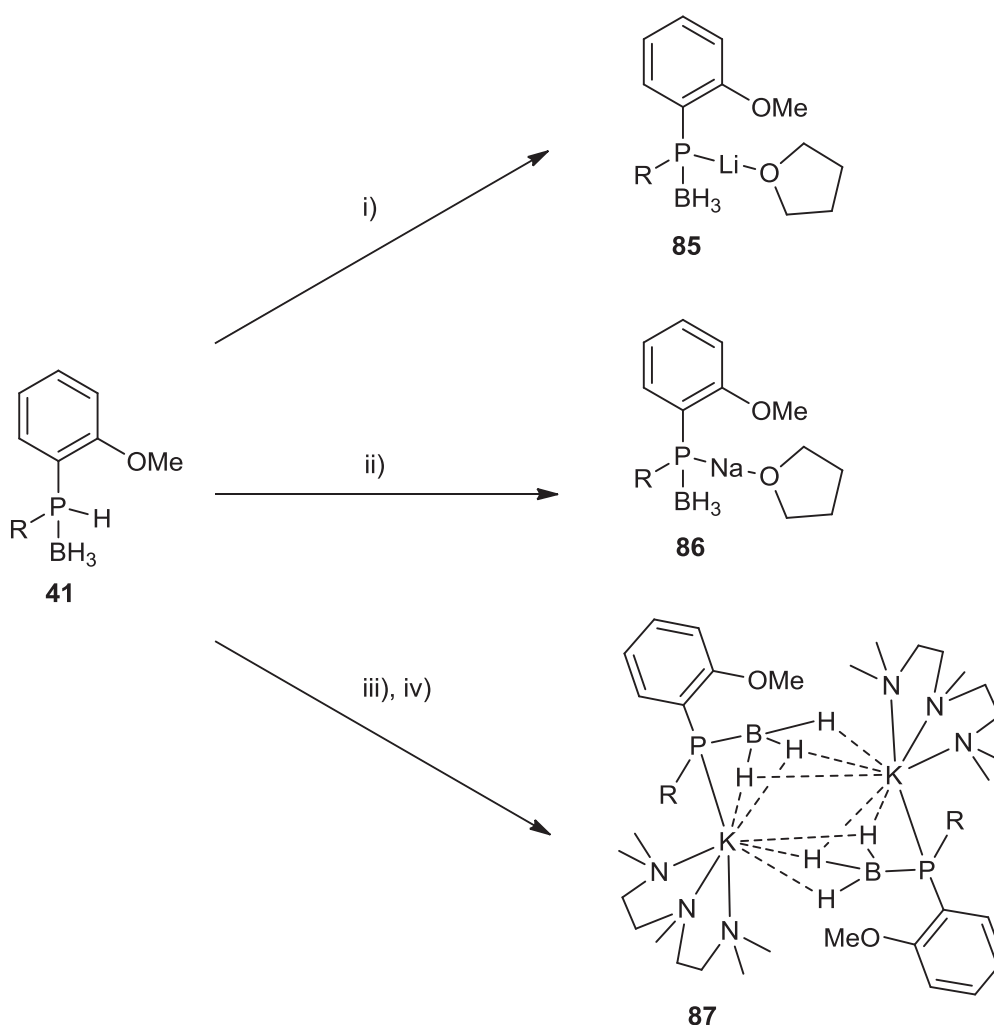
Scheme 5.3. Formation of **84** and **82** through facile C-O cleavage of compound **83**.

This chapter discusses the synthesis of several phosphido-borane adducts prepared from the anisole-functionalised phosphine-borane $\{(\text{Me}_3\text{Si})_2\text{CH}\}\text{P}(\text{C}_6\text{H}_4\text{-2-OMe})(\text{BH}_3)$ (**41**), and illustrates the effects that varying the metal centre and solvent have on the structures and reactivities of these complexes in solution.

5.2 Synthesis of alkali metal complexes $[\{(\text{Me}_3\text{Si})_2\text{CH}\}\text{P}(\text{C}_6\text{H}_4\text{-2-OMe})(\text{BH}_3)\text{M}(\text{L})]$ [$\text{M}(\text{L}) = \text{Li}(\text{THF})$ (**85**), $\text{Na}(\text{THF})$ (**86**), $\text{K}(\text{pmdeta})$ (**87**)]

The synthesis of compounds **85-87** is shown in Scheme 5.4. The reaction between **41** and one equivalent of $n\text{BuLi}$ in THF proceeds cleanly to yield the corresponding phosphido-borane $[\{(\text{Me}_3\text{Si})_2\text{CH}\}\text{P}(\text{C}_6\text{H}_4\text{-2-OMe})(\text{BH}_3)\text{Li}(\text{THF})]$ (**85**). Unfortunately, single crystals of

85 could not be isolated, and so the crystal structure of this compound could not be determined; its composition was confirmed by NMR spectroscopy. Treatment of **41** with one equivalent of either BnNa^{11} or BnK^{12} in THF yields the corresponding phosphido-boranes, which, upon removal of the solvent, yields yellow and orange solids respectively. The sodium compound may be crystallised from toluene in the presence of one equivalent of THF as the adduct $[\{(\text{Me}_3\text{Si})_2\text{CH}\}\text{P}(\text{C}_6\text{H}_4\text{-2-OMe})(\text{BH}_3)\text{Na}(\text{THF})]$ (**86**), whereas the potassium compound may be crystallised from toluene in the presence of pmdeta, as colourless blocks of the adduct $[\{(\text{Me}_3\text{Si})_2\text{CH}\}\text{P}(\text{C}_6\text{H}_4\text{-2-OMe})(\text{BH}_3)\text{K}(\text{pmdeta})]_2$ (**87**). Single crystals of **86** suitable for X-ray crystallography could not be isolated, however, its composition was confirmed by elemental analysis and NMR spectroscopy.



Scheme 5.4. Synthesis of **85**, **86** and **87**. i) $n\text{BuLi}$, THF, 1h, r.t. ii) BnNa , THF, 1h, r.t. iii) BnK , THF, 1h, r.t. iv) pmdeta, toluene [$\text{R} = (\text{Me}_3\text{Si})_2\text{CH}$].

5.3 Solution-phase characterisation of 85-87

Upon metalation of **41**, the $^{31}\text{P}\{^1\text{H}\}$ NMR signal shifts upfield from -22.3 ppm to between -62.5 and -64.3 ppm for compounds **85-87**. Although there are only slight variations in the $^{31}\text{P}\{^1\text{H}\}$ chemical shifts of the metalated compounds, the ^{31}P - ^{11}B coupling constants decrease in magnitude by 10 Hz steps between **41**, **85** and **86**, although this trend does not continue to compound **87** [$J_{\text{PB}} = 49.0$ (**41**), 39.4 (**85**), 29.8 (**86**), 29.4 (**87**) Hz].

The ^1H and $^{13}\text{C}\{^1\text{H}\}$ NMR spectra of **85-87** are as expected. In the ^1H NMR spectra of **85-87**, the diastereotopic SiMe_3 groups each give rise to sharp singlets between -0.3 and 0.5 ppm, whilst the adjacent CH protons appear as sharp doublets at 0.7 ppm for **85** and **86** [$^2J_{\text{PH}} = 6.9$ (**85**) and 7.3 Hz (**86**), and at 1.1 ppm for **87** [$^2J_{\text{PH}} = 7.8$ Hz]. The BH_3 protons appear as broad quartets, which collapse upon decoupling of the ^{11}B nucleus, to give sharp doublets at 0.6 [$^2J_{\text{PH}} = 3.2$ Hz], 0.7 [$^2J_{\text{PH}} = 6.9$ Hz] and 1.1 ppm [$^2J_{\text{PH}} = 5.5$ Hz] for **85**, **86** and **87**, respectively. In the $^{13}\text{C}\{^1\text{H}\}$ NMR spectra of **85-87**, the diastereotopic SiMe_3 groups give rise to two signals, a doublet [$^3J_{\text{PC}} = 8.6$ Hz for each compound] and a singlet, between 1.4 and 3.4 ppm, and the CH carbons appear as sharp doublets between 6.0-6.2 ppm [$^1J_{\text{PC}} = 44.1$ (**85**) and 41.2 Hz (**86** and **87**)].

5.4 Solid-state structure of 87

The adduct [$\{(\text{Me}_3\text{Si})_2\text{CH}\}\text{P}(\text{C}_6\text{H}_4\text{-2-CH}_2\text{OMe})(\text{BH}_3)\text{K}(\text{pmdeta})$] (**87**) crystallises as discrete centrosymmetric dimers in which the phosphido-borane ligand adopts a bidentate coordination mode; the structure of **87** is shown in Figure 5.2 with selected bond lengths and angles shown in Table 5.1. Each phosphido-borane ligand binds to the adjacent potassium ion through its phosphorus atom and an $\eta^2\text{-BH}_3$ interaction. The potassium ion is also bound by the second ligand in the dimer *via* an $\eta^2\text{-BH}_3$ interaction, such that each borane group acts as a $\mu_2\text{-}\eta^2:\eta^3$ bridge between the two cations, forming a pseudo-four-membered $\text{K}_2(\text{BH}_3)_2$ ring [B(1)-K(1)-B(1A) 93.94(5) $^\circ$]. Each potassium ion is coordinated by the three nitrogen atoms of a molecule of *pmdeta*. Unlike the related potassium salts [$\{(\text{Me}_3\text{Si})_2\text{CH}\}\text{P}(\text{C}_6\text{H}_4\text{-2-CH}_2\text{OMe})(\text{BH}_3)\text{K}(\text{pmdeta})$] (**51**) and [$\{(\text{Me}_3\text{Si})_2\text{CH}\}\text{P}(\text{C}_6\text{H}_4\text{-2-SMe})(\text{BH}_3)\text{K}(\text{pmdeta})$] (**66**), the potassium ions in **87** are not coordinated by the peripheral donor. This is rather unexpected, as a K-O interaction would be considered more favourable than a K-S

interaction, as observed in **66**, due to Pearson's hard-soft acid-base principle. Instead, the OMe groups in **87** are orientated away from the potassium ions, and the coordination about each potassium is completed by three short contacts to the central methyl group, and a methyl from each NMe₂ group of the pmdeta ligand. This is in contrast to **66**, which possesses a single K...Me contact to the central methyl of the pmdeta molecule. This shows that there is a fine balance between K-O and agostic type K...Me contacts.

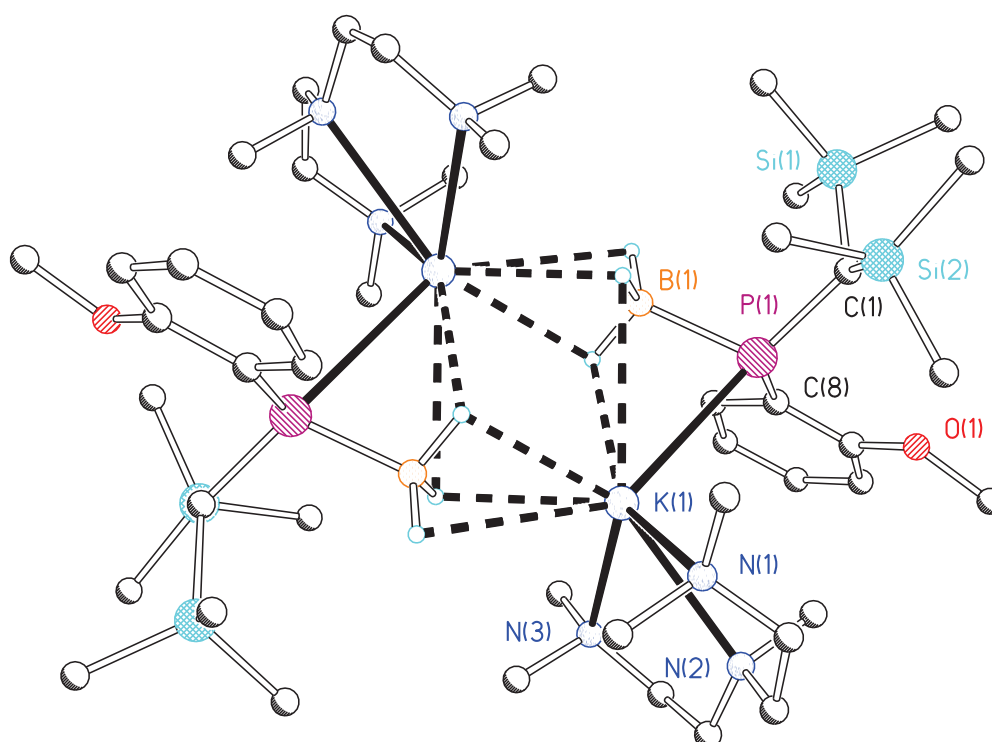


Figure 5.2. Molecular structure of compound **87**. All C-bound H atoms omitted for clarity.

The K-P bond lengths in **87** [K(1)-P(1) 3.2338(5) Å] are similar to the corresponding distance in **32** [3.320(2) Å], but are significantly shorter than the K-P distances in compounds **51** [3.7620(10) Å] and **66** [3.6617(6) Å]. This suggests that the K-P interactions are stronger when the metal centre is not bound by a peripheral donor atom. The K...B distances of 3.317(2) and 3.1365(8) Å in **87** are similar to the corresponding distances in **51** and **66**, and are consistent with η^2 - and η^3 -BH₃ coordination modes, respectively.

Compound **87** is very similar to **66**, except that the former has O- while the later has S-donor functionality. Both compounds crystallise as dimers, where dimerisation is afforded through $\mu^2\text{-}\eta^2\text{:}\eta^3$ bridging borane groups, and both have similar K...B and K-H distances. However, alongside K-P and K-BH₃ coordination modes, **66** also possesses coordination to potassium through the sulphur donor atom, to generate a five-membered chelate ring. In contrast, the oxygen donor atom in **87** does not coordinate to the adjacent potassium ion, as discussed above. Consequently, there are some variations between the structures of **66** and **87**. A comparison of the sum of angles within the C₂PB framework [312.33 and 321.34° for **66** and **87**, respectively] reveals that the geometry about the phosphorus anion in **87** is more planar than in **66**, whilst the K-P bond in **66** is significantly longer than the corresponding distance in **87**.

K(1)–P(1)	3.2338(5)	K(1)–N(1)	2.8320(13)
K(1)–B(1)	3.317(2)	K(1)–N(2)	2.9373(12)
K(1)–B(1A)	3.1365(18)	K(1)–N(3)	2.8555(13)
K(1)–H(1C)	3.359(17)		
K(1)–H(1B)	2.769(15)	P(1)–K(1)–B(1)	127.97(4)
K(1)–H(1AA)	3.311(16)	C(1)–P(1)–C(8)	104.00(6)
K(1)–H(1BA)	2.845(14)	B(1)–P(1)–C(1)	111.28(8)
K(1)–H(1CA)	2.735(17)	B(1)–P(1)–C(8)	106.06(8)
P(1)–B(1)	1.9568(18)	K(1)–P(1)–C(1)	147.31(4)
P(1)–C(1)	1.8772(15)	K(1)–P(1)–C(8)	104.76(5)
P(1)–C(8)	1.8375(15)	B(1)–K(1)–B(1A)	93.94(5)
		K(1)–P(1)–B(1)	74.97(6)

Table 5.1. Selected bond lengths (Å) and angles (°) of compound **87**.

5.5 Thermally-induced reactions of **85**

In chapter 4, the stabilities of the analogous phosphido-boranes **64**, **65** and **66** on exposure to heat and light were explored, and it was found that these complexes do not undergo any change. Compound **87** is also found to be thermally and photolytically stable in THF solutions over extended periods of time, as is the previously reported phosphide [$\{(Me_3Si)_2CH\}P(C_6H_4-2-OMe)K$ (**88**).⁷

In contrast, under certain conditions, compound **85** undergoes one of two competing, thermally-induced reactions. Heating a solution of **85** and one equivalent of tmeda in toluene to 60 °C for 72 h resulted in the conversion of the phosphido-borane complex into a mixture of the unusual aryloxide cluster [$\{(Me_3Si)CH\}PH(C_6H_4-2-O)Li$]₆ (**89**) and the tertiary phosphine-borane $\{(Me_3Si)_2CH\}PMe(BH_3)(C_6H_4-2-OMe)$ (**90**), which are observed in the ³¹P NMR spectrum as a sharp doublet [$^1J_{PH} = 217.6$ Hz] and a broad quartet [$^1J_{PB} = 58.8$ Hz] at -72.7 and 12.5 ppm, respectively, in an approximately 1:1 ratio (Figure 5.3). A broad signal is also observed in the ³¹P NMR spectrum at around 79.0 ppm, due to an unidentified side product (**A**) (see section 5.10).

The identity of **89** was confirmed by multi-element NMR spectroscopy (see section 5.6) and X-ray crystallography (see section 5.7), which demonstrates unequivocally that the structure of **89** results from elimination of the methyl and BH₃ groups from a phosphido-borane ligand, and concurrent formation of a P-H bond (Scheme 5.5). The cleaved methyl group appears to migrate to a second phosphido-borane ligand, forming a P-Me bond, thus generating **90**. It appears that **85** must be coordinated to THF for this thermolysis reaction to proceed; this is usually present as **85** is prepared in THF solutions. THF-free samples of **85** showed no evidence for conversion after heating in toluene for several days.

Alternatively, when a solution of **85** in toluene, in the presence of one equivalent of tmeda and an excess of THF is heated for 16 h at 60 °C, the formation of new phosphorus-containing species results. This compound gives rise to a broad peak in the ³¹P NMR spectrum at -69.7 ppm (Figure 5.4), which is consistent with a phosphido-borane-containing species, and is observed alongside compound **90**, which also forms in the reaction. Unfortunately, this new compound could not be separated from **90**.

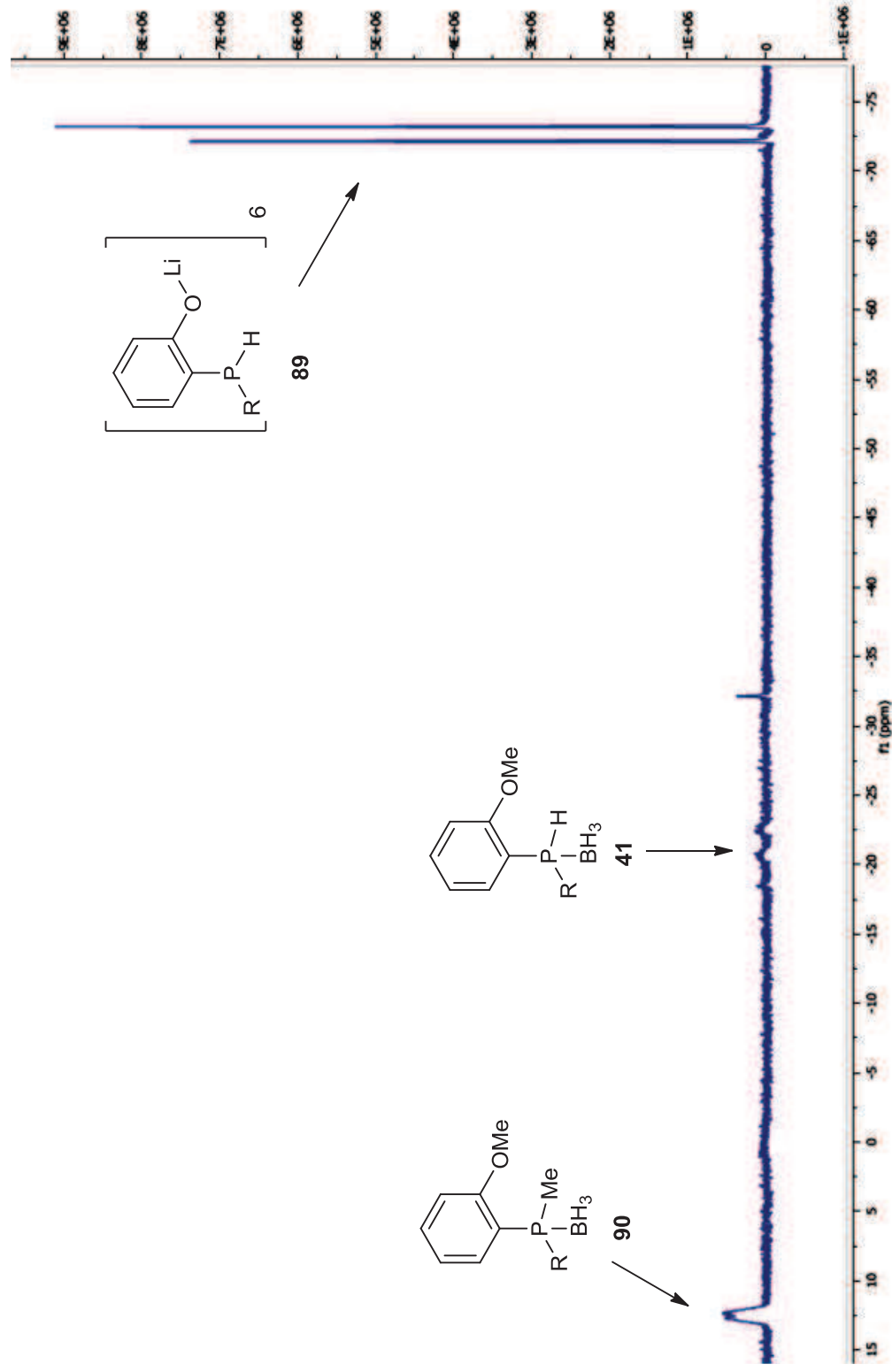
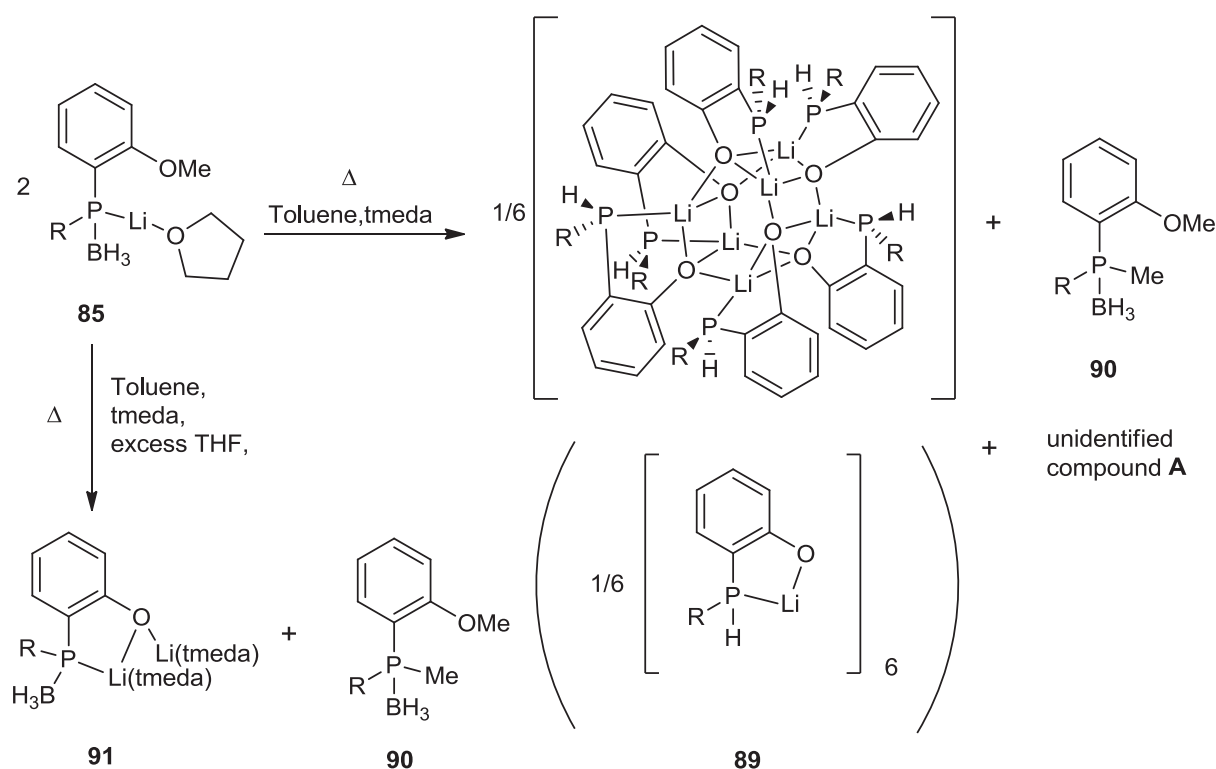


Figure 5.3. Proton-coupled ^{31}P NMR spectrum of **89** and **90** in THF, from the thermolysis of **85** in the presence of tmeda, after heating at 50°C for 16 h in toluene.

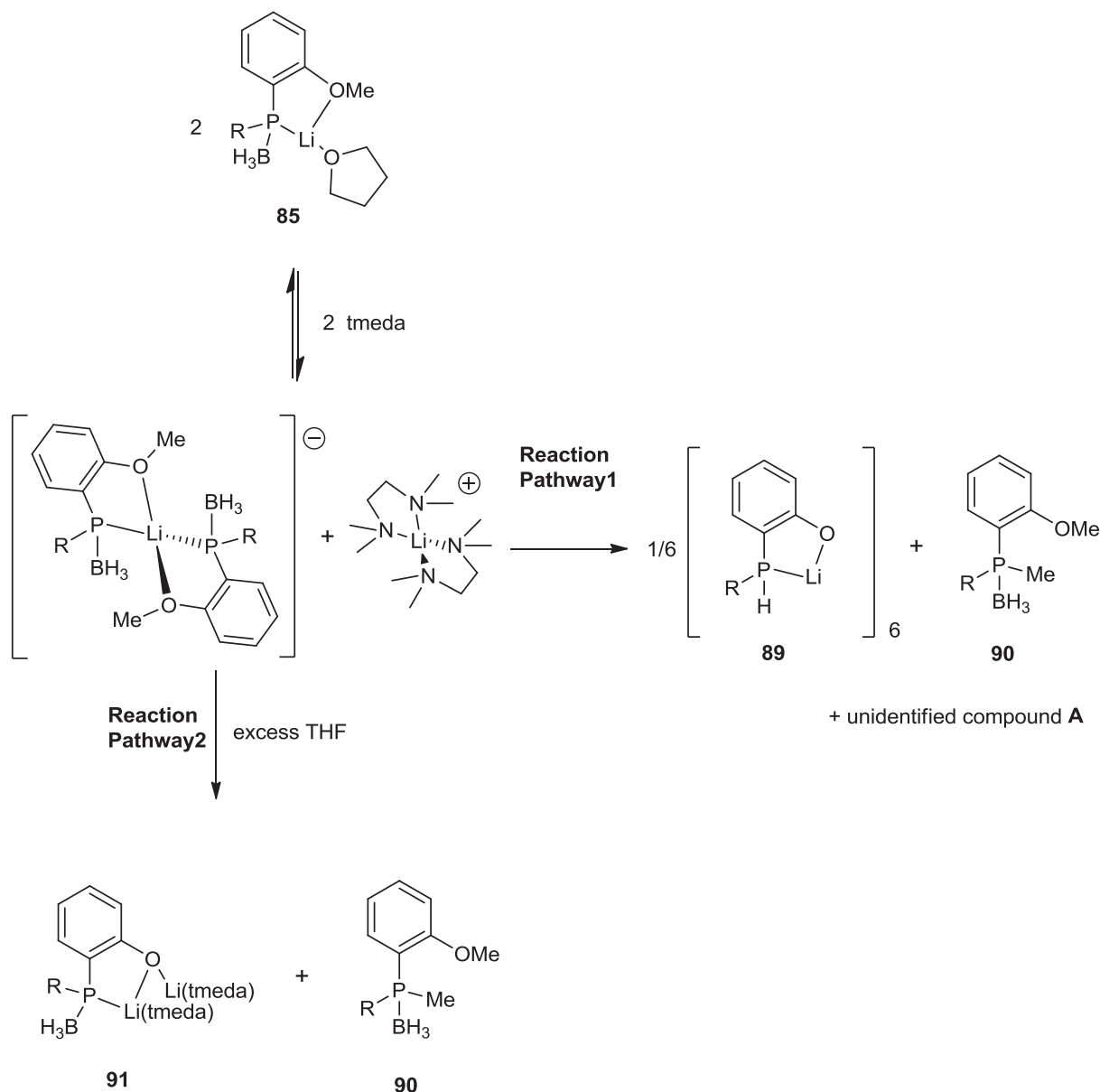
Previous studies have shown that degradation of the related calcium phosphide **78** in THF/ether results in the formation of the corresponding tertiary phosphine **82**, and a dianionic phosphide ligand, which forms the novel calcium cluster **80** (Section 5.1). On the basis of these observations and the presence of **90**, we propose that, in the presence of excess THF, **85** undergoes a similar ligand degradation to generate an alkoxo-functionalised phosphido-borane dianion, possibly forming the complex $[\{(Me_3Si)_2CH\}P(BH_3)(C_6H_4-2-O)Li_2(tmeda)_2]$ (**91**, Scheme 5.5).



Scheme 5.5. Thermolysis reactions of compound **85**.

The proposed mechanisms for the formation of **89**, **90** and **91** are shown in Scheme 5.6. Both processes may occur *via* an equilibrium to generate an “ate” species, analogous to the proposed mechanism for the formation of **83**, which is set up to undergo an intramolecular methyl migration, as also seen for the calcium and ytterbium complexes **80** and **81**. The reaction conditions are finely balanced; when THF is present in a stoichiometric amount, reaction pathway 1 is preferred, generating **89** and **90**, whilst in the presence of an excess of THF, pathway 2 is favoured, and **91** is generated alongside **90**.

In the absence of tmeda, yields of either **89** or **91** and **90** are noticeably lower. This may suggest that tmeda favours the formation of the intermediate ate complex, promoting the methyl-migration reaction.



Scheme 5.6. Proposed mechanisms for the formation of **89**, **90** and **91**.

Diorganolithates were first proposed as intermediates over 50 years ago, although only a few examples of complexes of this type have been characterised in the solid state. Examples include the phosphine-borane-stabilised carbanion complex $[(\text{THF})_3\text{Li}\{(\text{Me}_3\text{Si})_2\text{CPMe}_2(\text{BH}_3)\}_2\text{Li}]$ (**92**), which crystallizes as a contact ion multiple ate complex. In solution, **92** is subject to a dynamic equilibrium between the ate complex and a second, possibly

monomeric, species (Scheme 5.7).¹³ Therefore, it is reasonable to propose that in solution, **85** also exists in equilibrium between the monomeric species and the corresponding ate complex.



Scheme 5.7. Equilibrium between a mononuclear and an ate complex.

The conditions for these thermolysis reactions are finely balanced, where a slight variation in THF concentrations appears to be the only factor which determines the reaction pathway that is followed. The extent of aggregation in phosphide complexes with alkali metals in solution is dependent on the nature of donor solvents present e.g. the complex $[\text{Li}(\text{}^t\text{Bu}_2\text{P})]_n$ is tetrameric in THF (**1**), but is dimeric in DME (**2**), and as a consequence, this can have an effect on the reactivities of these species in solution. A well-known organometallic example which demonstrates this is $n\text{BuLi}$, which is hexameric in hexanes, but upon complexation with tmeda, the aggregate is broken down, generating a more reactive species.¹⁴ Therefore, it is possible that the reactivity of **85**, upon thermolysis, is governed by its aggregation state in solution, which can be affected by changes in THF concentration in solution; an excess of THF may favour the monomeric species over the ate complex.

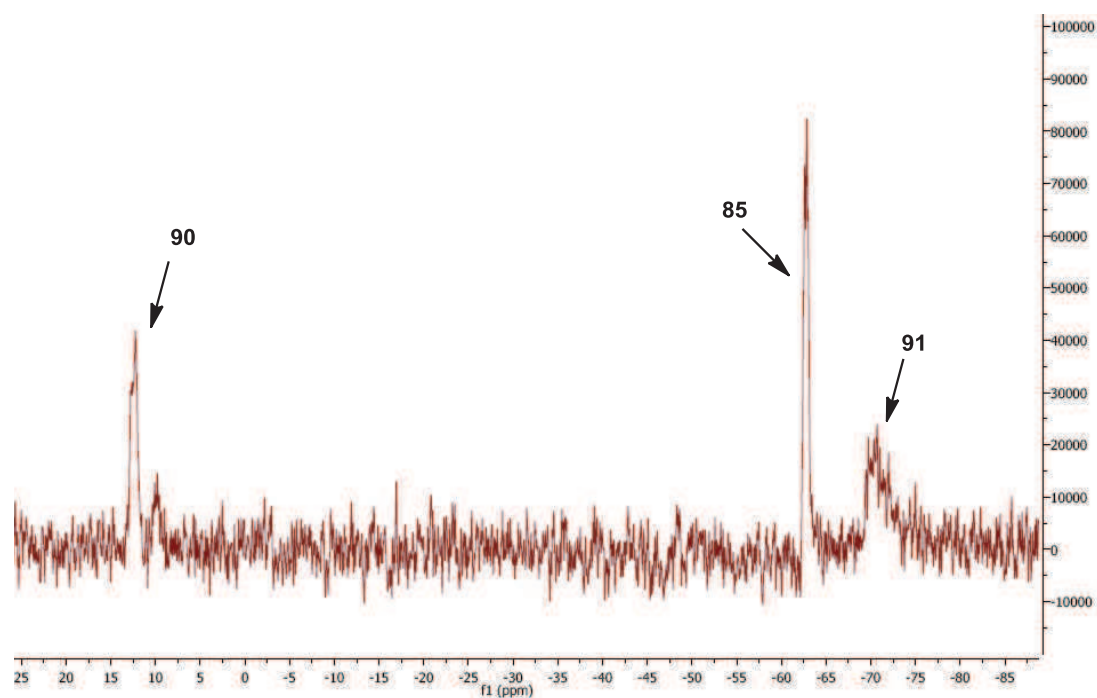


Figure 5.4. ^{31}P NMR spectrum of the conversion of **85** into **90** and **91** after heating at 50°C for 16 h in toluene/THF.

5.6 Solution-phase characterisation of compound **89**

The ^1H and $^{13}\text{C}\{^1\text{H}\}$ NMR spectra of **89** in d_6 -benzene is consistent with a single ligand environment. In the ^1H NMR spectrum, the P-H proton appears at 4.5 ppm as a doublet of doublets due to coupling of the proton to the ^{31}P nucleus [$^1J_{\text{PH}} = 217.6$ Hz] and coupling to the adjacent PCH proton [$^3J_{\text{HH}} = 5.5$ Hz]. The PCH proton gives rise to a doublet of doublets at 0.7 ppm [$^3J_{\text{HH}} = 5.5$ Hz, $^2J_{\text{PH}} = 1.9$ Hz], whilst the Me_3Si groups appear as a singlet at 0.2 ppm due, presumably, to rapid, reversible P-Li cleavage. In the $^{13}\text{C}\{^1\text{H}\}$ NMR spectrum, the Me_3Si groups also appear as a singlet at 1.1 ppm, whereas the adjacent CH appears as a doublet at 4.4 ppm due to coupling to the phosphorus nucleus, where $^1J_{\text{PC}} = 42.2$ Hz. The ^{31}P NMR spectrum of **89** exhibits a sharp doublet at -72.7 ppm due to the ^{31}P - ^1H coupling [$^1J_{\text{PH}} = 217.6$ Hz].

To gain a further understanding of the formation of **89**, the kinetics of the thermolysis reaction were studied. NMR samples containing solutions of known concentrations of **85** in toluene and a few drops of THF were prepared; the progress of the thermolysis reaction was then monitored by $^{31}\text{P}\{^1\text{H}\}$ NMR spectroscopy over a 16 h period for a range of

temperatures. Changes in the concentration of **85** were measured against the presence of impure quantities of **41**, which remained at a constant concentration throughout the experiment. The experiment was repeated at various temperatures (23.1 to 60 °C), to determine the rate of thermolysis, however, it was impossible to ascertain whether 1st or 2nd order kinetics were being obeyed under the conditions that the data was collected.

5.7 Solid-state structure of compound **89**

Compound **89** crystallises as a hexameric phosphine-substituted lithium aryloxide cluster with a puckered-hexagonal prismatic Li₆O₆ core; the structure of **89** is shown in Figure 5.5 (the Li₆O₆ core is shown in Figure 5.6), and selected bond lengths and angles are shown in Table 5.2. The Li and O atoms sit in alternating positions in the hexagonal prism, and are bridged through μ^3 -type interactions, thus linking the six units. The coordination about each lithium ion is completed by the P atom of an adjacent ligand, to give a five-membered chelate ring [P-Li-O 84.52(17)-85.20(2)°].

P–Li	2.523(5)-2.551(5)
P–H	1.31(3)-1.48(3)
Li–O (hexagonal face)	1.870(6)-1.924(6)
Li–O (edge)	2.051(5)-2.066(5)
Li–P–H	115.8(12)-118.1(10)
P–Li–O (bite angle)	84.52(17)-85.2(2)
O–Li–O (hexagonal face)	124.8(3)-126.9(3)
Li–O–Li (hexagonal face)	112.2(2)-113.7(2)
O–Li–O (edge)	94.8(2)-98.4(2)
Li–O–Li (edge)	81.9(2)-84.9(2)

Table 5.2. Selected ranges of bond lengths (Å) and angles (°) for compound **89**.

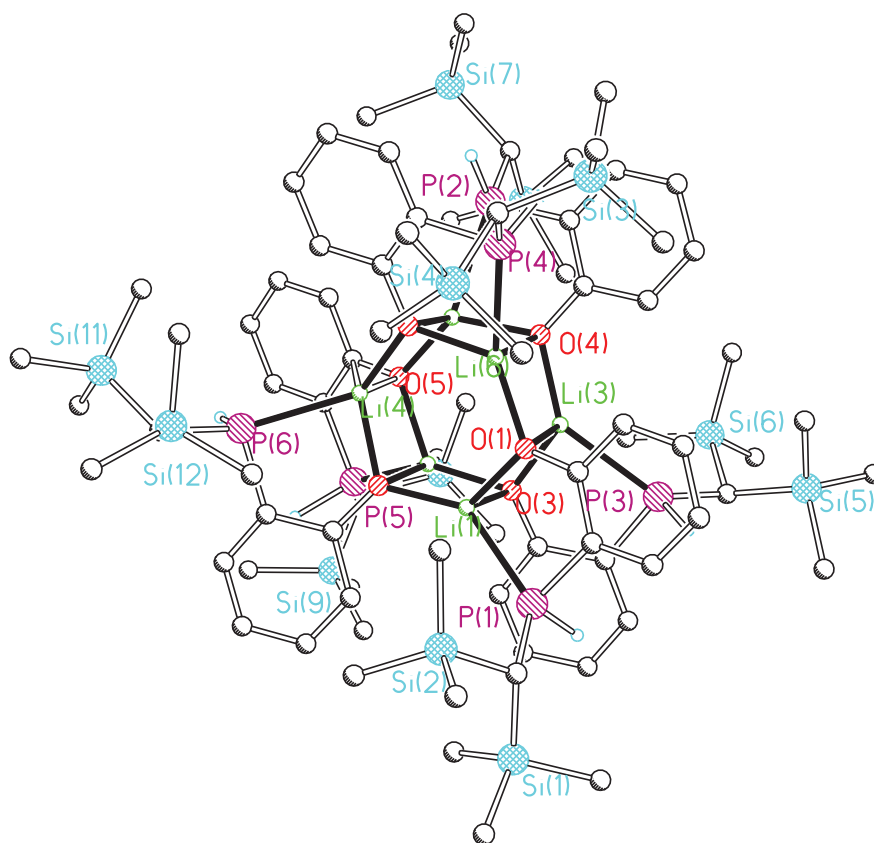


Figure 5.5. Molecular structure of compound **89**. All C-bound H atoms omitted for clarity.

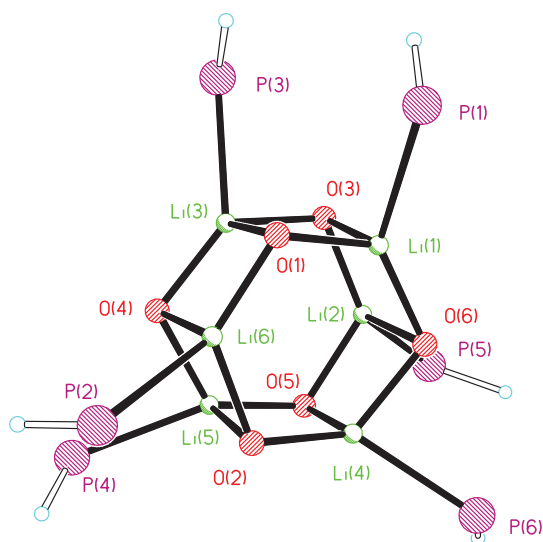


Figure 5.6. Structure of the core of **89**, with all C, Si and H atoms omitted bar phosphine protons.

The P-Li distances in **89** range from 2.523(5) to 2.551(5) Å, and are typical of P-Li distances of Li-PR₃ containing complexes, which range between 2.51 and 3.18 Å.¹⁵ The Li-O distances range from 1.901(5) to 2.055(5) Å, which are similar to Li-O distances observed in related lithium alkoxides.¹⁶⁻²⁰ The O-Li-O angles within the hexagonal face of the Li₆O₆ core, range from 112.5(2) to 125.6(3)°.

Lithium alkoxides have been extensively used as precursors to ceramic and electronic materials^{21,22} and have been investigated in great detail, with many of these compounds being crystallographically characterised. These complexes typically form aggregates, and usually adopt one of the structural motifs **I-V**, as shown in Figure 5.7. The contributing factors which govern the structures of these compounds include: the Lewis basicity of the solvent, the binding mode of the ligand (mono-, bi-, tri- or polydentate), the steric bulk of the ligand, and crystal packing effects.^{16,19,20}

The majority of simple solvent-free lithium alkoxide compounds that have been characterised typically crystallise as hexanuclear clusters.^{16,20,23,24} Three exceptions are polymeric [Li(OMe)]_∞ (**93**),^{25,26} dinuclear [Li(OC^tBu₃)]₂ (**94**),²⁷ and octanuclear [Li(μ₃-OCH₂CMe₃)]₈ (**95**), although **95** adopts a hexagon-cube prism structure **IV**, which maintains a high degree of solubility.¹⁷ The structures observed for these compounds are associated with the degree of steric hindrance introduced by the pendant hydrocarbon chain of the alkoxide ligand. Using less sterically hindered ligands tends to result in insoluble polymer aggregates, such as **93**, which limits the utility of these compounds. A number of related lithium-oxygen hexamers such as enolates,²⁸⁻³⁰ azaenolates,^{31,32} and a hydroxylamide³³ have previously been reported.

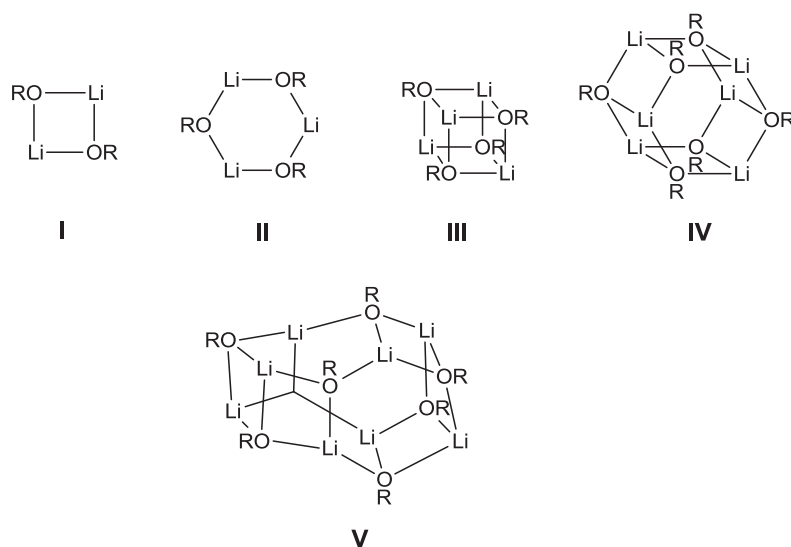


Figure 5.7. Typical $[\text{Li}(\text{OR})_n]$ structural motifs.

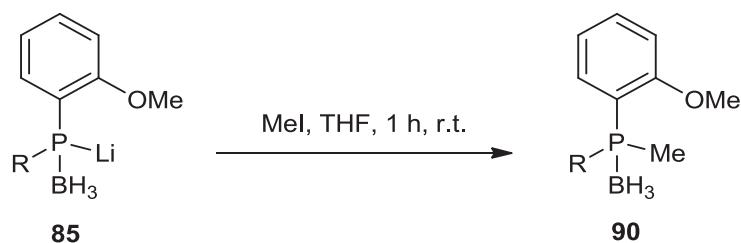
There have also been several reports detailing the structures of related α -amine-stabilised lithium alkoxides, some of which have also adopted the hexameric prism structure **IV**. The first such example was $[(4\text{-methoxybenzaldehyde})(N\text{-methylpiperazide})\text{Li}]_6 \cdot 2\text{PhMe} \cdot \text{THF}$ (**96**), which was reported by Armstrong *et al* in 1999, in which the lithium ions in the Li_6O_6 core are each coordinated by an N atom from the adjacent ligand, thus affording stable four-membered N-C-O-Li rings.¹⁸ This compound is closely related to the lithium enolate $\text{Li}_6[\text{OC}(\text{OEt})=\text{C}(\text{H})\text{NEt}_2]_6$ (**97**).³⁰

More recently, a series of lithium quinolates: $[\text{Li}(\text{NC}_9\text{H}_6\text{-8-O})]$ (**98**), $[\text{Li}(\text{NC}_9\text{H}_5\text{-2-Me-8-O})]$ (**99**) and $[\text{Li}(\text{NC}_9\text{H}_5\text{-2-Ph-8-O})]$ (**100**), were synthesised by Rajeswaran and co-workers.¹⁹ It was found that compounds **98** and **99** adopted the hexagonal prism motif **IV**, whilst **100** crystallises as a tetramer (**III**). Interestingly, computational studies of these complexes, which were carried out in tandem, showed that the observed tetrameric structure of **100** was less favourable (+1.2 kcal/mol/monomer) than the hexameric prism structure. However, in that particular case the crystal packing effects probably outweighed the small differences in cluster stability.

5.8 Synthesis and solution-phase characterisation of $\{(Me_3Si)_2CH\}PMe(BH_3)(C_6H_4-2-OMe)$ (**90**)

To confirm the identity of **90**, which was isolated from the thermolysis of **85** and characterised using multi-nuclear NMR spectroscopy and mass spectrometry, this compound was also prepared using a direct route.

The reaction between a solution of **85** in THF and one equivalent of MeI yields **90** as a white solid after aqueous work-up (Scheme 5.8); the 1H , $^{31}P\{^1H\}$, and $^{11}B\{^1H\}$ NMR spectra of this deliberately prepared sample are identical to those observed in the 1:1 mixture of **89** and **90** after thermolysis of **85**; in the $^{31}P\{^1H\}$ NMR spectrum a broad quartet is observed at 11.7 ppm [$^1J_{PB} = 58.8$ Hz], whilst in the $^{11}B\{^1H\}$ NMR spectrum **89** gives rise to a broad doublet at -37.5 ppm [$^1J_{BP} = 58.8$ Hz]. The 1H NMR spectrum is as expected; the P-methyl protons are observed as a sharp doublet at 1.7 ppm [$^2J_{PH} = 10.1$ Hz] due to coupling to phosphorus, and in the $^{13}C\{^1H\}$ NMR spectrum, the signal due to the PMe is a doublet [$^1J_{PC} = 9.6$ Hz] at 16.7 ppm. The borane protons appear as a broad peak at around 0.9 ppm, but upon ^{11}B decoupling the signal collapses into a sharp doublet [$^2J_{PH} = 14.7$ Hz].

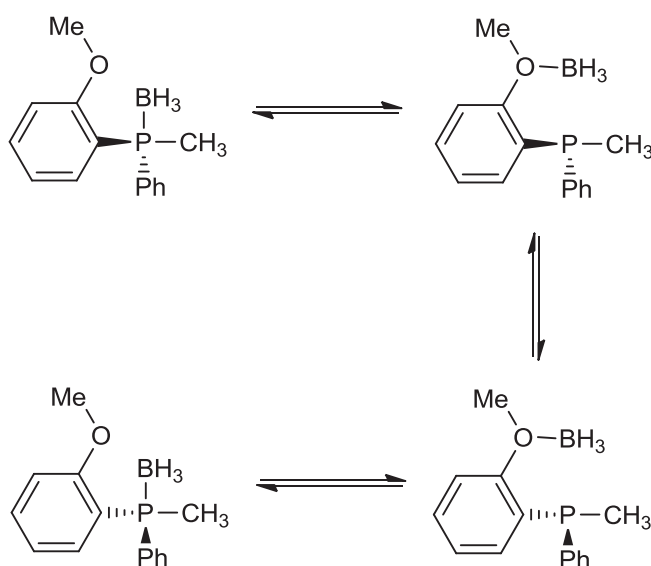


Scheme 5.8. Synthesis of **90** [R = $(Me_3Si)_2CH$].

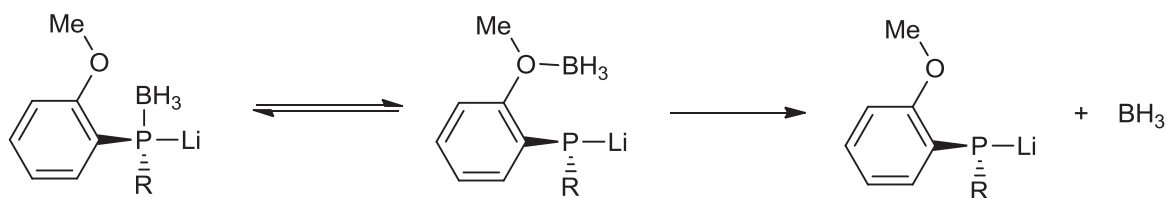
5.9 Investigation into the mechanism of formation of **89**

Although the mechanisms for the thermolysis reactions of **85** are clearly complex, NMR spectroscopic studies have given some insight into the processes occurring. The chemistry of facile O-Me cleavage is well established for the ligand $[\{(Me_3Si)_2CH\}P(C_6H_4-2-OMe)]^-$, however the borane elimination and P-H formation processes observed in the formation of **89** are highly unusual.

It has already been mentioned in section 5.1 that compound **73** was identified as a key intermediate in the synthesis of DIPAMP. In an attempt by Imamoto *et al* to develop synthetic routes to prepare enantiomerically pure **73**, it was observed that when **73** is prepared by the treatment of $(R_p,1'R,2'S,5'R)\text{-}((2'\text{-}^i\text{Pr-5-C}_6\text{H}_5\text{Me})\text{O})\text{MePhP}(\text{BH}_3)$ with *o*-anisyllithium in a solution of THF/DME at reflux, it is unexpectedly formed as a racemic mixture. The proposed mechanism for this observed behaviour is shown in Scheme 5.9. It is proposed that, in solution at high temperatures, an equilibrium is established where the oxygen atom can abstract the BH₃ group, breaking the P-B bond, thus allowing phosphorus to undergo an inversion, before the P-B bond is reformed.³⁴ This behaviour may apply to borane elimination observed in the formation of **89**; a suggested mechanism is shown in Scheme 5.10.



Scheme 5.9. Racemisation of **73**.



Scheme 5.10. Possible mechanism for borane elimination of **85** [R = (Me₃Si)₂CH].

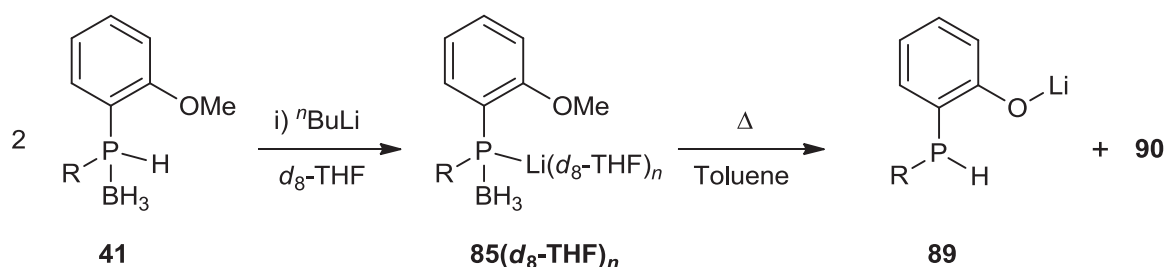
Perhaps the most intriguing aspect in the formation of **89** is the origin of the hydrogen atom of the P-H group. The hydrogen may be derived from the solvents used in synthesis, or

possibly the methyl or borane group which are cleaved during thermolysis. Several experiments were designed to identify the source from which the P-H proton is derived. These may be divided into two categories: deuterated solvents and deuterated phosphine-boranes. In each case, the potential proton sources were modified by replacing protons with deuterium atoms; the formation of a P-D bond can then be identified by ^{31}P and ^2D NMR spectroscopy.

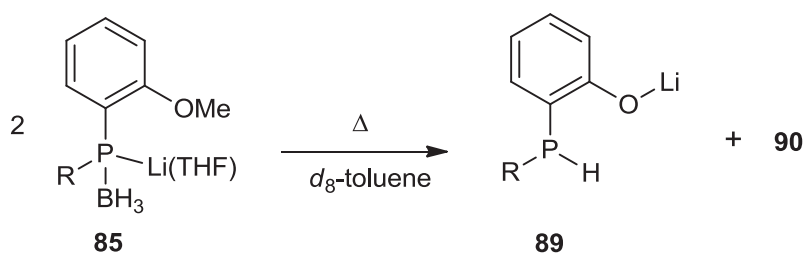
5.9.1 Deuterated solvents

Two solvents are used in the overall synthesis of **89**: THF in the synthesis of **85** and toluene, which is used in the thermolysis reaction. To determine if the P-H hydrogen atom is derived from one of these solvents, two experiments were performed using deuterated solvents. In the first instance, compound **41** was dissolved in d_8 -THF and treated with $^n\text{BuLi}$, to yield compound **85**(d_8 -THF) $_n$. The solvent was removed from the product *in vacuo* to give **85**(d_8 -THF) as a sticky yellow residue. Compound **85**(d_8 -THF) was then dissolved in toluene and heated for 16 h at 50 °C (Scheme 5.11). In the second experiment, compound **85** was synthesised using the general method as described in section 5.2. The THF used for the reaction was then removed *in vacuo* until **85** was left as a sticky residue, which was then dissolved in d_8 -toluene and heated for 16 h at 50 °C (Scheme 5.12).

Both reactions were monitored by ^{31}P NMR spectroscopy, which in each case saw the rise of the characteristic sharp doublet at -72.7 ppm associated with the P-H centre of **89**, thus eliminating the solvents as the proton source in this rearrangement.



Scheme 5.11. Thermolysis of **85**(d_8 -THF) $_n$ [R = (Me₃Si)₂CH].



Scheme 5.12. Thermolysis of **85** in d_8 -toluene [R = (Me₃Si)₂CH].

5.9.2 Synthesis of {(Me₃Si)₂CH}PH(BH₃)(C₆H₄-2-OCD₃) (**101**) and {(Me₃Si)₂CH}PH(BD₃)(C₆H₄-2-OMe) (**102**)

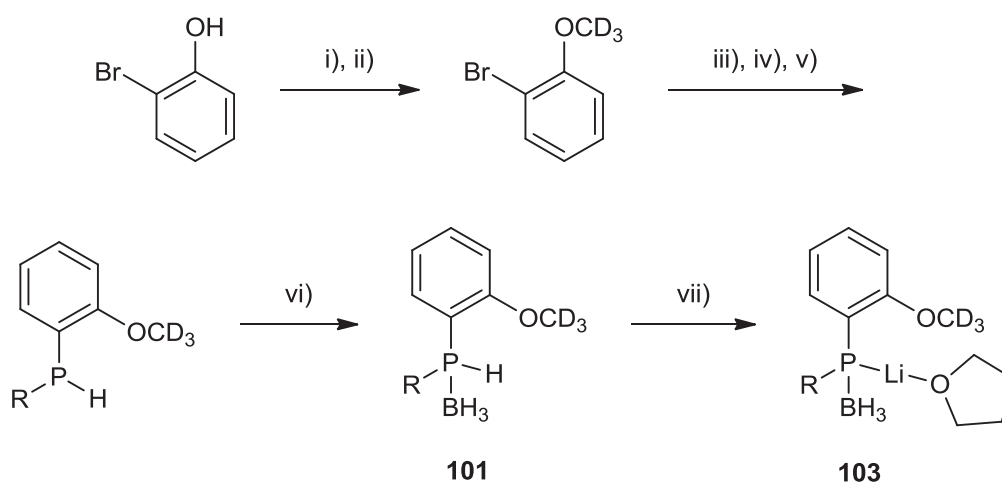
After it was determined that the P-H proton in **89** is not derived from the solvents used in its preparation, two variants of the precursor phosphine-borane **41**, modified with deuterium, were synthesised: {(Me₃Si)₂CH}PH(C₆H₄-2-OCD₃)(BH₃) (**101**) and {(Me₃Si)₂CH}PH(C₆H₄-2-OMe)(BD₃) (**102**). The syntheses of phosphine-boranes **101** and **102** are shown in Schemes 5.13 and 5.14, respectively.

The reaction between 2-bromophenol and potassium hydroxide in acetonitrile (MeCN) at low temperatures, followed by the addition of 1 equivalent of CD₃I yields BrC₆H₄-2-OCD₃, which can be isolated as an oil after aqueous work-up. Treatment of a solution BrC₆H₄-2-OCD₃ in Et₂O with ⁿBuLi at 0 °C yields LiC₆H₄-2-OCD₃, which is added *in situ* to a cold solution of {(Me₃Si)₂CH}PCl₂ (**43**), to yield the monochlorophosphine {(Me₃Si)₂CH}PCl(C₆H₄-2-OCD₃), which may then be reduced with LiAlH₄ *in situ* to yield the phosphine {(Me₃Si)₂CH}PH(C₆H₄-2-OCD₃), which is isolated as a colourless oil after aqueous work-up. Reaction of the phosphine with BH₃·SMe₂ yields **101**, which may be isolated as colourless, crystalline needles from cold light petroleum.

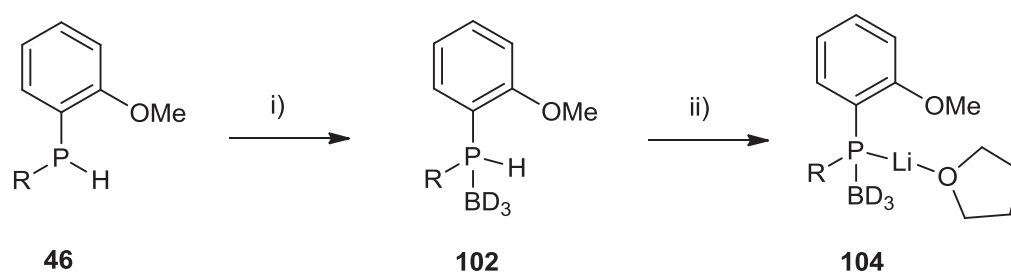
The reaction between {(Me₃Si)₂CH}PH(C₆H₄-2-OMe) (**46**) and BD₃·THF in a solution of THF yields **102**. Upon removal of the solvent *in vacuo*, **102** is isolated as a colourless oil.

Treatment of a THF solution of either **101** or **102** with one equivalent of ⁿBuLi yields the corresponding phosphido-boranes [{(Me₃Si)₂CH}P(C₆H₄-2-OCD₃)(BH₃)Li(THF)] (**103**) and [{(Me₃Si)₂CH}P(C₆H₄-2-OMe)(BD₃)Li(THF)] (**104**), respectively (Schemes 5.13 and 5.14).

The phosphido-boranes were dissolved in toluene and heated to 60 °C. The thermolysis of **103** was monitored by ^{31}P NMR spectroscopy; after 16 h stirring at 50 °C, the sharp doublet associated with the P-H centre of **89** appeared at -72.7 ppm, simultaneously with the appearance of a broad quartet at 11.7 ppm due to the CD_3 analogue of **90** [$\{(\text{Me}_3\text{Si})_2\text{CH}\}\text{P}(\text{CD}_3)(\text{BH}_3)(\text{C}_6\text{H}_4\text{-2-}\text{OCD}_3)$]. As a consequence the methyl group was eliminated as a potential proton source in the formation of **89**.



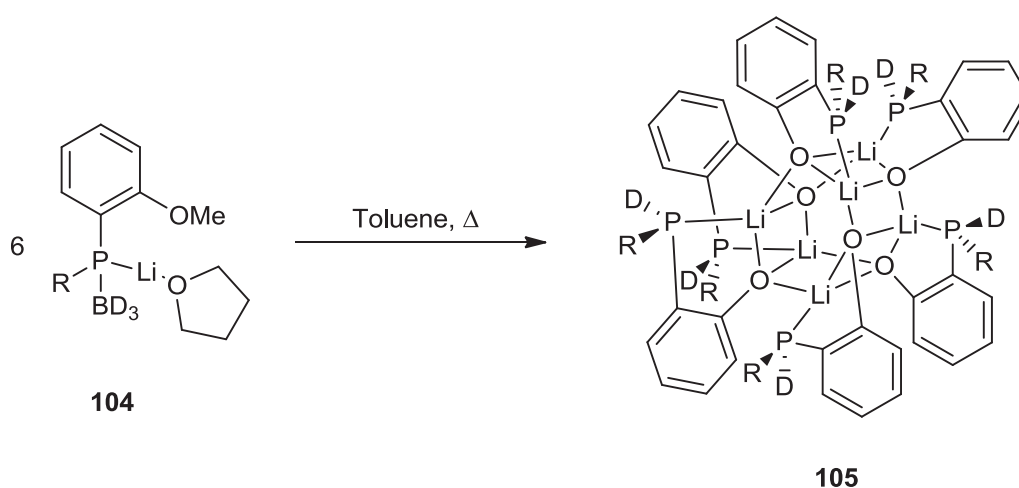
Scheme 5.13. Synthesis of **103**. i) KOH, MeCN, 0 °C, ½ h ii) CD_3I , MeCN, 0 °C, 1 h; r.t., 40 h. iii) $^n\text{BuLi}$, Et_2O , 0 °C, 2 h. iv) **43**, Et_2O , -78 °C, 16 h. v) LiAlH_4 , 35 °C, 2 h. vi) $\text{BH}_3\cdot\text{SMe}_2$, THF, 1 h, r.t. vii) $^n\text{BuLi}$, THF, 1 h, r.t. [R = $(\text{Me}_3\text{Si})_2\text{CH}$].



Scheme 5.14. Synthesis of compound **104**. i) $\text{BD}_3\cdot\text{SMe}_2$, THF, 1 h, r.t. ii) $^n\text{BuLi}$, THF, 1 h, r.t. [R = $(\text{Me}_3\text{Si})_2\text{CH}$].

The thermolysis of **104**, although not in the presence of tmeda, was also monitored by ^{31}P NMR spectroscopy. After heating for approximately two hours a new peak began to appear in the ^{31}P NMR spectrum at around -80.0 ppm. After 16 h hours stirring at 50 °C, the thermolysis of **104** had given rise to a broad quartet at 11.7 ppm (**90**), whilst the broad signal at -80.0 ppm grew in intensity; the sharp doublet associated with the P-H signal of **89** was not observed. The ^2D NMR spectrum of the thermolysis of **104** (Figure 5.8) exhibits a peak

at 3.9 ppm, which suggests the presence of a P-D bond, thus indicating that the complex $[\{(Me_3Si)CH\}PD(C_6H_4-2-O)]_6Li_6$ (**105**) has formed (Scheme 5.15); although the signal is not the expected doublet, this may be due to poorly resolved coupling and/or a small ^{31}P - 2D coupling constant. It therefore appears that the BH_3 group is the source of the P-H proton in compound **89**. Interestingly, a peak also appears at 2.1 ppm in the 2D NMR spectrum, which may possibly be attributed to the unidentified compound **A**, which will be discussed in the following section.



Scheme 5.15. Thermal rearrangement of compound **104** [$R = (Me_3Si)_2CH$].

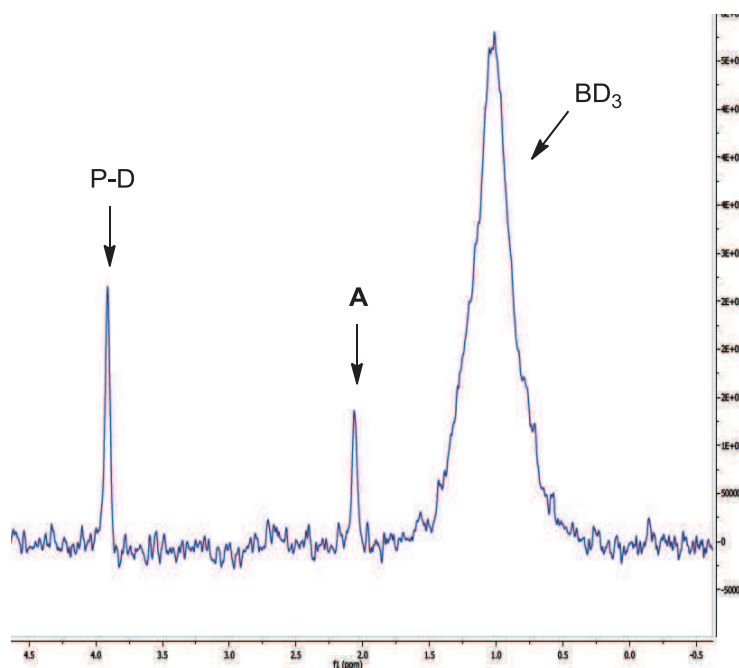
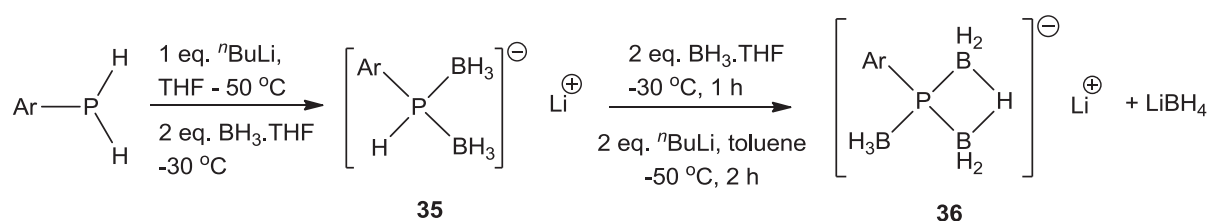


Figure 5.8. 2D NMR spectra of thermolysis of **104** in toluene.

5.10 Identity of unknown compound A

We were, unfortunately, unable to isolate and identify compound **A**, which gives rise to the broad signal at 79.0 ppm in the ^{31}P NMR spectra of the thermolysis products of **85**. However, it is likely that, since the proton in **89** is derived from a BH_3 group, compound **A** results from elimination of a borane proton from **85**. In this regard, it is notable that Romanenko and co-workers recently reported the synthesis of the complex $[(\text{mes}^*)\text{P}(\text{BH}_3)(\mu\text{-BH}_2)_2\text{HLi}(\text{THF})_2]_2$ (**36**). Compound **36** was prepared by the reaction of the phosphido-bis(borane) $[(\text{mes}^*)\text{P}(\text{BH}_3)_2\text{Li}(\text{THF})_3]$ (**35**) with an excess of $^n\text{BuLi}$, followed by addition of excess $\text{BH}_3\cdot\text{THF}$, and forms as a mixture with LiBH_4 (Scheme 5.16). The prominent feature in the structure of **36** (Figure 5.9) is the hydride-bridged $\mu\text{-B}_2\text{H}_5$ unit.³⁵



Scheme 5.16. Synthesis of compounds **35** and **36** [Ar = mes^*].

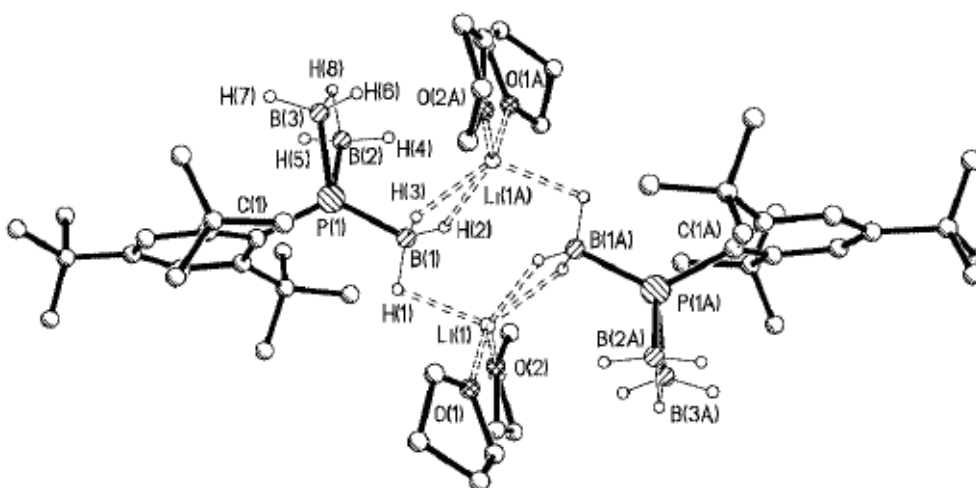
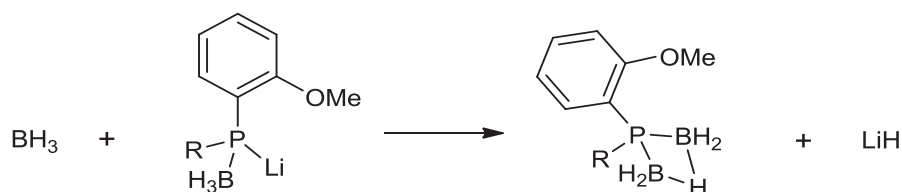


Figure 5.9. Structure of compound **36**.

It is tentatively proposed that, should **85** eliminate a proton from its borane group, the resulting species could react with a second borane fragment, possibly arising from BH_3 elimination in the formation of **89**, and a B_2H_5 containing species, stabilised by a bridging hydride, could form. That this suggested process is similar to the synthesis of **36** is unlikely, given that the mechanism for the formation of **36** results in the elimination of a hydride ion, whereas in the thermolysis of **85**, the P-H centre which arises in compound **89** must be formed by a proton. Scheme 5.17 highlights the possible products from a reaction between **85** and BH_3 , similar to the synthesis of **36**.

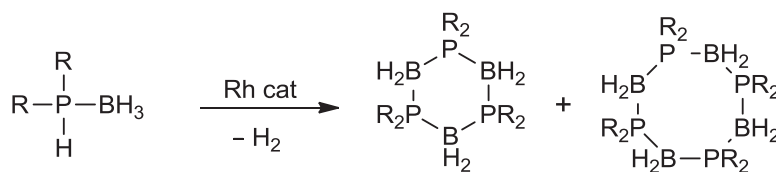


Scheme 5.17. Possible reaction between BH_3 and **85** [$\text{R} = (\text{Me}_3\text{Si})_2\text{CH}$].

It has been shown previously by Manners and co-workers that phosphine-boranes can undergo a Rh-catalysed dehydrogenation to give H_2 and (poly)phosphine-boranes (Scheme 5.18).³⁶ This process also occurs with elimination of a hydrogen atom from the borane group. It may also be possible that during the thermolysis of **85**, proton elimination from two BH_3 groups could generate H_2 , which could then be the source of the P-H proton in compound **89**.

Compound **A** gives rise to a very broad, poorly resolved signal in the $^{31}\text{P}\{^1\text{H}\}$ NMR spectrum, which is consistent with a phosphido/phosphine-poly(borane) species, whilst the signal observed in the ^2D NMR spectrum, from the thermolysis of **104**, at 2.1 ppm may possibly be attributed to a bridging borane deuteride. Although there is an example of a bridging B-H-B hydride containing species with a ^1H NMR resonance at 1.97 ppm,³⁷ other examples have been found to range from 1.1 to 8.2 ppm.³⁸⁻⁴¹

Since we have been unable to isolate **A**, to confirm its identity would be difficult; to prepare a phosphine/phosphido-borane species containing a hydride-bridged B_2H_5 group directly would be challenging, and as all previous examples of this type of compound have not been fully characterised by NMR spectroscopy, no comparisons can be drawn.^{42,43}

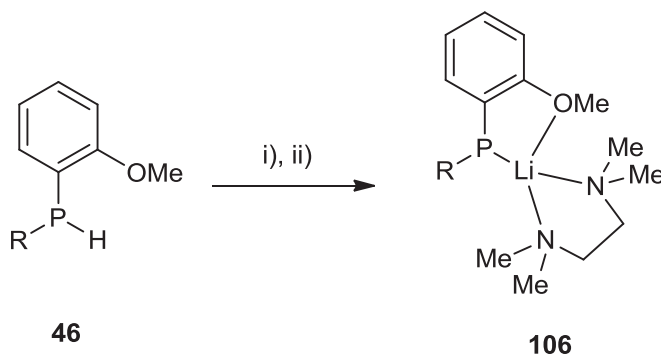


Scheme 5.18. Synthesis of a (Poly)phosphine-borane.

5.11 Comparison between the stability of **85** and $[\{(Me_3Si)_2CH\}P(C_6H_4-2-OMe)Li(tmeda)]$ (**106**)

5.11.1 Synthesis and solution-phase characterisation of **106**

In order to better understand the thermolysis behaviour of **85**, the related phosphide was prepared to ascertain if methyl migration is due to borane activation. The reaction between **46** and one equivalent of $nBuLi$ in THF proceeds cleanly to yield the corresponding lithium phosphide, which can be crystallised from cold toluene in the presence of one equivalent of tmeda as the adduct $[\{(Me_3Si)_2CH\}P(C_6H_4-2-OMe)Li(tmeda)]$ (**106**, Scheme 5.18).



Scheme 5.18. Synthesis of compound **106**. i) $nBuLi$, THF, 1 h, r.t. ii) tmeda, toluene. [R = $(Me_3Si)_2CH$].

The 1H , $^{13}C\{^1H\}$ and $^{31}P\{^1H\}$ NMR spectra of **106** are as expected. The $^{31}P\{^1H\}$ NMR spectrum consists of a sharp singlet at -85.1 ppm. In the 1H NMR spectra, the diastereotopic Me_3Si groups appear as a single peak, due to intermolecular exchange involving P–M bond scission/bond formation which is rapid on the NMR time-scale.

5.11.2 Solid-state structure of **106**

Compound **106** crystallises as discrete monomers, the structure of which is shown in Figure 5.10; details of selected bond lengths and angles are given in Table 5.3. Each lithium ion is coordinated by the P and O atoms of the phosphide ligand to give a five-membered chelate ring [P-Li-O bite angle $80.97(19)^\circ$]. The coordination about lithium is completed by two nitrogen atoms from a molecule of tmeda, to give the lithium ion a distorted tetrahedral geometry.

The P-Li distance of $2.428(5)$ Å falls within the range of previously reported lithium phosphides of 2.42 - 2.67 Å.¹⁵ The Li-O distance $1.986(6)$ Å is similar to the related distance reported for compound **49** [$1.982(7)$ Å], whilst the P-Li-O bite angle is somewhat smaller [P-Li-O bite angles: $80.97(19)$ (**106**) and $89.5(2)^\circ$ (**49**)].

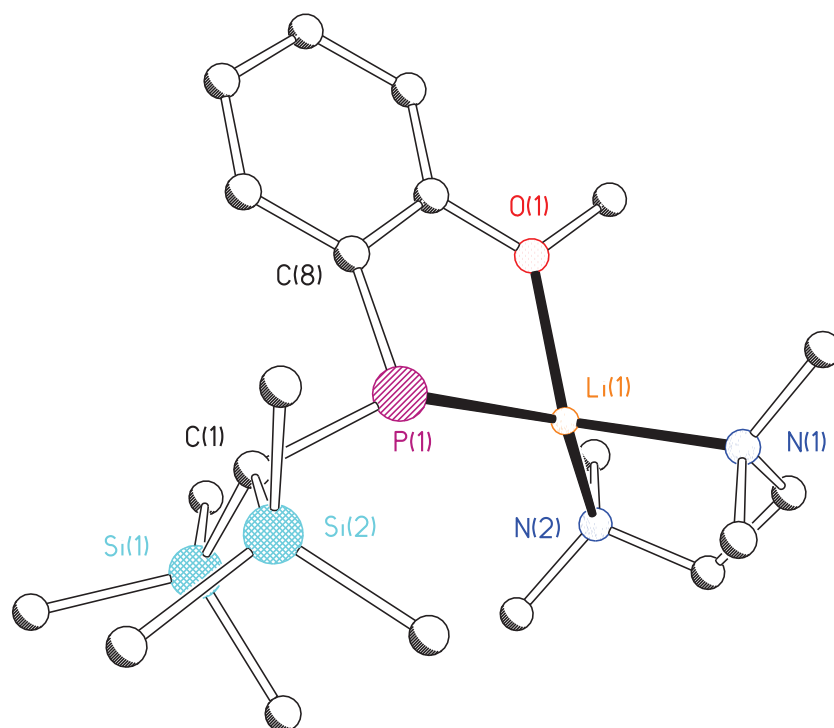


Figure 5.10. Molecular structure of compound **106**. All H atoms omitted for clarity.

P(1)–Li(1)	2.428(5)	P(1)–Li(1)–O(1)	80.97(19)
P(1)–C(1)	1.881(3)	Li(1)–P(1)–C(1)	143.37(17)
P(1)–C(8)	1.800(3)	Li(1)–P(1)–C(8)	96.39(17)
O(1)–Li(1)	1.986(6)	C(1)–P(1)–C(8)	104.65(14)
N(1)–Li(1)	2.091(6)	P(1)–C(1)–Si(1)	111.33(16)
N(2)–Li(1)	2.100(6)	P(1)–C(1)–Si(2)	108.14(16)
Si(1)–C(1)	1.868(3)		
Si(2)–C(1)	1.872(3)		

Table 5.3. Selected bond lengths (Å) and angles (°) for compound **106**.

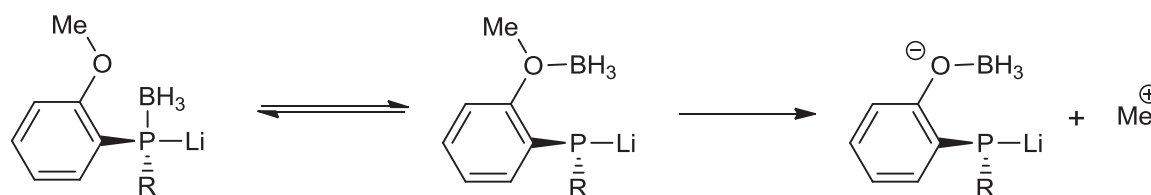
5.11.3 Reactivity of **106**

Samples of **106** in toluene in sealed NMR tubes were monitored by $^{31}\text{P}\{^1\text{H}\}$ NMR spectroscopy. After heating the sample, and after an extended period at room temperature, there was no evidence of O-Me cleavage. Similarly, heating a solution of **106** in toluene, in the presence of THF, resulted in no change, suggesting that the methyl migration seen in the thermolysis of compound **85** is borane activated.

The chemistry of group II and lanthanide metal complexes with the ligand [$\{(\text{Me}_3\text{Si})_2\text{CH}\}\text{P}(\text{C}_6\text{H}_4\text{-2-OMe})\}]^-$ has already been discussed, and highlights that O-Me cleavage is dependent on the Lewis acidity of the metal centre. As such, the stability of **106** suggests that lithium is insufficiently Lewis acidic to mediate O-Me cleavage in this ligand. However, the addition of a Lewis acidic borane group, generating **85**, may be sufficient enough to promote O-Me cleavage. This reactivity may be attributed to decreased electron density at phosphorus. However, whilst the combined Lewis acidity of a lithium metal centre and a borane substituent may promote O-Me cleavage, the potassium analogue (**87**) is stable.

Alternatively, it has been shown by Imamoto and co-workers that anisole-functionalised phosphine-boranes undergo racemisation at high-temperatures *via* a $\text{P-BH}_3/\text{O-BH}_3$ equilibrium (Scheme 5.8). It has already been proposed that borane elimination in the preparation of **89** occurs *via* this mechanism, but it could also contribute to methyl

migration; the formation of the O-B bond could promote O-Me cleavage, and generate alkoxy-functionality, which is otherwise unobserved in **106** (Scheme 5.19).



Scheme 5.19. Possible mechanism for Me elimination for **85** [R = (Me₃Si)₂CH].

5.12 Synthesis and solution-phase characterisation of [{(Me₃Si)₂CH}P(C₆H₄-2-OMe)(BH₃)₂Li(THF)] (**107**)

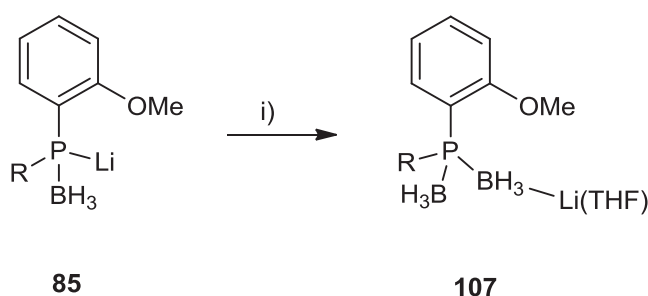
In an analogous manner to that observed for the complex [{(Me₃Si)₂CH}P(C₆H₄-2-SMe)(BH₃)Li(THF)]₂ (**64**) (see chapter 4), heating a THF solution of **85** in the presence of the free phosphine-borane **41**, results in the conversion of **85** into the phosphine-bis(borane) [{(Me₃Si)₂CH}P(BH₃)₂(C₆H₄-2-OMe)Li] and the secondary phosphine **46**, due to borane-redistribution.

The formation of [{(Me₃Si)₂CH}P(BH₃)₂(C₆H₄-2-OMe)Li] can be observed by ³¹P{¹H} and ¹¹B{¹H} NMR spectroscopy, however we were unable to isolate a pure sample from the thermolysis reactions. Therefore, in order to confirm the identity of the phosphido-bis(borane), this compound was prepared using a direct route.

The reaction between **85** and one equivalent of BH₃·SMe₂ in THF proceeds cleanly to yield [{(Me₃Si)₂CH}P(BH₃)₂(C₆H₄-2-OMe)Li], which, upon removal of the solvent, is isolated as a viscous, colourless oil. The product may be crystallised from light petroleum in the presence of THF as the adduct [{(Me₃Si)₂CH}P(C₆H₄-2-OMe)(BH₃)₂Li(THF)] (**107**, Scheme 5.20).

Upon addition of the second equivalent of borane, the ³¹P{¹H} NMR signal for **85** [-62.5 ppm] is replaced by a new, very broad signal at -12.7 ppm, which is indistinguishable from that of the sample of **107** prepared from the thermolysis of **85** in the presence of **41** in solutions of THF.

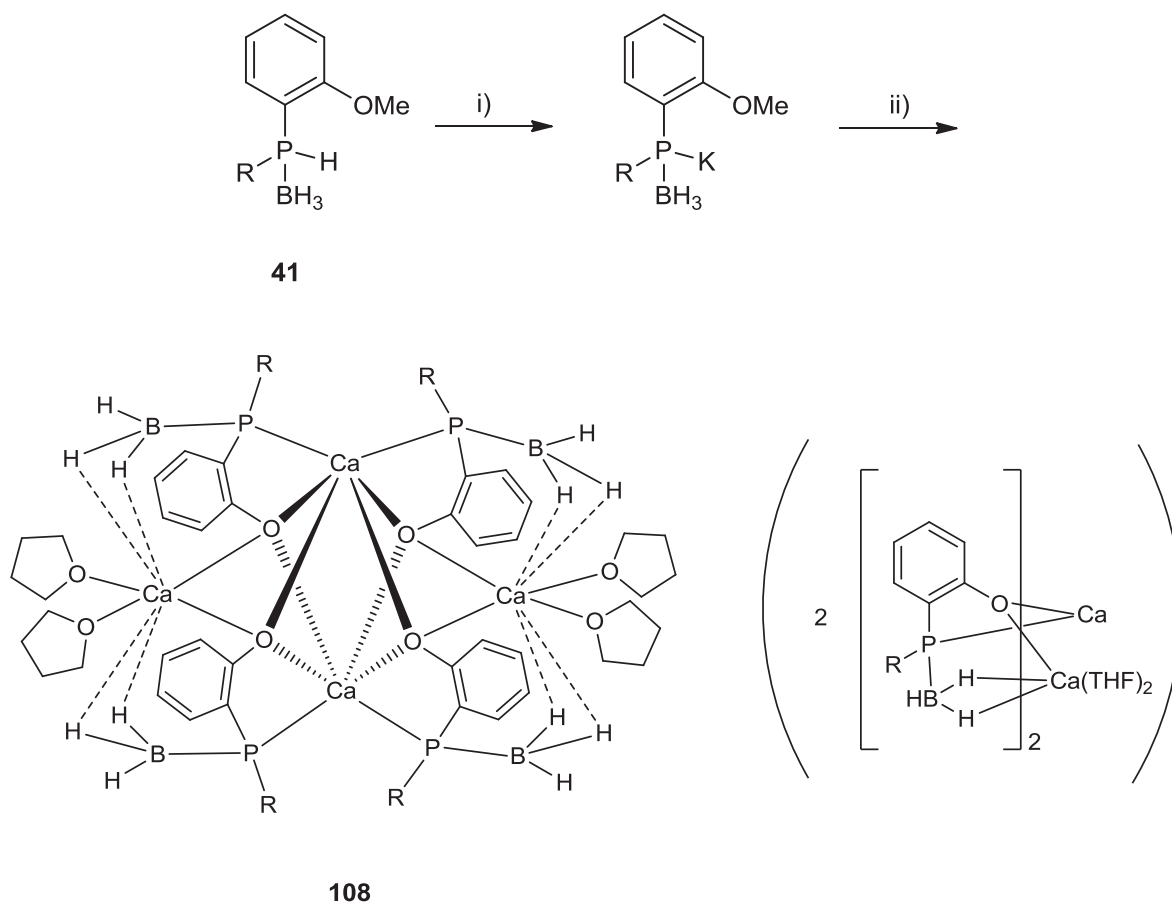
The ^1H NMR spectrum of **107** in d_8 -THF is as expected; the SiMe_3 groups appear as a sharp singlet, whilst the six BH_3 protons appear as a broad signal at 0.7 ppm, which, upon decoupling of the ^{11}B nucleus, resolves as a sharp doublet [$^2J_{\text{PH}} = 11.0$ Hz]. As observed in **72**·(**12-crown-4**), all six borane protons appear to be identical. This suggests that in solution there is either rapid exchange between the free and coordinated borane groups, or that the compound exists as a separated ion pair in THF. In the $^{13}\text{C}\{^1\text{H}\}$ NMR spectrum the SiMe_3 carbons appear as a doublet [$^3J_{\text{PC}} = 1.9$ Hz], whilst the adjacent CH carbon also gives rise to a doublet [$^1J_{\text{PC}} = 1.9$ Hz].



Scheme 5.20. Synthesis of **107**. i) $\text{BH}_3 \cdot \text{SMe}_2$, THF, 1 h, r.t. [$\text{R} = (\text{Me}_3\text{Si})_2\text{CH}$].

5.13 Synthesis of the alkaline earth metal complex $[\{(\text{Me}_3\text{Si})_2\text{CH}\}\text{P}(\text{C}_6\text{H}_4\text{-2-O})(\text{BH}_3)\text{Ca}(\text{THF})_4]$ (**108**)

To probe the effects of varying the metal centre in complexes with $[\{(\text{Me}_3\text{Si})_2\text{CH}\}\text{P}(\text{C}_6\text{H}_4\text{-2-O})(\text{BH}_3)]^-$, the related calcium compound was prepared. The reaction between **41** and one equivalent of BnK in THF proceeds cleanly to yield the corresponding phosphido-borane $[\{(\text{Me}_3\text{Si})_2\text{CH}\}\text{P}(\text{C}_6\text{H}_4\text{-2-O})(\text{BH}_3)]\text{K}$, which was added *in situ* to a solution of CaI_2 in THF, which yields the adduct $[\{(\text{Me}_3\text{Si})_2\text{CH}\}\text{P}(\text{C}_6\text{H}_4\text{-2-O})(\text{BH}_3)\text{Ca}(\text{THF})_4]$ (**108**) and the tertiary phosphine-borane **90** (Scheme 5.21) after 16 hours stirring. Compound **108** was extracted into hexamethyldisiloxane, and upon cooling, formed as colourless crystals suitable for X-ray crystallography. This is in stark contrast to the related complex $[\{(\text{Me}_3\text{Si})_2\text{CH}\}\text{P}(\text{C}_6\text{H}_4\text{-2-O})\text{Ca}(\text{THF})_4]$ (**80**) which is sparingly soluble in ether solvents, but may be obtained as pale yellow needles by recrystallization from hot THF.



Scheme 5.21. Synthesis of **108**. i) BnK, THF, 1 h, r.t. ii) CaI₂, THF, 16 h, r.t. [R = (Me₃Si)₂CH].

5.14 Solution-phase characterisation of **108**

The ³¹P{¹H} NMR spectrum of **108** in *d*₈-toluene at room temperature indicates the presence of several phosphorus-containing species with signals between -62 and -76 ppm, alongside traces of compound **90** at 12.1 ppm, and another compound, which gives rise to a broad signal at -30 ppm, possibly a phosphido-bis(borane) species (Figure 5.11). The peaks between -62 and -76 ppm are very broad, and suggest that in solution, **108** exists as a mixture of species, which are in dynamic equilibrium.

Variable-temperature ³¹P{¹H} NMR (Figure 5.12) supports the thesis that **108** is subject to dynamic equilibria. At 90 °C, the ³¹P{¹H} NMR spectrum exhibits a single broad peak at -69.1 ppm, suggesting that the dynamic equilibria are fast on the NMR time scale at

elevated temperatures. As the temperature is decreased to 40 °C, this peak de-coalesces into two very broad peaks at -64.5 and -75.6 ppm, which are of similar intensity. Upon further cooling, a third and a fourth peak begin to emerge, whilst the signals at -64.5 and -75.6 ppm begin to partially de-coalesce into overlapping peaks. Unfortunately, even at the lowest attainable temperature (-90 °C), these signals are very broad and poorly resolved.

In *d*₈-toluene it is possible that **108** fragments into smaller species (possibly dimers and/or monomers). In addition, where two or more ligands are present in a complex, multiple diastereoisomers are possible. Dynamic equilibria between these species would be consistent with the observed NMR spectra. This is in contrast to compound **80**, which, in *d*₈-THF, gives rise to a single resonance in the ³¹P{¹H} NMR spectrum, whilst its ¹H and ¹³C{¹H} NMR spectra show only a single sets of signals for the ligands, which suggests that either its cubane structure is maintained in solution, or that any equilibria are very rapid.

The ¹H and ¹³C{¹H} NMR spectra of **108** consist of many broad and overlapping resonances, consistent with dynamic behaviour in solution, and as such are not amenable to interpretation.

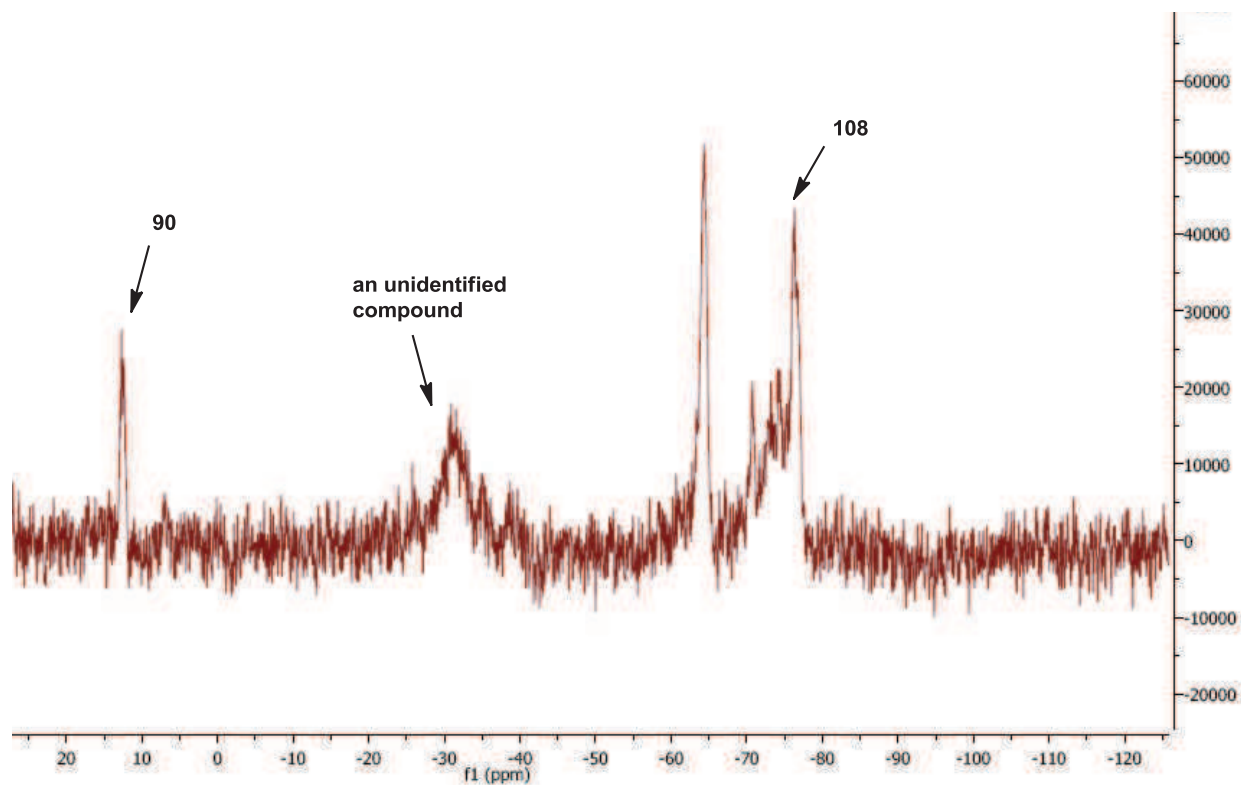


Figure 5.11. $^{31}\text{P}\{^1\text{H}\}$ spectra of **108**, **90** and an unknown compound at 0 °C in d_8 -toluene.

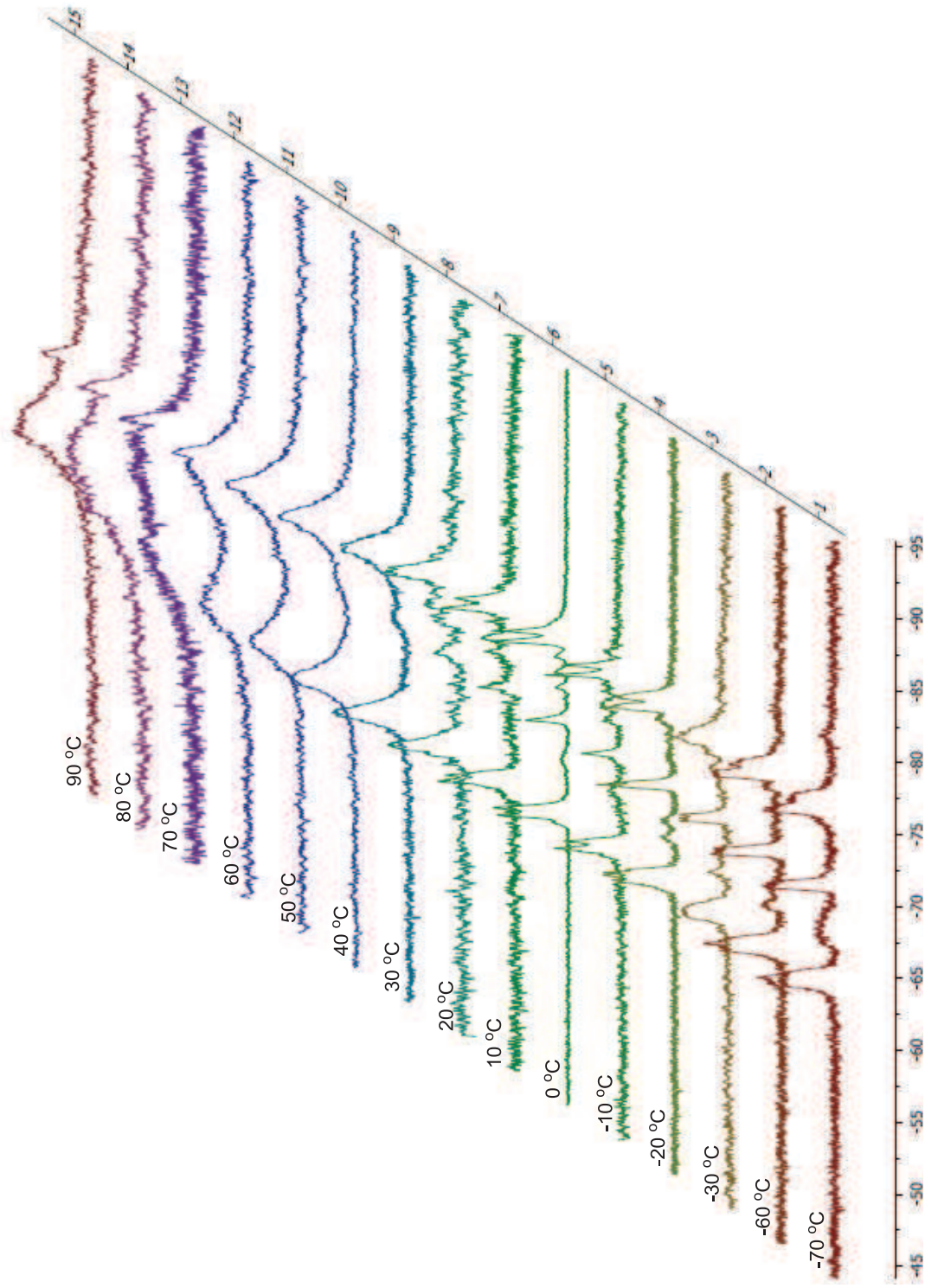


Figure 5.12. Stacked variable-temperature $^{31}\text{P}\{^1\text{H}\}$ NMR spectra of **108** in d_8 -toluene.

5.15 Solid-state structure of 108

Compound **108** crystallises as discrete tetramers, with a Ca_4O_4 core consisting of a square of O atoms with a Ca ion over each face and along two opposing edges; the structure of **108** is shown in Figure 5.13 (with the core structure shown in Figure 5.14), with selected bond lengths and angles given in Table 5.4. The alkoxophosphido-borane ligands in the complex are essentially identical, but the complex contains two independent calcium environments; one set of Ca ions are coordinated by two adjacent ligands *via* their phosphorus and oxygen atoms, and by an $\eta^1\text{-BH}_3$ interaction. The coordination sphere of these Ca ions is completed by the alkoxo oxygen atoms of the remaining two ligands. In the second set, the Ca ions are coordinated by two alkoxo oxygen atoms, such that each oxygen is acting as a μ_3 bridge between the calcium ions. The coordination about each of these ions is completed by two adjacent ligands *via* $\eta^2\text{-BH}_3$ interactions, so that each borane group acts as a $\mu_2\text{-}\eta^2\text{:}\eta^1$ bridge between two Ca ions, and also by two molecules of THF.

Ca–P	2.8454(12) and 2.8778(11)
Ca–O	2.297(2)-2.524(2)
Ca–B	2.873(5)-3.280(5)
Ca–H	2.33(3)-2.54(4)
P–B	1.965(5) and 1.980(5)
<hr/>	
P(2A)–Ca(1)–P(1)	120.94(4)
Ca–P–B	81.03(13)-83.60(15)
P–Ca–O (bite angle)	67.04(6) and 67.53(6)
Ca–O–Ca	78.08(7)-102.63(8)
O–Ca–O	63.51(7)-165.6(10)

Table 5.4. Selected ranges of bond lengths (Å) and angles (°) for compound **108**.

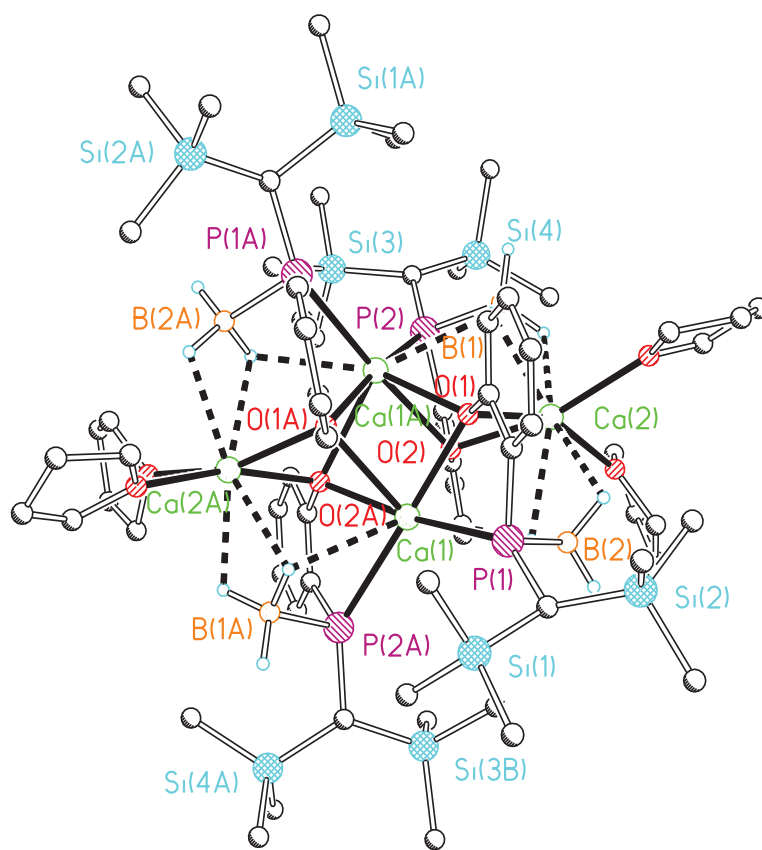


Figure 5.13. Molecular structure of compound **108**. All C-bound H atoms omitted for clarity.

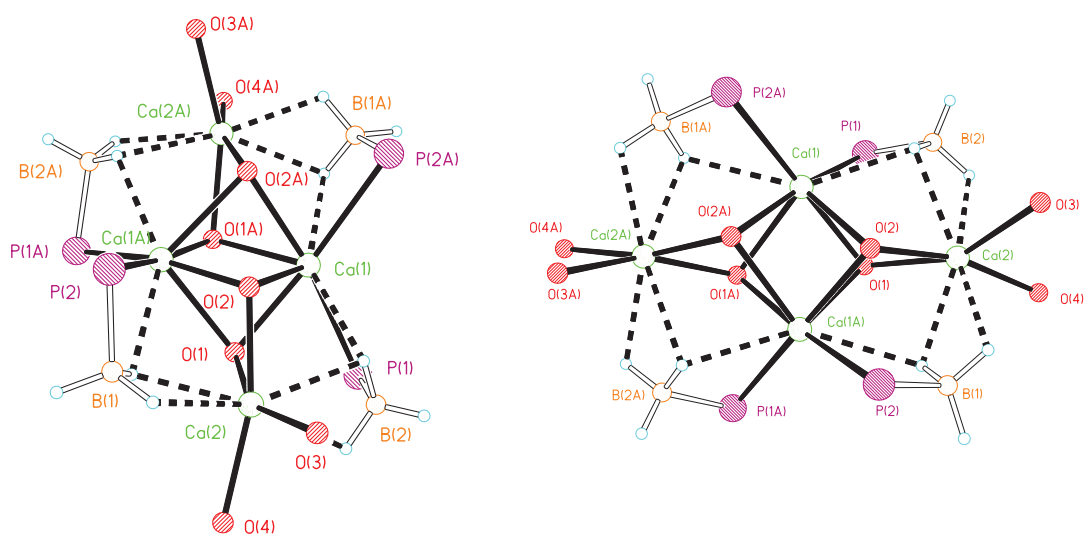


Figure 5.14. Structure of the central core of **108**, with all Si, C and C-bound H atoms omitted for clarity.

To date, only a small number of calcium complexes with phosphides have been structurally characterised.⁴⁴⁻⁵⁵ These are typically isolated as solvated monomers (e.g. $[(\text{Ph}_2\text{P})\text{CaPh}(\text{THF})_4]^{51}$ although dimers, a trimer, a hexamer and a number of alkaline earth-tin heterometallic clusters have been isolated.

The P-Ca distances of 2.8454(12) Å and 2.8778(11) in **108** are slightly shorter than the corresponding distance in the related alkoxophosphide **80** [2.9612(6) and 2.9695(7) Å], reported by Izod and co-workers,⁹ and other P-Ca distances that have been reported previously.^{32-45,51,55,56} For example, the compound $[(\text{Ph}_2\text{P})\text{CaPh}(\text{THF})_4]$ (**109**) has a P-Ca distance of 3.010(2) Å. The Ca-O (alkoxo) distances range from 2.369(2) to 2.524(2) Å, which are similar to the Ca-O distances reported for the oxo-alkoxide clusters $[\text{Ca}(\text{tmhd})(\mu_3\text{-OEt})(\text{EtOH})]_4$ (**110**, $\text{tmhd} = \text{Bis}(2,2,6,6\text{-tetramethyl-3,5-heptanedionate})$ [Ca-O 2.328(6)-2.367(6) Å] and $[\text{Ca}_6(\mu_4\text{-O})_2-(\mu_3\text{-OEt})_4(\text{EtOH})_4] \cdot 14\text{EtOH}$ (**111**) [Ca-O 2.312(6)-2.529(5) Å].^{57,58} Compound **108** is the first example of a phosphido-borane complex with calcium to be characterised in the solid-state.

5.16 Conclusions

The synthesis of alkali metal and calcium complexes of the phosphido-borane $[\{(\text{Me}_3\text{Si})_2\text{CH}\}\text{P}(\text{C}_6\text{H}_4\text{-2-OMe})(\text{BH}_3)]^-$ are readily achievable through straightforward synthetic procedures. However, the lithium and calcium compounds were found to undergo unusual thermally-driven rearrangements.

The thermolytic reactivity of **85** in solution is finely balanced, with two possible reaction pathways, which can result in the formation of either complex **89** along with side products **90** and another unidentified compound (**A**) or complex **91**, which is postulated to be an alkoxo-functionalised phosphido-borane, also alongside the formation of **90**. The formation of compounds **89**, **90** and **91** is thought to arise *via* the formation of an ate complex intermediate, which is favoured in the presence of *tmeda*. The formation of **89** involves concurrent O-Me and P-BH₃ cleavage and P-H bond formation.

Through comparison with **87** and the phosphide **106**, activation of the O-Me bond in **85** towards cleavage may be attributed to a combination of the Lewis acidity of the lithium metal centre and the borane group.

The reaction between $[(\text{Me}_3\text{Si})_2\text{CH}]\text{P}(\text{C}_6\text{H}_4\text{-2-OMe})(\text{BH}_3)]\text{K}$ and CaI_2 in THF yields the unusual alkoxophosphido-borane complex **108**, which proceeds with intramolecular methyl migration, generating **90** *in situ*. The structure adopted by **108** is rather unique; it is tetranuclear in the solid-state, with two distinct Ca ion environments. In *d*₈-toluene **108** is subject to dynamic equilibria, possibly between diastereoisomers and/or oligomers.

5.17 References

- (1) Imamoto, T.; Kusumoto, T.; Suzuki, N.; Sato, K. *J. Am. Chem. Soc.* **1985**, *107*, 5301.
- (2) Pican, S.; Gaumont, A.-C. *Chem. Commun.* **2005**, 2393.
- (3) Aspinall, H. C.; Moore, S. R.; Smith, A. K. *J. Chem. Soc., Dalton Trans.* **1993**, 993.
- (4) Aspinall, H. C.; Tillotson, M. R. *Inorg. Chem.* **1996**, *35*, 5.
- (5) Clegg, W.; Doherty, S.; Izod, K.; Kagerer, H.; O'Shaughnessy, P.; Sheffield, J. M. *J. Chem. Soc., Dalton Trans.* **2000**, 1825.
- (6) Izod, K.; O'Shaughnessy, P.; Sheffield, J. M.; Clegg, W.; Liddle, S. T. *Inorg. Chem.* **2000**, *39*, 4741.
- (7) Clegg, W.; Izod, K.; Liddle, S. T.; O'Shaughnessy, P.; Sheffield, J. M. *Organometallics* **2000**, *19*, 2090.
- (8) Blair, S.; Izod, K.; Clegg, W.; Harrington, R. W. *Eur. J. Inorg. Chem.* **2003**, 3319.
- (9) Izod, K.; Clegg, W.; Liddle, S. T. *Organometallics* **2000**, *19*, 3640.
- (10) Blair, S.; Izod, K.; Clegg, W.; Harrington, R. W. *Inorg. Chem.* **2004**, *43*, 8526.

- (11) Bertz, S. H.; Gibson, C. P.; Dabbagh, G. *Organometallics* **1988**, *7*, 227.
- (12) Lochmann, L.; Trekoval, J. J. *Organomet. Chem.* **1987**, *326*, 1.
- (13) Izod, K.; Wills, C.; Clegg, W.; Harrington, R. W. *Organometallics* **2006**, *25*, 38.
- (14) Harmin, T. E.; Shirley, D. A. *J. Org. Chem.* **1974**, *39*, 3164.
- (15) Izod, K. *Adv. Inorg. Chem.* **2000**, *50*, 33.
- (16) Boyle, T. J.; Pedrotty, D. M.; Alam, T. M.; Vick, S. C.; Rodriguez, M. A. *Inorg. Chem.* **2000**, *39*, 5133.
- (17) Boyle, T. J.; Alam, T. M.; Peters, K. P.; Rodriguez, M. A. *Inorg. Chem.* **2001**, *40*, 6281.
- (18) Armstrong, D. R.; Davies, R. P.; Raithby, P. R.; Snaith, R.; Wheatley, A. E. H. *New J. Chem.* **1999**, *23*, 499.
- (19) Rajeswaran, M.; Begley, W. J.; Olson, L. P.; Huo, S. *Polyhedron* **2007**, *26*, 3653.
- (20) Pauer, F.; Power, P. P. In *Lithium Chemistry. A Theoretical and Experimental Overview*; Sapse, A.-M., Schleyer, P. V. R.; Eds.; John Wiley & Sons: New York: 1995, p 295.
- (21) Bradley, D. C. *Chem. Rev.* **1989**, *89*, 1317.
- (22) Herrmann, W. A.; Huber, N. W.; Runte, O. *Angew. Chem. Int. Ed. Engl.* **1995**, *34*, 2187.
- (23) Chisholm, M. H.; Drake, S. R.; Naiini, A. A.; Streib, W. E. *Polyhedron* **1991**, *10*, 805.
- (24) Jackman, L. M.; Cizmeciyan, D.; Williard, P. G.; Nichols, M. A. *J. Am. Chem. Soc.* **1993**, *115*, 6262.
- (25) Wheatley, P. J. *J. Chem. Soc.* **1960**, 4270.

- (26) Williard, P. G.; MacEwan, G. J. *J. Am. Chem. Soc.* **1989**, *111*, 7671.
- (27) Beck, G.; Hitchcock, P. B.; Lappert, M. F.; Mackinnon, I. A. *Chem Commun.* **1989**, 1312.
- (28) Williard, P. G.; Carpenter, G. B. *J. Am. Chem. Soc.* **1985**, *107*, 3345.
- (29) Williard, P. G.; Carpenter, G. B. *J. Am. Chem. Soc.* **1986**, *108*, 462.
- (30) Jastrzebski, J. T. B. H.; van Koten, G.; van de Mieroop, W. F. *Inorg. Chim. Acta* **1988**, *142*, 169.
- (31) Maetzke, T.; Hidber, C. P.; Seebach, D. *J. Am. Chem. Soc.* **1990**, *112*, 8248.
- (32) Maetzke, T.; Seebach, D. *Organometallics* **1990**, *9*, 3032.
- (33) Armstrong, D. R.; Clegg, W.; Hodgson, S. M.; Snaith, R.; Wheatley, A. E. H. *J. Organomet. Chem.* **1998**, *550*, 233.
- (34) Imamoto, T.; Osaiki, T.; Onoznuva, T.; Kusumoto, T.; Sato, K. *J. Am. Chem. Soc.* **1990**, *112*, 5245.
- (35) Rudzevich, L. R.; Gornitzka, H.; Romanenko, V. D.; Bertrand, G. *Chem. Commun.* **2001**, 1634.
- (36) Dorn, H.; Vejzovic, E.; Lough, A. J.; Manners, I. *Inorg. Chem.* **2001**, *40*, 4327.
- (37) Paetzold, P.; Englert, U.; Finger, R.; Thomas, S. *Z. Anorg. Allg. Chem.* **2004**, *630*, 508.
- (38) Prasang, C.; Sahin, Y.; Hofmann, M.; Geiseler, G.; Massa, W.; Berndt, A. *Eur. J. Inorg. Chem.* **2008**, 5046.
- (39) Sahin, Y.; Ziegler, A.; Happel, T.; Meyer, H.; Bayer, M. J.; Pritzkow, H.; Massa, W.; Hofmann, M.; Schleyer, P. V. R.; Siebert, W.; Berndt, A. *J. Organomet. Chem.* **2003**, *680*, 244.

- (40) Saturnino, D. J.; Yamauchi, M.; Clayton, W. R.; Nelson, R. W.; Shore, S. G. *J. Am. Chem. Soc.* **1975**, *97*, 6063.
- (41) Wehmschulte, R. J.; Diaz, A. A.; Khan, M. A. *Organometallics* **2003**, *22*, 83.
- (42) Hofstötter, H.; Mayer, E. *Angew. Chem. Int. Ed. Engl.* **1973**, *12*, 413.
- (43) Nöth, H.; Staude, S.; Thomann, M.; Paine, R. T. *Chem. Ber.* **1993**, *126*, 611.
- (44) Crimmin, M. R.; Barrett, A. G. M.; Hill, M. S.; Hitchcock, P. B.; Procopiou, P. A. *Inorg. Chem.* **2007**, *26*, 2953.
- (45) Gärtner, M.; Görls, H.; Westerhausen, M. *Z. Anorg. Allg. Chem.* **2007**, *633*, 2025.
- (46) Westerhausen, M.; Digeser, M. H.; Nöth, H.; Ponikwar, W.; Seifert, T.; Polborn, K. *Inorg. Chem.* **1999**, *38*, 3207.
- (47) Westerhausen, M.; Schwarz, W. *J. Organomet. Chem.* **1993**, *463*, 51.
- (48) Kopecky, P.; von Hänisch, C.; Weigend, F.; Kracke, A. *Eur. J. Inorg. Chem.* **2010**, 258.
- (49) Westerhausen, M.; Low, R.; Schwarz, W. *J. Organomet. Chem.* **1996**, *513*, 213.
- (50) Westerhausen, M.; Digiser, M. H.; Krofta, M.; Weiberg, N.; Nöth, H.; Knizek, J.; Ponikwar, W.; Siefert, T. *Eur. J. Inorg. Chem.* **1999**, 743.
- (51) Gärtner, M.; Görls, H.; Westerhausen, M. *Organometallics* **2007**, *26*, 1077.
- (52) Westerhausen, M.; Krofta, M.; Mayer, P. *Z. Anorg. Allg. Chem.* **2000**, *626*, 2307.
- (53) von Hänisch, C.; Kopecky, P. *Z. Anorg. Allg. Chem.* **2010**, *636*, 1522.
- (54) Westerhausen, M.; Schwarz, W. *Z. Anorg. Allg. Chem.* **1996**, *622*, 903.
- (55) Blair, S.; Izod, K.; Clegg, W. *Inorg. Chem.* **2002**, *41*, 3886.
- (56) Knapp, V.; Müller, G. *Angew. Chem. Int. Ed. Engl.* **2001**, *40*, 183.

- (57) Arunasalam, V.-C.; Baxter, I.; Drake, S. R.; Hursthouse, M. B.; Malik, K. M.; Otway, D. J. *Inorg. Chem.* **1995**, *34*, 5295.
- (58) Turova, N. Y.; Turevskaya, E. P.; Kessler, V. G.; Yanovsky, A. I.; Struchkov, Y. T. *Chem. Commun.* **1993**, 21.

Chapter 6. Alkali and alkaline earth metal complexes of a phenyl-functionalised phosphido-borane

6.1 Introduction

Chapters 3, 4 and 5 have explored the effects that varying the peripheral donor-functionalised substituent on phosphido-boranes has on the structures and stabilities of these complexes. In this regard, to gain further insight into the role of the peripheral donor substituent, this chapter discusses the synthesis and characterisation of complexes of the phosphido-borane $[(\text{Me}_3\text{Si})_2\text{CH}\text{P}(\text{C}_6\text{H}_5)(\text{BH}_3)]^-$, which does not contain additional donor functionality, and explores the factors which determine the structure of its complexes. For a comprehensive overview of the effects that the cation has on structure, complexes of this ligand with both alkali and alkaline earth metal cations have been synthesised.

It is expected that removing the donor functionality will have a significant effect on the structures adopted by the alkali metal complexes of this phosphido-borane ligand. A similar effect was observed for complexes of the phosphide $[(\text{Me}_3\text{Si})_2\text{CH}\text{P}(\text{C}_6\text{H}_5)\text{M}(\text{L})]$, $[\text{M}(\text{L}) = \text{Li}(\text{THF})_3$ (**112**), $\text{Na}(\text{tmeda})$ (**113**), $\text{K}(\text{pmdeta})$ (**114**)], which were reported in 2010 by Izod and co-workers,¹ and the related N-donor functionalised phosphides $[(\text{Me}_3\text{Si})_2\text{CH}\text{P}(\text{C}_6\text{H}_4\text{-}2\text{-CH}_2\text{NMe}_2)\text{M}(\text{L})]$ $[\text{M}(\text{L}) = \text{Li}(\text{THF})_2$ (**17**), $\text{Na}(\text{tmeda})$ (**18**), $\text{K}(\text{pmdeta})$ (**19**)], which were reported by the same group.² Compounds **113** and **114** crystallise as dimers, each containing a rhombus-shaped M_2P_2 core, whereas the corresponding N-donor-functionalised phosphide complexes **18** and **19** crystallise as monomers (Figure 6.1).

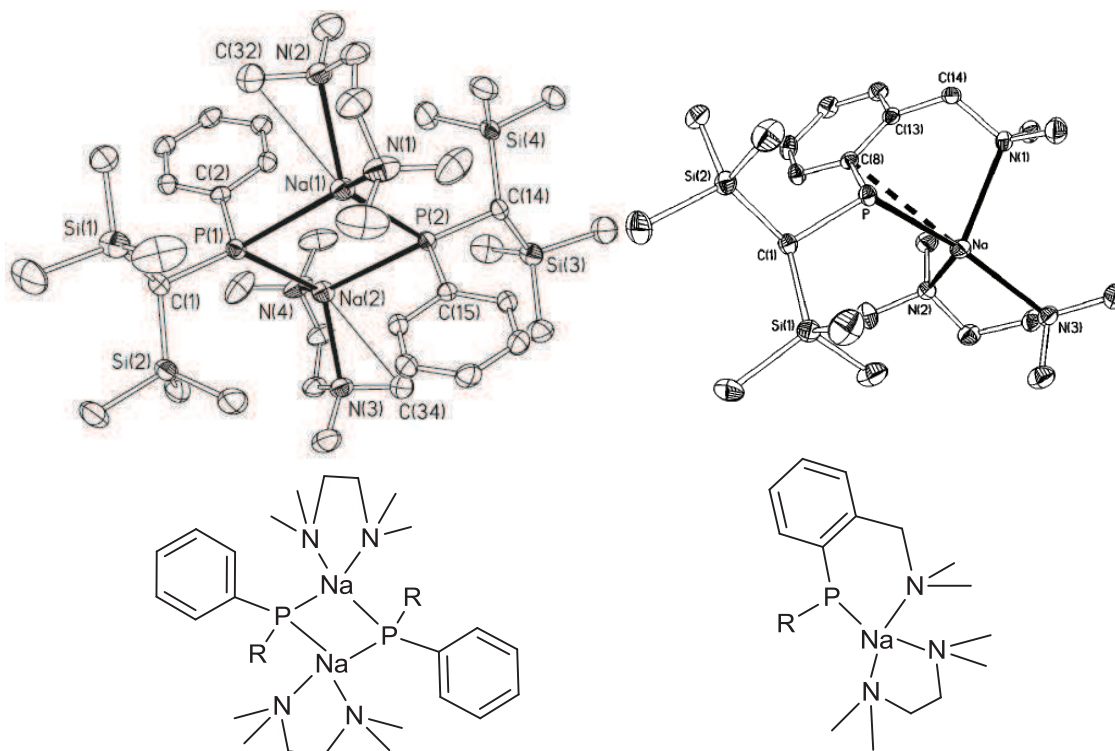
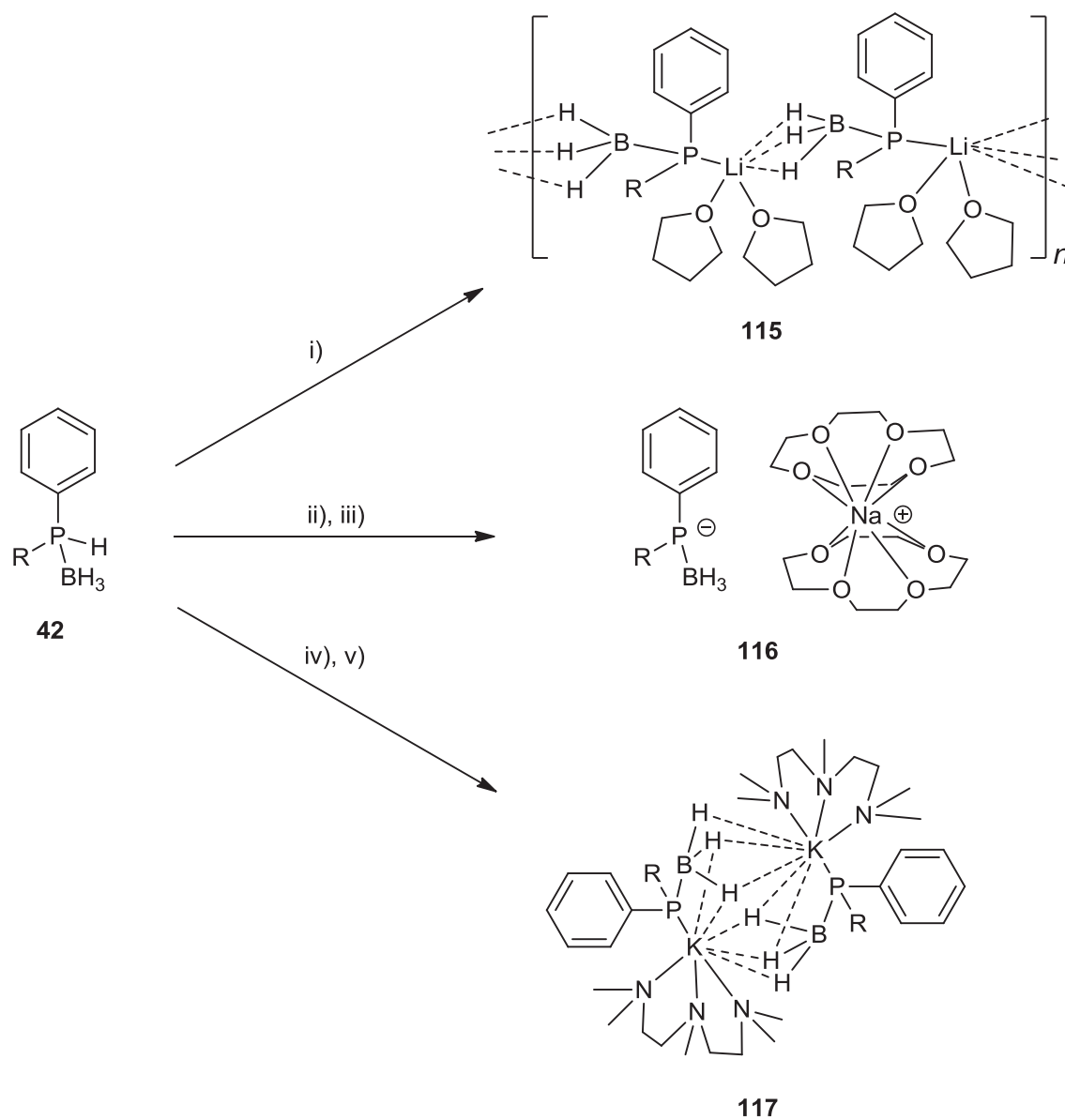


Figure 6.1. Structures of compounds **113** and **18** [R = (Me₃Si)₂CH].^{1,2}

6.2 Synthesis of the alkali metal complexes [{(Me₃Si)₂CH}P(C₆H₅)(BH₃)M(L)]_n [M(L) = Li(THF)₂, *n* = ∞ (**115**), M(L) = Na(12-crown-4)₂, *n* = 1 (**116**), M(L) = K(pmdeta)₂, *n* = 2 (**117**)]

The reaction between a solution of **42** in THF and ⁿBuLi yields the corresponding phosphido-borane, which may be crystallised from a mixture of toluene and THF as the adduct [{(Me₃Si)₂CH}P(C₆H₅)(BH₃)Li(THF)₂]_∞ (**115**). The sodium and potassium salts were prepared from the reaction between **42** and a solution of either BnNa³ or BnK⁴ in THF, giving the corresponding phosphido-boranes [{(Me₃Si)₂CH}P(C₆H₅)(BH₃)Na] and [{(Me₃Si)₂CH}P(C₆H₅)(BH₃)K], respectively, in quantitative yield. The sodium salt may be crystallised from a solution of 12-crown-4 and toluene, containing a small amount of THF, as single crystals of the adduct [{(Me₃Si)₂CH}P(C₆H₅)(BH₃)[Na(12-crown-4)₂] (**116**), suitable for X-ray crystallography, whilst the potassium salt may be crystallised from toluene containing one equivalent of pmdeta as the adduct [{(Me₃Si)₂CH}P(C₆H₅)(BH₃)K(pmdeta)]₂ (**117**).



Scheme 6.1. Synthesis of compounds **115**, **116** and **117**. Reagents and conditions: i) ${}^n\text{BuLi}$, THF, 1 h, r.t. ii) BnNa, THF, 1 h, r.t. iii) 12-crown-4, toluene. iv) BnK, THF, 1 h, r.t. v) pmdeta, toluene [$\text{R} = (\text{Me}_3\text{Si})_2\text{CH}$].

6.3 Solution-phase characterisation of **115-117**

The $^{31}\text{P}\{^1\text{H}\}$ NMR spectra of **115-117** exhibit broad quartets, with chemical shifts that range from -48.2 to -56.8 ppm. The P-B coupling constant in **115** [$^1J_{\text{PB}} = 49.0$ Hz] is unchanged from that of the phosphine-borane **42**, however the coupling constant decreases in magnitude for the sodium and potassium salts [$^1J_{\text{PB}} = 29.4$ (**116**), 19.6 Hz (**117**)].

The ^1H and $^{13}\text{C}\{^1\text{H}\}$ spectra of **115** and **117** are as expected. In the ^1H NMR spectra of **115** and **117**, the diastereotopic SiMe_3 groups give rise to two sharp signals between 0.0 and 0.4 ppm. The PCH proton in **115** and **117** affords a doublet at 0.6 ppm [$^2J_{\text{PH}} = 7.8$ and 6.0 Hz, respectively], whilst the BH_3 protons give rise to broad quartets, which collapse upon decoupling of the ^{11}B nucleus. The BH_3 signals appear as a doublet at 1.1 ppm [$^2J_{\text{PH}} = 4.1$ Hz] for **117**, however, the corresponding signal in the $^1\text{H}\{^{11}\text{B}\}$ NMR spectrum of **115** could only be resolved as a broad singlet at 1.0 ppm. In the $^{13}\text{C}\{^1\text{H}\}$ NMR spectra, the SiMe_3 carbons give rise to two signals, a doublet and a singlet between 2.3 and 3.3 ppm for **115** and **117**, respectively [$^3J_{\text{PC}} = 7.7$ Hz (**115** and **117**)], whilst the adjacent CHP carbon gives rise to a doublet at 8.9 and 9.8 for **115** and **117**, respectively [$^1J_{\text{PC}} = 34.6$ (**115**) and 43.1 Hz (**117**)].

In contrast, the ^1H NMR spectrum of **116** in d_8 -THF exhibits two rather broad singlets for the diastereotopic SiMe_3 groups. At low temperatures these signals sharpen to give two singlets at -0.1 (A) and 0.2 ppm (B), whilst at higher temperatures these signals coalesce to give a broad signal at 0.1 ppm (C) (Figure 6.2).

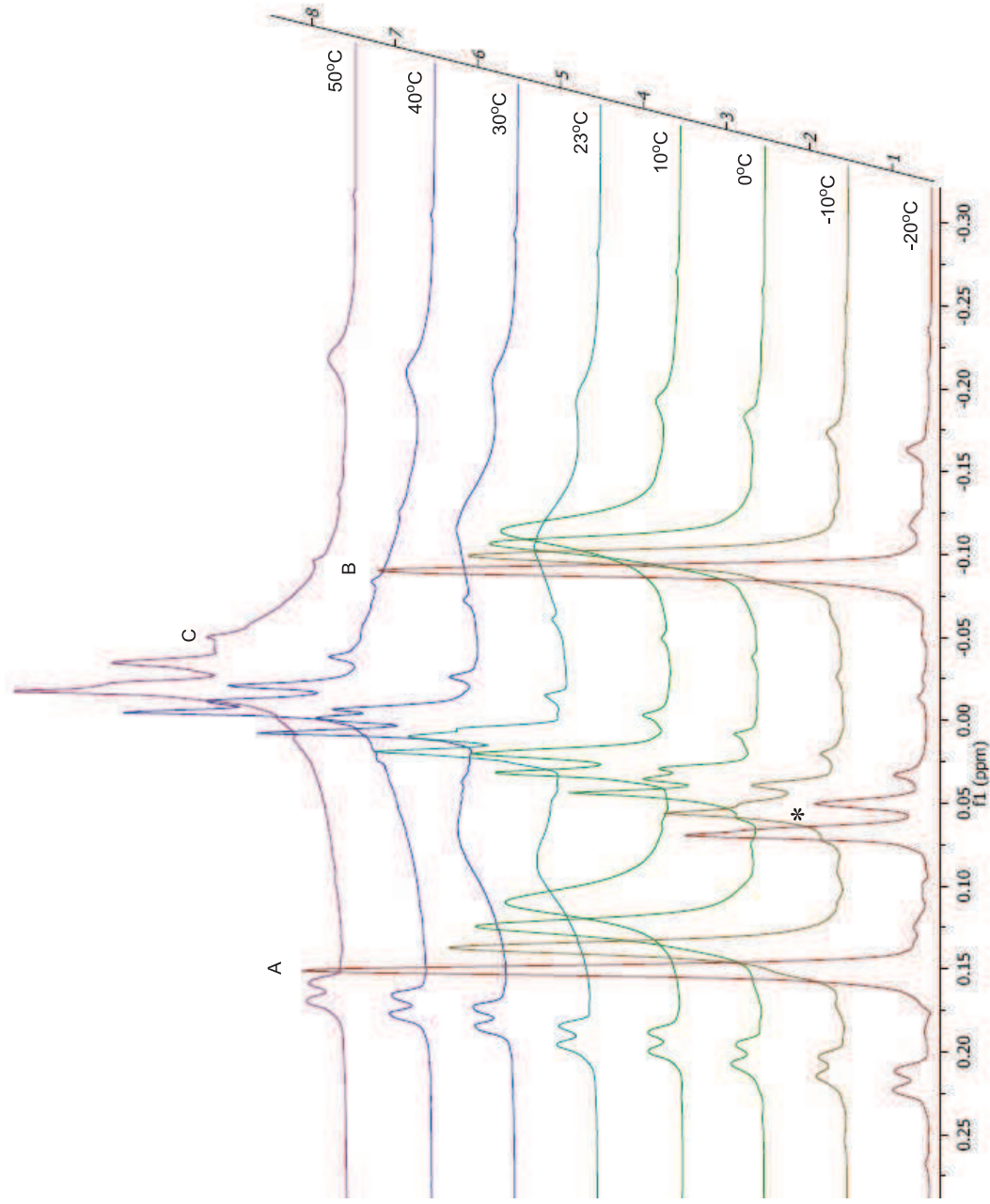
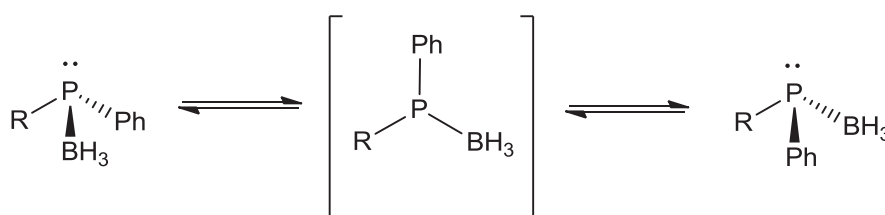


Figure 6.2. Variable-temperature $^1\text{H}\{^{11}\text{B}\}$ NMR spectra of **116** in d_8 -THF. Only SiMe_3 region shown [$*$ free phosphine-borane **42**].

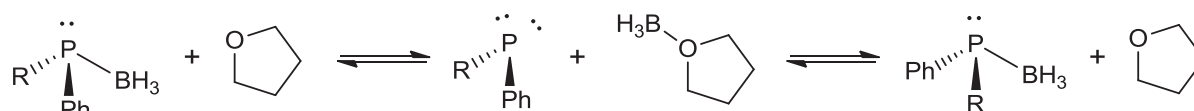
The rate of exchange between the SiMe₃ groups at each temperature was calculated using simulated ¹H{¹¹B} NMR spectra (Appendix 1). From the data collected, an Eyring plot could be obtained, from which, the enthalpy of activation, Δ*H*‡ and the entropy of activation, Δ*S*‡, were calculated: Δ*H*‡ = 52.78 kJ mol⁻¹, Δ*S*‡ = -28.33 J K⁻¹ mol⁻¹. The low value of Δ*S*‡ suggests that this is an intramolecular exchange process.

Also in the ¹H NMR spectrum of **116**, the PCH proton gives rise to a doublet at 0.2 ppm [²*J*_{PH} = 5.5 Hz], whilst the borane protons appear as a broad quartet at around 1.0 ppm, which collapse upon decoupling of the ¹¹B nucleus into a sharp doublet at 1.0 ppm [²*J*_{PH} = 4.1 Hz]; these signals do not change with temperature. In the ¹³C{¹H} spectrum of **116** the SiMe₃ groups give rise to two broad signals, which also shows its dynamic behaviour in solution, whilst the adjacent PCH carbon give rise to a sharp doublet at 10.5 ppm [¹*J*_{PC} = 47.9].

The dynamic behaviour observed for **116** is rather surprising, given that the two SiMe₃ are diastereotopic due to the chiral P centre, and as such should always give two signals. Hence the exchange process cannot be attributed to rotation about the Si₂CH-P bond. Instead, the only way for the two SiMe₃ signals to coalesce in the ¹H NMR spectrum, is if the chiral centre is lost or inverted. For this to happen, there must either be inversion at the P centre (Scheme 6.2),⁵ or reversible P-B cleavage, which could be facilitated by the THF present in solution (Scheme 6.3).⁶



Scheme 6.2. Inversion of the P centre of **116** [R = (Me₃Si)₂CH].



Scheme 6.3. Reversible P-B cleavage of **116** in THF [R = (Me₃Si)₂CH].

The inversion behaviour of tertiary phosphines has been extensively studied, and there is a substantial amount of information regarding the factors that affect barriers to inversion in these compounds; for phosphorus, the inversion barrier is reduced by i) bulky substituents, and ii) electropositive substituents. For instance, the silyl groups in the compound ($^i\text{Pr}_3\text{Si}$) $_3\text{P}$, have a combination of both steric bulk and electropositivity, which results in near planar geometry of the PSi_3 framework in the solid state.⁷

The influence of electropositivity on inversion has been extensively studied by Mislow and co-workers, who have shown that substitution of tertiary phosphines with increasingly electropositive EMe_3 groups ($\text{E} = \text{C}, \text{Si}, \text{Ge}, \text{Sn}$) leads to progressive reduction of the inversion barrier.^{8,9,10,11} For example, variable-temperature NMR experiments reveal that the free energies of inversion of $^i\text{PrPhP}(\text{EMe}_3)$ are 136.8, 89.5, and 80.8 kJ mol^{-1} for $\text{E} = \text{C}, \text{Ge}$, and Sn , respectively.⁹

In contrast, Izod and co-workers have calculated that the barrier to inversion at phosphorus for the phosphagermylenes $\{(\text{Me})\text{P}(\text{C}_6\text{H}_4\text{-2-CH}_2\text{NMe}_2)\}\text{GeX}$ [$\text{X} = \text{F}, \text{Cl}, \text{Br}, \text{H}, \text{Me}$] decreases with increasing electronegativity of the substituent X , however this is thought to be due to increasing delocalization of the p-type phosphorus lone pair in the transition state. As part of an ongoing study, the same group have also observed by multi-element and variable-temperature NMR analysis, that the related compound $[\{(\text{Me}_3\text{Si})_2\text{CH}\}(\text{C}_6\text{H}_4\text{-2-CH}_2\text{NMe}_2)\text{P}]\text{GeCl}$ is highly dynamic in solution, due to rapid interconversion of diastereoisomers most likely due to inversion at phosphorus.

The Pauling electronegativity of Ge (2.01) and B (2.04) are rather similar and so it is tempting to attribute the dynamic behaviour observed for **116** to a similar inversion process. However on the available evidence it is not possible to do so unambiguously.

As mentioned above, the other possible process that may be occurring for **116** is reversible P-B cleavage. It is well documented that the formation of phosphine-borane adducts is reversible, and decomplexation can be achieved using a strong Lewis base. For example, treatment of a phosphine-borane adduct with excess amine yields the amine-borane and free phosphine *via* an equilibrium process.

It has also been previously proposed by Imamoto and co-workers that the methoxy group in the phosphine-borane $\text{PhP}(\text{BH}_3)(\text{CH}_3)(\text{C}_6\text{H}_4\text{-2-OMe})$ (**73**) can abstract the borane fragment,

cleaving the P-B bond.⁶ It is possible therefore that a THF·BH₃ adduct could form in THF solutions of **116** in a similar fashion, resulting in rapid conversion between enantiomers, as shown in Scheme 6.3.

6.4 Solid-state structures of **115**, **116** and **117**

6.4.1 Solid-state structure of **115**

Compound **115** crystallises as essentially linear polymers, in contrast to the donor-functionalised lithium phosphido-boranes **49** and **64**, which crystallise as dimers. The molecular structure of **115** is shown in Figure 6.3, with details of selected bond lengths and angles given in Table 6.1. Each lithium ion is coordinated by the P atom of a phosphido-borane ligand and by the oxygen atoms of two molecules of THF. The coordination of Li is completed by an η^2 -interaction with the BH₃ group of an adjacent unit in the polymer chain, so that each Li ion is pseudo-four-coordinate. The phosphido-borane ligands thus adopt a bridging coordination mode.

P(1)–Li(1)	2.741(3)	B(1)–P(1)–Li(1)	123.04(8)
P(1)–B(1)	1.9611(17)	B(1)–P(1)–C(8)	106.09(7)
P(1)–C(1)	1.8850(14)	Li(1)–P(1)–C(1)	111.64(7)
P(1)–C(8)	1.8394(14)	B(1)–P(1)–C(1)	110.56(7)
Li(1)–B(1B)	2.440(3)	Li(1)–P(1)–C(8)	99.81(7)
Li(1)–H(2A)	2.182(19)	C(1)–P(1)–C(8)	102.95(6)
Li(1)–H(3A)	2.084(18)	P(1)–B(1)–Li(1A)	157.42(11)
Li(1)–C(1)	3.857(30)	P(1)–C(1)–Si(1)	119.63(7)
		P(1)–C(1)–Si(2)	109.93(7)
		Si(1)–C(1)–Si(2)	115.59(7)

Table 6.1. Selected bond lengths (Å) and angles (°) for **115**.

The Li-P distance of 2.741(3) Å is slightly longer than the corresponding distances in [Me₂PH(BH₃)Li(tmeda)] (**29**) [2.620(4) Å], [{(Me₃Si)₂CH}P(C₆H₄-2-CH₂OMe)(BH₃)Li(THF)]₂ (**49**) [2.611(6) Å] and [{(Me₃Si)₂CH}P(C₆H₄-2-SMe)(BH₃)Li(THF)]₂ (**64**) [2.527(3) Å], but is typical of Li-P distances in lithium phosphides.^{1,2,12-16} The Li...B distance and Li-H distances in **115** of 2.440(3) Å and 2.182(19) and 2.084(18) Å, respectively, are similar to the corresponding interactions in **29** [Li...B 2.372(4); Li-H 2.03(2) Å] and **64** [Li...B 2.403(3); Li-H 2.053(14) Å], which is consistent with an η²-BH₃-Li interaction.

The B-P-Li bridging angle in **115** of 123.04(8)° is comparable to the B-P-Li angle in **29** [120.2(1)°], which also crystallises as a linear polymer.¹⁷

Figures 6.4 and 6.5 show in detail the packing arrangement between two adjacent polymer chains; Figure 6.4 shows how one chain sits above the other, so that the phenyl groups are directed towards each other, and so that the (Me₃Si)₂CH substituents are orientated in opposite directions. At first glance it appears that this could be a consequence of aromatic π-π stacking, particularly with C...C distances of 3.976 Å, but in Figure 6.5, it can be clearly seen that the phenyl rings are arranged in a staggered manner, such that steric interactions between the two chains are reduced.

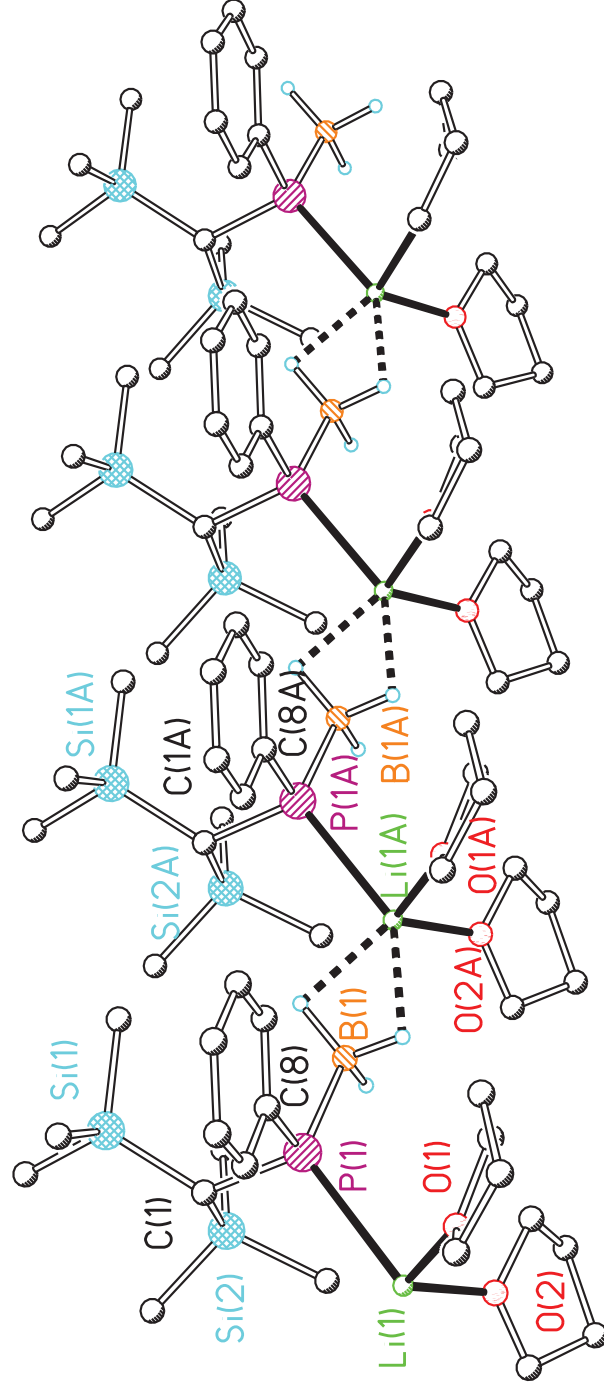


Figure 6.3. Part of the polymeric structure of compound **115**. All C-bound H atoms omitted for clarity.

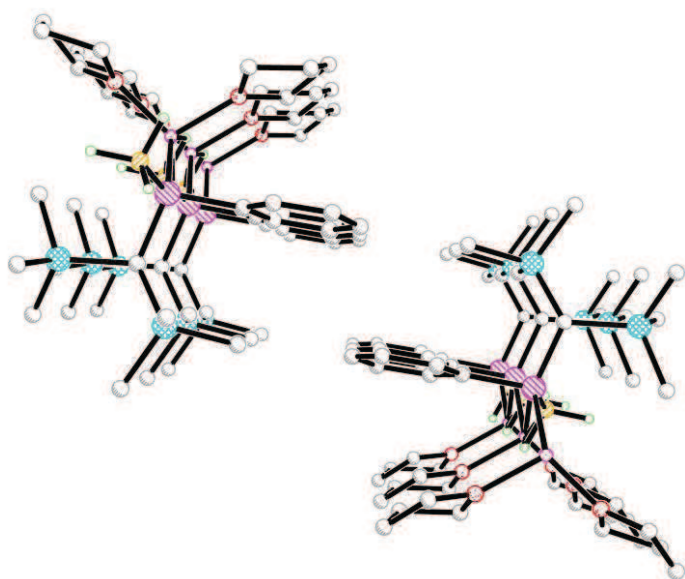


Figure 6.4. Structure of compound **115** viewed along a section of two adjacent polymer chains. All C-bound H atoms omitted for clarity.

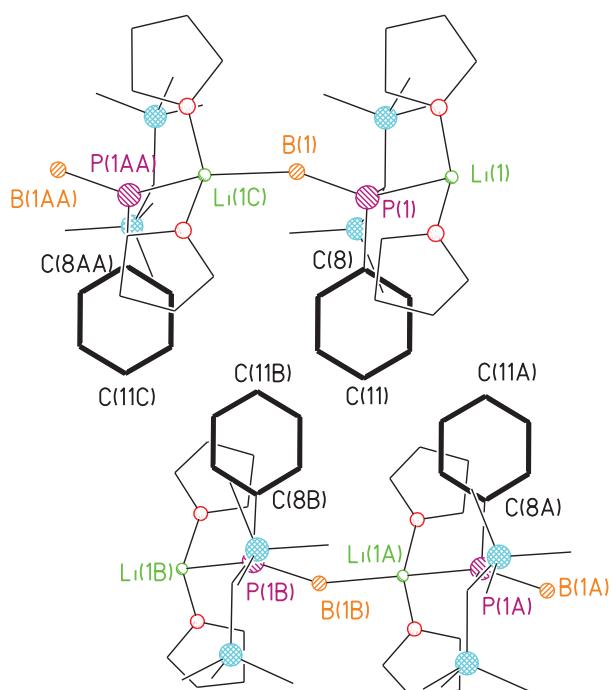


Figure 6.5. Structure of compound **115** viewed from above a section of two polymer chains. All H atoms omitted for clarity.

6.4.2 Solid-state structure of **116**

Compound **116** crystallises as a solvent-separated ion pair; the structure of **116** is shown in Figure 6.6, with selected bond lengths and angles shown in Table 6.2. This is the first example of a phosphido-borane complex that has been isolated as a solvent-separated ion pair; all previous examples of phosphido-boranes that have been characterised in the solid-state demonstrate $\text{BH}_3\cdots\text{M}$ interactions, even when there is no direct contact between the phosphorus atom and the metal centre.

Interestingly, a comparison between **116** and compound **115**, which crystallises as a contact ion pair, shows that the P-B and P-C bond distances within the ligand have similar values; for instance, the P-B distances are 1.9611(17) and 1.9688(15) Å for **115** and **116**, respectively. Also, the P-C(1) distances are 1.8850(14) and 1.8899(13) Å for **115** and **116**, respectively, whilst the P-C(8) distances are 1.8394(14) Å for **115** and 1.8400(14) Å for **116**.

The sum of angles within the C_2PB framework in **116** is 318.13° , which is similar to the sum of angles about the P atom in compound **115** [319.6°], which demonstrates that the geometry about phosphorus is not appreciably affected by its interaction with the metal centre.

These traits suggest that phosphido-boranes which exist as an isolated anion are likely to possess the same structural parameters as those that form a tight contact ion-pair with the metal cation.

P(1)–C(8)	1.8400(14)	C(1)–P(1)–B(1)	110.57(6)
P(1)–B(1)	1.9688(15)	C(8)–P(1)–C(1)	101.50(6)
P(1)–C(1)	1.8899(13)	C(8)–P(1)–B(1)	106.06(7)
Na(1)–O(1)	2.4982(12)	Si(2)–C(1)–P(1)	117.10(6)
Na(1)–O(2)	2.5032(13)	Si(1)–C(1)–P(1)	106.99(6)
Na(1)–O(3)	2.4375(11)	Si(2)–C(1)–Si(1)	118.99(7)
Na(1)–O(4)	2.4264(12)	C(8)–P(1)–C(1)	101.50(6)
		C(1)–P(1)–B(1)	110.57(6)
		C(8)–P(1)–B(1)	106.06(7)

Table 6.2. Selected bond lengths (Å) and angles ($^\circ$) for **116**.

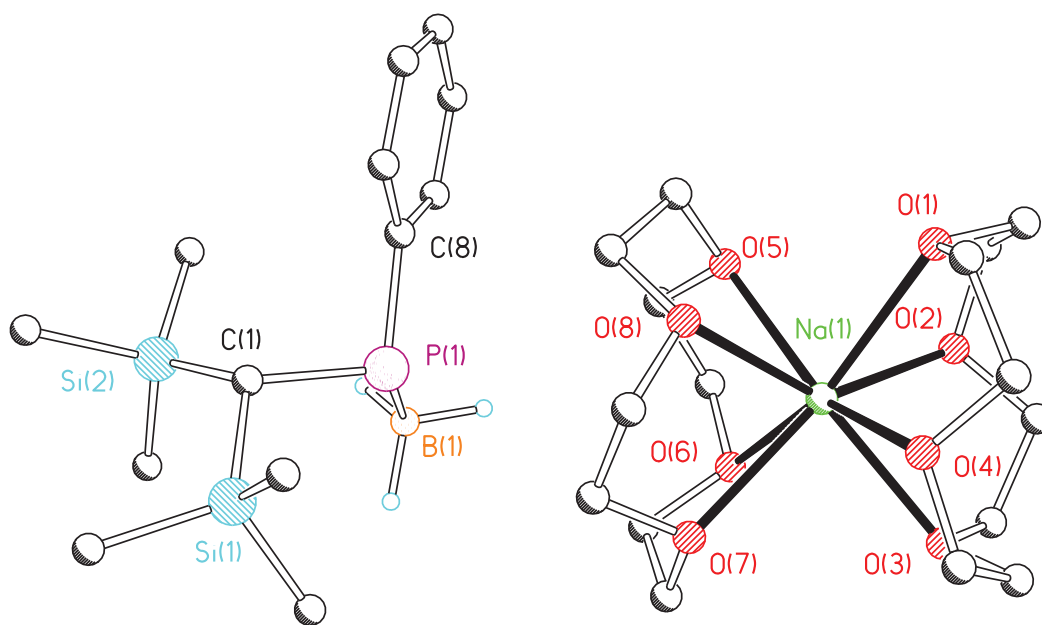


Figure 6.6. Structure of compound **116**. All C-bound H atoms omitted for clarity.

6.4.3 Solid-state structure of **117**

Compound **117** crystallises as discrete centrosymmetric dimers; the molecular structure of **117** is shown in Figure 6.7 and details of selected bond lengths and angles are shown in Table 6.3. Each phosphido-borane ligand is bound to an adjacent potassium ion via its P atom and an η^1 -BH₃ interaction, generating a pseudo-three-membered B-P-K ring [B-P-K bite angle 72.11(9)°]. The phosphido-borane ligand also coordinates to the second potassium ion in the dimer *via* its borane group in an η^3 -type fashion such that each BH₃ fragment acts as a μ_2 - η^1 : η^3 bridge; thus the two halves of the dimer are linked, generating a planar, pseudo-six-membered [PK(BH₃)₂]₂ ring. The coordination sphere of each potassium ion is completed by the three nitrogen atoms of a molecule of pmdeta, so that each potassium ion is pseudo-six-coordinate.

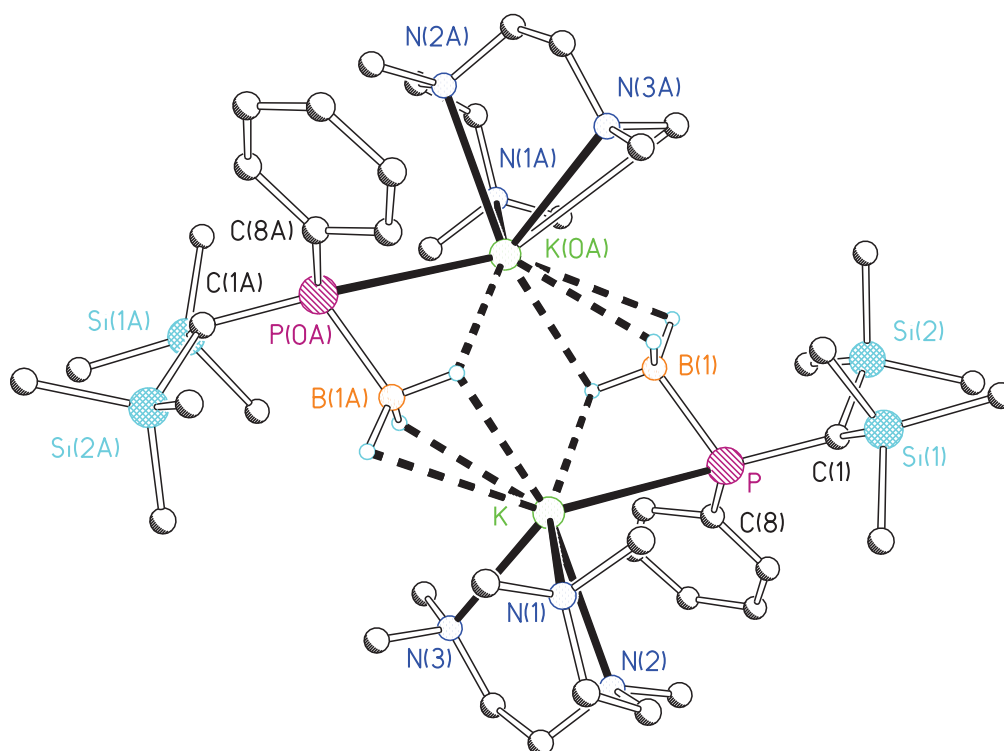


Figure 6.7. Structure of compound **117**. All C-bound H atoms omitted for clarity.

K–P	3.2754(8)	P–C(1)	1.874(2)
K–B(1)	3.262(3)	P–C(8)	1.831(2)
K–B(1A)	3.107(3)		
K–H(1AA)	2.7640 (0.0230)	K–P–B(1)	72.11(9)
K–H(1BA)	3.2499 (0.0282)	K–P–C(1)	151.87(7)
K–H(1CA)	2.7715 (0.0285)	K–P–C(8)	102.79(7)
K–H1A	2.7093 (0.0246)	B(1)–P–C(1)	111.20(11)
K–N(1)	2.830(2)	B(1)–P–C(8)	107.46(12)
K–N(2)	2.9132(18)	C(1)–P–C(8)	102.57(10)
K–N(3)	2.801(2)	P–K–B(1A)	131.08(6)
P–B(1)	1.969(3)		

Table 6.3. Selected bond lengths (Å) and angles (°) for **117**.

The K-P distance in **117** of 3.2754(8) Å is somewhat shorter than the corresponding distance in the related phosphide **114** [3.3351(12) Å].¹ Interestingly, in comparison to related potassium phosphido-borane complexes, the K-P distance in **117** is similar to the corresponding distances in [Ph₂P(BH₃)K(18-crown-6)] (**32**) [3.320(2) Å] and [{(Me₃Si)₂CH}P(C₆H₄-2-OMe)(BH₃)K(pmdeta)]₂ (**87**) [3.2338(5) Å], but is far shorter than the K-P distances in [{(Me₃Si)₂CH}P(C₆H₄-2-CH₂OMe)(BH₃)K(pmdeta)] (**51**) and [{(Me₃Si)₂CH}P(C₆H₄-2-SMe)(BH₃)K(pmdeta)]₂ (**66**) [3.6617(6) and 3.7620(10) Å, respectively], which have additional intramolecular coordination to potassium through a peripheral donor (the phosphido-borane ligand in **87**, although containing donor functionality, does not coordinate to potassium *via* the donor oxygen atom).

That compounds **51** and **66** have longer P-K distances than **32**, **87** and **117** suggests that P-K interactions are weaker in phosphido-boranes where the potassium ion is coordinated by a peripheral donor atom. Interestingly, however, this behaviour is only observed in phosphido-borane complexes with potassium, and not with lithium contact ion pairs.

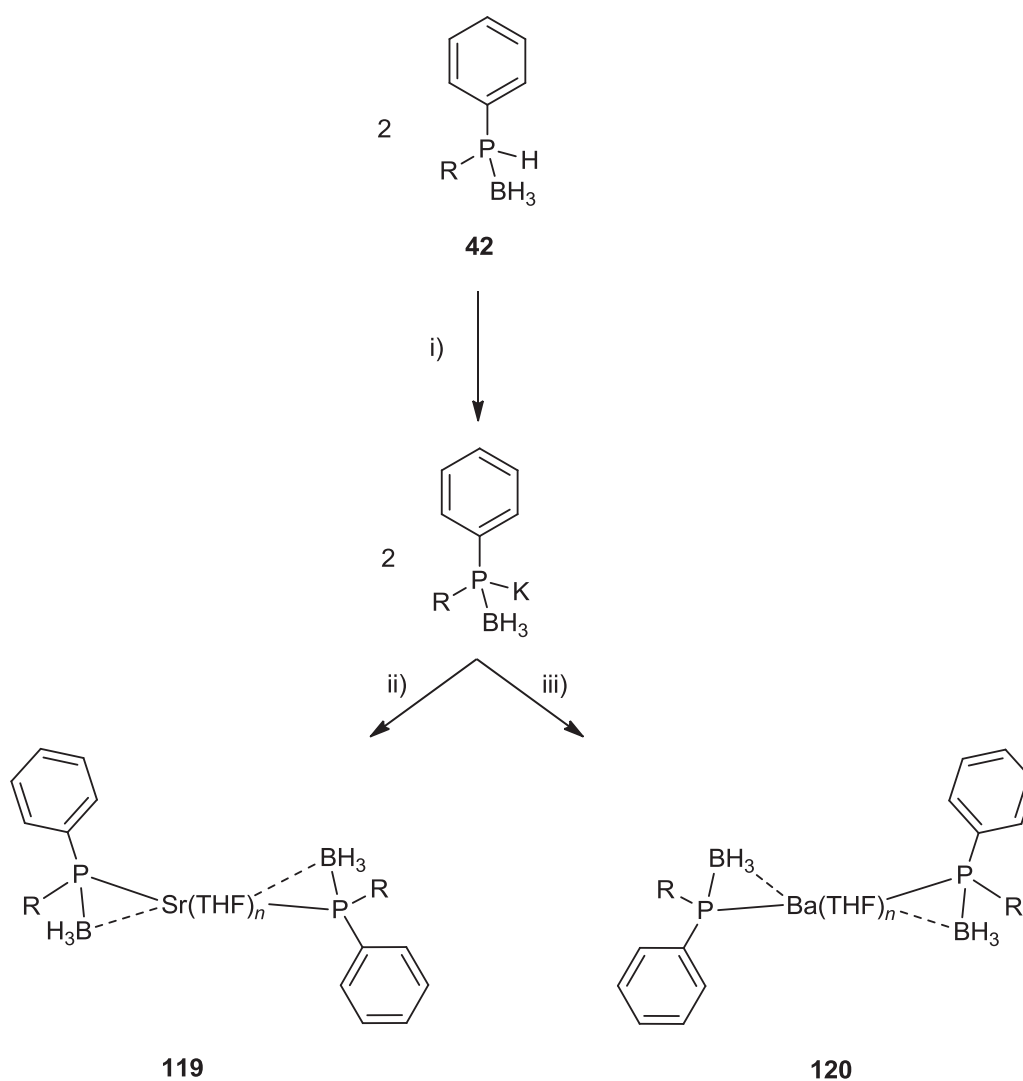
The K...B(1A) distance in **117** of 3.107(3) Å is comparable to other η³-BH₃-K distances,^{18,19} for example, the K...B distance in [K(BH₄)(18-crown-6)] (**60**) is 2.964(9) Å. The K-H distances for the bridging borane hydrogen in **117** [2.71(2) Å] are similar to the corresponding distances in the compound [(Et₃BH)K(pmdeta)]₂ (**118**), which also possesses a μ₂-bridging hydrogen [K-H 2.64(3) and 2.69(3) Å].²⁰

The K-P-B(1) angle in **117** [72.11(9)°] is somewhat larger than the corresponding angles in the ‘tridentate’ complexes **51** and **66** [61.79(7) and 62.01(7)° respectively], which may account for the difference in binding mode between the borane group and potassium; **117** adopts an η¹-BH₃-K binding mode, whereas **51** and **66** adopt an η²-BH₃-K coordination mode, which results in shorter B...K distances.

6.5 Synthesis of alkaline earth metal complexes [{(Me₃Si)₂CH}P(C₆H₅)(BH₃)₂M [M = Sr(**119**), Ba(**120**)]

The compounds [{(Me₃Si)₂CH}P(C₆H₅)(BH₃)₂Sr (**119**) and [{(Me₃Si)₂CH}P(C₆H₅)(BH₃)₂Ba (**120**)] were prepared by the addition of two equivalents of

[{(Me₃Si)₂CH}P(C₆H₅)(BH₃)K] in THF to a cold (-78 °C) slurry of either SrI₂ or BaI₂ in cold toluene (Scheme 6.4). The products were crystallised from cold toluene as an orange and a yellow solid, respectively. Unfortunately, however, single crystals of **119** and **120** could not be isolated, and so the X-ray crystal structures of these compounds could not be determined; the identity of **119** and **120** was confirmed by multi-element NMR spectroscopy and elemental analysis. It is reasonable to assume that **119** and **120** are coordinated by 4 or 5 molecules of THF molecules in THF solutions, as seen with group 2 complexes of related phosphides^{21,22,23} and phosphine-borane-stabilised carbanions.²⁴ However, NMR spectroscopy of compounds **119** and **120** alongside elemental analysis of **120** show no evidence of THF coordinated to the metal centres, which suggests that THF is easily lost when these compounds are exposed to vacuum.



Scheme 6.4. Synthesis of compounds **119** and **120**. Reagents and conditions: i) 2 BnK, THF, 1 h r.t. ii) SrI₂, toluene/THF, -78 °C, 16 h. iii) BaI₂, toluene/THF, -78 °C, 16 h [R = (Me₃Si)₂CH].

6.6 Solution-phase characterisation of **119** and **120**

The ^1H , $^{13}\text{C}\{^1\text{H}\}$, and $^{31}\text{P}\{^1\text{H}\}$ NMR spectra of **119** and **120** are as expected, and show that in both cases, the phosphido-borane ligands are equivalent. The $^{31}\text{P}\{^1\text{H}\}$ NMR spectra show broad quartets at -46.7 and -48.7 ppm, respectively, whilst the magnitude of the P-B coupling decreases from 39.7 Hz for **119** to 29.8 Hz for **120** (49.0 Hz for **42**), which is consistent with the greater ionic character in the P-M bonding interaction in the latter case.

In the ^1H NMR spectra of **119** and **120**, the diastereotopic SiMe_3 protons give rise to two sharp singlets between -0.05 and 0.14 ppm. The BH_3 protons give rise to a very broad quartet in each case, which collapses upon decoupling of the ^{11}B nucleus to give sharp doublets [$^2J_{\text{PH}} = 4.1$ Hz (**119** and **120**)] centred at 0.82 and 0.84 ppm for **119** and **120**, respectively. In the $^{13}\text{C}\{^1\text{H}\}$ NMR spectra of **119**, the SiMe_3 groups give rise to two singlets at 1.5 and 2.7 ppm, whilst in **120**, they appear as a doublet and a singlet at 1.68 [$^3J_{\text{PC}} = 5.8$ Hz] and 2.8 ppm. The adjacent CHP carbon gives rise to a doublet at 9.54 [$^1J_{\text{PC}} = 45.1$ Hz] and 6.34 ppm [$^1J_{\text{PC}} = 44.1$ Hz] for **119** and **120**, respectively.

6.7 Conclusions

Complexes of the phosphido-borane anion [$\{(\text{Me}_3\text{Si})_2\text{CH}\}\text{P}(\text{C}_6\text{H}_5)(\text{BH}_3)\text{P}^-$] with Li, Na, K, Sr and Ba have been prepared using straightforward synthetic procedures.

Compound **115** adopts a polymeric structure, where each unit is bridged by an $\eta^2\text{-BH}_3\text{-Li}$ interaction, in a comparable fashion to compound **29**. This is in stark contrast to the related compounds **49** and **64**, which possess a peripheral donor coordination to lithium, and which crystallise as dimers. This suggests that phosphido-borane complexes with lithium are more likely to exist as high-order aggregates if the lithium ion is not coordinated by a peripheral donor, or a sterically demanding co-ligand.

Compound **116** is the first example of a phosphido-borane to be characterised as a solvent-separated ion pair. A study of the phosphido-borane anion in **116** shows that there are no significant structural differences compared with phosphido-borane complexes that crystallise as a contact ion pair, and that coordination of the P and BH_3 centres has little influence on ligand structure.

The structure of compound **117** demonstrates that complexes of phosphido-boranes with potassium which do not possess additional chelation from a peripheral donor atom, have shorter P-K distances than the related compounds **51** and **66**, which do possess coordination from a peripheral donor. Compound **117** also has a larger M-P-B angle than that of the related ‘tridentate’ phosphido-boranes, and as a result, the borane group in **117** acts as a $\mu_2\text{-}\eta^1:\eta^3$ bridge between the two halves of the dimer, as opposed to a $\mu_2\text{-}\eta^2:\eta^3$ interaction as seen with compounds **51** and **66**.

Compounds **119** and **120** are the first examples of phosphido-borane complexes with strontium and barium. The structures of compounds **119** and **120** were deduced by ^1H , $^1\text{H}\{^{11}\text{B}\}$, $^{31}\text{P}\{^1\text{H}\}$, $^{11}\text{B}\{^1\text{H}\}$ and $^{13}\text{C}\{^1\text{H}\}$ NMR spectroscopy, alongside elemental analysis of **120**.

6.8 References

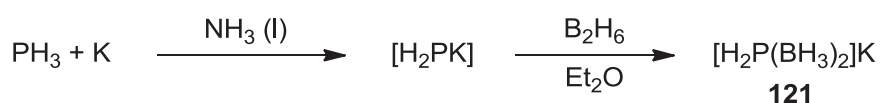
- (1) Izod, K.; Stewart, J.; Clark, E. R.; Clegg, W.; Harrington, R. W. *Inorg. Chem.* **2010**, *49*, 4698.
- (2) Clegg, W.; Doherty, S.; Izod, K.; Kagerer, H.; O’Shaughnessy, P. *J. Chem. Soc. Dalton Trans.* **1999**, 1825.
- (3) Bertz, S. H.; Gibson, C. P.; Dabbagh, G. *Organometallics.* **1988**, *7*, 227.
- (4) Lochmann, L.; Trekoval, J. *J. Organomet. Chem.* **1987**, *326*, 1.
- (5) Izod, K.; Clark, E. R.; Stewart, J. *Inorg. Chem.* **2011**, *50*, 3651.
- (6) Imamoto, T.; Oshiki, T.; Onozawa, T.; Kusumoto, T.; Sato, K. *J. Am. Chem. Soc.* **1990**, *112*, 5244.
- (7) Dreiss, M.; Merz, K.; Monsé, C. *Z. Anorg. Allg. Chem.* **2000**, *626*, 2264.
- (8) Beachler, R. D.; Mislow, K. *J. Am. Chem. Soc.* **1970**, *92*, 4758.
- (9) Beachler, R. D.; Mislow, K. *J. Am. Chem. Soc.* **1971**, *93*, 773

- (10) Beachler, R. D.; Casey, J. P.; Cook, R. J.; Senkler, G. H., Jr.; Mislow, K. *J. Am. Chem. Soc.* **1972**, *94*, 2859.
- (11) Beachler, R. D.; Andose, J. D.; Stackhouse, J.; Mislow, K. *J. Am. Chem. Soc.* **1972**, *94*, 8060.
- (12) Izod, K. *Adv. Inorg. Chem.* **2000**, *50*, 33.
- (13) Steiglitz, G.; Neumüller, B.; Dehnicke, K. *Z. Naturforsch* **1993**, *48b*, 156.
- (14) Izod, K.; Liddle, S. T.; Clegg, W.; Harrington, R. W. *Dalton Trans.* **2006**, 3431.
- (15) Blair, S.; Izod, K.; Harrington, R. W.; Clegg, W. *Organometallics* **2003**, *22*, 302.
- (16) Clegg, W.; Izod, K.; Liddle, S. T.; O'Shaughnessy, P.; Sheffield, J. M. *Organometallics* **2000**, *19*, 2090.
- (17) Müller, G.; Brand, J. *Organometallics* **2003**, *22*, 1463.
- (18) Dornhaus, F.; Bolte, M.; Lerner, H.-W.; Wagner, M. *Eur. J. Inorg. Chem.* **2006**, 1777.
- (19) Gálvez Ruiz, J. C.; Nöth, H.; Warchhold, M. *Eur. J. Inorg. Chem.* **2008**, 251.
- (20) Haywood, J.; Wheatley, A. E. H. *Eur. J. Inorg. Chem.* **2009**, 5010.
- (21) Westerhausen, M. *J. Organomet. Chem.* **1994**, *479*, 141.
- (22) Westerhausen, M.; Digeser, M. H.; Nöth, H.; Ponikwar, W.; Seifert, T.; Polborn, K. *Inorg. Chem.* **1999**, *38*, 3207.
- (23) Crimmin, M. R. Anthony G. M. Barrett, A. G. M.; Hill, M. S.; Hitchcock, P. B.; Procopiu, P. A. *Inorg. Chem.* **2007**, *46*, 10410.
- (24) Izod, K.; Wills, C.; Clegg, W.; Harrington, R. W. *Inorg. Chem.* **2007**, *46*, 4320.

Chapter 7. Alkali and alkaline earth metal complexes of phosphido-bis(boranes)

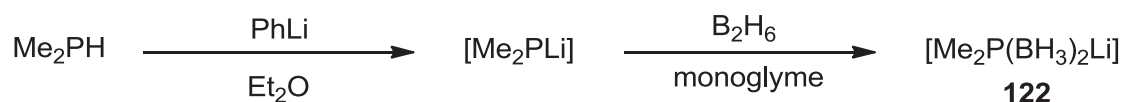
7.1 Introduction

The first example of a phosphido-bis(borane), reported by Thompson in 1965, was the compound $[\text{H}_2\text{P}(\text{BH}_3)_2\text{K}]$ (**121**). Compound **121** was prepared by reducing PH_3 with potassium in liquid ammonia to give the corresponding phosphide, followed by removal of the ammonia and addition of excess diborane in a cold solution of diethylether (Scheme 7.1). The unreacted diborane was recovered and showed that only one equivalent had reacted. That the compound was of empirical formula $[\text{H}_2\text{P}(\text{BH}_3)_2\text{K}]$ and not a mixture of potassium borohydride and $(\text{H}_2\text{P}\cdot\text{BH}_2)_n$ was shown by a comparison of X-ray powder diffraction patterns.¹



Scheme 7.1. Preparation of **121**.

In 1971 Keller and Schwartz reported the synthesis of lithium dimethylphosphido-bis(borane) (**122**).² Similar to **121**, compound **122** was prepared by reaction of the phosphide with diborane in monoglyme (Scheme 7.2). Interestingly, even when an excess of the phosphide was reacted with diborane only **122** was observed, with no $[\text{Me}_2\text{P}(\text{BH}_3)\text{Li}]$ present, indicating that diborane reacts directly with the phosphide.



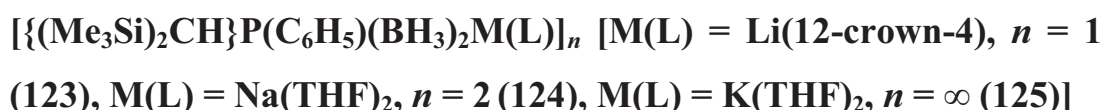
Scheme 7.2. Preparation of **122**.

This type of compound could have applications as reactive intermediates, as seen in their phosphido-borane counterparts. However, to date there are only a handful of examples of

structurally characterised phosphido-bis(borane) compounds (see chapter 1.4), hence a clearer understanding of the relationship between structure and reactivity is needed.

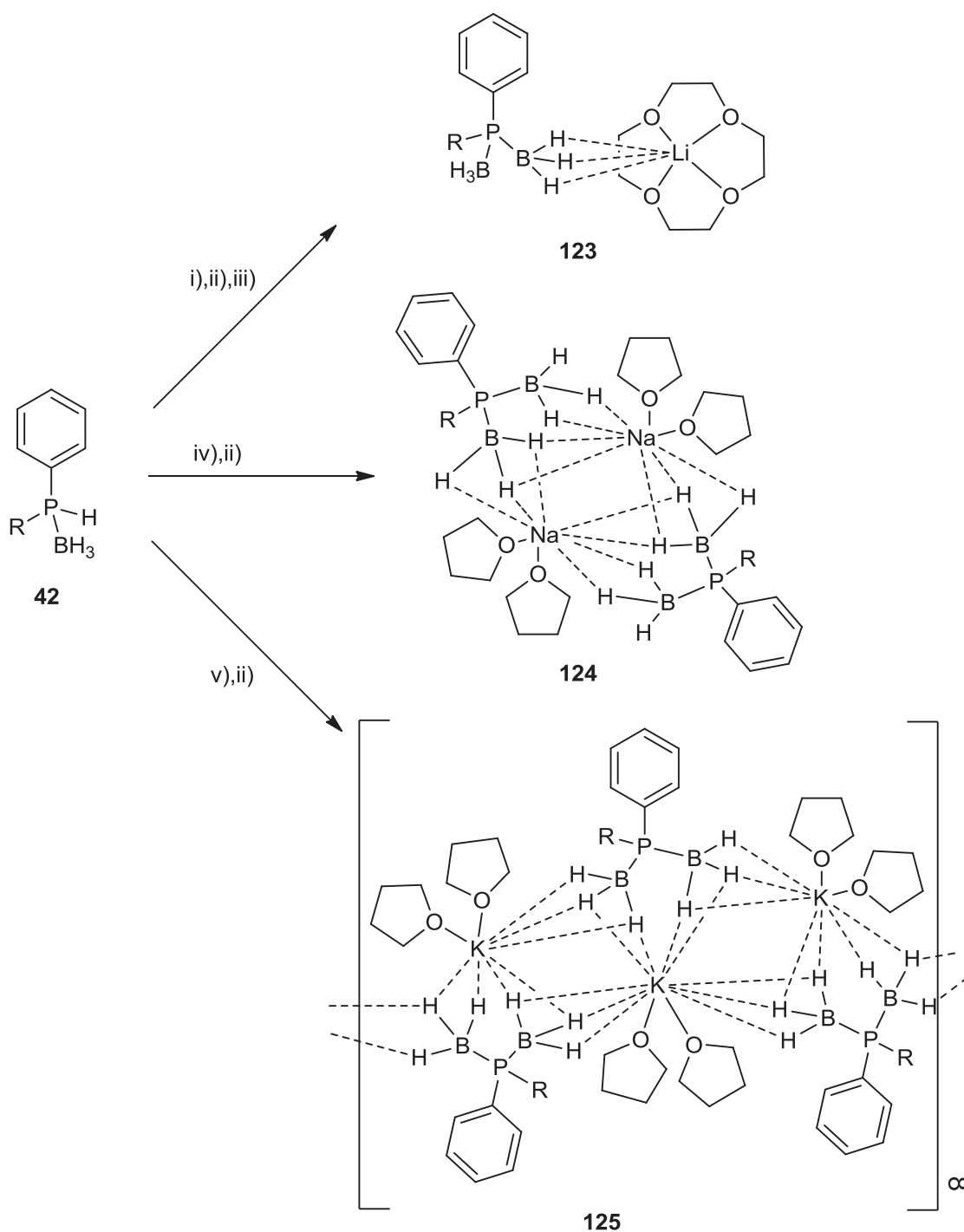
This chapter reports the synthesis and solid- and solution-state characterisation of a series of phosphido-bis(borane) complexes with group I and II metals.

7.2 Synthesis and characterisation of the alkali metal complexes



Reaction between a solution of compound **42** in THF and n BuLi, followed by addition of one equivalent of $\text{BH}_3 \cdot \text{SMe}_2$ yields the corresponding phosphido-bis(borane), which can be crystallised from toluene containing one equivalent of 12-crown-4 as the adduct $[\{(\text{Me}_3\text{Si})_2\text{CH}\}\text{P}(\text{C}_6\text{H}_5)(\text{BH}_3)_2\text{Li}(\text{12-crown-4})]$ (**123**, Scheme 7.3). The sodium and potassium salts are prepared from the reaction of a solution of **42** in THF and either a solution of BnNa^3 or BnK^4 in THF, followed by addition of $\text{BH}_3 \cdot \text{SMe}_2$ *in situ*. The products may be crystallised in good yield at room temperature, from toluene/methylcyclohexane/THF or toluene/THF, respectively, as the adducts $[\{(\text{Me}_3\text{Si})_2\text{CH}\}\text{P}(\text{C}_6\text{H}_5)(\text{BH}_3)_2\text{Na}(\text{THF})_2]_2$ (**124**) and $[\{(\text{Me}_3\text{Si})_2\text{CH}\}\text{P}(\text{C}_6\text{H}_5)(\text{BH}_3)_2\text{K}(\text{THF})_2]_\infty$ (**125**), which are colourless square plates.

The $^{31}\text{P}\{^1\text{H}\}$, ^1H and $^{13}\text{C}\{^1\text{H}\}$ NMR spectra of **123-125** are as expected. The $^{31}\text{P}\{^1\text{H}\}$ NMR spectra of compounds **123-125** exhibit broad signals at -8.8, -14.9 and -14.1 ppm respectively, which is a considerable downfield shift from -56.8, -49.4 and -48.2 ppm in the corresponding phosphido-boranes **115**, **116** and **117**, respectively. The signals should appear as septets due to coupling to two equivalent ^{11}B nuclei, but the coupling is unresolved due to quadrupolar broadening by ^{11}B . The P-B coupling constant can be measured through $^{11}\text{B}\{^1\text{H}\}$ NMR spectroscopy [$^1J_{\text{PB}} = 49.0$ (**123**), 68.6 (**124**) and 58.8 Hz (**125**)]. It is interesting that in compound **123**, only one BH_3 resonance is observed in the ^{11}B and ^1H spectra, although the solid-state structure of this compound (see section 7.4.1) shows that the two BH_3 groups are distinct. This suggests that in solution, **123** exists in a dynamic equilibrium, or as a solvent-separated ion pair.



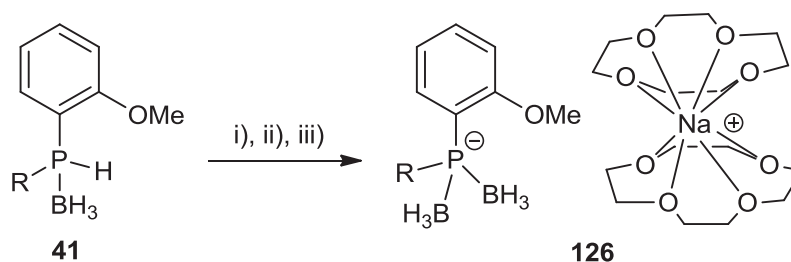
Scheme 7.3. Synthesis of compounds **123**, **124** and **125**. Reagents and conditions: i) $n\text{BuLi}$, THF, 1 h, r.t. ii) $\text{BH}_3 \cdot \text{SMe}_2$, 1 h, r.t. iii) 12-crown-4. iv) BnNa , THF, 1 h, r.t. v) BnK , THF, 1 h, r.t. [$\text{R} = (\text{Me}_3\text{Si})_2\text{CH}$].

In the ^1H NMR spectra, the SiMe_3 protons of **123-125** appear as sharp singlets, centred at -0.1 ppm for **123** and 0.1 ppm for **124** and **125**, whilst the CHP protons appear as doublets, centred around 0.6 ppm [$^2J_{\text{PH}} = 13.8, 15.1, 14.7$ Hz, for **123-125**, respectively]. The six borane hydrogens give rise to a broad signal centred between $0.6\text{-}0.8$ ppm in each case,

which, upon decoupling of the ^{11}B nucleus, collapse into sharp doublets [$^2J_{\text{PH}} = 10.1$ (**123**), 8.7 (**124**) and 9.6 (**125**) Hz]. The $^{13}\text{C}\{^1\text{H}\}$ NMR spectrum is as expected; the SiMe_3 carbons appear as a singlet at 3.2 ppm for **123**, and as doublets at 2.8 and 2.9 ppm for **124** and **125**, respectively [$^3J_{\text{PC}} = 1.9$ Hz (**124** and **125**)], whilst the CHP carbon gives rise to a doublet between 10.6 and 11.9 ppm for **123-125** [$^1J_{\text{PC}} = 6.7$ (**123**), 2.9 (**124**) and 3.8 Hz (**125**)].

7.3 Synthesis and characterisation of the alkali metal complex [$\{(\text{Me}_3\text{Si})_2\text{CH}\}\text{P}(\text{C}_6\text{H}_4\text{-2-OMe})(\text{BH}_3)_2\}[\text{Na}(\text{12-crown-4})_2]$ (**126**)

Reaction between a solution of compound **41** in THF with one equivalent of BnNa ,³ followed by addition of one equivalent of $\text{BH}_3\cdot\text{SMe}_2$ yields the corresponding phosphido-bis(borane), which may be crystallised from light petroleum ether containing two equivalents of 12-crown-4 as the adduct [$\{(\text{Me}_3\text{Si})_2\text{CH}\}\text{P}(\text{C}_6\text{H}_4\text{-2-OMe})(\text{BH}_3)_2\}[\text{Na}(\text{12-crown-4})_2]$ (**126**, Scheme 7.4).



Scheme 7.4. Synthesis of **126**. Reagents and conditions: i) BnNa , THF, 1 h, r.t. ii) $\text{BH}_3\cdot\text{SMe}_2$, 1 h, r.t. iii) 12-crown-4. [$\text{R} = (\text{Me}_3\text{Si})_2\text{CH}$].

The $^{31}\text{P}\{^1\text{H}\}$, ^1H and $^{13}\text{C}\{^1\text{H}\}$ NMR spectra of **126** are as expected. The $^{31}\text{P}\{^1\text{H}\}$ NMR spectrum of compound **126** exhibits a broad signal at -8.1 ppm, which is in the same region as those of compounds **123-125**. Unfortunately, the P-B coupling could not be resolved by either ^{31}P or $^{11}\text{B}\{^1\text{H}\}$ NMR spectroscopy; the $^{11}\text{B}\{^1\text{H}\}$ spectrum of **126** gives rise to a broad, poorly resolved signal at -32.7 ppm.

In the ^1H NMR spectrum, the SiMe_3 groups of **126** give rise to a singlet at 0.1 ppm, whilst the PCH hydrogen appears as a doublet, centred at 0.6 ppm [$^2J_{\text{PH}} = 10.1$ Hz], whilst the six borane hydrogens generate a broad signal centred at 0.8 ppm, which upon decoupling of the ^{11}B nucleus, collapses into a sharp doublet [$^2J_{\text{PH}} = 9.6$ Hz].

7.4 Solid-state structures of 123-126

7.4.1 Solid-state structure of 123

The lithium complex **123** crystallises as discrete monomers, with two distinct BH₃ groups: one shows contacts between all three hydrogen atoms and Li through an η^3 -type interaction [Li(1)-H(1A) 2.02(4) Å, Li(1)-H(1B) 2.27(5) Å, Li(1)-H(1C) 2.26(5) Å], while the hydrogen atoms of the other borane group have no intra- or intermolecular contacts with the metal. Coordination of the lithium ion is completed by the four oxygen atoms of the crown ether molecule. The Li...B distance in **123** is somewhat shorter than the corresponding interaction in [(mes*)PH(BH₃)₂Li(THF)₃] (**35**) [Li...B 2.281(7) (**123**), 2.430(5) (**35**) Å], which is consistent with their respective η^3 -BH₃-Li and η^2 -BH₃-Li type coordination. The distance between phosphorus and the boron engaged in Li coordination in **123** is slightly shorter than that for the ‘free’ BH₃ group [P(1)-B(1) 1.928(4), P(1)-B(2) 1.947(4) Å], as seen for compound **35** [P(1)-B(1) 1.955(3) Å, P(1)-B(2) 1.984(3) Å].⁵ The molecular structure of **123** is shown in Figure 7.1, with details of selected bond lengths and angles given in Table 7.1.

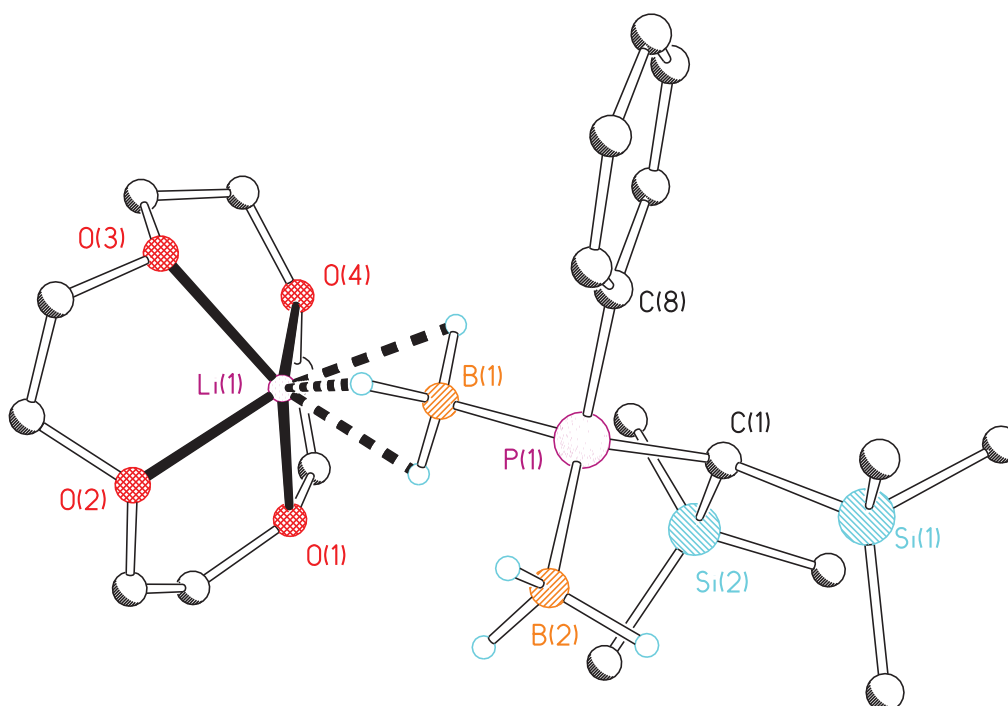


Figure 7.1. Structure of compound **123**. All C-bound H atoms omitted for clarity.

P(1)–B(1)	1.928(4)	B(1)–P(1)–B(2)	111.0(2)
P(1)–C(1)	1.853(3)	B(1)–P(1)–C(8)	102.50(17)
B(1)–Li(1)	2.281(7)	B(2)–P(1)–C(8)	113.5(2)
Li(1)–H(1B)	2.27(5)	B(1)–P(1)–C(1)	115.40(19)
P(1)–B(2)	1.947(4)	B(2)–P(1)–C(1)	111.71(18)
P(1)–C(8)	1.832(4)	C(1)–P(1)–C(8)	102.17(15)
Li(1)–H(1A)	2.02(4)	P(1)–B(1)–Li(1)	171.2(3)
Li(1)–H(1C)	2.26(5)		

Table 7.1. Selected bond lengths (Å) and angles (°) for **123**.

The range of Li-H distances in **123** [2.02(4)-2.27(5) Å] is also similar to other η^3 -BH_n-Li distances reported, such as in complexes **49**, [Ph₂^tBuSi(BH₃)Li(THF)₃] (**127**) and the borohydrides [Li(BH₄)(THF)₃] (**53**) and [Li(η^3 -BH₄)(NC₅H₄-4-Me)₃] (**54**). For example, the Li-H distances in **127** are 2.07, 2.13 and 2.21 Å.⁶⁻¹⁰

7.4.2 Solid-state structure of **124**

Compound **124** crystallises as discrete centrosymmetric dimers and is the first example of a sodium complex of a phosphido-bis(borane) anion to be crystallographically characterised; the molecular structure of **124** is shown in Figure 7.2, with selected bond lengths and angles shown in Table 7.2. Within the phosphido-bis(borane) ligand there are two distinctly different types of borane groups. In the first, the borane group binds to the adjacent sodium ion through two hydrogen atoms in an η^2 -manner, with the third hydrogen atom not involved in any Na-H interactions. The second borane group bridges both sodium ions in the dimer *via* an η^2 -type interaction with two hydrogen atoms, which forms a planar pseudo-four-membered Na₂B₂ ring, with the third hydrogen forming an η^1 contact to the second Na atom in the dimer, such that the borane group acts as a μ_2 - η^2 : η^3 bridge. In all, the sodium ions are coordinated to three BH₃ groups, with coordination completed by two molecules of THF on each ion. The B...Na distances in **124** range from 2.782(3) to 3.011(3) Å, and these values are consistent with η^3 or η^2 -BH_n-Na coordination modes, respectively.^{7,10} For example, the η^3 - and η^2 -BH₄...Na distances in [NaBH₄(pmdeta)]₂ (**57**) are 2.727(4) and 2.837(4) Å, respectively. The Na-H distances in **124** [2.42(2)-2.67(3) Å] also lie in the typical range for Na-H-B containing

species; for example, the Na-H distances in $[\{(Me_3Si)_2CH\}P(C_6H_4-2-SMe)(BH_3)Na(tmeda)]_\infty$ (**65**) range from 2.35(3) to 2.69(4) Å.

Na(1)–B(1A)	2.782(3)	B(1)–P(1)–B(2)	109.59(12)
Na(1)–B(1)	3.011(3)	B(1)–P(1)–C(1)	114.59(12)
Na(1)–B(2)	2.864(3)	B(2)–P(1)–C(1)	113.75(11)
Na(1)–H(1A)	2.63(2)	B(1)–P(1)–C(8)	104.19(12)
Na(1)–H(1B)	2.67(3)	B(2)–P(1)–C(8)	109.06(12)
Na(1)–H(2A)	2.42(2)	C(1)–P(1)–C(8)	104.99(10)
Na(1)–H(2B)	2.54(3)	P(1)–C(1)–Si(1)	113.44(12)
P(1)–B(1)	1.950(3)	P(1)–C(1)–Si(2)	113.39(12)
P(1)–C(1)	1.862(2)	Si(1)–C(1)–Si(2)	116.56(12)
P(1)–B(2)	1.958(3)	B(1)–Na(1)–B(2)	65.79(8)
P(1)–C(8)	1.846(2)	Na(1)–B(1)–Na(1A)	91.12(9)
		B(1)–Na(1)–B(1A)	88.88(9)

Table 7.2. Selected bond lengths (Å) and angles (°) for **124**.

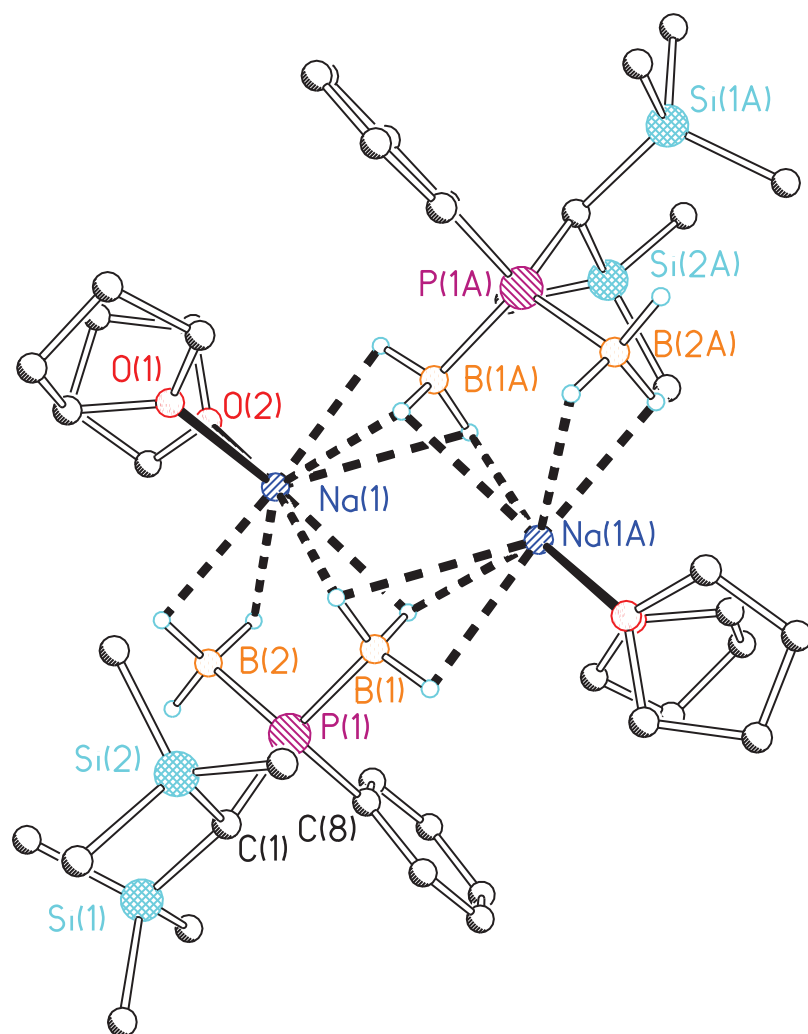


Figure 7.2. Structure of compound **124**. All C-bound H atoms omitted for clarity.

7.4.3 Solid-state structure of **125**

Compound **125** crystallises as a linear polymer; the structure of **125** is shown in Figure 7.3, with selected bond lengths and angles shown in Table 7.3. In each polymer unit, the phosphido-bis(borane) ligand is coordinated *via* both BH_3 groups to the potassium centre in an η^2 -manner, thus forming a pseudo-four-membered $\text{K}(\text{BH}_3)_2\text{P}$ ring. Each borane group also coordinates in an η^3 fashion to the potassium ion in an adjacent unit, such that the potassium

ions in the polymer are bridged by two $\mu_2\text{-}\eta^2\text{:}\eta^3$ borane groups, generating a series of pseudo-four-membered $\text{K}_2(\text{BH}_3)_2$ rings along the polymer chain, thus the polymer adopts a zig-zag ladder structural motif (Figure 7.4). The coordination about each potassium ion is completed by two molecules of THF, making the K ion pseudo-six-coordinate.

The K...B distances in **125** [3.316(4), 3.131(4), 3.417(4) and 3.183(4) Å] are much longer than the corresponding Li...B and Na...B distances in **123** and **124**, consistent with the larger ionic radius of potassium, and are similar in length to the K...B distance in the related phosphido-bis(borane) compound **37** [3.205 Å].¹¹ The B-P-B angle in **125** [111.48(16)°] is slightly larger than the related angle in **124** [109.59(12)°], which is as expected, due to the larger ionic radius of the potassium ion.

K(1)–H(1A)	3.06(3)	P(1)–C(8)	1.838(3)
K(1)–H(1B)	2.76(3)		
K(1)–H(2B)	2.88(3)	B(1)–P(1)–B(2)	111.48(16)
K(1)–B(1)	3.316(4)	K(1)–B(2)–K(1A)	88.35(9)
K(1)–B(1A)	3.131(4)	B(1)–K(1)–B(2)	56.89(9)
K(1)–B(2)	3.417(4)	B(1)–P(1)–C(8)	109.26(16)
K(1)–B(2B)	3.183(4)	B(2)–P(1)–C(8)	104.06(16)
P(1)–B(1)	1.933(4)	B(2)–P(1)–C(1)	115.12(15)
P(1)–B(2)	1.949(4)	C(1)–P(1)–C(8)	103.45(14)
P(1)–C(1)	1.850(3)		

Table 7.3. Selected bond lengths (Å) and angles (°) for **125**.

7.4.4 Solid-state structure of **126**

Compound **126** crystallises with two crystallographically independent molecular ion pairs in the asymmetric unit; the structures of both ion pairs are shown in Figure 7.5, with selected bond distances and angles shown in Table 7.4. In a similar fashion to the related sodium phosphido-borane complex $[\{(Me_3Si)_2CH\}P(C_6H_5)(BH_3)][Na(12\text{-crown-}4)_2]$ (**116**), **126** crystallises as solvent separated ion pairs; the sodium ions are coordinated by eight oxygen atoms of two molecules of 12-crown-4.

The angles about the phosphorus centre in **126** are similar to those seen in **124**; the B-P-B and C-P-C angles are $109.59(12)$ and $104.99(10)^\circ$ for **124** and $111.7(3)$ and $105.0(2)^\circ$ for **126**, respectively, whilst the B-P-C angles lie in the same range of $104\text{--}116^\circ$. There are no significant differences in the bond distances about phosphorus in **124** and **126**, which suggests that phosphido-bis(borane) complexes are likely to possess the same structural parameters whether they exist as a solvent-separated ion species or as a contact ion pair.

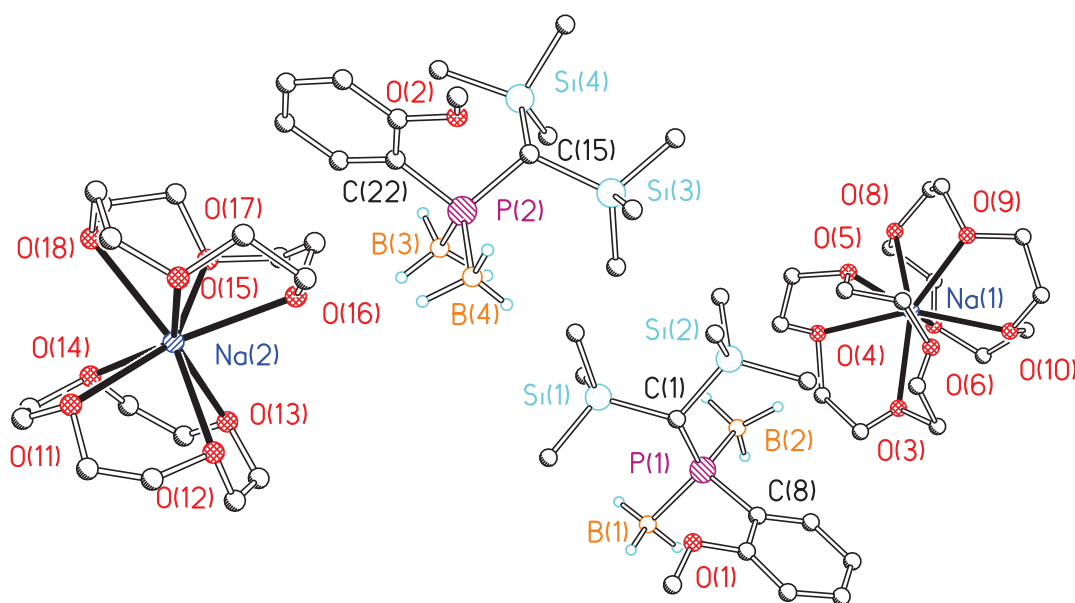


Figure 7.5. Structure of compound **126** (both independent molecules shown). All C-bound H atoms omitted for clarity.

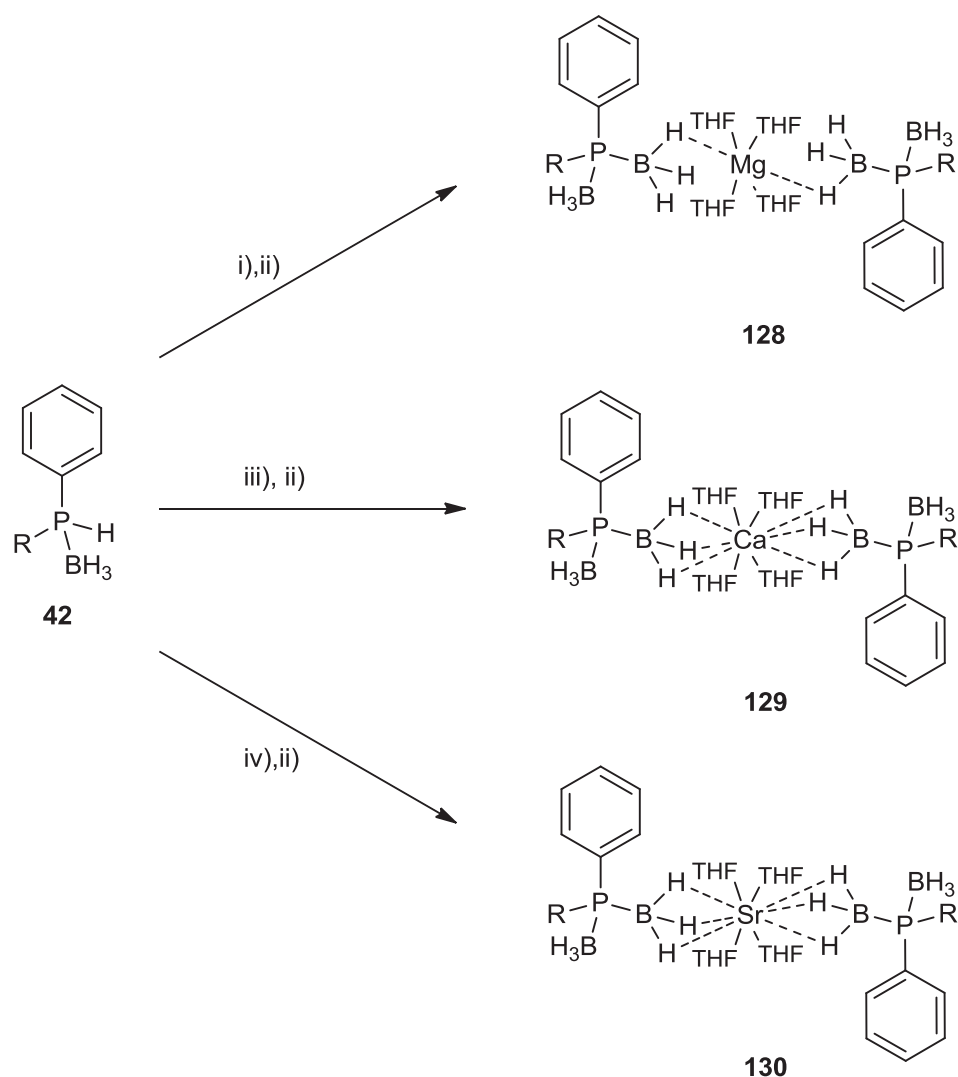
P(1)–B(1)	1.943(7)	C(1)–P(1)–B(1)	116.3(3)
P(1)–B(2)	1.954(6)	C(8)–P(1)–B(2)	110.1(3)
P(1)–C(1)	1.858(5)	B(1)–P(1)–B(2)	111.7(3)
P(1)–C(8)	1.841(5)	C(22)–P(2)–C(15)	103.5(2)
P(2)–B(3)	1.956(7)	C(22)–P(2)–B(3)	108.6(3)
P(2)–B(4)	1.963(6)	C(15)–P(2)–B(3)	110.3(3)
P(2)–C(22)	1.825(5)	C(22)–P(2)–B(4)	104.9(3)
P(2)–C(15)	1.855(5)	C(15)–P(2)–B(4)	116.4(3)
Na(1)–O(6)	2.385(6)	B(3)–P(2)–B(4)	112.4(3)
Na(2)–O(18)	2.507(4)	P(1)–C(1)–Si(2)	115.3(3)
C(8)–P(1)–C(1)	105.0(2)	P(1)–C(1)–Si(1)	113.1(3)
C(8)–P(1)–B(1)	103.4(3)	Si(2)–C(1)–Si(1)	116.4(3)

Table 7.4 Selected bond lengths (Å) and angles (°) for **126**.

7.5 Synthesis and characterisation of alkaline earth metal complexes [[{(Me₃Si)₂CH}P(C₆H₅)(BH₃)₂]M(THF)₄] [M = Mg (**128**), Ca(**129**), Sr(**130**)]

Treatment of a solution of two equivalents of **42** in toluene with one equivalent of MgBu₂ in heptane, followed by addition of one equivalent of BH₃·SMe₂ *in situ*, yields the corresponding phosphido-bis(borane) (Scheme 7.5), which crystallises from toluene/THF at room temperature as the adduct [({(Me₃Si)₂CH}P(BH₃)₂(C₆H₅))₂Mg(THF)₄] (**128**).

To prepare the related calcium and strontium derivatives, the basic reagents [Bn₂Ca(THF)₄] and [(Me₃Si)₂CH]₂Sr(THF)₃] were synthesised using previously reported procedures.^{12,13} The reaction between a solution of two equivalents of **42** in toluene and one equivalent of either [Bn₂Ca(THF)₄] or [(Me₃Si)₂CH]₂Sr(THF)₃] in THF, followed by addition of BH₃·SMe₂ *in situ*, yields the corresponding alkaline earth metal salts. The compounds may be crystallised from toluene/THF by concentrating the reaction solution *in vacuo*, as the adducts [({(Me₃Si)₂CH}P(BH₃)₂(C₆H₅))₂Ca(THF)₄] (**129**) and [({(Me₃Si)₂CH}P(BH₃)₂(C₆H₅))₂Sr(THF)₄] (**130**).

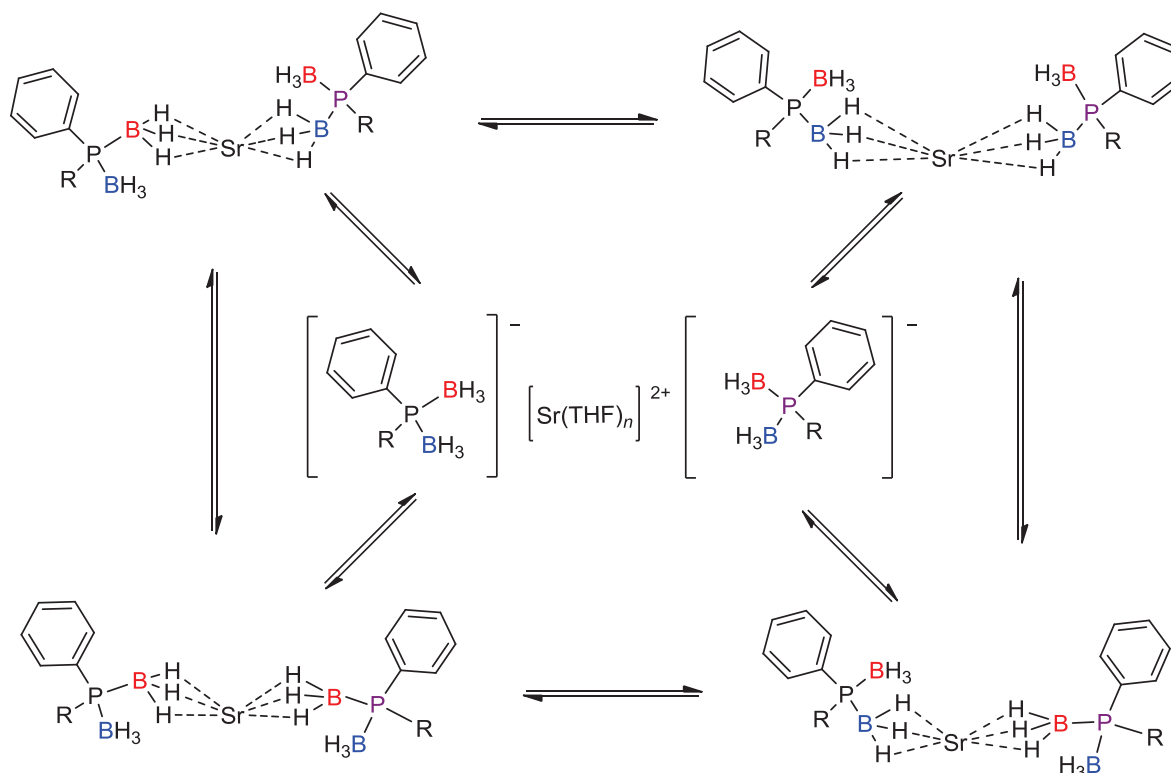


Scheme 7.5. Synthesis of compounds **128-130**. Reagents and conditions: i) MgBu_2 , 1 h, r.t. ii) $\text{BH}_3 \cdot \text{SMe}_2$, THF, 1 h, r.t. iii) $[\text{Bn}_2\text{Ca}(\text{THF})_3]$, THF, 1 h, r.t. v) $[\text{R}_2\text{Sr}(\text{THF})_3]$, THF, 1 h, r.t. [$\text{R} = (\text{Me}_3\text{Si})_2\text{CH}$].

The $^{31}\text{P}\{^1\text{H}\}$, $^1\text{H}\{^{11}\text{B}\}$ and $^{13}\text{C}\{^1\text{H}\}$ NMR spectra of **128-130** are as expected. The $^{31}\text{P}\{^1\text{H}\}$ NMR spectra of compounds **128-130** in d_3 -THF exhibit broad, poorly resolved multiplets at -11.5, -15.9 and -16.4 ppm respectively, due to coupling to two ^{11}B nuclei.

In the ^1H NMR spectra, the SiMe_3 protons of **128-130** are equivalent, and give rise to a sharp singlet at 0.1 ppm in each case. The twelve borane protons give rise to a broad signal centred around 0.7-0.8 ppm, and, upon decoupling of the ^{11}B nucleus, the broad signals collapse into sharp doublets due to coupling to the ^{31}P nucleus [$^2J_{\text{PH}} = 10.5$ (**128**), 12.9 (**129**) and 11.0 Hz (**130**)].

That the BH₃ groups in compounds **128-130** are equivalent by NMR spectroscopy is rather surprising, given the crystal structures of these complexes in the solid-state show that they are inequivalent (see chapter 7.6). This indicates that, in THF, either there is rapid exchange between the free and bound BH₃ groups, or that the complexes exist as solvent separated ion multiples (Scheme 7.6).



Scheme 7.6. Possible behaviour of compound **130** in solution.

7.6 Solid-state structures of compounds 128-130

Compounds **128-130** crystallise as discrete centrosymmetric monomers, and are essentially isostructural in the solid state. The structures of **128-130** are shown in Figures 7.8, 7.9 and 7.10 with selected bond lengths and angles given in Tables 7.6-7.8, respectively.

In each complex, the metal centres are coordinated by two phosphido-bis(borane) ligands *via* one of the BH₃ groups. The coordination about each metal ion is completed by four molecules of THF. This is rather surprising, as it would be assumed that the larger cations would adopt higher coordination numbers. Indeed the ionic radius of Sr²⁺ is over 60% greater than the

radius of Mg^{2+} , with coordination numbers, which typically lie in the range of 8-12 compared to four for Mg^{2+} . However, in compound **128** the borane groups adopt an $\eta^1\text{-BH}_3\text{-Mg}$ type interaction, whereas compounds **129** and **130** adopt $\eta^3\text{-BH}_3\text{-M}$ binding modes.

Cation (2+)	Ionic Radius Å	Coordination No.
Mg	0.78	6
Ca	1.06	6-9
Sr	1.27	8-12

Table 7.5. Ionic radii of group 2 metals.

The Mg...B distance of 2.7800(18) Å is slightly longer than related $\eta^1\text{-BH}_n\text{-Mg}$ distances that have been reported.^{14,15} For example the complex $[(\text{B}_3\text{H}_8)_2(\text{Et}_2\text{O})_2\text{Mg}]$ (**131**) has a Mg...B distance of 2.575(5). However the Mg-H distance of 2.069(19) Å lies in the typical range of 1.9-2.4 Å. For example, in compound **131**, the Mg-H distances are 1.99(3) and 2.01(4) Å.

The Ca...B distances in **129** of 2.751(2) Å are similar to the corresponding $\eta^3\text{-BH}_n\text{-Ca}$ interactions in $(\text{BH}_4)_2\text{Ca}(\text{DME})_2$ (**132**)¹⁶ [2.67(5) and 2.65(4) Å], and the Ca-H distances of **132** [2.637(19) 2.834(19) and 2.374(19) Å] are also similar to those in **129** [2.345(29)–2.577(29)]. As expected the Ca-H distances in **129** [2.637(19), 2.834(19) and 2.374(19) Å] are longer than the corresponding Mg-H distances in **128**.

Mg(1)–B(1)	2.8700(18)	B(1)–P(1)–C(1)	110.83(8)
Mg(1)–H(1A)	2.069(19)	B(1)–P(1)–C(8)	102.07(8)
Mg(1)–H(1B)	3.020(19)	B(2)–P(1)–C(1)	112.53(8)
Mg(1)–H(1C)	3.209(20)	B(2)–P(1)–C(8)	110.02(9)
P(1)–B(1)	1.9465(18)	O(3)–Mg(1)–B(1)	92.66(5)
P(1)–B(2)	1.937(2)	O(3A)–Mg(1)–B(1)	89.60(5)
P(1)–C(1)	1.8520(16)	O(1)–Mg(1)–O(3A)	94.25(3)
P(1)–C(8)	1.8311(16)	O(1)–Mg(1)–B(1)	74.62(4)
		O(2)–Mg(1)–B(1)	105.38(4)
B(1)–Mg(1)–B(1A)	149.24(8)	B(1)–Mg(1)–B(1A)	149.24(8)
B(1)–P(1)–B(2)	114.39(8)		

Table 7.6. Selected bond lengths (Å) and angles (°) for **128**.

Ca(1)–B(1)	2.751(2)	O(1A)–Ca(1)–O(2)	87.43(6)
Ca(1)–H(1A)	2.637(19)	O(1)–Ca(1)–B(1)	89.97(7)
Ca(1)–H(1B)	2.834(19)	O(1)–Ca(1)–B(1A)	90.03(7)
Ca(1)–H(1C)	2.374(19)	B(1)–Ca(1)–B(1A)	180.00(5)
P(1)–B(1)	1.926(2)	B(1)–P(1)–B(2)	111.97(11)
P(1)–B(2)	1.941(2)	B(1)–P(1)–C(1)	114.30(10)
P(1)–C(1)	1.8426(18)	B(1)–P(1)–C(8)	100.73(10)
P(1)–C(8)	1.8286(19)	B(2)–P(1)–C(1)	113.42(10)
		B(2)–P(1)–C(8)	110.14(10)
O(1)–Ca(1)–O(2)	92.57(6)	C(1)–P(1)–C(8)	105.22(8)

Table 7.7. Selected bond lengths (Å) and angles (°) for compound **129**.

The Sr–H distances of 2.54(6), 2.78(7) and 2.81(7) Å and the Sr...B distance of 2.871(12) Å in **130** are comparable to the η^3 -BH_n-Sr distances in the phosphine-borane-stabilised carbanion [(Me₃Si)₂{Me₂(H₃B)P}C]₂Sr(THF)₅ (**133**)¹⁷ [Sr–H 2.65(3), 2.76(3) and 2.89(4) Å; Sr...B 2.893(7) Å] and the tetrahydridoborate complex (BH₄)₂Sr(diglyme)₂ (**134**)¹⁸ [Sr–H 2.64(4), 2.77(4) and 2.65(4) Å; Sr...B 2.916(7) Å].

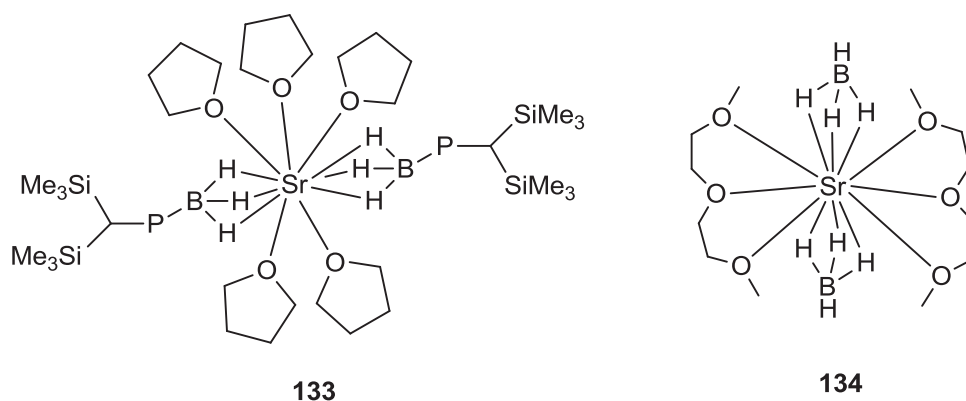


Figure 7.6. Examples of η^3 -BH_n-Sr interactions.

Sr(1)–B(1)	2.871(12)	B(1)–Sr(1)–B(1A)	179.998(1)
Sr(1)–B(1A)	2.871(12)	B(1)–P(1)–B(2)	110.7(6)
Sr(1)–H(1A)	2.54(6)	B(1)–P(1)–C(1)	114.9(4)
Sr(1)–H(1B)	2.81(7)	B(1)–P(1)–C(8)	100.8(5)
Sr(1)–H(1C)	2.78(7)	B(2)–P(1)–C(1)	112.6(5)
P(1)–B(1)	1.914(12)	B(2)–P(1)–C(8)	111.8(5)
P(1)–B(2)	1.957(12)	C(1)–P(1)–C(8)	105.4(4)
P(1)–C(1)	1.858(8)	O(1)–Sr(1)–O(2A)	91.4(2)
		O(1A)–Sr(1)–B(1A)	91.0(3)
		O(1A)–Sr(1)–B(1)	89.0(3)

Table 7.8. Selected bond lengths (Å) and angles (°) for **130**.

From compounds **128-130** it is clear to see that there is a trend of increasing M-H distances with increasing ionic radius of the metal cation [for example: M-H(1) 2.069(19) (**128**), 2.374(19) (**129**) and 2.54(6) Å (**130**)]. However, the overall M...B distances in **128-130** do not exhibit any trend, in fact quite surprisingly, the Mg...B distance in **128** and the Sr...B distance in **130** are identical [2.8700(18) and 2.871(12) Å, respectively].

As seen with compound **123**, the P-B distances in compounds **129** [1.926(2) and 1.941(2)] and **130** are shorter for the BH₃ group engaged with the metal centre [P-B_{bound} 1.928(4) (**123**), 1.926(2) (**129**) and 1.914(12) Å (**130**)] than for the free BH₃ group [P-B_{free} 1.947(4) (**123**), 1.941(2) (**129**) and 1.957(12) Å (**130**)]. In contrast to these observations, the P-B distances of the compound **128** are very similar, where the P-B distance for the magnesium-bound borane group is only marginally longer than the P-B distance to the free BH₃ group [1.9465(18) and 1.937(2) Å, respectively]. This may be attributed to the η¹ binding mode of the metal bound borane group in **128** which closer resembles a separated ion pair, where the P-B distances would be identical.

Interestingly, as you move down the series, the P-B distances for the metal-bound borane groups decrease, whilst the P-B distances for the non-bound BH₃ groups increase, which comes with an increasing disparity between the P-B_{bound} and P-B_{free} distances.

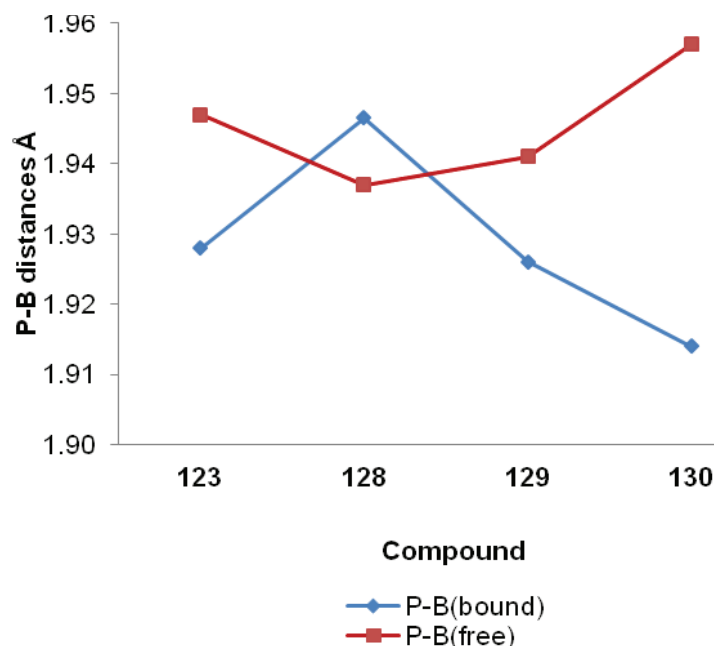


Figure 7.7. P-B bond lengths in compounds **123**, **128**, **129** and **130**.

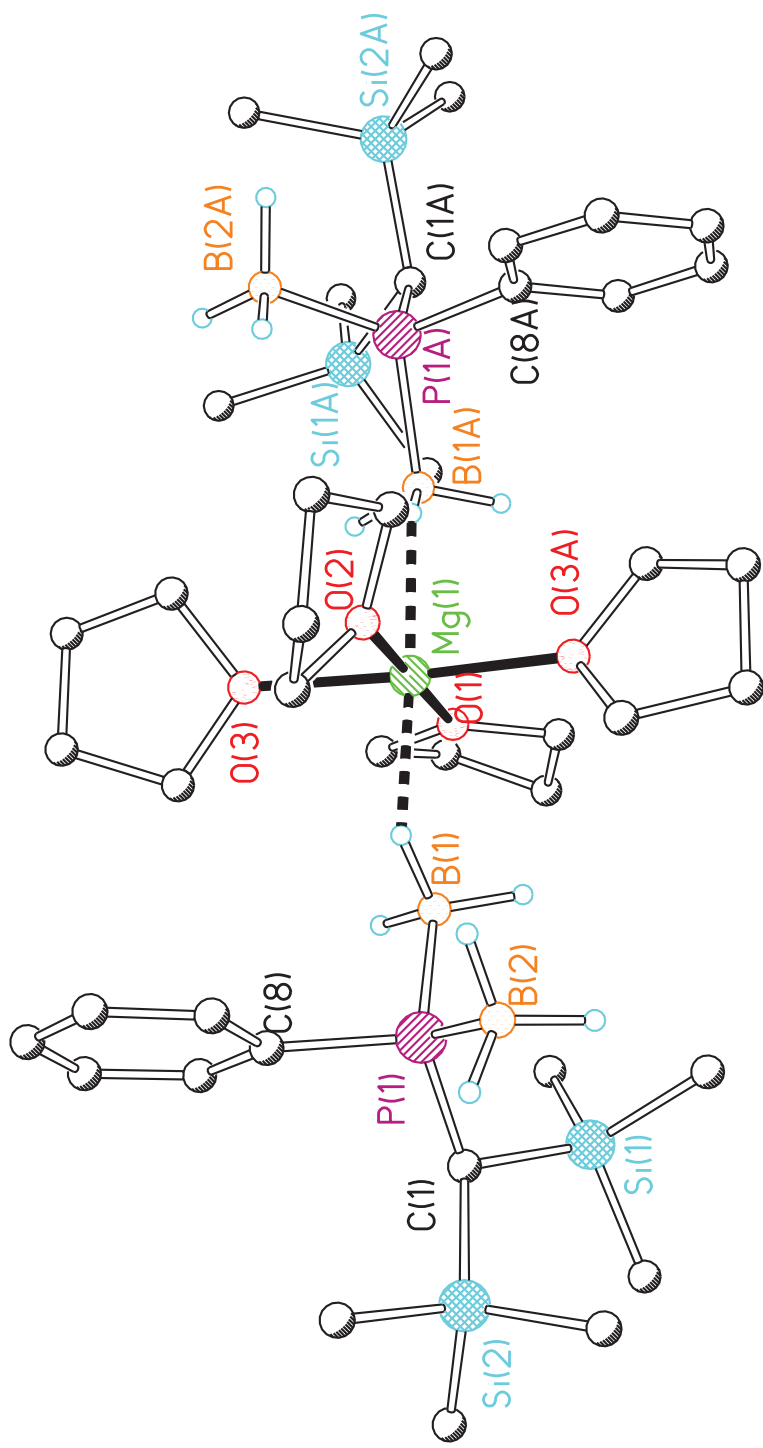


Figure 7.8. Structure of compound 128. All C-bound H atoms omitted for clarity.

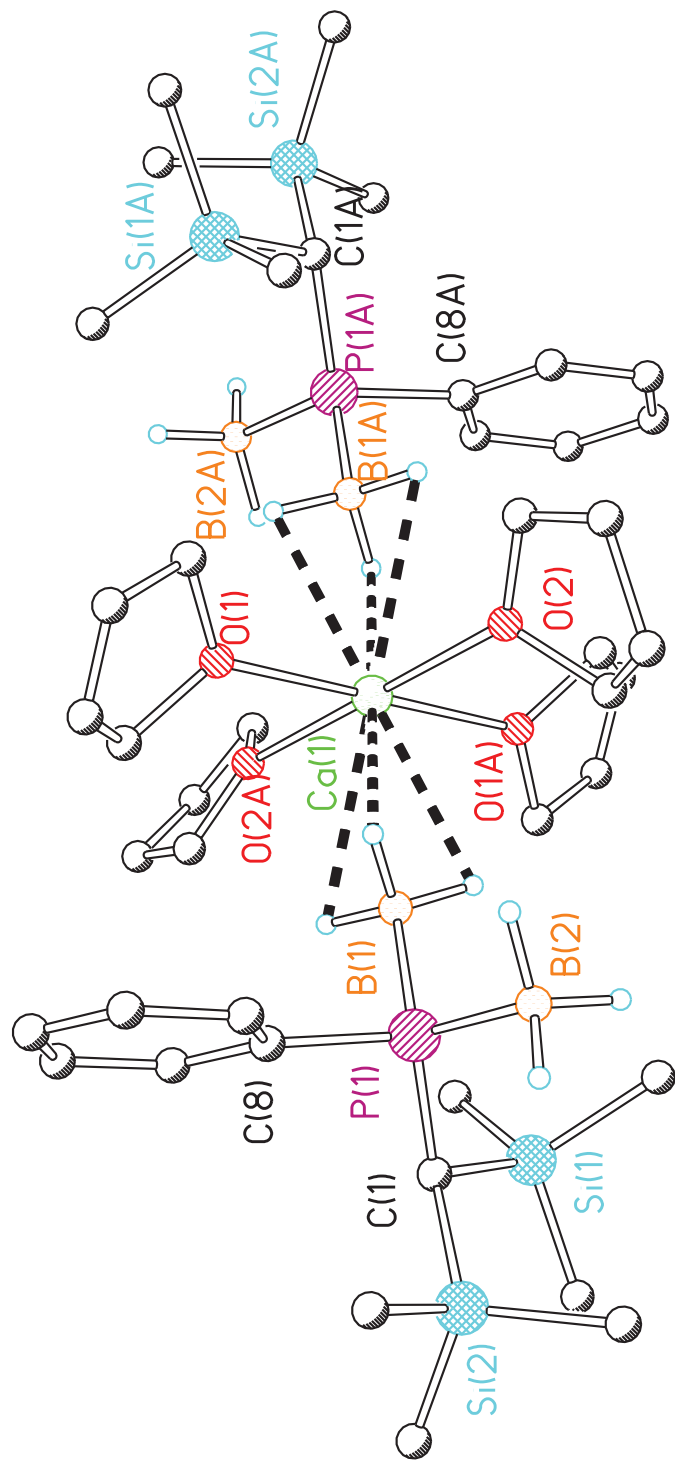


Figure 7.9. Structure of compound **129**. All C-bound H atoms omitted for clarity.

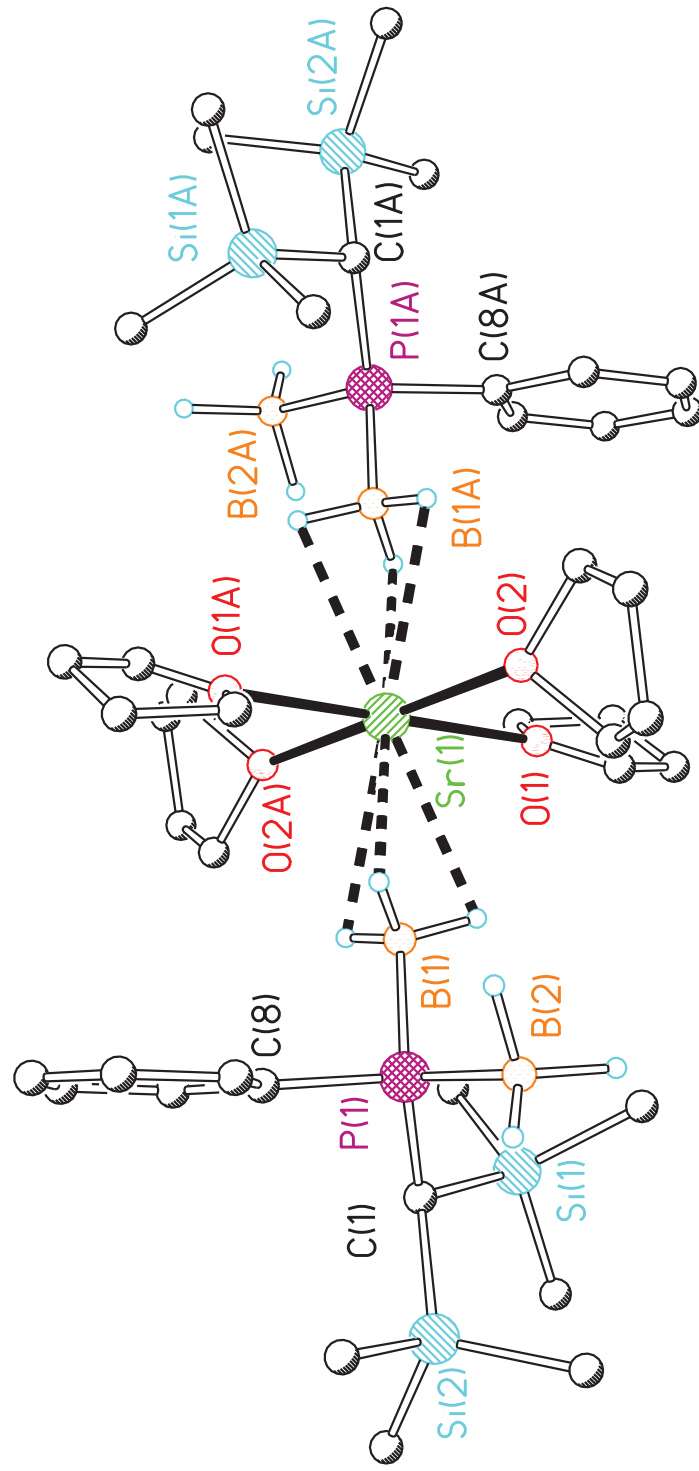


Figure 7.10. Structure of compound **130**. All C-bound H atoms omitted for clarity.

7.7 Conclusions

The alkali metal complexes of the phosphido-bis(borane) [$\{(Me_3Si)_2CH\}P(C_6H_5)(BH_3)_2\}^-$] are prepared using straightforward synthetic techniques. The lithium complex may be crystallised as the 12-crown-4 adduct **123**, which is monomeric in structure and has similar characteristics to the related complex **35**. In contrast to previous reports of phosphido-bis(boranes), the sodium and potassium complexes **124** and **125** are shown to have dimeric and polymeric structures, respectively, in the solid state; where previous reports show that this type of ligand coordinates to the metal ion through only one borane group, in the case of **124** and **125** each ligand is bound to an adjacent metal centre through both BH_3 groups.

Similarly, the sodium complex of the phosphido-(bis)borane [$\{(Me_3Si)_2CH\}P(C_6H_4-2-OMe)(BH_3)_2\}^-$], is easily synthesised and can be crystallised as an adduct with 12-crown-4 (**126**) as a separated ion pair. In comparison to the sodium complex **124**, which crystallises as a tight contact ion pair, there are no significant differences in their structural parameters.

Phosphido-bis(borane) complexes with the alkaline earth metals Mg, Ca and Sr have also been prepared and characterised in the solid state. Complexes **128**, **129** and **130** are isostructural in the solid state, with each metal adopting a pseudo-coordination number of 6; two ligands are bound to the metal centre through BH_3 hydrogen interactions, with coordination completed by four molecules of THF. This is rather surprising, given the markedly different ionic radii of the metal centres. As you move down the series, the P-B distances for the bound borane groups decrease, whilst the P-B distances for the free borane group decrease.

7.7 References

- (1) Thompson, N. R. *Journal of the Chemical Society (Resumed)* **1965**, 6290.
- (2) Keller, P. C.; Schwartz, L. D. *Inorg. Chem.* **1971**, *10*, 645.
- (3) Bertz, S. H.; Gibson, C. P.; Dabbagh, G. *Organometallics* **1988**, *7*, 227.
- (4) Lochmann, L.; Trekoval, J. J. *Organomet. Chem.* **1987**, 326, 1.

- (5) Rudzevich, L. R.; Gornitzka, H.; Romanenko, V. D.; Bertrand, G. *Chem. Commun.* **2001**, 1634.
- (6) Giese, H.-H.; Nöth, H.; Schwenk, H.; Thomas, S. *Eur. J. Inorg. Chem.* **1998**, 941.
- (7) Giese, H.-H.; Habereeder, T.; Nöth, H.; Ponikwar, W.; Thomas, S.; Warchhold, M. *Inorg. Chem.* **1999**, 38, 4188.
- (8) Giese, H.-H.; Habereeder, T.; Knizek, J.; Nöth, H.; Warchhold, M. *Eur. J. Inorg. Chem.* **2001**, 1195.
- (9) Lippert, W.; Nöth, H.; Ponikwar, W.; Seifert, T. *Eur. J. Inorg. Chem.* **1999**, 817.
- (10) Gálvez Ruiz, J. C.; Nöth, H.; Warchhold, M. *Eur. J. Inorg. Chem.* **2008**, 251.
- (11) Dornhaus, F.; Bolte, M.; Lerner, H.-W.; Wagner, M. *Eur. J. Inorg. Chem.* **2006**, 1777.
- (12) Harder, S.; Müller, S.; Hübner, E. *Organometallics* **2003**, 23, 178.
- (13) Crimmin, M. R.; Barrett, A. G. M.; Hill, M. S.; MacDougall, D. J.; Mahon, M. F.; Procopiou, P. A. *Chem.-Eur. J.* **2008**, 14, 11292.
- (14) Kim, D. Y.; Yang, Y.; Abelson, J. R.; Girolami, G. S. *Inorg. Chem.* **2007**, 46, 9060.
- (15) Spielmann, J.; Piesik, D. F. J.; Harder, S. *Chemistry – A European Journal* **2010**, 16, 8307.
- (16) Soloveichik, G.; Her, J.-H.; Stephens, P. W.; Gao, Y.; Rijssenbeek, J.; Andrus, M.; Zhao, J. C. *Inorg. Chem.* **2008**, 47, 4290.
- (17) Power, P. P. *J. Organomet. Chem.* **2004**, 689, 3904.
- (18) Izod, K.; McFarlane, W.; Tyson, B. V.; Clegg, W.; Harrington, R. W.; Liddle, S. T. *Organometallics* **2003**, 22, 3684.

Chapter 8. Conclusions

The work presented in this thesis has explored the effects that varying the metal centre and peripheral donor have on the structure and stabilities of complexes of phosphido-boranes. A series of phosphido-borane and phosphido-bis(borane) complexes with group I and II metals has been isolated, with the majority of these compounds characterised in the solid-state, using X-ray crystallography. This chapter aims to draw comparisons between the structures of these compounds and highlight the trends that have been observed.

8.1 Effects of varying the peripheral donor on group I complexes of phosphido-boranes

The synthesis, isolation and characterisation of group I complexes with phosphido-boranes illustrates the variety of structures these complexes can adopt (Figure 8.1). The structural motifs and aggregation states of these species are highly dependent on a number of factors, including cation size and polarisability, the nature of the peripheral donor, the presence of coligands, and agostic-type $\text{BH}_3 \dots \text{M}$ interactions.

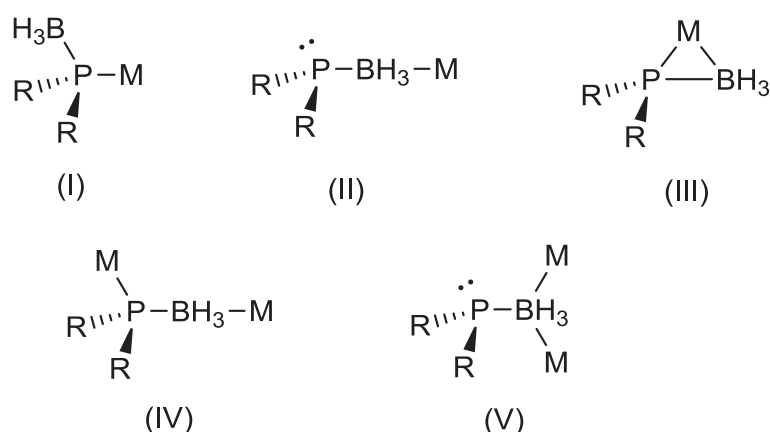


Figure 8.1. Coordination modes adopted by phosphido-boranes.

The P-M distances between lithium, sodium or potassium, and phosphido-borane ligands prepared from either $\{(Me_3Si)_2CH\}PH(C_6H_4-2-CH_2OMe)(BH_3)$ (**39**), $\{(Me_3Si)_2CH\}PH(C_6H_4-2-SMe)(BH_3)$ (**40**) or $\{(Me_3Si)_2CH\}PH(C_6H_5)(BH_3)$ (**42**), are shown in Figure 8.2. The effect of cation size is as expected, with P-M distances increasing with increasing radius of the alkali metal, where $P-Li < P-Na < P-K$. Figure 8.2 also shows that phosphido-boranes prepared from compound **39** possess slightly longer P-M distances compared with the corresponding thioanisole-functionalised phosphido-borane complexes prepared from **40**. Whether this is a result of the nature of the donor atom or the flexibility of the chelate ring is unclear at this time; an X-ray study of $[\{(Me_3Si)_2CH\}P(C_6H_4-2-OMe)(BH_3)Li]$ (**85**) would provide further understanding of this trend, however, due to its poor stability tendency to decompose into **89** and **90**, the isolation of single crystals of **85** for X-ray analysis has proved to be particularly challenging.

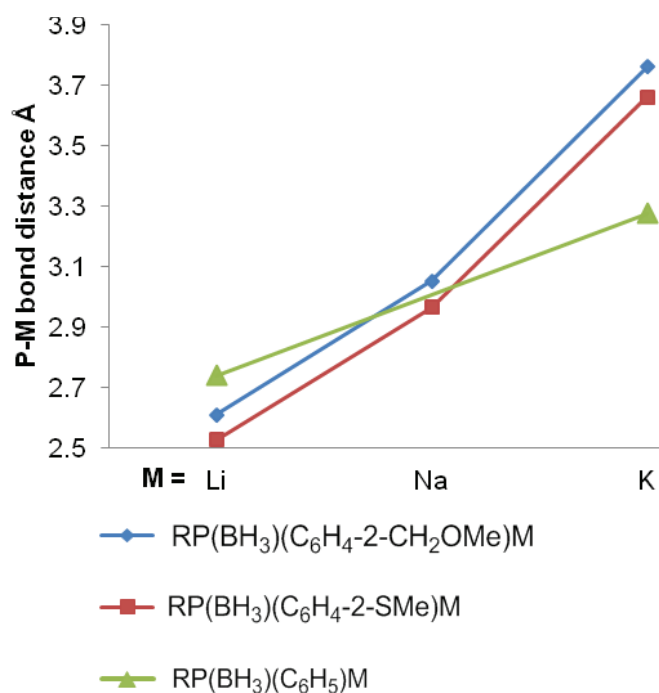


Figure 8.2. P-M distances in selected phosphido-borane complexes [R = (Me₃Si)₂CH].

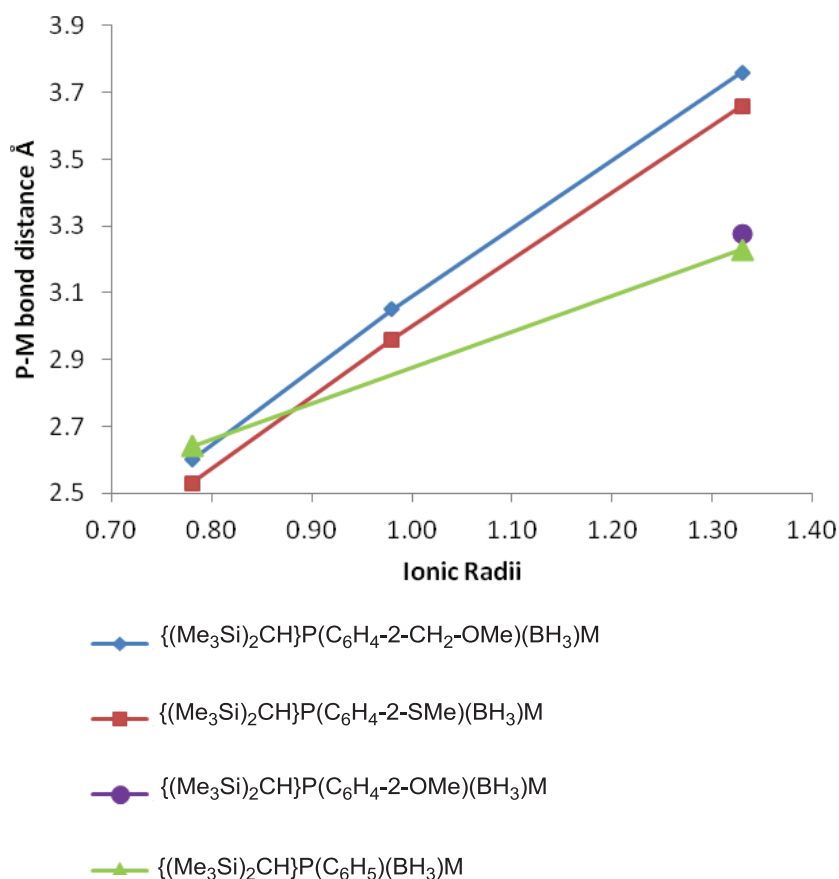


Figure 8.3. Correlation between P-M distance and ionic radii.

Compounds $[\{(\text{Me}_3\text{Si})_2\text{CH}\}\text{P}(\text{C}_6\text{H}_4\text{-2-CH}_2\text{OMe})(\text{BH}_3)\text{K}(\text{pmdeta})]$ (**51**) and $[\{(\text{Me}_3\text{Si})_2\text{CH}\}\text{P}(\text{C}_6\text{H}_4\text{-2-SMe})(\text{BH}_3)\text{K}(\text{pmdeta})]$ (**66**) are the first examples of potassium complexes with phosphido-boranes to be structurally characterised that contain peripheral donor coordination of the metal centre. Figure 8.3 highlights the drastic increase in P-K bond length observed in these two compounds compared to the corresponding distances in the related complexes $[\text{Ph}_2\text{P}(\text{BH}_3)\text{K}(\text{18-crown-6})]$ (**32**), $[\{(\text{Me}_3\text{Si})_2\text{CH}\}\text{P}(\text{C}_6\text{H}_4\text{-2-OMe})(\text{BH}_3)\text{K}(\text{pmdeta})]$ (**87**) and $[\{(\text{Me}_3\text{Si})_2\text{CH}\}\text{P}(\text{C}_6\text{H}_5)\text{K}(\text{pmdeta})]$ (**117**), which do not exhibit intramolecular coordination from a peripheral donor. Interestingly, this trend is not observed for the phosphido-borane complexes with lithium, which possess similar Li-P distances, irrespective of whether the ligand possesses peripheral donor functionality (Figure 8.5).

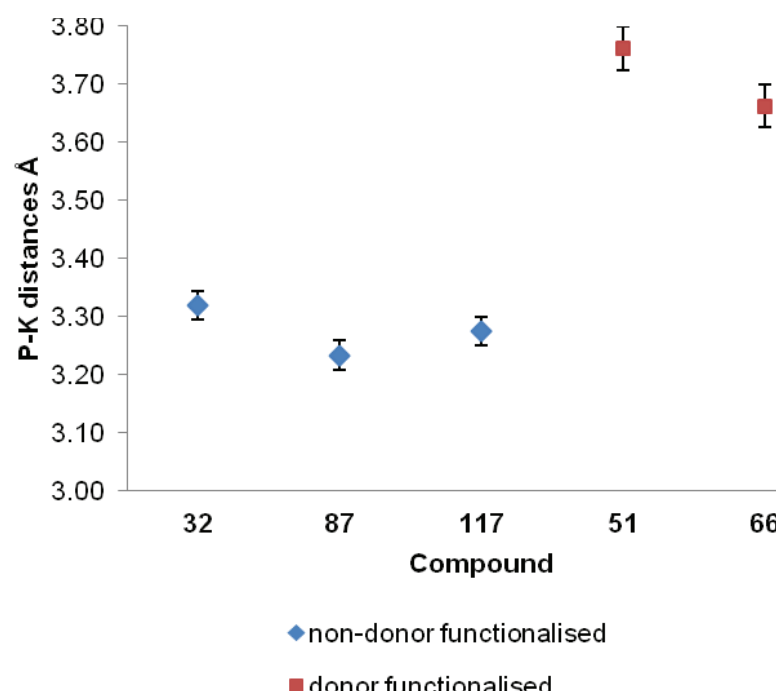


Figure 8.4. P-K distances of phosphido-boranes.

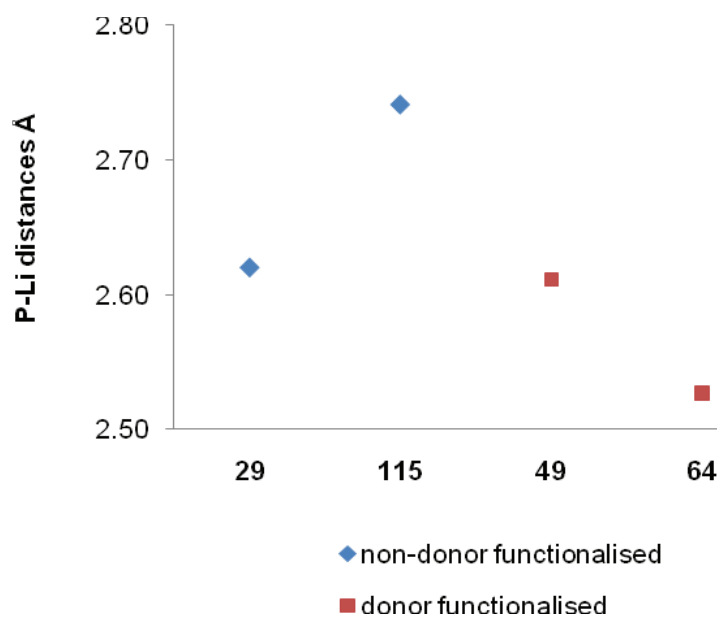


Figure 8.5. P-Li distances of phosphido-boranes.

An important feature of the structures of group I complexes with phosphido-boranes is the coordination mode adopted by the borane group, which provides additional stabilisation through agostic-type B-H-M interactions. The borane group can adopt a range of coordination modes, illustrated by the structures discussed previously. In addition to straightforward η^1 , η^2 or η^3 coordination, the borane group can bridge metal centres in a μ_2 - $\eta^1:\eta^2$, μ_2 - $\eta^1:\eta^3$, μ_2 - $\eta^2:\eta^2$ or μ_2 - $\eta^2:\eta^3$ manner (Figure 8.6).

The B...M distances in phosphido-boranes are expected to vary depending on the size of the metal centre and hapticity of the BH₃ group. It is unsurprising, therefore, that B...M distances increase with increasing radius of the alkali metal and with lower hapticities (Figure 8.7). The M-H distances correlate well with η^1 -, η^2 - and η^3 -BH₃ coordination modes.

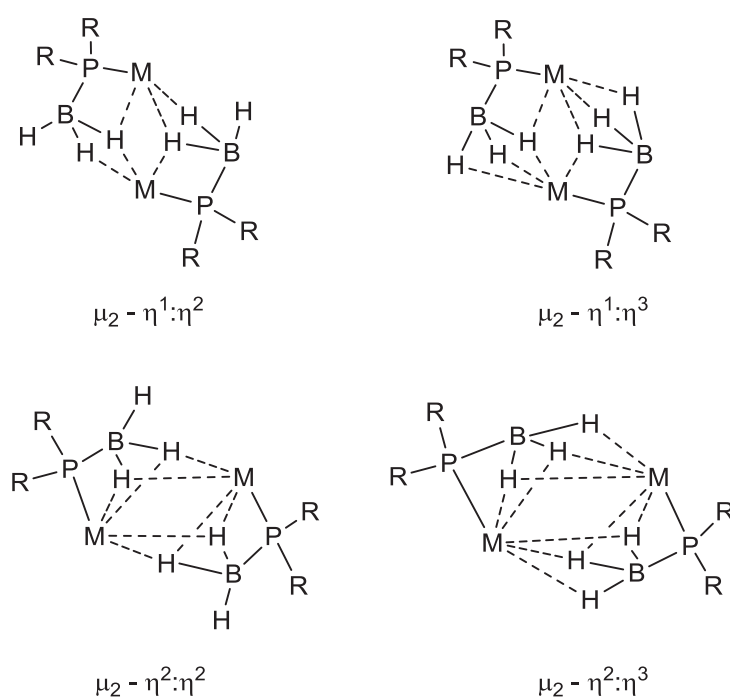
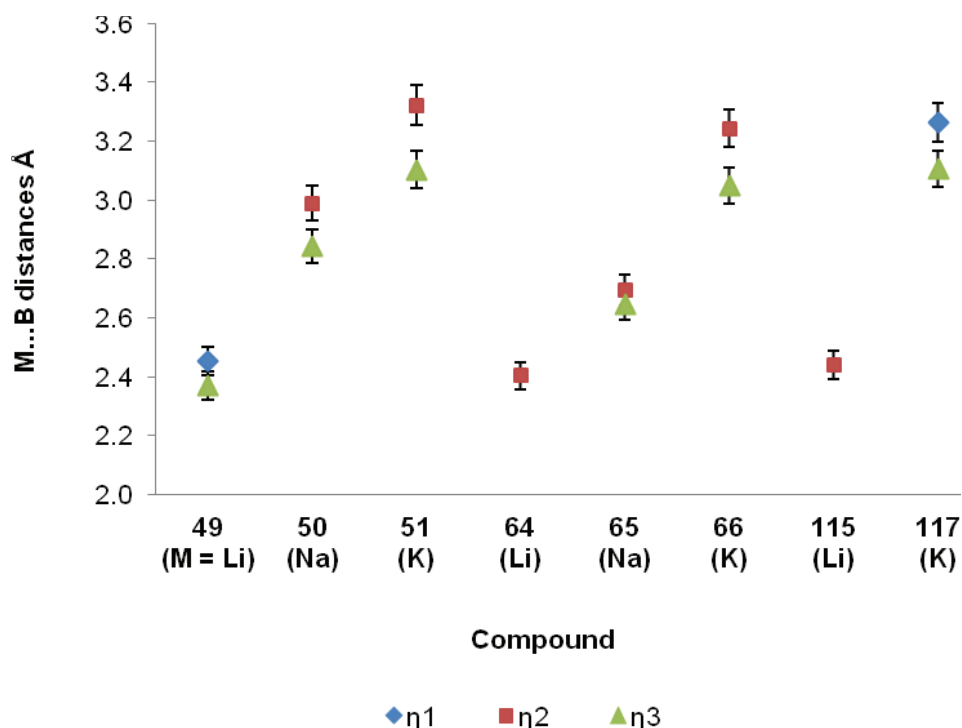


Figure 8.6. Examples of BH₃...M bridging modes.



Numbers Figure 8.7. M...B distances of phosphido-boranes.

Aggregation states are markedly affected by the presence of peripheral donor functionalisation. Whereas the lithium salt $[\{(Me_3Si)_2CH\}P(C_6H_5)(BH_3)Li(THF)_2]$ (**115**) crystallises as a polymer, the donor-functionalised compounds $[\{(Me_3Si)_2CH\}P(C_6H_4-2-CH_2OMe)(BH_3)Li(THF)_2]$ (**49**) and $[\{(Me_3Si)_2CH\}P(C_6H_4-2-SMe)(BH_3)Li(THF)_2]$ (**64**) crystallise as dimers; both of the latter complexes possess a direct P-Li bond and η^2 -type BH_3 -Li coordination. In the absence of a peripheral donor, the lithium ions in **115** adopt a four-coordinate geometry, through an additional molecule of THF; however, as a consequence of removing peripheral functionality, **115** exhibits a larger B-P-Li angle [the B-P-Li angles of **49**, **64** and **115** are $94.28(19)$, $109.30(8)$ and $123.04(8)^\circ$, respectively], which is an important feature of the polymeric structure, confirming that steric bulk is insufficient to stabilise the species in a dimeric state.

The sodium complex $[\{(Me_3Si)_2CH\}P(C_6H_4-2-SMe)(BH_3)Na(tmeda)]$ (**65**), also crystallises as a polymer, whereas the related complex $[\{(Me_3Si)_2CH\}P(C_6H_4-2-CH_2OMe)(BH_3)Na(tmeda)]$ (**50**) crystallises as a dimer. Compounds **65** and **50** (Figure 8.8) are essentially constitutionally identical, except for their donor-functionalities, hence their aggregation states must be attributed to the nature of the chelate ring generated by the

peripheral donor. Compound **50** contains a six-membered chelate ring, and has a Na-P-C(8) angle of $107.31(9)^\circ$ and a P-Na-O bite angle of $76.40(6)^\circ$, whereas **65** has a sulphur-containing five-membered chelate ring, a corresponding Na-P-C(8) angle of $98.10(12)^\circ$ and a P-Na-S bite angle of $62.93(4)^\circ$. As a consequence of these distortions, the B-P-Na angle in **65** is somewhat larger than the corresponding angle in **50** [$118.70(15)$ and $69.21(11)^\circ$, respectively], which may be ascribed to the borane-bridged polymer structure in **65**.

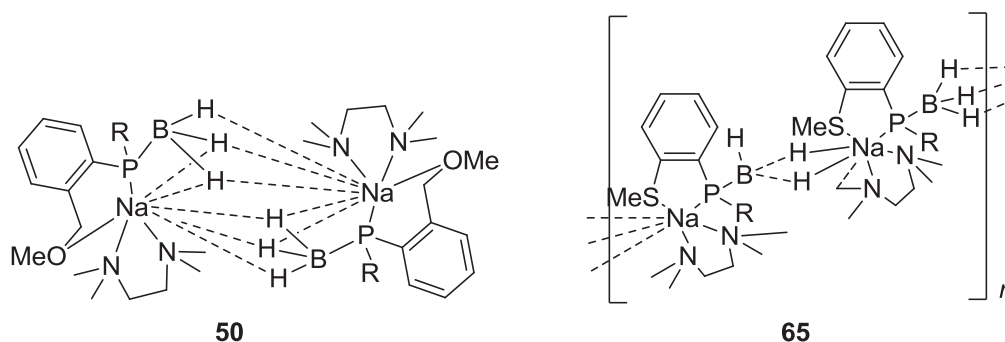


Figure 8.8. Structures of compounds **50** and **65**.

From this result, it may be expected that the potassium complex **66** would also adopt a higher order aggregate than the related compound **51**, which crystallises as a dimer. However, the presence of pmdeta as a co-ligand in **66** provides sufficient coordination about the potassium cation to prevent aggregation beyond a dimer.

A comparison of the sum of angles within the C₂PB framework reveals some interesting trends in the geometry of the phosphorus centre in the phosphine- and phosphido-borane structures (Figure 8.8). The phosphido-borane anions adopt a more pyramidal geometry about phosphorus compared with the corresponding phosphine-boranes, which may be expected, as the metal cations are able to localise negative charge on the phosphorus atom. The geometry about the phosphorus centre is dependent upon the nature of each phosphido-borane structure adopted, however, it is apparent that for each metal cation, the phosphorus anion is more pyramidal in complexes with the ligand [$\{(Me_3Si)_2CH\}P(C_6H_4-2-CH_2OMe)(BH_3)^-$]. The lithium salt [$\{(Me_3Si)_2CH\}P(C_6H_4-2-CH_2OMe)(BH_3)Li(THF)$] (**49**) exhibits the most pyramidal phosphorus centre, although in general, the size of the metal cation does not appear to significantly affect the geometry about the phosphorus atom.

In summary, it appears that there is a fine balance between the formation of dimeric and polymeric structures in these species, which depends on a combination of: the peripheral donor, chelate ring size, the size of the cation, B...M interactions and chelating coligands. The distances between phosphorus and the alkali metal vary with respect to the functionality of the peripheral donor. In particular, P-K distances are substantially longer when the potassium ion is coordinated by a peripheral donor.

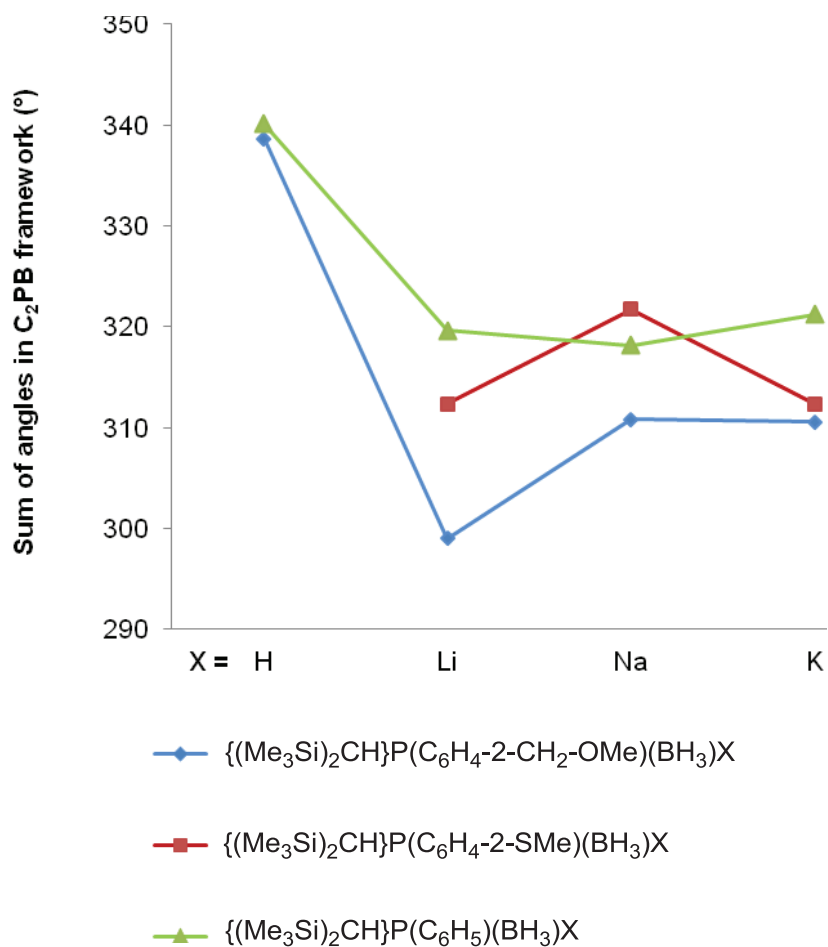


Figure 8.9. Sum of angles about phosphorus atoms with C_2PB frameworks.

8.2 Comparisons between group I complexes of the ligands $[\{(Me_3Si)_2CH\}P(C_6H_5)BH_3]^-$ and $[\{(Me_3Si)_2CH\}P(C_6H_5)(BH_3)_2]^-$

Alkali metal complexes of the ligands $[\{(Me_3Si)_2CH\}P(C_6H_5)(BH_3)]^-$ and $[\{(Me_3Si)_2CH\}P(C_6H_5)(BH_3)_2]^-$ have been prepared from the corresponding phosphine-borane **42**; the coordination modes that have been adopted by these ligands are shown in Figure 8.10.

The complexes of the phosphido-mono(borane) ligand with lithium (**115**) and potassium (**117**), in the presence of THF and pmdeta, respectively, crystallise as tight contact ion pairs, whilst the sodium complex crystallises as a solvent-separated ion pair in the presence of 12-crown-4 (**116**).

Alkali metal complexes of the related phosphido-bis(borane) ligand, **123**, **124** and **125** crystallise as contact ion pairs; the ligand may coordinate to the metal cation through either one or both borane groups, with no direct contact between the formally anionic phosphorus and the alkali metal (VI, VII).

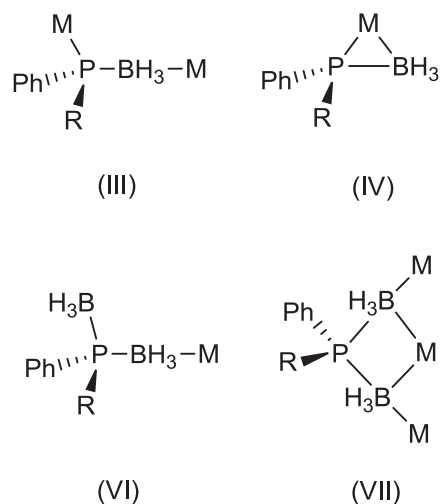


Figure 8.10. Coordination modes adopted by $[RP(C_6H_5)(BH_3)]^-$ and $[RP(C_6H_5)(BH_3)_2]^-$ complexes with alkali metals [R = $(Me_3Si)_2CH$].

A comparison between the phosphido-boranes **115** and **117** and the related phosphido-bis(boranes) **123** and **125** highlights that the additional P-B bond has no effect on the B...M distances between the borane groups and metal cation; the B...Li distances for **115** and **123** are 2.440(3) and 2.281(7) Å, respectively, whilst the B...K distances are 3.262(3) and 3.107(3) Å for **117** and range between 3.131(4) and 3.417(4) Å for **125**. It was observed in compound **123**, that the P-B distance for the boron group engaged in bonding to the lithium ion is slightly shorter than the P-B distance for the 'free' borane group. In general, however, the P-B distances of the phosphido-(bis)borane complexes are very similar, and differences between these and the corresponding P-B distances in the phosphido-borane complexes are negligible.

8.3 Summary

The structures of a number of phosphido-borane and phosphido-bis(borane) complexes with group I and II metals and the trends that are observed have been discussed. As expected, P-M distances in phosphido-complexes with alkali metals increase with increasing size of the metal cation. Varying the peripheral donor has also been shown to have an effect on P-M distances, where complexes of the ligand [$\{(Me_3Si)_2CH\}P(C_6H_4-2-CH_2OMe)(BH_3)]^-$ have longer P-M distances than the corresponding complexes with [$\{(Me_3Si)_2CH\}P(C_6H_4-2-SMe)(BH_3)]^-$.

The structures of phosphido-borane/bis(borane) complexes have been shown to adopt a variety of coordination modes not previously reported. These may be rationalised by considering the charge/size ratio of the metal cations, which affects the hapticity of the borane groups, peripheral functionality, and the nature of co-ligands used.

Chapter 9. Experimental

9.1 General procedure

All manipulations were carried out using standard Schlenk techniques under an atmosphere of dry nitrogen or in a nitrogen filled MBraun dry-box. Diethyl ether, THF, light petroleum (bp 40-60), toluene, benzene and methylcyclohexane were dried prior to use by distillation under nitrogen from sodium, potassium or sodium/potassium alloy as appropriate. *n*-Hexane was distilled under nitrogen from sodium/benzophenone, and hexamethyldisiloxane was distilled under nitrogen from calcium hydride. THF and hexamethyldisiloxane were stored over activated 4Å molecular sieves; all other solvents were stored over a potassium film. Deuterated-THF, -toluene and -benzene were distilled from potassium and deoxygenated by three freeze-pump-thaw cycles and were stored over activated 4Å molecular sieves.

ⁿButyllithium was purchased from Aldrich as a 2.5 M solution in hexanes. Dibutylmagnesium was purchased as a 1.0 M solution in heptanes from Aldrich. The adduct H₃B·SMe₂ was obtained as a 2.0 M solution in THF from Aldrich. Potassium *t*-butoxide and sodium *t*-butoxide were purchased from Lancaster and were heated under vacuum at 100 °C (0.01 mmHg) for 3 h prior to use. All other compounds were used as supplied by the manufacturer, with the exception of tmeda and pmdeta, which were freshly distilled from CaH₂, and 12-crown-4, which was dried over activated 4 Å molecular sieves.

The compounds (Me₃Si)₂CHPCl₂ (**43**),¹ {(Me₃Si)₂CH}PH(C₆H₄-2-SMe) (**45**),² {(Me₃Si)₂CH}PH(C₆H₄-2-OMe) (**46**),³ {(Me₃Si)₂CH}PH(C₆H₅) (**48**),⁴ benzylna⁺,⁵ benzylpotassium,⁶ bis-benzylcalcium⁷ and {(Me₃Si)₂CH}₂Sr⁸ were prepared by previously published procedures.

9.2 NMR Spectroscopy and elemental analyses

¹H and ¹³C{¹H} NMR spectra were recorded on a JEOL Lambda500 spectrometer operating at 500.16 and 125.65 MHz, respectively, or a JEOL ECS400 spectrometer operating at

399.78 and 100.53 MHz, respectively; chemical shifts are quoted in ppm relative to tetramethylsilane. $^{31}\text{P}\{^1\text{H}\}$, $^7\text{Li}\{^1\text{H}\}$ and $^{11}\text{B}\{^1\text{H}\}$ NMR spectra were recorded on a JEOL Lambda500 spectrometer operating at 202.35, 194.25 and 160.35 MHz, respectively; chemical shifts are quoted in ppm relative to external 85% H_3PO_4 , external 0.1 M LiCl, and external $\text{BF}_3(\text{OEt})_2$ respectively. Elemental analyses were obtained by the Elemental Analysis Service of London Metropolitan University.

9.3 Crystal structure determinations

Measurements were made at 150 K on either a Bruker AXS SMART, a Nonius KappaCCD or an Oxford Diffraction Gemini A Ultra diffractometer using either graphite-monochromated $\text{MoK}\alpha$ or $\text{CuK}\alpha$ radiation ($\lambda = 0.71073$ and 1.54184 Å, respectively). Cell parameters were refined from the observed positions of all strong reflections. Intensities were corrected semi-empirically for absorption, based on symmetry-equivalent and repeated reflections. The structures were solved by direct methods and refined on F^2 values for all unique data. All non-hydrogen atoms were refined anisotropically, H atoms bonded to boron were freely refined isotropically and the remaining H atoms were constrained with a riding model; $U(\text{H})$ was set at 1.2 (1.5 for methyl groups) times U_{eq} for the parent atom. Programmes were Oxford Diffraction CrysAlisPro Bruker AXS SMART and SAINT or Nonius COLLECT and EvalCCD, and SHELXTL for structure solution, refinement, and molecular graphics.^{9,10,11}

9.4 Preparative methods

$\{(\text{Me}_3\text{Si})_2\text{CH}\}\text{PH}(\text{C}_6\text{H}_4\text{-2-CH}_2\text{OMe})(\text{BH}_3)$ (**39**):

To a cold (0 °C) solution of 2- $\text{BrC}_6\text{H}_4\text{CH}_2\text{OMe}$ (2.39 g, 11.9 mmol) was added one equivalent of $^n\text{BuLi}$ (4.8 mL of a 2.5 M solution in hexane, 11.9 mmol). The reaction was stirred for 2 h at 0 °C, then added *in situ* to a cold -78 °C solution of **43** (2.85 g, 11.0 mmol) in THF (30 mL). The mixture was stirred for 16 h and allowed to reach room temperature. Solid LiAlH_4 (0.41 g, 11.0 mmol) was carefully added, and the reaction mixture was stirred

under reflux for 2 h. The reaction mixture was allowed to cool to room temperature, and excess LiAlH_4 was quenched by the careful addition of deoxygenated water (30 mL). The organic layer was decanted, and the aqueous layer was extracted into Et_2O (3 x 20 mL). The combined organic extracts were dried over 4\AA molecular sieves, the solution was filtered, and the solvent was removed *in vacuo* from the filtrate to give $\{(\text{Me}_3\text{Si})_2\text{CH}\}\text{PH}(\text{C}_6\text{H}_4\text{-2-CH}_2\text{OMe})$ **44** as a colourless oil. Isolated yield: 2.62 g, 76%.

To a solution of **44** (4.62 g, 14.88 mmol) in THF (20 mL) was added $\text{BH}_3\cdot\text{SMe}_2$ (7.4 mL of a 2.0 M solution in THF, 14.80 mmol). After one hour stirring the solvent was removed *in vacuo* to yield a white solid. The product was dissolved in hot petroleum-ether 40-60 (10 mL) and crystallised upon cooling. Isolated yield: 2.91 g, 60%. $^1\text{H}\{^{11}\text{B}\}$ NMR (CDCl_3 , 25 °C): δ -0.04 (s, 9H, SiMe_3), 0.29 (s, 9H, SiMe_3), 0.89 (dd, $^1J_{\text{PH}} = 13.8$ Hz, $^3J_{\text{HH}} = 6.4$ Hz, 3H, BH_3), 1.14 (d, $J_{\text{PH}} = 20.2$ Hz, 1H, CH), 3.41 (s, OMe), 4.48 (d, $J_{\text{HH}} = 11.9$ Hz, 1H, CH_2), 4.65 (d, $J_{\text{HH}} = 11.5$ Hz, 1H, CH_2), 5.97 (dq, $^1J_{\text{PH}} = 375.5$ Hz, $^3J_{\text{HH}} = 6.4$ Hz, $^3J_{\text{HH}} = 4.0$ Hz, 1H, PH), 7.41 (m, 2H, ArH), 7.46 (d, $J_{\text{HH}} = 9.2$ Hz, 1H, ArH), 8.05 (dd, $J_{\text{HH}} = 13.7$ Hz, $J_{\text{HH}} = 7.8$ Hz, 1H, ArH). $^{13}\text{C}\{^1\text{H}\}$ NMR (CDCl_3 , 25 °C): δ 1.52 (d, $^3J_{\text{PC}} = 2.9$ Hz, SiMe_3), 2.29 (d, $^3J_{\text{PC}} = 2.9$ Hz, SiMe_3), 8.85 (d, $^1J_{\text{PC}} = 1.9$ Hz, CHP), 58.22 (OMe), 73.47 (CH_2), 128.43 (d, $J_{\text{PC}} = 13.4$ Hz, ArC), 128.97 (d, $J_{\text{PC}} = 47.0$ Hz, ArC), 130.37 (d, $J_{\text{PC}} = 6.7$ Hz, ArC), 131.58 (d, $J_{\text{PC}} = 1.9$ Hz, ArC), 135.83 (d, $J_{\text{PC}} = 18.2$ Hz, ArC), 140.37 (ArC). $^{11}\text{B}\{^1\text{H}\}$ NMR (CDCl_3 , 25 °C): δ -39.8 (d, br, $^1J_{\text{PB}} = 49.0$ Hz). $^{31}\text{P}\{^1\text{H}\}$ NMR (CDCl_3 , 25 °C): δ -16.2 (q, broad, $^1J_{\text{PB}} = 49.0$ Hz).

$\{(\text{Me}_3\text{Si})_2\text{CH}\}\text{PH}(\text{C}_6\text{H}_4\text{-2-SMe})(\text{BH}_3)$ (**40**):

To a solution of **45** (6.64 g, 21.11 mmol) in THF (20 mL) was added $\text{BH}_3\cdot\text{SMe}_2$ (10.6 mL of a 2.0 M solution in THF, 21.20 mmol). After one hour stirring the solvent was removed *in vacuo* to yield an off-white oil. The product was dissolved in *n*-hexane and crystallised upon cooling (-30 °C). The product was then washed with petrol (3 x 10 mL) and dried *in vacuo*, to give a white powder. Isolated crystalline yield: 7.22 g, 83%. $^1\text{H}\{^{11}\text{B}\}$ NMR (CDCl_3 , 25 °C): δ -0.06 (s, 9H, SiMe_3), 0.32 (s, 9H, SiMe_3), 0.92 (dd, $^2J_{\text{PH}} = 14.9$ Hz, $^3J_{\text{HH}} = 6.5$ Hz, 3H, BH_3), 1.46 (dd, $^2J_{\text{PH}} = 20.6$ Hz, $^3J_{\text{HH}} = 2.8$ Hz, 1H, CHP), 2.56 (s, 3H, SMe), 6.04 (dq, $^1J_{\text{PH}} = 375.2$ Hz, $^3J_{\text{HH}} = 6.5$ Hz, $^3J_{\text{HH}} = 2.8$ Hz, 1H, PH), 7.24 (t, $J_{\text{HH}} = 7.8$ Hz, 1H, ArH), 7.29 (d, $J_{\text{HH}} = 6.9$ Hz, 1H, ArH), 7.46 (t, $J_{\text{HH}} = 7.6$ Hz, 1H, ArH), 8.02 (dd, $J_{\text{HH}} = 13.8$ Hz, $J_{\text{HH}} = 6.0$ Hz,

1H, ArH). $^{13}\text{C}\{^1\text{H}\}$ NMR (CDCl_3 , 25 °C): δ 1.53 (d, $^3J_{\text{PC}} = 3.8$ Hz, SiMe_3), 2.18 (d, $^3J_{\text{PC}} = 2.8$ Hz, SiMe_3), 6.34 (CHP), 16.59 (SMe), 125.25 (d, $J_{\text{PC}} = 12.5$ Hz, ArC), 126.02 (d, $J = 4.8$ Hz, ArC), 127.51 (d, $J_{\text{PC}} = 49.8$ Hz, ArC), 132.08 (d, $J_{\text{PC}} = 1.9$ Hz, ArC), 136.14 (d, $^2J_{\text{PC}} = 18.2$ Hz, ArC), 143.08 (ArC). $^{11}\text{B}\{^1\text{H}\}$ NMR (CDCl_3 , 25 °C): δ -40.1 (d, br, $^1J_{\text{BP}} = 49.0$ Hz). ^{31}P NMR (CDCl_3 , 25 °C): δ -15.7 (dq, br, $^1J_{\text{PH}} = 375.2$ Hz, $^1J_{\text{PB}} = 49.0$ Hz).

$\{(\text{Me}_3\text{Si})_2\text{CH}\}\text{PH}(\text{C}_6\text{H}_4\text{-2-OMe})(\text{BH}_3)$ (41):

To a solution of **46** (6.55 g, 21.94 mmol) in THF (20 mL) was added $\text{BH}_3\cdot\text{SMe}_2$ (11.0 mL of a 2.0 M solution in THF, 22.0 mmol). After one hour stirring the solvent was removed *in vacuo* to yield a white solid. The product was dissolved in *n*-hexane (20 mL) and THF (1 mL) with heating, and crystallised upon cooling (-30 °C). Isolated yield: 5.00 g, 73%. $^1\text{H}\{^{11}\text{B}\}$ NMR (CDCl_3 , 25 °C): δ -0.01 (s, 9H, SiMe_3), 0.29 (s, 9H, SiMe_3), 0.89 (dd, $^2J_{\text{PH}} = 14.9$ Hz, $^3J_{\text{HH}} = 6.6$ Hz, 3H, BH_3), 1.08 (d, $J_{\text{PH}} = 20.2$ Hz, 1H, CHP), 3.90 (s, 3H OMe), 5.86 (dq, $J_{\text{PH}} = 384.0$ Hz, $^3J_{\text{HH}} = 6.6$ Hz, $^3J_{\text{HH}} = 1.4$ Hz, 1H, PH), 6.90 (dd, $^1J_{\text{HH}} = 7.6$ Hz, $^2J_{\text{HH}} = 2.5$ Hz, 1H, ArH), 7.06 (t, $J_{\text{HH}} = 7.3$ Hz, 1H, ArH), 7.48 (t, $J_{\text{HH}} = 7.8$ Hz, 1H, ArH), 7.92 (dd, $^1J_{\text{HH}} = 13.1$ Hz, $^2J_{\text{HH}} = 7.6$ Hz, 1H, ArH). $^{13}\text{C}\{^1\text{H}\}$ NMR (CDCl_3 , 25 °C): δ 1.25 (d, $^3J_{\text{PC}} = 3.8$ Hz, SiMe_3), 2.11 (d, $^3J_{\text{PC}} = 2.8$ Hz, SiMe_3), 6.51 (d, $^1J_{\text{PC}} = 4.8$ Hz, CHP), 55.54 (OMe), 110.28 (d, $J_{\text{PC}} = 3.8$ Hz, ArC), 116.87 (d, $J_{\text{PC}} = 50.8$ Hz, ArC), 121.05 (d, $J_{\text{PC}} = 12.5$ Hz, ArC), 133.50 (ArC), 136.19 (d, $^2J_{\text{PC}} = 15.3$ Hz, ArC), 160.78 (ArC). $^{11}\text{B}\{^1\text{H}\}$ NMR (CDCl_3 , 25 °C): δ -40.6 (d, br, $^1J_{\text{PB}} = 49.0$ Hz). $^{31}\text{P}\{^1\text{H}\}$ NMR (CDCl_3 , 25 °C): δ -22.3 (q, br, $^1J_{\text{PB}} = 49.0$ Hz).

$\{(\text{Me}_3\text{Si})_2\text{CH}\}\text{PH}(\text{C}_6\text{H}_5)(\text{BH}_3)$ (42):

To a solution of **48** (9.78 g, 36.43 mmol) in THF (20 mL) was added $\text{BH}_3\cdot\text{SMe}_2$ (18.2 mL of a 2.0 M solution in THF, 36.40 mmol). After one hour stirring the solvent was removed *in vacuo* to yield a white solid. THF was added to a solution of **42** in methylcyclohexane (20 mL), until the product dissolved. Compound **42** was then crystallised upon cooling to -30 °C. Isolated yield: 8.89 g, 63%. $^1\text{H}\{^{11}\text{B}\}$ NMR (CDCl_3 , 25 °C): δ 0.36 (s, 9H, SiMe_3), 0.29 (s, 9H, SiMe_3), 0.76 (d, $J_{\text{PH}} = 19.3$ Hz, 1H, CHP), 0.94 (dd, $^1J_{\text{PH}} = 15.3$ Hz, $^3J_{\text{HH}} = 6.4$ Hz, 3H, BH_3), 5.72 (dq, $^1J_{\text{PH}} = 368.9$ Hz, $^3J_{\text{HH}} = 6.4$ Hz, 1H, PH), 7.46 (m, 3H, ArH), 0.77 (dd, $J_{\text{HH}} = 11.2$

Hz, $J_{\text{HH}} = 7.1$ Hz, 2H, ArH). $^{13}\text{C}\{^1\text{H}\}$ NMR (CDCl_3 , 25 °C): δ 1.26 (d, $^3J_{\text{PC}} = 2.9$ Hz, SiMe_3), 2.10 (d, $^3J_{\text{PC}} = 2.9$ Hz, SiMe_3), 9.41 (d, $^1J_{\text{PC}} = 2.9$ Hz, CHP), 128.81 (d, $J_{\text{PC}} = 10.5$ Hz, ArC), 129.21 (d, $J_{\text{PC}} = 51.8$ Hz, ArC), 131.29 (d, $J_{\text{PC}} = 2.9$ Hz, ArC), 133.16 (d, $J_{\text{PC}} = 9.6$ Hz, ArC). $^{11}\text{B}\{^1\text{H}\}$ NMR (CDCl_3 , 25 °C): δ -40.6 (d, br, $^1J_{\text{PB}} = 49.0$ Hz). $^{31}\text{P}\{^1\text{H}\}$ NMR (CDCl_3 , 25 °C): δ -8.6 (q, br, $^1J_{\text{PB}} = 49.0$ Hz).

$\{[(\text{Me}_3\text{Si})_2\text{CH}]_2\text{P}(\text{C}_6\text{H}_4\text{-2-CH}_2\text{OMe})(\text{BH}_3)\text{Li}(\text{THF})\}_2$ (49):

To a solution of **39** (0.41 g, 1.26 mmol) in THF (15 mL) was added $n\text{BuLi}$ (0.5 mL of a 2.5 M solution in hexane, 1.25 mmol). After 1 h stirring the solvent was removed *in vacuo* to yield an off-white solid. THF was added to a solution of **39** in methylcyclohexane until the product had dissolved. Upon cooling (-30 °C) colourless crystals suitable for X-ray crystallography were deposited. Isolated crystalline yield: 0.06g, 18%. Anal. Calcd for $\{[(\text{Me}_3\text{Si})_2\text{CH}]_2\text{P}(\text{C}_6\text{H}_4\text{-2-CH}_2\text{OMe})(\text{BH}_3)\text{Li}(\text{THF})\}_2$: C 56.43, H 9.72%. Found C 56.29, H 9.62%. $^1\text{H}\{^{11}\text{B}\}$ NMR (d_8 -THF, 25 °C): δ -0.05 (s, 9H, SiMe_3), 0.25 (s, 9H, SiMe_3), 0.75 (d, $^2J_{\text{PH}} = 16.0$ Hz, 1H, CHP), 0.83 (d, $^2J_{\text{PH}} = 14.7$ Hz, 3H, BH_3), 1.69 (m, 4H, THF), 3.54 (m, 4H, THF), 3.38 (s, 3H, OMe), 4.82 (d, $J_{\text{HH}} = 11.5$ Hz, 1H, CH_2), 5.12 (d, $J_{\text{HH}} = 11.5$ Hz, 1H, CH_2), 7.14 (t, $J_{\text{HH}} = 7.1$ Hz, 1H, ArH), 7.20 (t, $J_{\text{HH}} = 7.3$ Hz, 1H, ArH), 7.33 (d, $J_{\text{HH}} = 7.3$ Hz, 1H, ArH), 8.08 (d, $J_{\text{HH}} = 7.6$ Hz, 1H, ArH). $^{13}\text{C}\{^1\text{H}\}$ NMR (d_8 -THF, 25 °C): δ 1.98 (SiMe_3), 3.23 (SiMe_3), 25.44 (THF), 57.08 (OMe), 67.28 (THF), 72.80 (CH_2), 125.84 (ArC), 127.83 (ArC), 129.02 (d, $J_{\text{PC}} = 5.8$ Hz, ArC), 133.74 (d, $J_{\text{PC}} = 17.3$ Hz, ArC), 139.54 (ArC), 145.90 (d, $J_{\text{PC}} = 37.4$ Hz). $^{11}\text{B}\{^1\text{H}\}$ NMR (d_8 -THF, 25 °C): δ -31.4 (d, br, $^1J_{\text{BP}} = 37.2$ Hz). $^{31}\text{P}\{^1\text{H}\}$ NMR (d_8 -THF, 25 °C): δ -66.6 (q, br, $^1J_{\text{PB}} = 37.2$ Hz). $^7\text{Li}\{^1\text{H}\}$ NMR (d_8 -THF, 25 °C): δ -0.7.

$\{[(\text{Me}_3\text{Si})_2\text{CH}]_2\text{P}(\text{C}_6\text{H}_4\text{-2-CH}_2\text{OMe})(\text{BH}_3)\text{Na}(\text{tmeda})\}_2$ (50):

To a solution of **39** (0.37 g, 1.14 mmol) in THF (15 mL) was added a solution of benzylna (0.13 g, 1.14 mmol) in THF (15 mL). After 1 h stirring the solvent was removed *in vacuo* to yield an off-white solid. The product was dissolved in the minimal amount of toluene containing tmeda (0.2 mL, 1.14 mmol). The solvent was then carefully reduced *in vacuo* until the product began to precipitate slightly. The solution was allowed to

warm to room temperature, dissolving the product, and upon cooling (-30 °C) colourless crystals of **50** suitable for X-ray crystallography were deposited. Isolated crystalline yield: 0.46 g, 43%. Anal. Calcd for $[\{(Me_3Si)_2CH\}P(C_6H_4-2-CH_2OMe)(BH_3)Na(tmeda)]_2$: C 54.29, H 10.20, N 6.03%. Found C 54.14, H 10.16, N 5.93%. $^1H\{^{11}B\}$ NMR (d_8 -THF, 25 °C): δ -0.02 (s, 9H, SiMe₃), 0.06 (s, 9H, SiMe₃), 0.40 (s, 1H, CHP), 0.62 (d, $^2J_{PH} = 5.5$ Hz, 3H, BH₃), 3.31 (s, 3H, OMe), 4.61 (d, $J_{HH} = 12.4$ Hz, 1H, CH₂), 4.92 (d, $J_{HH} = 12.4$ Hz, 1H, CH₂), 6.90 (t, $J = 7.1$ Hz, 1H, ArH), 6.95 (t, $J = 7.3$ Hz, 1H, ArH), 7.18 (d, $J = 5.5$ Hz, 1H, ArH), 7.68 (dd, $J_{HH} = 7.1$ Hz, $J_{HH} = 3.4$ Hz, 1H, ArH). $^{13}C\{^1H\}$ NMR (d_8 -THF, 25 °C): δ 1.27 (d, $^1J_{PC} = 6.7$ Hz, SiMe₃), 2.88 (SiMe₃), 8.01 (d, $^1J_{PC} = 47.9$ Hz, CHP), 42.29 (NMe₂), 56.86 (OMe), 57.95 (NCH₂), 73.52 (d, $J = 32.6$ Hz, CH₂), 123.34 (ArC), 125.19 (ArC), 125.81 (d, $^2J_{PC} = 3.8$ Hz, ArC), 132.30 (ArC), 139.88 (d, $^2J_{PC} = 18.2$ Hz, ArC), 151.69 (d, $^1J_{PC} = 32.6$ Hz). $^{11}B\{^1H\}$ NMR (d_8 -THF, 25 °C): δ -31.9 (d, br, $^1J_{BP} = 29.4$ Hz). $^{31}P\{^1H\}$ NMR (d_8 -THF, 25 °C): δ -65.3 (d, br, $^1J_{PB} = 29.4$ Hz).

$[\{(Me_3Si)_2CH\}P(C_6H_4-2-CH_2OMe)(BH_3)K(pmdeta)]_2$ (51**):**

To a solution of **39** (0.39 g, 1.20 mmol) in THF (15 mL) was added a solution of benzylpotassium (157 mg, 1.20 mmol) in THF (10 mL). After 1 h stirring the solvent was removed *in vacuo*, yielding an orange powder. The product was dissolved in toluene upon addition of pmdeta (0.3 mL, 1.44 mmol). The solvent was then carefully reduced *in vacuo* until the product began to precipitate slightly. The solution was allowed to warm to room temperature, dissolving the product, and upon cooling (-30 °C) colourless crystals of **51** suitable for X-ray crystallography were deposited. Isolated crystalline yield: 0.25 g, 39%. Anal. Calcd for $[\{(Me_3Si)_2CH\}P(C_6H_4-2-CH_2OMe)(BH_3)K(pmdeta)]_2$: C 53.60, H 10.12, N 7.81%. Found C 53.48, H 10.24, N 7.81%. $^1H\{^{11}B\}$ NMR (d_8 -THF, 25 °C): δ -0.07 (s, 9H, SiMe₃), 0.09 (s, 9H, SiMe₃), 0.43 (s, 1H, CHP), 0.68 (d, $^2J_{PH} = 5.0$ Hz, 3H, BH₃), 2.15 (s, 12H, NMe₂), 2.19 (s, 3H, NMe), 2.31 (m, 4H, CH₂N), 2.41 (m, 4H, CH₂N), 3.29 (s, 3H, OMe), 4.53 (d, $J_{HH} = 11.9$ Hz, 1H, CH₂), 5.00 (d, $J_{HH} = 11.9$ Hz, 1H, CH₂), 6.92 (t, $J = 7.3$ Hz, 1H, ArH), 6.98 (t, $J = 7.3$ Hz, 1H, ArH), 7.17 (d, $J = 6.9$ Hz, 1H, ArH), 7.71 (d, $J = 4.6$ Hz, 1H, ArH). $^{13}C\{^1H\}$ NMR (d_8 -THF, 25 °C): δ 2.86 (SiMe₃), 8.26 (d, $^1J_{PC} = 49.8$ Hz, CHP), 42.32 (NMe), 45.27 (NMe₂), 56.40 (NCH₂), 56.69 (OMe), 57.86 (NCH₂), 73.48 (d, $J_{PC} = 24.0$ Hz, CH₂), 123.28 (ArC), 125.38 (ArC), 126.17 (d, $J_{PC} = 2.9$ Hz, ArC), 132.41 (ArC),

139.78 (d, $J_{PC} = 18.2$ Hz, ArC), 152.93 (d, $J_{PC} = 32.6$ Hz, ArC). $^{11}\text{B}\{^1\text{H}\}$ NMR (d_8 -THF, 25 °C): δ -29.2 (d, br, $^1J_{BP} = 19.6$ Hz). $^{31}\text{P}\{^1\text{H}\}$ NMR (d_8 -THF, 25 °C): δ -64.2 (d, br, $^1J_{PB} = 19.6$ Hz).

[{(Me₃Si)₂CH}P(BH₃)(C₆H₄-2-SMe)Li(THF)]₂ (64):

To a solution of **40** (0.47 g, 1.43 mmol) in diethyl ether (15 mL) was added *n*-BuLi (0.7 mL of a 2.5 M solution in hexanes, 1.75 mmol) and this mixture was stirred at room temperature for 1 h. Solvent was removed *in vacuo* to yield a white powder, which was crystallized from cold (5 °C) toluene (5 mL) containing a few drops of THF, to yield **64** as colourless blocks suitable for X-ray crystallography. Crude yield: 0.48 g, 100%. Anal. Calcd. For [(Me₃Si)₂CH}P(BH₃)(C₆H₄-2-SMe)Li(THF)]₂: C 50.29, H 8.74%. Found C 50.40, H 8.65%. ^1H NMR (d_8 -THF, 25 °C): δ -0.03 (s, 9H, SiMe₃), 0.07 (s, 9H, SiMe₃), 0.59 (q, $J_{BH} = 87.0$ Hz, 3H, BH₃), 0.85 (s, 1H, CHP), 1.77 (m, 4H, THF), 2.32 (s, 3H, SMe), 3.62 (m, 4H, THF), 6.80 (m, 1H, ArH), 6.91 (m, 2H, ArH), 7.76 (d, $J_{HH} = 7.3$ Hz, 1H, ArH). $^{13}\text{C}\{^1\text{H}\}$ NMR (d_8 -THF, 25 °C): δ 1.50 (d, $^3J_{PC} = 6.7$ Hz, SiMe₃), 2.88 (SiMe₃), 7.52 (d, $^1J_{PC} = 48.0$ Hz, CHP), 15.05 (d, $^4J_{PC} = 13.4$ Hz, SMe), 122.28 (ArC), 122.52 (ArC), 124.68 (ArC), 133.51 (ArC), 143.35 (d, $^2J_{PC} = 24.0$ Hz, ArC), 149.95 (d, $^1J_{PC} = 32.6$ Hz, ArC). $^{11}\text{B}\{^1\text{H}\}$ NMR (d_8 -THF, 25 °C): δ -32.9 (d, br, $^1J_{BP} = 39.2$ Hz). $^{31}\text{P}\{^1\text{H}\}$ NMR (d_8 -THF, 25 °C): δ -59.5 (q, br, $^1J_{PB} = 39.2$ Hz). ^7Li NMR (d_8 -THF, 25 °C): δ 2.3.

[{(Me₃Si)₂CH}P(BH₃)(C₆H₄-2-SMe)Na(tmeda)]_∞ (65):

To a solution of **40** (0.48 g, 1.46 mmol) in Et₂O (15 mL) was added a solution of benzylsodium (167 mg, 1.46 mmol) in Et₂O (15 mL). After stirring at room temperature for 1 h the solvent was removed *in vacuo*, yielding a yellow powder. This powder was dissolved in toluene (5 mL) and tmeda (0.20 mL, 1.33 mmol). The solvent was then carefully reduced *in vacuo* until the product began to precipitate slightly. The solution was then allowed to warm to room temperature, dissolving the product, and upon cooling to 5 °C colourless crystals of **65** suitable for X-ray crystallography were deposited. Crude yield: 0.48 g, 94%. Anal. Calcd. For [(Me₃Si)₂CH}P(BH₃)(C₆H₄-2-SMe)Na(tmeda)]_∞: C 51.48, H 9.72%

Found C 51.38, H 9.76%. $^1\text{H}\{^{11}\text{B}\}$ NMR (d_8 -THF, 25 °C): δ -0.05 (s, 9H, SiMe₃), 0.11 (s, 9H, SiMe₃), 0.72 (d, $^2J_{\text{PH}} = 6.9$ Hz, 3H, BH₃), 0.87 (d, $^2J_{\text{PH}} = 5.5$ Hz, 1H, CHP), 2.15 (s, 12H, NMe₂), 2.30 (s, 4H, NCH₂), 2.33 (s, 3H, SMe), 6.84 (t, $J_{\text{HH}} = 7.1$ Hz, 1H, ArH), 6.92 (d, $J_{\text{HH}} = 8.3$ Hz, 1H, ArH), 6.96 (t, $J_{\text{HH}} = 6.7$ Hz, 1H, ArH), 7.84 (d, $J_{\text{HH}} = 7.3$ Hz, 1H, ArH). $^{13}\text{C}\{^1\text{H}\}$ NMR (d_8 -THF, 25 °C): δ 1.60 (d, $^3J_{\text{PC}} = 6.7$ Hz, SiMe₃), 2.90 (s, SiMe₃), 6.94 (d, $^1J_{\text{PC}} = 43.2$ Hz, CHP), 14.85 (d, $^4J_{\text{PC}} = 10.6$ Hz, SMe), 46.20 (NMe), 58.90 (NCH₂), 123.57 (d, $^2J_{\text{PC}} = 3.7$ Hz, ArC), 124.04, 125.88, 132.72, 134.86 (ArC), 143.45 (d, $^1J_{\text{PC}} = 22.6$ Hz, ArC). $^{11}\text{B}\{^1\text{H}\}$ NMR (d_8 -THF, 25 °C): δ -33.5 (d, br, $^1J_{\text{BP}} = 29.4$ Hz). $^{31}\text{P}\{^1\text{H}\}$ NMR (d_8 -THF, 25 °C): δ -58.6 (q, br, $^1J_{\text{PB}} = 29.4$ Hz).

[{(Me₃Si)₂CH}P(BH₃)(C₆H₄-2-SMe)K(pmdeta)]₂ (66**):**

To a solution of **40** (0.55 g, 1.67 mmol) in diethyl ether (15 mL) was added a slurry of benzylpotassium (224 mg, 1.72 mmol) in diethyl ether (15 mL). This mixture was stirred at room temperature for 1 h and then solvent was removed *in vacuo* to give a white powder. This powder was dissolved in toluene (5 mL) and pmdeta (0.3 ml, 1.44 mmol). The solvent was then carefully reduced *in vacuo* until the product began to precipitate slightly. The solution was allowed to warm to room temperature, dissolving the product, and upon cooling to 5 °C colourless crystals of **66** suitable for X-ray crystallography were deposited. Crude yield: 0.57 g, 93%. Anal. Calcd. For [(Me₃Si)₂CH}P(BH₃)(C₆H₄-2-SMe)K(pmdeta)]₂: C 51.18, H 9.71, N 7.78%. Found C 51.09, H 9.75, N 7.74%. $^1\text{H}\{^{11}\text{B}\}$ NMR (d_8 -THF, 25 °C): δ 0.01 (s, 9H, SiMe₃), 0.04 (s, 9H, SiMe₃), 0.73 (d, $^2J_{\text{PH}} = 5.5$ Hz, 3H, BH₃), 0.83 (d, $^2J_{\text{PH}} = 4.2$ Hz, 1H, CHP), 2.16 (s, 12H, NMe₂), 2.19 (s, 3H, NMe), 2.31(m, 4H, CH₂N), 2.32 (s, 3H, SMe), 2.42 (m, 4H, CH₂N), 6.84 (t, $J_{\text{HH}} = 7.4$ Hz, 1H, ArH), 6.90 (d, $J_{\text{HH}} = 6.9$ Hz, 1H, ArH), 6.95 (t, $J_{\text{HH}} = 7.55$ Hz, 1H, ArH), 7.75 (d, $J_{\text{HH}} = 7.8$ Hz, 1H, ArH). $^{13}\text{C}\{^1\text{H}\}$ NMR (d_8 -THF, 25 °C): δ 2.36 (d, $^3J_{\text{PC}} = 6.71$ Hz, SiMe₃), 3.73 (d, $^3J_{\text{PC}} = 1.9$ Hz, SiMe₃), 8.03 (d, $^1J_{\text{PC}} = 47.0$ Hz, CHP), 15.75 (d, $^4J_{\text{PC}} = 13.4$ Hz, SMe), 43.15 (NMe), 46.16 (NMe₂), 57.24 (NCH₂), 58.70 (NCH₂), 122.03 (d, $^2J_{\text{PC}} = 3.8$ Hz, ArC), 122.45, 125.78, 134.25 (ArC), 143.48 (d, $^2J_{\text{PC}} = 22.0$ Hz, ArC), 150.42 (d, $^1J_{\text{PC}} = 27.8$ Hz, ArC). $^{11}\text{B}\{^1\text{H}\}$ NMR (d_8 -THF, 25 °C): δ -30.6 (d, br, $^1J_{\text{BP}} = 19.6$ Hz). $^{31}\text{P}\{^1\text{H}\}$ NMR (d_8 -THF, 25 °C): δ -58.3 (q, br, $^1J_{\text{PB}} = 19.6$ Hz).

[{(Me₃Si)₂CH}P(BH₃)₂(C₆H₄-2-SMe)Li(12-crown-4)] (72·(12-crown-4)) :

To a solution of **40** (0.57 g, 1.74 mmol) in THF (10 mL) was added *n*-BuLi (0.7 mL of a 2.5 M solution in hexane, 1.75 mmol). After 1 h stirring, H₃B·SMe₂ (0.90 mL, of 2 M solution in THF, 1.80 mmol) was added to the reaction mixture, turning the solution from yellow to colourless. After 1 h further stirring, the solvent was removed *in vacuo* to yield a colourless solid., which was promptly dissolved in a solution toluene (10 mL) containing a few drops of Et₂O and 12-crown-4 (0.3 mL, 1.84 mmol). The solution was then filtered, and the compound precipitated from solution at room temperature. Isolated yield: 0.55 g, 60%. Anal. Calcd for [(SiMe₃)₂CH}P(BH₃)₂(C₆H₄-2-SMe)Li(12-crown-4)]: C 50.29, H 9.40%. Found C 50.13, H 9.39%. ¹H{¹¹B} NMR (*d*₈-THF, 25 °C): δ 0.07 (s, 18H, SiMe₃), 0.34 (d, ²J_{PH} = 8.3 Hz, 1H, CHP), 0.80 (d, ²J_{PH} = 10.5 Hz, 6H, BH₃), 2.42 (s, 3H, SMe), 3.74 (s, 16H, 12-crown-4), 6.93 (t, *J*_{HH} = 7.3 Hz, 1H, ArH), 7.09 (t, *J*_{HH} = 7.6 Hz, 1H, ArH), 7.22 (d, *J*_{HH} = 7.8 Hz, 1H, ArH), 8.11 (t, *J*_{HH} = 8.9 Hz, 1H, ArH). ¹³C{¹H} NMR (*d*₈-THF, 25 °C): δ 3.09 (SiMe₃), 6.98 (d, ¹J_{PC} = 3.8 Hz, CHP), 17.40 (SMe), 68.53 (12-crown-4), 123.7 (d, *J*_{PC} = 8.6 Hz, ArC), 127.32 (ArC), 128.10 (d, *J*_{PC} = 3.8 Hz, ArC), 135.07 (d, *J*_{PC} = 12.46 Hz, ArC), 143.23 (ArC), 143.62 (d, ¹J_{PC} = 26.8 Hz, ArC). ¹¹B{¹H} NMR (*d*₈-THF, 25 °C): δ -32.6 (d, br, ¹J_{BP} = 68.6 Hz). ³¹P{¹H} NMR (*d*₈-THF, 25 °C): δ -4.6 (m, br, ¹J_{PB} = 68.6 Hz). ⁷Li NMR (*d*₈-THF, 25 °C): δ -0.7.

[{(Me₃Si)₂CH}P(C₆H₄-2-OMe)(BH₃)Li(THF)] (85):

To a solution of **41** (0.20 g, 0.64 mmol) in Et₂O (20 mL) was added ⁿBuLi (0.4 mL of 1.9 M solution in hexane, 0.76 mmol). After 1 h stirring, the solvent was removed to yield a yellow solid. The product was dissolved in the minimal amount of THF, which was removed *in vacuo*, leaving a sticky residue. Upon addition of light petroleum, the product precipitated as a white powder. The mother liquor was removed *via* cannula, isolating the solid, which was then washed with cold light petroleum. Isolated yield: 0.13 g, 54%. ¹H{¹¹B} NMR (*d*₈-THF, 25 °C): δ -0.11 (s, 9H, SiMe₃), 0.15 (s, 9H, SiMe₃), 0.62 (d, ²J_{PH} = 3.2 Hz, 3H, BH₃), 0.73 (d, ²J_{PH} = 6.9 Hz, 1H, CHP), 1.76 (m, 4H, THF), 3.65 (m, 4H, THF), 3.75 (s, 3H, OMe), 6.61 (dd, ³J_{HH} = 7.8 Hz, ⁴J_{HH} = 5.1 Hz, 1H, ArH), 6.65 (t, *J*_{HH} = 7.6 Hz, 1H, ArH), 6.90 (d, *J*_{HH} = 7.6 Hz, 1H, ArH), 7.69 (d, *J*_{HH} = 6.9 Hz, 1H, ArH). ¹³C{¹H} NMR (*d*₈-THF, 25 °C): δ 1.46 (d, ³J_{PC} = 8.6 Hz, SiMe₃), 2.82 (SiMe₃), 6.17 (d, ¹J_{PC} = 44.1 Hz, CHP), 25.46 (THF), 54.55

(OMe), 67.40 (THF), 109.25 (ArC), 119.44 (ArC), 124.65 (ArC), 133.76 (ArC), 140.28 (d, $J_{PC} = 36.4$ Hz, ArC), 161.39 (d, $J_{PC} = 10.5$ Hz, ArC). $^{11}\text{B}\{^1\text{H}\}$ NMR (d_8 -THF, 25 °C): δ -34.3 (d, $^1J_{PB} = 39.2$ Hz). $^{31}\text{P}\{^1\text{H}\}$ NMR (d_8 -THF, 25 °C): δ -62.5 (d, $^1J_{PB} = 39.2$ Hz). ^7Li NMR (d_8 -THF, 25 °C): δ -0.58.

[{(Me₃Si)₂CH}P(C₆H₄-2-OMe)(BH₃)Na(THF)] (86):

A solution of **41** (0.21 g, 0.67 mmol) and benzylna (0.08 g, 0.67 mmol) in Et₂O (30 mL) was stirred for 1 h. The solvent was removed *in vacuo* to yield a yellow solid. The product was dissolved in the minimal amount of THF, and upon addition of light petroleum ether the product precipitated from solution as a white powder, which was isolated by removing the mother liquor *via* canula and then washed with cold light petroleum. Crude yield: 0.25 g, 96%. Anal. Calcd for [(Me₃Si)₂CH}P(C₆H₄-2-OMe)(BH₃)Na(THF)]: C 53.19, H 9.18%. Found C 53.06, H 9.31%. $^1\text{H}\{^{11}\text{B}\}$ NMR (d_8 -THF, 25 °C): δ -0.07 (s, 9H, SiMe₃), 0.15 (s, 9H, SiMe₃), 0.66 (d, $^2J_{PH} = 7.3$ Hz, 1H, CHP), 0.72 (d, $^2J_{PH} = 6.9$ Hz, 3H, BH₃), 1.79 (m, 4H, THF), 3.63 (m, 4H, THF), 3.77 (s, 3H, OMe), 6.66 (m, 2H, ArH), 6.92 (t, $J = 7.3$ Hz, 1H, ArH), 7.72 (m, 1H, ArH). $^{13}\text{C}\{^1\text{H}\}$ NMR (d_8 -THF, 25 °C): δ 1.41 (d, $^2J_{PC} = 8.6$ Hz, SiMe₃), 2.79 (SiMe₃), 6.09 (d, $^1J_{PC} = 41.2$ Hz, CHP), 25.46 (THF), 54.57 (OMe), 67.33 (THF), 109.16 (ArC), 119.60 (ArC), 124.91 (ArC), 133.93 (ArC), 139.43 (d, $J_{PC} = 29.7$ Hz ArC), 161.08 (d, $J_{PC} = 9.6$ Hz). $^{11}\text{B}\{^1\text{H}\}$ NMR (d_8 -THF, 25 °C): δ -34.5 (d, br, $^1J_{BP} = 29.4$ Hz). $^{31}\text{P}\{^1\text{H}\}$ NMR (d_8 -THF, 25 °C): δ -64.3 (d, br, $^1J_{PB} = 29.4$ Hz).

[{(Me₃Si)₂CH}P(C₆H₄-2-OMe)(BH₃)K(pmdeta)] (87):

To a solution of **41** (0.88 g, 2.82 mmol) in THF (20 mL) was added a solution of BnK (0.37 g, 2.82 mmol) in THF (20 mL). After 1 h stirring the solvent was removed *in vacuo* to yield a yellow solid. The product was dissolved in the minimal amount of toluene and pmdeta (0.6 mL, 2.87 mmol). The solvent was then carefully reduced *in vacuo* until the product began to precipitate slightly. The solution was allowed to warm to room temperature, dissolving the product, and upon cooling (5 °C) colourless crystals of **87** suitable for X-ray crystallography were deposited. Isolated crystalline yield: 0.54 g, 37%. Anal. Calcd for

[{(Me₃Si)₂CH}P(C₆H₄-2-OMe)(BH₃)K(pmdeta)]: C 52.75, H 10.01, N 8.02%. Found C 56.69, H 9.92, N 7.87%. ¹H{¹¹B} NMR (C₆D₆, 25 °C): δ -0.27 (s, 9H, SiMe₃), 0.45 (s, 9H, SiMe₃), 1.05 (d, ²J_{PH} = 5.5 Hz, 3H, BH₃), 1.07 (d, ²J_{PH} = 7.8 Hz, 1H, CHP), 2.01 (s, 8H, NCH₂), 2.05 (s, 3H, NMe), 2.11 (s, 12H, NMe₂), 3.53 (s, 3H, OMe), 6.54 (dd, *J* = 7.8 Hz, *J* = 2.8 Hz, 1H, ArH), 6.94 (t, *J* = 7.3 Hz, 1H, ArH), 7.06 (d, *J* = 7.6 Hz, 1H, ArH), 8.04 (m, br, 1H, ArH). ¹³C{¹H} NMR (C₆D₆, 25 °C): δ 2.21 (d, ³J_{PC} = 8.6 Hz, SiMe₃), 3.39 (SiMe₃), 6.00 (d, ¹J_{PC} = 41.2 Hz, CHP), 41.11 (NMe), 44.93 (NMe₂), 54.29 (OMe), 55.74 (NCH₂), 56.88 (NCH₂), 108.92 (ArC), 120.07 (ArC), 125.76 (ArC), 133.87 (ArC), 138.48 (d, ¹J_{PC} = 29.7 Hz, ArC), 161.24 (d, ²J_{PC} = 9.58 Hz, ArC). ¹¹B{¹H} NMR (C₆D₆, 25 °C): δ -32.3 (d, br, ¹J_{BP} = 29.8 Hz). ³¹P{¹H} NMR (C₆D₆, 25 °C): δ -63.0 (d, br, ¹J_{PB} = 29.8 Hz).

[{(Me₃Si)₂CH}PH(C₆H₄-2-O)Li]₆ (**89**):

To a solution of **41** (0.23 g, 0.74 mmol) in THF (20 mL) was added ⁿBuLi (0.4 mL of 2.0 M solution in hexane, 0.80 mmol). After 1 h stirring, the solvent was removed to yield **85**. The product was dissolved in toluene (20 mL) and tmeda (0.2 mL, 1.30 mmol) was added. After 16 h stirring **85** was fully converted into **89** and other side products. **89** was extracted into hexamthylidisiloxane, then the solvent was removed *in vacuo* to yield an oil. Single crystals of **89** were grown from cold (-30 °C) methylcyclohexane. Isolated yield 0.09 g, 38%. ¹H NMR (C₆D₆, 25 °C): δ 0.24 (s, 18 H, SiMe₃), 0.65 (dd, ³J_{HH} = 5.5 Hz, ²J_{PH} = 1.9 Hz, 1H, CHP), 4.51 (dd, ¹J_{PH} = 217.6 Hz, ³J_{HH} = 5.5 Hz), 6.47 (d, *J*_{HH} = 8.3 Hz, 1H, ArH), 6.79 (t, *J*_{HH} = 7.3 Hz, 1H, ArH), 7.20 (t, *J*_{HH} = 7.3 Hz, 1H, ArH), 7.47 (t, *J*_{HH} = 7.3 Hz, 1H, ArH). ¹³C{¹H} NMR (C₆D₆, 25 °C): δ 1.07 (SiMe₃), 4.38 (d, ¹J_{PC} = 42.2 Hz, CHP), 109.4 (ArC), 120.52 (d, *J*_{PC} = 5.8 Hz, ArC), 129.7 (ArC), 134.94 (d, *J*_{PC} = 18.2 Hz, ArC), 160.99 (d, *J*_{PC} = 6.7 Hz, ArC), 161.20 (d, *J*_{PC} = 2.9 Hz, ArC). ³¹P NMR (C₆D₆, 25 °C): δ -72.7 (d, ¹J_{PH} = 219.6 Hz). ⁷Li NMR (C₆D₆, 25 °C): δ 0.7.

{(Me₃Si)₂CH}PMe(C₆H₄-2-OMe)(BH₃) (**90**):

To a solution of **41** (0.31 g, 0.99 mmol) in THF (15 mL) was added ⁿBuLi (0.4 mL of a 2.5 M solution in hexane, 1.00 mmol). After ½ h stirring MeI (0.07 mL, 1.12 mmol) was added to

the solution. After a further ½ h stirring, the solvent was removed *in vacuo* to yield a white solid. Isolated yield: 0.32 g, 99%. $^1\text{H}\{^{11}\text{B}\}$ NMR (CDCl_3 , 25 °C): δ -0.08 (s, 9H, SiMe_3), 0.31 (s, 9H, SiMe_3), 0.88 (d, $^2J_{\text{PH}} = 14.7$ Hz, 3H, BH_3), 1.46 (d, $^2J_{\text{PH}} = 20.2$ Hz, 1H, CHP), 1.66 (d, $^2J_{\text{PH}} = 10.1$ Hz, 3H, PMe), 3.91 (s, 3H, OMe), 6.88 (dd, $^1J_{\text{HH}} = 8.3$ Hz, $^2J_{\text{HH}} = 3.2$ Hz, 1H, ArH), 7.06 (t, $J_{\text{HH}} = 7.3$ Hz, 1H, ArH), 7.48 (t, $J_{\text{HH}} = 7.8$ Hz, 1H, ArH), 7.92 (dd, $^1J_{\text{HH}} = 13.1$ Hz, $^2J_{\text{HH}} = 7.6$ Hz, 1H, ArH). $^{13}\text{C}\{^1\text{H}\}$ NMR (CDCl_3 , 25 °C): δ 2.40 (d, $^3J_{\text{PC}} = 2.9$ Hz, SiMe_3), 3.50 (d, $^3J_{\text{PC}} = 1.9$ Hz, SiMe_3), 10.40 (d, $J_{\text{PC}} = 4.8$ Hz, CHP), 16.68 (d, $J_{\text{PC}} = 39.3$ Hz, PMe), 55.17 (OMe), 110.58 (d, $J_{\text{PC}} = 3.83$ Hz, ArC), 120.93 (d, $J_{\text{PC}} = 12.5$ Hz, ArC), 121.63 (d, $J_{\text{PC}} = 50.8$ Hz ArC), 132.90 (ArC), 135.77 (d, $J_{\text{PC}} = 15.3$ Hz, ArC), 161.33 (ArC). $^{11}\text{B}\{^1\text{H}\}$ NMR (CDCl_3 , 25 °C): δ -37.5 (d, br, $J_{\text{PB}} = 58.8$ Hz). $^{31}\text{P}\{^1\text{H}\}$ NMR (CDCl_3 , 25 °C): δ 11.7 (q, br, $J_{\text{PB}} = 58.8$ Hz).

$\{(\text{Me}_3\text{Si})_2\text{CH}\}\text{PH}(\text{C}_6\text{H}_4\text{-2-OCD}_3)(\text{BH}_3)$ (101**):**

To a cold (0 °C) solution of KOH (0.63 g, 12.00 mmol) in acetonitrile (10 mL) was added a solution of 2-bromophenol (2.0 mL of 5.0 M solution in acetonitrile, 10.00 mmol) in acetonitrile (10 mL). After ½ h stirring at 0 °C CD_3I (0.75 mL, 12 mmol) was added to the solution. The reaction was stirred for 40 h. The solvent was removed *in vacuo*, and the residue was washed with light petroleum (3 x 20 mL). The solvent was removed to yield a colourless oil (2-bromo- d_3 -anisole). Yield 1.19 g, 62 %. To a cold (0 °C) solution of 2-bromo- d_3 -anisole (1.19 g, 6.23 mmol) in Et_2O (10 mL) was added $n\text{BuLi}$ (2.5 mL of a 2.5 M solution in hexane, 6.25 mmol). After 2 h stirring at 0 °C, the solution was added dropwise to a cold (-78 °C) solution of **43** (1.70 g, 6.51 mmol) in Et_2O (20 mL). The reaction was stirred for 16 h and allowed to reach room temperature. Solid LiAlH_4 (0.28 g, 7.3 mmol) was added to the solution *in situ*, then the mixture was heated under reflux for 2 h. When the solution was cool, $\text{BH}_3\cdot\text{SMe}_2$ (3.2 mL of 2 M solution in THF, 6.4 mmol) was added, and the solution stirred for 1 h at room temperature. The reaction was quenched with water. The product was extracted into THF (3 x 20 mL) and the extracts were washed with brine (30 mL). The organic phase was dried with MgSO_4 , filtered, and then the solvent was removed *in vacuo*. The product was dissolved in hot *n*-hexane, and crystals of $\{(\text{Me}_3\text{Si})_2\text{CH}\}\text{PH}(\text{C}_6\text{H}_4\text{-2-OCD}_3)(\text{BH}_3)$ (**101**) were deposited upon cooling to -30 °C. Isolated yield: 0.83 g, 42%. $^1\text{H}\{^{11}\text{B}\}$ NMR (CDCl_3 , 25 °C): δ -0.01 (s, 9H, SiMe_3), 0.28 (s, 9H, SiMe_3), 0.89 (dd, $^3J_{\text{HH}} =$

6.6 Hz, $^2J_{\text{PH}} = 14.9$ Hz, 3H, BH_3), 1.07 (d, $J_{\text{PH}} = 20.2$ Hz, 1H, CHP), 5.84 (dq, $^1J_{\text{PH}} = 384.0$ Hz, $^3J_{\text{HH}} = 12.9$, 1H, PH), 6.89 (dd, $J_{\text{HH}} = 8.2$ Hz, $J_{\text{HH}} = 2.8$ Hz, 1H, ArH), 7.04 (t, $J_{\text{HH}} = 6.9$ Hz, 1H, ArH), 7.47 (t, $J_{\text{HH}} = 7.8$ Hz, 1H, ArH), 7.91 (dd, $J_{\text{HH}} = 13.3$ Hz, $J_{\text{HH}} = 7.3$ Hz, 1H, ArH). $^{13}\text{C}\{^1\text{H}\}$ NMR (CDCl_3 , 25 °C): δ 1.25 (d, $J_{\text{PC}} = 2.9$ Hz, SiMe_3), 2.10 (d, $J_{\text{PC}} = 2.9$ Hz, SiMe_3), 6.49 (d, $^2J_{\text{PC}} = 3.8$ Hz, CHP), 110.20 (d, $J_{\text{PC}} = 3.8$ Hz, ArC), 116.88 (d, $J = 50.8$ Hz, ArC), 121.07 (d, $J_{\text{PC}} = 12.5$ Hz, ArC), 133.47 (ArC), 136.25 (d, $J_{\text{PC}} = 15.3$ Hz, ArC), 160.78 (ArC). $^{11}\text{B}\{^1\text{H}\}$ NMR (CDCl_3 , 25 °C): δ -40.4 (d, br, $J_{\text{PB}} = 49.0$ Hz). $^{31}\text{P}\{^1\text{H}\}$ NMR (CDCl_3 , 25 °C): δ -22.3 (q, br, $J_{\text{PB}} = 49.0$ Hz).

$\{(\text{Me}_3\text{Si})_2\text{CH}\}\text{PH}(\text{C}_6\text{H}_4\text{-2-OMe})(\text{BD}_3)$ (102):used in situ

To a solution of **46** (0.37 g, 1.24 mmol) in THF (5 mL) was added $\text{BD}_3 \cdot \text{THF}$ (1.2 mL of a 1.0 M solution in THF, 1.20 mmol). After one hour stirring the solvent was removed *in vacuo* to yield a white solid (**102**). **102** was dissolved in THF (5 mL) and used *in situ*.

$\{(\text{Me}_3\text{Si})_2\text{CH}\}\text{P}(\text{C}_6\text{H}_4\text{-2-OMe})\text{Li}(\text{tmeda})$ (106):

To a solution of **46** (0.39 g, 1.31 mmol) in THF (20 mL) was added $^n\text{BuLi}$ (0.5 mL of a 2.5 M solution in hexanes, 1.25 mmol). After 1 h stirring the solvent was removed *in vacuo* to yield a yellow solid. The product was dissolved in toluene and tmeda (0.2 mL, 1.31 mmol). The solvent was then carefully reduced *in vacuo* until the product began to precipitate slightly. The solution was allowed to warm to room temperature, dissolving the product, and upon cooling (-30 °C), crystals of the adduct $[\{(\text{Me}_3\text{Si})_2\text{CH}\}\text{P}(\text{C}_6\text{H}_4\text{-2-OMe})\text{Li}(\text{tmeda})]$ suitable for X-ray crystallography were deposited. Isolated crystalline yield: 0.32 g, 58%. Anal. Calcd for $[\{(\text{Me}_3\text{Si})_2\text{CH}\}\text{P}(\text{C}_6\text{H}_4\text{-2-OMe})\text{Li}(\text{tmeda})]$: C 57.11, H 10.06, N 6.66%. Found C 56.98, H 9.91, N 6.53%. ^1H NMR (d_8 -THF, 25 °C): δ 0.11 (s, 18H, SiMe_3), 0.18 (s, 1H, CHP), 2.18 (s, 12H, NMe_2), 2.31 (s, 4H, NCH_2), 3.81 (s, 3H, OMe), 6.19 (t, $J_{\text{HH}} = 7.6$ Hz, 1H, ArH), 6.37 (dd, $^1J_{\text{HH}} = 6.9$ Hz, $^2J_{\text{HH}} = 4.2$ Hz, 1H, ArH), 6.51 (t, $J_{\text{HH}} = 7.6$ Hz, 1H, ArH), 6.77 (d, $J_{\text{HH}} = 7.7$ Hz, 1H, ArH). $^{13}\text{C}\{^1\text{H}\}$ NMR (CDCl_3 , 25 °C): δ 0.53 (d, $^3J_{\text{PC}} = 5.8$ Hz, SiMe_3), 4.06 (d, $^2J_{\text{PC}} = 42.2$ Hz, CHP), 45.30 (NMe_2), 55.09 (OMe), 57.95 (NCH_2), 107.75 (ArC), 113.07 (d, $J_{\text{PC}} = 3.8$ Hz, ArC), 121.84 (ArC), 125.48 (d, $J_{\text{PC}} = 2.9$ Hz, ArC), 129.68 (ArC), 154.9 (d,

$^2J_{\text{PC}} = 22.0$ Hz, ArC). $^{31}\text{P}\{^1\text{H}\}$ NMR (d_8 -THF, 25 °C): δ -85.1. ^7Li NMR (d_8 -THF, 25 °C): δ 3.7.

[{(Me₃Si)₂CH}P(BH₃)₂(C₆H₄-2-OMe)Li(THF)] (107):

To a solution of **41** (0.52 g, 1.67 mmol) in THF (10 mL) was added $n\text{BuLi}$ (0.9 mL of a 1.9 M solution in hexane, 1.71 mmol). After 1 h stirring, $\text{H}_3\text{B}\cdot\text{SMe}_2$ (0.9 mL, of a 2.0 M solution, 1.80 mmol) was added to the reaction mixture turning the solution from yellow to colourless. After 1 h further stirring, the solvent was removed *in vacuo* to yield **107**. The product was crystallised from light petroleum in the presence of a few drops of THF as a colourless powder. Isolated yield: 0.06 g, 9%. Anal. Calcd for [(SiMe₃)₂CH}P(BH₃)₂(C₆H₄-2-OMe)Li(THF)]: C 53.48, H 9.97%. Found C 53.03, H 9.82%. $^1\text{H}\{^{11}\text{B}\}$ NMR (d_8 -THF, 25 °C): δ 0.04 (s, 18H, SiMe₃), 0.66 (dd, $^2J_{\text{PH}} = 11.0$ Hz, 6H, BH₃), 1.56 (dd, $^2J_{\text{PH}} = 15.6$ Hz, 1H, CHP), 1.78 (m, 4 H, THF), 3.62 (m, 4 H, THF), 2.42 (d, $J_{\text{HH}} = 2.8$ Hz, 3H, OMe), 6.73 (t, $J_{\text{HH}} = 7.3$ Hz, 1H, ArH), 7.76 (d, $J_{\text{HH}} = 8.3$ Hz, 1H, ArH), 7.11 (t, $J_{\text{HH}} = 7.8$ Hz, 1H, ArH), 7.87 (t, $J_{\text{HH}} = 9.2$ Hz, 1H, ArH). $^{13}\text{C}\{^1\text{H}\}$ NMR (d_8 -THF, 25 °C): δ 3.00 (d, $^3J_{\text{PC}} = 1.9$ Hz, SiMe₃), 7.52 (d, $^1J_{\text{PC}} = 1.9$ Hz, CHP), 25.46 (THF), 54.74 (OMe), 67.39 (THF), 110.64 (d, $J_{\text{PC}} = 2.9$ Hz, ArC), 119.33 (d, $J_{\text{PC}} = 8.6$ Hz, ArC), 128.39 (ArC), 132.26 (d, $J_{\text{PC}} = 29.7$ Hz, ArC), 134.55 (d, $J_{\text{PC}} = 9.6$ Hz, ArC), 162.34 (ArC). $^{11}\text{B}\{^1\text{H}\}$ NMR (d_8 -THF, 25 °C): δ -33.3 (d, br, $^1J_{\text{BP}} = 68.6$ Hz). $^{31}\text{P}\{^1\text{H}\}$ NMR (d_8 -THF, 25 °C): δ -12.7 (m, br, $^1J_{\text{PB}} = 68.6$ Hz). ^7Li NMR (d_8 -THF, 25 °C): δ -0.8.

[{(Me₃Si)₂CH}P(C₆H₄-2-O)(BH₃)Ca(THF)]₄ (108):

To a solution of **41** (0.98 g, 3.14 mmol) in THF (15 mL) was added BnK (0.47 g, 3.30 mmol) in THF (20 mL). After 1 h stirring the solution was added to a slurry of CaI₂ (0.48 g, 1.63 mmol) in THF (20 mL). After 16 h stirring the solvent was removed, then the residue was extracted into diethyl ether (50 mL). The solvent was again removed *in vacuo*, and the product was extracted into hexamethyldisiloxane. The product was crystallised from cold (5 °C) methylcyclohexane. Isolated yield: 0.63 g, 22% Anal. Calcd for [(Me₃Si)₂CH}P(C₆H₄-

2-O)(BH₃)]Ca(THF)₄: C 51.67, H 8.79%. Found C 51.56, H 8.64%. ³¹P{¹H} NMR (*d*₈-THF, 25 °C): δ -69.1 (m, br).

[{(Me₃Si)₂CH}P(C₆H₅)(BH₃)Li(THF)₂]_∞ (115):

To a solution of **42** (0.41 g, 1.26 mmol) in THF (15 mL) was added ⁿBuLi (0.5 mL of 2.5 M solution in hexane, 1.25 mmol). After 1 h stirring the solvent was removed *in vacuo* to yield an off-white solid. THF was added to a solution of **115** in methylcyclohexane until product was dissolved. THF was carefully removed *in vacuo*, until the point of precipitation. Upon cooling to -30 °C colourless crystals of **115** suitable for X-ray crystallography were deposited. Isolated crystalline yield: 0.19 g, 35%. Anal. Calcd for [(Me₃Si)₂CH}P(C₆H₅)(BH₃)Li(THF)₂]_∞: C 58.32, H 10.02%. Found C 58.29, H 9.95%. ¹H{¹¹B} NMR (*d*₈-toluene, 25 °C): δ 0.29 (s, 9H, SiMe₃), 0.39 (s, 9H, SiMe₃), 0.63 (d, ²J_{PH} = 7.8 Hz, 1H, CHP), 1.04 (s, 3H, BH₃), 1.40 (m, 8H, THF), 3.54 (m, 8H, THF), 6.99 (t, *J*_{HH} = 7.3 Hz, 1H, ArH), 7.17 (t, *J*_{HH} = 7.1 Hz, 2H, ArH), 7.78 (t, *J*_{HH} = 6.9 Hz, 2H, ArH). ¹³C{¹H} NMR (*d*₈-toluene, 25 °C): δ 2.29 (d, ³J_{PC} = 7.7 Hz, SiMe₃), 3.32 (SiMe₃), 8.86 (d, ¹J_{PC} = 34.6 Hz, CHP), 25.12 (THF), 68.13 (THF), 124.23 (ArC), 127.14 (d, *J*_{PC} = 4.8 Hz, ArC), 131.84 (d, *J*_{PC} = 11.5 Hz, ArC), 149.62 (d, *J*_{PC} = 16.3 Hz, ArC). ¹¹B{¹H} NMR (*d*₈-toluene, 25 °C): δ -32.7 (d, br, ¹J_{BP} = 49.0 Hz). ³¹P{¹H} NMR (*d*₈-toluene, 25 °C): δ -56.8 (q, br, ¹J_{PB} = 49.0 Hz). ⁷Li{¹H} NMR (*d*₈-toluene, 25 °C): δ 3.1.

[{(Me₃Si)₂CH}P(C₆H₅)(BH₃)] [Na(12-crown-4)] (116):

A solution of **42** (0.37 g, 1.31 mmol) and benzylna (0.15 g, 1.31 mmol) in THF (30 mL) was stirred for 1 h. The solvent was removed to yield a yellow solid. The product was dissolved in the minimal amount of toluene and THF. 12-crown-4 (0.4 mL, 2.62 mmol) was added to the solution, and THF was carefully removed *in vacuo*, until the product began to precipitate from solution. Upon warming to room temperature, the product had dissolved back into the solution. After cooling (-30 °C) colourless crystals of **116** suitable for X-ray crystallography were deposited. Isolated crystalline yield: 0.73 g, 86%. ¹H{¹¹B} NMR (*d*₈-THF, 25 °C): δ -0.05 (s, br, 9H, SiMe₃), 0.14 (s, br, 9H, SiMe₃), 0.20 (d, ²J_{PH} = 5.5 Hz, 1H,

CHP), 0.97 (d, $^2J_{\text{PH}} = 4.1$ Hz, 3H, BH_3), 3.63 (s, 32 H, 12-crown-4), 6.70 (t, $J_{\text{HH}} = 7.6$ Hz, 1H, ArH), 6.91 (t, $J_{\text{HH}} = 7.1$ Hz, 2H, ArH), 7.55 (m, 2H, ArH). $^{13}\text{C}\{^1\text{H}\}$ NMR (d_8 -THF, 25 °C): δ 1.81 (s, br, SiMe_3), 2.91 (s, br, SiMe_3), 10.51 (d, $^1J_{\text{PC}} = 47.9$ Hz, CHP), 66.13 (12-crown-4), 121.11 (ArC), 125.73 (ArC), 131.84 (d, $J_{\text{PC}} = 11.5$ Hz, ArC), 157.07 (d, $J_{\text{PC}} = 35.5$ Hz, ArC). $^{11}\text{B}\{^1\text{H}\}$ NMR (d_8 -THF, 25 °C): δ -32.4 (s, br). $^{31}\text{P}\{^1\text{H}\}$ NMR (d_8 -THF, 25 °C): δ -41.0 (d, br, $^1J_{\text{PB}} = 26.1$ Hz).

[{(Me₃Si)₂CH}P(C₆H₅)(BH₃)K(pmdeta)]₂ (117):

To a solution of **42** (0.45 g, 1.59 mmol) in THF (15 mL) was added a solution of benzylpotassium (0.21 g, 1.59 mmol) in THF (10 mL). After 1 h stirring the solvent was removed *in vacuo* yielding an orange powder. The product was dissolved in toluene and pmdeta (0.3 mL, 1.44 mmol). The solvent was then carefully reduced *in vacuo* until the product began to precipitate slightly. The solution was allowed to warm to room temperature, dissolving the product, and upon cooling (-30 °C) colourless crystals of **117** suitable for X-ray crystallography were deposited. Isolated crystalline yield: 0.41 g, 39%. Anal. Calcd for [(Me₃Si)₂CH}P(C₆H₅)(BH₃)K(pmdeta)]₂: C 53.52, H 10.21, N 8.51%. Found C 53.41, H 10.14, N 8.42%. $^1\text{H}\{^{11}\text{B}\}$ NMR (d_8 -toluene, 25 °C): δ 0.28 (s, 9H, SiMe_3), 0.42 (s, 9H, SiMe_3), 0.61 (d, $^2J_{\text{PH}} = 6.9$ Hz, 1H, CHP), 1.08 (d, $^2J_{\text{PH}} = 4.1$ Hz, 3H, BH_3), 1.93 (m, 4H, NCH_2), 1.95 (m, 4H, NCH_2), 1.99 (s, 3H, NMe), 2.09 (s, 12H, NMe_2), 6.98 (t, $J_{\text{HH}} = 7.3$ Hz, 1H, ArH), 7.20 (t, $J_{\text{HH}} = 7.3$ Hz, 2H, ArH), 7.80 (t, $J_{\text{HH}} = 6.4$ Hz, 2H, ArH). $^{13}\text{C}\{^1\text{H}\}$ NMR (d_8 -toluene, 25 °C): δ 2.25 (d, $^3J_{\text{PC}} = 7.7$ Hz, SiMe_3), 3.20, (SiMe_3), 9.78 (d, $^1J_{\text{PC}} = 43.1$ Hz, CHP), 41.00 (NMe), 44.80 (NMe_2), 55.60 (NCH_2), 56.76 (NCH_2), 123.42 (ArC), 127.09 (d, $J_{\text{PC}} = 2.9$ Hz, ArC), 131.83 (d, $J_{\text{PC}} = 11.5$ Hz, ArC), 153.07 (d, $J_{\text{PC}} = 25.9$ Hz). $^{11}\text{B}\{^1\text{H}\}$ NMR (d_8 -toluene, 25 °C): δ -31.6 (d, br, $^1J_{\text{BP}} = 19.6$ Hz). $^{31}\text{P}\{^1\text{H}\}$ NMR (d_8 -toluene, 25 °C): δ -50.6 (d, br, $^1J_{\text{PB}} = 19.6$ Hz).

[{(Me₃Si)₂CH}P(C₆H₅)(BH₃)₂Sr (119):

A solution of **42** (0.97 g, 3.44 mmol) and BnK (0.45 mmol 3.44 mmol) in diethyl ether (20 mL) was stirred for 1 h. The solvent was removed *in vacuo* to yield a yellow/ orange solid.

The product was dissolved in toluene (20 mL) and added to a cold (-78 °C) solution of SrI₂ (0.59 g, 1.72 mmol) in toluene (20 mL). The solution was stirred overnight and allowed to reach room temperature. The solution was filtered through celite to remove KI and the solvent was removed *in vacuo*. The product was dissolved in methylcyclohexane containing a few drops of THF and upon cooling (-30 °C) crystals of **119** were deposited. The product was washed with cold (0 °C) light petroleum and isolated as a yellow powder. Isolated yield: 0.20 g, 18 %. ¹H{¹¹B} NMR (*d*₈-THF, 25 °C): δ -0.05 (s, 9H, SiMe₃), 0.10 (s, 9H, SiMe₃) 0.25 (d, ²J_{PH} = 5.5 Hz, 1H, CHP), 0.82 (d, ²J_{PH} = 4.1 Hz, 3H, BH₃), 6.76 (d, J_{HH} = 7.3 Hz, 1H, ArH), 6.94 (t, J_{HH} = 7.6 Hz, 2H, ArH), 7.50 (t, J_{HH} = 6.0 Hz, 2H, ArH). ¹³C{¹H} NMR (*d*₈-THF, 25 °C): δ 1.52 (SiMe₃), 2.66 (SiMe₃), 9.54 (d, ¹J_{PC} = 45.1 Hz, CHP), 121.80 (ArC), 126.88 (d, J_{PC} = 3.8 Hz, ArC), 131.55 (d, J_{PC} = 12.5 Hz, ArC), 155.04 (d, J_{PC} = 30.7 Hz, ArC). ¹¹B{¹H} NMR (*d*₈-THF, 25 °C): δ -31.8 (m, br, ¹J_{PB} = 39.7 Hz). ³¹P{¹H} NMR (*d*₈-THF, 25 °C): δ -46.7 (q, br, ¹J_{PB} = 39.7 Hz).

[{(Me₃Si)₂CH}P(C₆H₅)(BH₃)₂Ba (**120**):

A solution of **42** (0.72 g, 2.55 mmol) and BnK (0.33 mmol 2.55 mmol) in diethyl ether (20 mL) was stirred for 1 h. The solvent was removed *in vacuo* to yield a yellow/ orange solid. The product was dissolved in toluene (20 mL) and added to a cold (-78 °C) solution of BaI₂ (0.50 g, 1.28 mmol) in toluene (20 mL). The solution was stirred overnight and allowed to reach room temperature. The solution was filtered through celite to remove KI and the solvent was removed *in vacuo*. The product was dissolved in methylcyclohexane containing a few drops of THF and upon cooling (-30 °C) crystals of **120** were deposited. The product was washed with cold (0 °C) light petroleum and isolated as a yellow powder. Isolated yield: 0.27 g, 30% Anal. Calcd for [(Me₃Si)₂CH}P(C₆H₅)(BH₃)₂Ba: C 44.62, H 7.78%. Found C 44.72, H 7.88%. ¹H{¹¹B} NMR (*d*₈-THF, 25 °C): δ 0.01 (s, 9H, SiMe₃), 0.14 (s, 9H, SiMe₃) 0.32 (d, ²J_{PH} = 5.5 Hz, 1H, CHP), 0.84 (d, ²J_{PH} = 4.1 Hz, 3H, BH₃), 6.84 (d, J_{HH} = 7.1 Hz, 1H, ArH), 7.01 (t, J_{HH} = 7.3 Hz, 2H, ArH), 7.53 (t, J_{HH} = 6.2 Hz, 2H, ArH). ¹³C{¹H} NMR (*d*₈-THF, 25 °C): δ 1.68 (d, ³J_{PC} = 5.8 Hz, SiMe₃), 2.76 (SiMe₃), 6.34 (d, ¹J_{PC} = 44.1 Hz, CHP), 126.02 (ArC), 126.25 (d, J_{PC} = 3.8 Hz, ArC), 131.53 (d, J_{PC} = 12.5 Hz, ArC), 154.02 (d, J_{PC} = 28.8 Hz, ArC). ¹¹B{¹H} NMR (*d*₈-THF, 25 °C): δ -31.5 (m, br, ¹J_{PB} = 29.8 Hz). ³¹P{¹H} NMR (*d*₈-THF, 25 °C): δ -48.7 (q, br, ¹J_{PB} = 29.8 Hz).

[{(Me₃Si)₂CH}P(C₆H₅)(BH₃)₂Li(12-crown-4)] (123):

To a solution of **42** (0.54 g, 1.91 mmol) in THF (10 mL) was added ⁿBuLi (0.8 mL of a 2.5 M solution in hexane, 2.0 mmol). After 1 h stirring, a solution of BH₃.SMe₂ (1.0 mL, of a 2.0 M solution in THF, 2.0 mmol) was added to the reaction mixture turning the solution from yellow to colourless. After 1 h further stirring, the solvent was removed *in vacuo* to yield a colourless solid. The product was dissolved in toluene (5 mL) and 12-crown-4 (0.3 mL, 1.85 mmol) was added. Colourless crystals suitable for X-ray crystallography were obtained upon cooling this solution to 5 °C. Isolated crystalline yield: 0.46 g, 50%. Anal. Calcd for [(Me₃Si)₂CH}P(C₆H₅)(BH₃)₂Li(12-crown-4)]: C 52.73, H 9.69%. Found C 52.67, H 9.81%. ¹H{¹¹B} NMR (*d*₈-THF, 25 °C): δ -0.05 (s, 18H, SiMe₃), 0.57 (d, ²J_{PH} = 13.8 Hz, 1H, CHP), 0.77 (d, ²J_{PH} = 10.1 Hz, 6H, BH₃), 3.75 (s, 16H, 12-crown-4), 7.07 (t, J_{HH} = 7.1 Hz, 2H, ArH), 7.12 (t, J_{HH} = 7.2 Hz, 2H, ArH), 7.79 (t, J_{HH} = 10.1 Hz, 1H, ArH). ¹³C{¹H} NMR (*d*₈-THF, 25 °C): δ 3.20 (SiMe₃), 11.85 (d, ¹J_{PC} = 6.7 Hz, CHP), 67.15 (12-crown-4), 126.02 (ArC), 126.31 (d, J_{PC} = 7.7 Hz, ArC), 132.32 (d, J_{PC} = 6.7 Hz, ArC), 146.78 (d, J_{PC} = 29.7 Hz, ArC), ¹¹B{¹H} NMR (*d*₈-THF, 25 °C): δ -32.5 (d, br, ¹J_{BP} = 49.0 Hz). ³¹P{¹H} NMR (*d*₈-THF, 25 °C): δ -8.8 (m, ¹J_{PB} = 49.0 Hz). ⁷Li{¹H} NMR (*d*₈-THF, 25 °C): δ -0.7.

[{(Me₃Si)₂CH}P(C₆H₅)(BH₃)₂Na(THF)₂]₂ (124):

To a solution of **42** (0.45 g, 1.59 mmol) in THF (10 mL) was added a solution of BnNa (184 mg, 1.61 mmol). After 1 h stirring, a solution of BH₃.SMe₂ (0.8 mL, of a 2.0 M solution in THF, 1.60 mmol) was added to the reaction mixture, turning the solution from yellow to colourless. After 1 h further stirring, the solvent was removed to yield a colourless solid. The product was dissolved in a mixture of methylcyclohexane (10 mL), toluene (2 mL), and THF (5 mL). Colourless crystals suitable for X-ray crystallography were obtained upon cooling (-30 °C). Isolated crystalline yield: 0.46 g, 50%. Anal. Calcd for [(Me₃Si)₂CH}P(C₆H₅)(BH₃)₂Na(THF)₂]₂: C 49.08, H 9.51%. Found C 48.89, H 9.45%. ¹H{¹¹B} NMR (*d*₈-THF, 25 °C): δ 0.07 (s, 18 H, SiMe₃), 0.63 (d, ²J_{PH} = 8.7 Hz, 6H, BH₃), 0.64 (d, ²J_{PH} = 15.1 Hz, 1H, CHP), 1.78 (m, 8H, THF), 3.61 (m, 8H, THF), 7.12 (t, J_{HH} = 8.5 Hz, 1H, ArH), 7.17 (t, J_{HH} = 9.1 Hz, 2H, ArH), 7.74 (t, J_{HH} = 8.5 Hz, 2H, ArH). ¹³C{¹H} NMR (*d*₈-THF, 25 °C): δ 2.79 (d, ³J_{PC} = 1.9 Hz, SiMe₃), 10.55 (d, ¹J_{PC} = 2.9 Hz, CHP), 25.30 (THF), 67.14 (THF), 126.58 (ArC), 126.68 (d, J_{PC} = 7.7 Hz, ArC), 132.03 (d, J_{PC} = 7.7 Hz, ArC), 143.84 (d, J_{PC} = 36.4

Hz, ArC). $^{11}\text{B}\{^1\text{H}\}$ NMR (d_8 -THF, 25 °C): δ -33.8 (d, br, $^1J_{\text{BP}} = 68.6$ Hz). $^{31}\text{P}\{^1\text{H}\}$ NMR (d_8 -THF, 25 °C): δ -14.9 (m, $^1J_{\text{PB}} = 68.6$ Hz).

[{(Me₃Si)₂CH}P(C₆H₅)(BH₃)₂K(THF)₂]_∞ (125):

To a solution of **42** (0.42 g, 1.49 mmol) in THF (10 mL) was added a solution of BnK (194 mg, 1.49 mmol) in THF (10 mL). After 1 h stirring, a solution of BH₃.SMe₂ (0.8 mL of a 2.0 M solution in THF, 1.60 mmol) was added to the reaction mixture, turning the solution from yellow/orange to colourless. After 1 h further stirring, the solvent was removed to yield a colourless solid. THF was added to a solution of **125** in toluene (5 mL) until the product was dissolved. THF was carefully removed *in vacuo*, until the point of precipitation. Upon cooling to 5 °C, colourless crystals of **125** suitable for X-ray crystallography were obtained. Isolated crystalline yield: 1.30 g, 88%. Anal. Calcd for [(Me₃Si)₂CH}P(C₆H₅)(BH₃)₂K(THF)₂]_∞: C 49.71, H 9.05%. Found C 46.78, H 8.95%. $^1\text{H}\{^{11}\text{B}\}$ NMR (d_8 -THF, 25 °C): δ 0.07 (s, 18H, SiMe₃), 0.62 (d, $^2J_{\text{PH}} = 14.7$ Hz, 1H, CHP), 0.70 (d, $^2J_{\text{PH}} = 9.6$ Hz, 6H, BH₃), 1.78 (m, 8H, THF), 3.62 (m, 8H, THF), 7.10 (t, $J_{\text{HH}} = 6.8$ Hz, 1H, ArH), 7.14 (t, $J_{\text{HH}} = 6.8$ Hz, 2H, ArH), 7.77 (t, $J_{\text{HH}} = 8.5$ Hz, 1H, ArH). $^{13}\text{C}\{^1\text{H}\}$ NMR (d_8 -THF, 25 °C): δ 2.91 (d, $J_{\text{PC}} = 1.9$ Hz, SiMe₃), 11.37 (d, $J_{\text{PC}} = 3.8$ Hz, CHP), 25.01 (THF), 66.85 (THF), 126.38 (ArC), 126.46 (ArC), 132.27 (d, $^3J_{\text{PC}} = 6.7$ Hz, ArC), 144.58 (d, $J_{\text{PC}} = 34.5$ Hz, ArC), $^{11}\text{B}\{^1\text{H}\}$ NMR (d_8 -THF, 25 °C): δ -32.9 (d, br, $^1J_{\text{BP}} = 58.8$ Hz). $^{31}\text{P}\{^1\text{H}\}$ NMR (d_8 -THF, 25 °C): δ -14.1 (m, br, $^1J_{\text{PB}} = 58.8$ Hz).

[{(Me₃Si)₂CH}P(C₆H₄-2-OMe)(BH₃)₂][Na(12-crown-4)] (126):

To a solution of **41** (0.38 g, 1.22 mmol) in THF (10 mL) was added a solution of benzylsodium (0.14 g, 1.22 mmol). After 1 h stirring, a solution of BH₃.SMe₂ (0.6 mL of a 2.0 M solution in THF, 1.20 mmol) was added to the reaction mixture, turning the solution from yellow to colourless. After 1 h further stirring, the solvent was removed to yield a colourless solid. The product was dissolved in a mixture of methylcyclohexane (10 mL), toluene (2 mL), and THF (5 mL). Colourless crystals suitable for X-ray crystallography were obtained at room temperature. Isolated crystalline yield: 0.28 g, 33%. Anal. Calcd for

[{(Me₃Si)₂CH}P(C₆H₅)(BH₃)₂][Na(12-crown-4)]₂: C 51.43, H 9.21%. Found C 52.37, H 8.94%. ¹H{¹¹B} NMR (*d*₈-THF, 25 °C): δ 0.06 (s, 18 H, SiMe₃), 0.68 (d, ²J_{PH} = 10.1 Hz, 1H, CHP), 0.78 (d, ²J_{PH} = 9.6 Hz, 6H, BH₃), 3.65 (s, 32H, 12-crown-4), 6.71 (m, 2H, ArH), 7.05 (t, J_{HH} = 7.6 Hz, 1H, ArH), 7.90 (t, J_{HH} = 8.5 Hz, 1H, ArH). ¹³C{¹H} NMR (*d*₈-THF, 25 °C): δ 3.22 (SiMe₃), 7.77 (d, ¹J_{PC} = 4.8 Hz, CHP), 54.99 (OMe), 67.30 (12-crown-4), 110.96 (ArC), 119.32 (d, J_{PC} = 8.6 Hz, ArC), 127.59 (ArC), 134.35 (d, J_{PC} = 25.9 Hz, ArC), 134.99 (d, J_{PC} = 9.6 Hz, ArC), 162.63 (ArC). ¹¹B{¹H} NMR (*d*₈-THF, 25 °C): δ -32.7 (m, br). ³¹P{¹H} NMR (*d*₈-THF, 25 °C): δ -8.1 (m, br).

[{(Me₃Si)₂CH}P(C₆H₅)(BH₃)₂]₂Mg(THF)₄ (128):

To a solution of **42** (0.50 g, 1.77 mmol) in toluene (10 mL) was added Bu₂Mg (0.90 mL of a 1.0 M solution in heptane, 0.9 mmol). After 1 h stirring, a solution of BH₃.SMe₂ (1.4 mL of a 2.0 M solution in THF, 2.80 mmol) was added to the reaction mixture, turning the solution from pale yellow to colourless. After 1 h further stirring, the solvent volume was reduced *in vacuo* to 5 mL, and the solution was filtered. Colourless crystals suitable for X-ray crystallography were obtained on standing at room temperature for 16 h. Isolated crystalline yield: 0.36 g, 45%. Anal. Calcd for [(Me₃Si)₂CH}P(C₆H₅)(BH₃)₂]₂Mg(THF)₄: C 55.86, H 10.27%. Found C 55.94, H 10.39%. ¹H{¹¹B} NMR (*d*₈-THF, 25 °C): δ 0.05 (s, 18H, SiMe₃), 0.59 (d ¹J_{PH} = 14.2 Hz, 1H, CHP), 0.74 (d, ²J_{PH} = 10.5 Hz, 6H, BH₃), 1.77 (m, 8H, THF), 3.61 (m, 8H, THF), 7.08 (t, J_{HH} = 7.5 Hz, 2H, ArH), 7.18 (t, J_{HH} = 7.5 Hz, 2H, ArH), 7.78 (t, J_{HH} = 7.5 Hz, 2H, ArH). ¹³C{¹H} NMR (*d*₈-THF, 25 °C): δ 2.53 (SiMe₃), 11.26 (d, ¹J_{PC} = 4.8 Hz, CHP), 25.44 (THF), 67.24 (THF), 125.10 (ArC), 126.43 (d, J_{PC} = 7.7 Hz, ArC), 132.33 (d, J_{PC} = 6.7 Hz, ArC), 137.49 (ArC). ¹¹B{¹H} NMR (*d*₈-THF, 25 °C): δ -32.8 (d, br, ¹J_{BP} = 58.8 Hz). ³¹P{¹H} NMR (*d*₈-THF, 25 °C): δ -11.5 (m, br, ¹J_{PB} = 58.8 Hz).

[{(Me₃Si)₂CH}P(C₆H₅)(BH₃)₂]₂Ca(THF)₄ (129):

To a solution of **42** (0.77 g, 2.73 mmol) in toluene (10 mL) was added a solution of (4-^tbutylbenzyl)₂Ca (0.85 g, 1.36 mmol) in THF (10 mL). After 1 h stirring, the solution was concentrated, and a solution of BH₃.SMe₂ (1.4 mL of a 2.0 M solution in THF, 2.80 mmol)

was added to the reaction mixture, turning the solution from yellow to colourless. After 1 h further stirring, the solvent volume was reduced *in vacuo* until the product crystallised from solution. The solution was warmed until the product re-dissolved. Colourless crystals suitable for X-ray crystallography were obtained on standing at room temperature for 16 h. Isolated crystalline yield: 0.85 g, 80%. Anal. Calcd for $[(\{\text{Me}_3\text{Si}\}_2\text{CH}\}\text{P}(\text{C}_6\text{H}_5)(\text{BH}_3)_2)_2\text{Ca}(\text{THF})_4$: C 52.72, H 9.89%. Found C 52.69, H 9.77%. $^1\text{H}\{^{11}\text{B}\}$ NMR (d_8 -THF, 25 °C): δ 0.07 (s, 18H, SiMe₃), 0.68 (d, $^2J_{\text{PH}} = 15.1$ Hz, 1H, CHP), 0.72 (d, $^2J_{\text{PH}} = 12.9$ Hz, 6H, BH₃), 1.79 (m, 8H, THF), 3.60 (m, 8H, THF), 7.15 (t, $J_{\text{HH}} = 6.9$ Hz, 1H, ArH), 7.19 (t, $J_{\text{HH}} = 6.9$ Hz, 2H, ArH), 7.76 (t, $J_{\text{HH}} = 8.0$ Hz, 2H, ArH). $^{13}\text{C}\{^1\text{H}\}$ NMR (d_8 -THF, 25 °C): δ 2.55 (d, $^3J_{\text{PC}} = 1.9$ Hz, SiMe₃), 10.80 (d, $^1J_{\text{PC}} = 1.9$ Hz, CHP), 25.30 (THF), 67.15 (THF), 126.82 (d, $^3J_{\text{PC}} = 7.7$ Hz, ArC), 127.08 (ArC), 132.09 (d, $^2J_{\text{PC}} = 7.7$ Hz, ArC), 143.69 (d, $^1J_{\text{PC}} = 36.4$ Hz, ArC), $^{11}\text{B}\{^1\text{H}\}$ NMR (d_8 -THF, 25 °C): δ -32.4 (d, br, $^1J_{\text{BP}} = 68.6$ Hz). $^{31}\text{P}\{^1\text{H}\}$ NMR (d_8 -THF, 25 °C): δ -15.9 (m, br, $^1J_{\text{PB}} = 68.6$ Hz).

$[(\{\text{Me}_3\text{Si}\}_2\text{CH}\}\text{P}(\text{C}_6\text{H}_5)(\text{BH}_3)_2)_2\text{Sr}(\text{THF})_4$ (130):

To a solution of **42** (0.24 g, 0.84 mmol) in toluene (10 mL) was added a solution of $\{\text{Me}_3\text{Si}\}_2\text{CH}\}_2\text{Sr}$ (0.26 g 0.42 mmol) in THF (10 mL) followed by a solution of BH₃.SMe₂ (0.4 mL of a 2.0 M solution in THF, 0.80 mmol). After 1 h stirring, the solvent volume was reduced *in vacuo* to 10 mL. Upon cooling (5 °C) colourless crystals suitable for X-ray crystallography were deposited. Isolated yield: 0.34 g, 84%. Anal. Calcd for $[(\{\text{Me}_3\text{Si}\}_2\text{CH}\}\text{P}(\text{C}_6\text{H}_5)(\text{BH}_3)_2)_2\text{Sr}(\text{THF})_4$: C 52.20, H 9.60%. Found C 52.00, H 9.47%. $^1\text{H}\{^{11}\text{B}\}$ NMR (d_8 -THF, 25 °C): δ 0.08 (s, 18H, SiMe₃), 0.67 (d, $^2J_{\text{PH}} = 15.1$ Hz, 1H, CHP), 0.81 (d, $^2J_{\text{PH}} = 11.0$ Hz, 6H, BH₃), 1.77 (m, 8H, THF), 3.62 (m, 8H, THF), 7.16 (t, $J_{\text{HH}} = 6.6$ Hz, 1H, ArH), 7.19 (t, $J_{\text{HH}} = 7.1$ Hz, 2H, ArH), 7.77 (t, $J_{\text{HH}} = 8.0$ Hz, 2H, ArH). $^{13}\text{C}\{^1\text{H}\}$ NMR (d_8 -THF, 25 °C): δ 2.07 (d, $^3J_{\text{PC}} = 1.9$ Hz, SiMe₃), 10.58 (d, $^1J_{\text{PC}} = 2.9$ Hz, CHP), 25.45 (THF), 67.37 (THF), 126.84 (d, $J_{\text{PC}} = 7.7$ Hz, ArC), 127.14 (ArC), 132.14 (d, $J_{\text{PC}} = 6.7$ Hz, ArC), 143.31 (d, $J_{\text{PC}} = 37.4$ Hz, ArC), $^{11}\text{B}\{^1\text{H}\}$ NMR (d_8 -THF, 25 °C): δ -31.5 (d, br, $^1J_{\text{BP}} = 58.8$ Hz). $^{31}\text{P}\{^1\text{H}\}$ NMR (d_8 -THF, 25 °C): δ -16.4 (m, br, $^1J_{\text{PB}} = 58.8$ Hz).

9.5 References

- (1) Gynane, M. J. S.; Hudson, A.; Lappert, M. F.; Power, P. P.; Goldwhite, H. J. *Chem. Soc., Chem. Commun.* **1980**, 2428.
- (2) Blair, S.; Izod, K.; Harrington, R. W.; Clegg, W. *Organometallics* **2003**, 22, 302.
- (3) Clegg, W.; Izod, K.; Liddle, S. T.; O'Shaughnessy, P.; Sheffield, J. M. *Organometallics* **2000**, 19, 2090.
- (4) Izod, K.; Stewart, J.; Clark, E. R.; Clegg, W.; Harrington, R. W. *Inorg. Chem.* **2010**, 49, 4698.
- (5) Bertz, S. H.; Gibson, C. P.; Dabbagh, G. *Organometallics* **1988**, 7, 227.
- (6) Lochmann, L.; Trekoval, J. J. *Organomet. Chem.* **1987**, 326, 1.
- (7) Harder, S.; Müller, S.; Hübner, E. *Organometallics* **2003**, 23, 178.
- (8) Crimmin, M. R.; Barrett, A. G. M.; Hill, M. S.; MacDougall, D. J.; Mahon, M. F.; Procopiou, P. A. *Chem.-Eur. J.* **2008**, 14, 11292.
- (9) Sheldrick, G. M. *SHELXTL user manual*, version 6; Bruker AXS Inc., Madison, WI, **2001**.
- (10) *COLLECT* software; Nonius BV, Delft, The Netherlands, **2000**.
- (11) *CrysAlisPro*; Oxford Diffraction Ltd, Oxford, UK, **2008**.

Appendix 1.

1. Dynamic NMR spectroscopy

In chapter 6.3 it was shown using variable-temperature NMR spectroscopy that the SiMe₃ groups in the compound [{(Me₃Si)₂CH}P(C₆H₅)(BH₃)] [Na(12-crown-4)₂] (**116**) exhibit dynamic exchange behaviour in solution. As the temperature is increased rate of exchange becomes increasingly rapid. This results in the two signals coalescing into a single peak, so that the two groups can no longer be distinguished.

2. Line-shape analysis

The variable-temperature ¹H{¹¹B} NMR spectra for compound **116** were simulated using the programme gNMR. Using this programme, the rate constant, *k*, for the SiMe₃ exchange process could be calculated from line-shape analysis at each temperature. As there is no coupling between the exchanging nuclei, the line shape can be calculated using the modified Bloch equations.

For uncoupled exchanging groups which are equally populated, three parameters determine the shape of the NMR peak: i) lifetime of exchanging sites τ ($1/\tau$ = exchange rate) ii) peak separation δ , (shift difference between exchanging sites in Hz), and iii) signal width.

3. The free enthalpy of activation ΔG^\ddagger

By applying the Eyring equation (1) it is possible to determine the free enthalpy of activation ΔG^\ddagger :

$$k = x \frac{k_B T}{h} e^{-\Delta G^\ddagger / RT} \quad (1)$$

$$\begin{aligned}
 k_B &= \text{Boltzmann constant} = 3.2995 \times 10^{-24} \text{ cal K}^{-1} \\
 &= 1.3805 \times 10^{-23} \text{ J K}^{-1}
 \end{aligned}$$

x = transmission coefficient (assumed to be exactly 1)

$$\begin{aligned}
 h &= \text{Planck constant} = 1.5836 \times 10^{-34} \text{ cal s} \\
 &= 6.6256 \times 10^{-34} \text{ J s}
 \end{aligned}$$

Equations (2) and (3) describe the relationship between the free enthalpy of activation ΔG^\ddagger , with enthalpy of activation ΔH^\ddagger and the entropy of activation ΔS^\ddagger , and thermodynamic equilibrium constant K

$$\Delta G^\ddagger = \Delta H^\ddagger - T\Delta S^\ddagger \quad (2)$$

$$\Delta G^\ddagger = -RT\ln K^\ddagger \quad (3)$$

By combining (2) and (3) and solving for $\ln K^\ddagger$ yields equation (4)

$$\ln K^\ddagger = \frac{\Delta G^\ddagger}{RT} + \frac{\Delta H^\ddagger}{R} - \frac{T\Delta S^\ddagger}{R} \quad (4)$$

If we insert this expression into the Eyring equation (1), and take the natural log, assuming $x = 1$, the following is obtained:

$$\ln \frac{k}{T} = 23.76 - \frac{\Delta H^\ddagger}{RT} + \frac{\Delta S^\ddagger}{R} \quad (5)$$

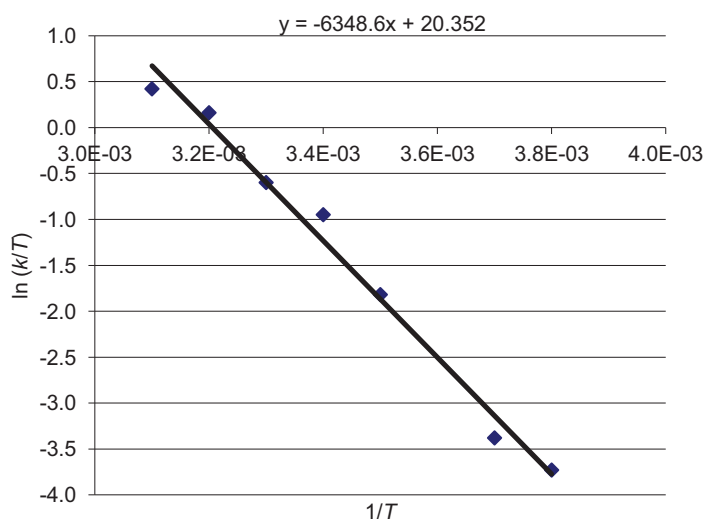
Thus plotting $\ln(k/T)$ against $1/T$ yields ΔH^\ddagger and ΔS^\ddagger . For mononuclear reactions the relationship between enthalpy of activation and the Arrhenius activation energy is:

$$\Delta H^\ddagger = E_A - RT \quad (6)$$

4. Line shape data for SiMe₂ groups of **116** in *d*₈-THF

<i>T</i> / K	<i>k</i>	<i>k</i> / <i>T</i>	ln(<i>k</i> / <i>T</i>)	1 / <i>T</i> , K ⁻¹ (10 ⁻³)
263.15	6.30 × 10 ⁰	0.024	-3.73	3.8
273.15	9.30 × 10 ⁰	0.034	-3.38	3.7
283.15	4.60 × 10 ¹	0.16	-1.82	3.5
296.25	1.15 × 10 ²	0.39	-0.95	3.4
303.15	1.66 × 10 ²	0.55	-0.60	3.3
313.15	3.66 × 10 ²	1.17	0.16	3.2
323.15	4.94 × 10 ²	1.53	0.42	3.1

5. Eyring plot



6. Calculation of ΔH^\ddagger , ΔS^\ddagger and ΔG^\ddagger of **116** using (5) and (2)

Where ΔH^\ddagger can be calculated from the slope ($m = -\Delta H^\ddagger/R$), whilst ΔS^\ddagger can be calculated from the intercept ($c = \frac{\Delta S^\ddagger}{R} + 23.76$).

$$\Delta H^\ddagger = 52.78 \text{ kJ mol}^{-1}$$

$$\Delta S^\ddagger = -28.33 \text{ J K}^{-1} \text{ mol}^{-1}$$

As ΔS^\ddagger is so small and has an inherent large degree of error, it can be considered as 0 kJ mol⁻¹, thus ΔG^\ddagger is essentially equal to ΔH^\ddagger . The low value also suggests that the exchange process in **116** is an intramolecular process.

Appendix 2. X-ray crystallographic data

List of crystal structures

No.	Compound	file no.
39	$\{(\text{Me}_3\text{Si})_2\text{CH}\}\text{PH}(\text{C}_6\text{H}_4\text{-2-CH}_2\text{OMe})(\text{BH}_3)$	ki476
41	$\{(\text{Me}_3\text{Si})_2\text{CH}\}\text{PH}(\text{C}_6\text{H}_4\text{-2-OMe})(\text{BH}_3)$	ki467
42	$\{(\text{Me}_3\text{Si})_2\text{CH}\}\text{PH}(\text{C}_6\text{H}_5)(\text{BH}_3)$	ki367
49	$[\{(\text{Me}_3\text{Si})_2\text{CH}\}\text{P}(\text{C}_6\text{H}_4\text{-2-CH}_2\text{OMe})(\text{BH}_3)\text{Li}(\text{THF})]_2$	ki316
50	$[\{(\text{Me}_3\text{Si})_2\text{CH}\}\text{P}(\text{C}_6\text{H}_4\text{-2-CH}_2\text{OMe})(\text{BH}_3)\text{Na}(\text{tmeda})]_2$	ki468
51	$[\{(\text{Me}_3\text{Si})_2\text{CH}\}\text{P}(\text{C}_6\text{H}_4\text{-2-CH}_2\text{OMe})(\text{BH}_3)\text{K}(\text{pmdeta})]_2$	ki314
64	$[\{(\text{Me}_3\text{Si})_2\text{CH}\}\text{P}(\text{C}_6\text{H}_4\text{-2-SMe})(\text{BH}_3)\text{Li}(\text{THF})]_2$	ki397
65	$[\{(\text{Me}_3\text{Si})_2\text{CH}\}\text{P}(\text{C}_6\text{H}_4\text{-2-SMe})(\text{BH}_3)\text{Na}(\text{tmeda})]_\infty$	ki385
66	$[\{(\text{Me}_3\text{Si})_2\text{CH}\}\text{P}(\text{C}_6\text{H}_4\text{-2-SMe})(\text{BH}_3)\text{K}(\text{pmdeta})]_2$	ki450
87	$[\{(\text{Me}_3\text{Si})_2\text{CH}\}\text{P}(\text{C}_6\text{H}_4\text{-2-OMe})(\text{BH}_3)\text{K}(\text{pmdeta})]_2$	ki474
89	$[\{(\text{Me}_3\text{Si})\text{CH}\}\text{PH}(\text{C}_6\text{H}_4\text{-2-O})\text{Li}]_6$	ki390a
106	$[\{(\text{Me}_3\text{Si})_2\text{CH}\}\text{P}(\text{C}_6\text{H}_4\text{-2-OMe})\text{Li}(\text{tmeda})]$	ki404
108	$[[\{(\text{Me}_3\text{Si})_2\text{CH}\}\text{P}(\text{C}_6\text{H}_4\text{-2-O})]\text{Ca}(\text{THF})]_4$	ki469
115	$[\{(\text{Me}_3\text{Si})_2\text{CH}\}\text{P}(\text{C}_6\text{H}_5)(\text{BH}_3)\text{Li}(\text{THF})_2]_\infty$	ki319
116	$[\{(\text{Me}_3\text{Si})_2\text{CH}\}\text{P}(\text{C}_6\text{H}_5)(\text{BH}_3)][\text{Na}(12\text{-crown-4})]_2$	ki334
117	$[\{(\text{Me}_3\text{Si})_2\text{CH}\}\text{P}(\text{C}_6\text{H}_5)(\text{BH}_3)\text{K}(\text{pmdeta})]_2$	ki493
123	$[\{(\text{Me}_3\text{Si})_2\text{CH}\}\text{P}(\text{C}_6\text{H}_5)(\text{BH}_3)_2\text{Li}(12\text{-crown-4})]$	ki462
124	$[\{(\text{Me}_3\text{Si})_2\text{CH}\}\text{P}(\text{C}_6\text{H}_5)(\text{BH}_3)_2\text{Na}(\text{THF})_2]_2$	ki320
125	$[\{(\text{Me}_3\text{Si})_2\text{CH}\}\text{P}(\text{C}_6\text{H}_5)(\text{BH}_3)_2\text{K}(\text{THF})_2]_\infty$	ki437
126	$[\{(\text{Me}_3\text{Si})_2\text{CH}\}\text{P}(\text{C}_6\text{H}_4\text{-2-OMe})(\text{BH}_3)_2][\text{Na}(12\text{-crown-4})]_2$	ki494
128	$[[\{(\text{Me}_3\text{Si})_2\text{CH}\}\text{P}(\text{BH}_3)_2(\text{C}_6\text{H}_5)]_2\text{Mg}(\text{THF})_4]$	ki463
129	$[[\{(\text{Me}_3\text{Si})_2\text{CH}\}\text{P}(\text{BH}_3)_2(\text{C}_6\text{H}_5)]_2\text{Ca}(\text{THF})_4]$	ki461
130	$[[\{(\text{Me}_3\text{Si})_2\text{CH}\}\text{P}(\text{BH}_3)_2(\text{C}_6\text{H}_5)]_2\text{Sr}(\text{THF})_4]$	ki480